KfK 3709
März 1985

Experimental Investigation of Flow Dynamics in the SNR-Upper-Core Structure

L. Meyer
Institut für Neutronenphysik und Reaktortechnik
Projekt Schneller Brüter

Kernforschungszentrum Karlsruhe

KERNFORSCHUNGSZENTRUM KARLSRUHE

Institut für Neutronenphysik und Reaktortechnik

Projekt Schneller Brüter

KfK 3709

EXPERIMENTAL INVESTIGATION OF FLOW DYNAMICS IN THE SNR-UPPER-CORE STRUCTURE

L. Meyer

Dieser Bericht erscheint gleichzeitig als Report des
Los Alamos National Laboratory, Los Alamos, N.M.,U.S.A.

Kernforschungszentrum Karlsruhe GmbH, Karlsruhe

Kernforschungszentrum Karlsruhe GmbH
ISSN 0303-4003

Experimentelle Untersuchung der Fluiddynamik in den oberen Kernstrukturen des SNR

Zusammenfassung

Dieser Bericht beschreibt die Ergebnisse von Experimenten mit Simulationsmaterialien, die durchgeführt wurden, um die Fluiddynamik in den oberen Kernstrukturen während eines Kernzerlegungsunfalles in einem Natriumgekühlten Schnellen Brutreaktor zu untersuchen. Anhand der Experimente sollten einige der thermohydraulischen Modelle in SIMMER-II überprüft werden. Es wurden vier verschiedene Flüssigkeiten verwendet, um das expandierende UO_2 zu simulieren; die experimentellen Anfangs- und Randbedingungen, wie z.B. Anfangsdruck und Temperatur und der Aufbau der Teststrecke, wurden in großer Zahl variiert. Die Experimente zeigten den großen Einfluß der Wärmeübertragung in den oberen Kernstrukturen und den relativ kleinen Einfluß der Reibung. Die Umsetzung des thermischen Energiepotentials in kinetische Energie wird durch die Präsenz der oberen Kernstrukturen reduziert. Die Größe dieser Reduktion ist eine Funktion des Anfangdruckes und der Temperaturdifferenz zwischen Kern und oberen Kernstrukturen.

Nachrechnungen sehr verschiedener Experimente mit SIMMER-II ergaben Werte für die kinetische Energie innerhalb einer Bandbreite eines Faktors von zwei verglichen mit den experimentellen Werten, ohne daß Eingabeparameter künstlich angepasst wurden. Es zeigte sich, daß die minimale Tröpfchengröße und der künstliche Wärmedurchgangskoeffizient in der Struktur die kritischen und empfindlichsten Eingabeparameter sind. Das weist auf Schwächen bei der Modellierung des Verdampfungsprozesses unter schneller Druckabsenkung und der transienten Wärmeleitung in der Struktur hin.

ABSTRACT

This report describes the results of a simulant-material experimental investigation of flow dynamics in the upper-core structure (UCS) during a hypothetical core disruptive accident of a liquid-metal fast breeder reactor. The experiments were designed to verify some of the thermal-hydraulic models in SIMMER-II. Four different liquids were used to simulate the flashing UO_2; and numerous parameter variations were made regarding initial pressure, temperature, and configurations of the test apparatus. The experiments showed the large effect of the heat transfer in the UCS and the relatively small effect of friction. The reduction in final kinetic energy by the presence of the UCS is shown as a function of the initial pressure and the temperature difference between core and UCS.

Calculations with SIMMER-II for the wide range of experiments produced results for the kinetic energy within a factor of 2 of the experimental results without changing the crucial input parameters. The minimum droplet size during the flashing process and the structure-side heat transfer coefficient were determined to be the crucial and most sensitive parameters. This reflects deficiencies in modeling of both the flashing process and the transient heat conduction in the structure.

CONTENTS

ABSTRACT

I. INTRODUCTION 3

II. THE EXPERIMENT 5
A. Apparatus 5
B. Instrumentation 7
1. Pressure Measurement 7
2. Temperature Measurement 7
3. Optical Observation of the Flow 8
4. Measurement of Piston Motion 8
C. Experimental Procedure and Data Acquisition 9
D. Experimental Results 9
1. Reproducibility of the Experiments 10
2. Transient Temperature 11
3. Test Matrix 12

III. SIMMER CALCULATIONS 17
A. Numerical Model 17
B. Physical Properties 18
C. Results 19
1. Helium Tests 19
2. Flashing Experiment 21
3. Tests with no Piston 22
4. Reduction of Kinetic Energy by the UCS 25
5. Effect of Parameter Variations 26
6. Calculation with a Fixed Set of Input Parameters. 28
7. Tests with Vapor below Liquid in the Core 30

IV. SUMMARY AND CONCLUSIONS 32

REFERENCES 34

TABLES I - XI 35
FIGURES 1 - 82 48
APPENDIX A 146
APPENDIX B 150
APPENDIX C 155

I. INTRODUCTION

The consequences of hypothetical core-disruptive accidents (HCDAs) in liquid-metal fast breeder reactors (LMFBRs) depend to a large degree on the conversion rate of thermal energy, developed during the neutronic transient, into kinetic energy. During the postdisassembly phase of an HCDA, the high-temperature core material passes through the upper-core structure (UCS) as a multicomponent, multiphase fluid into the sodium pool. The upper-structure dynamics (USD) experiment was designed to study the transient two-phase flow of a flashing fluid interacting with the relatively cold upper-core structures. The objective of the USD experiment was to provide data for evaluating the adequacy of models used in the SIMMER code (Ref. 2,4) and for the development of new models.

The USD experiment was set up at the Los Alamos National Laboratory. The apparatus was tested and a first series of experiments were completed in 1981 and are described in Ref. 1. These experiments were performed with a UCS typical of the Clinch River Breeder Reactor (CRBR), while the experiments described in this report were performed with a UCS of the German sodium-cooled fast reactor (Schneller Natriumgekuhlter Reactor, SNR).

In the prototypic case of an HCDA, the main working fluid is UO_2 at very high temperatures (4000 - 5000 K) and pressures (5 - 25 MPa). For the experiment, a simulant fluid was sought that shows similar behavior at lower temperatures and pressures. A similarity analysis was performed (Ref. 3) and was described extensively in Ref. 1; here, only its main features will be outlined. Basic scaling requirements can be derived by considering the homogeneous part of the three conservation equations of mass, momentum, and energy. The latent heat of evaporation (h_v) is used as the main normalization parameter. Three non-dimensional parameters are obtained, $\rho h_v/p$, gx/h_v, and $c_v T/h_v$, where ρ is density, g is the acceleration of gravity, and c_v is the vapor specific heat at constant volume, which set the scales for pressure (p), length (x), and temperature (T), respectively. The combination of two of these parameters and the application of the perfect gas law yields another parameter ($c_v m$) with the molecular weight m, which serves to select the appropriate simulant fluid. Propyl alcohol and ethylene glycol were chosen because their values of ($c_v m$) were similar to that of UO_2. The scaling factors for pressure, length, and temperature were approximately 25:1, 2.5:1, and 10:1, respectively. To study the effect of different physical properties, two additional simulant fluids, methyl and heptane, were used in one experiment each.

This kind of scaling analysis leads to similitude in the important aspects of liquid/vapor phase change, during the HCDA. Of course, it is impossible to simultaneously achieve similarity of all aspects of transient two-phase flow with heat transfer. Also, the properties of both the prototypic material and the simulants vary greatly in the relevant temperature and pressure ranges; and the importance of the liquid and vapor phases to the flow characteristics vary at different times during the HCDA. A discussion of these problems can be found in Refs. 1 and 3.

Calculations with the SIMMER code for the same geometry and similar boundary conditions for both prototypic and simulant materials will help to clarify these questions of similarity. In this report, we present SIMMER calculations of the simulant experiments.

In the USD experiment, the upper sodium pool is simulated by a solid piston. The piston approximately simulates the movement of the interface between the HCDA bubble emerging from the UCS and the sodium pool and also provides a convenient way of tracing interfacial velocity. The mass of the piston and the length of its flight path have to be modeled according to scaling laws and by taking into consideration the simulation of a three-dimensional expansion by a one-dimensional movement (see Appendix A). The effects of any fuel/coolant thermal interactions were not modeled.

In the first section of this report, all relevant data of the experiments are presented. No additional information is necessary to perform SIMMER calculations or to compare the theoretical and experimental results. The test matrix is a result of a learning process during the experimental program. Of course, this learning process did not end when we completed the experimental program, and different experiments might be desirable in the future. For most of the experiments, calculations with SIMMER were performed. The main results of these calculations are presented in the second section of the report.

II. THE EXPERIMENT

A. Apparatus

The experimental apparatus is of a 1/2.5 geometrically scaled subassembly, along with a similarly scaled region extending upward to the vessel head. A schematic is shown in Fig. 1. The lower part represents the molten core region. The heated and pressurized simulation fluids are separated from the (UCS) by a diaphragm. A fast-acting opening mechanism is used to simulate the rapid expansion of the molten core materials into the UCS. Former experiments[1] had employed prescored, two- or four-petal rupture disks.* They were selected so that their rupture pressure was approximately 20 Pa above the pressure in the lower vessel (core). A rupture-disk-breaking mechanism opens the petals fully and controls the experimental timing. It operates by electrically initiating 150 mg of high explosive that in turn drives a rod equipped with a rounded head into the rupture disk. The excess energy of the moving rod is transformed into deformation energy to minimize the transmission of oscillations to the test section.

At the beginning of this series of experiments, the experimental apparatus was the same as in the preceding experiments except that the UCS section was replaced by one containing the SNR upper axial blanket pin array and SNR mixing head.** Photographs of the UCS and its components are shown in Figs. 2 through 5. The pin bundle (Fig. 3) has 169 pins, each with a length of 172 mm, a diameter of 2.4 mm, and pitch-to-diameter ratio of 1.317. The pins are held by two honeycomb spacer grids (Fig. 4) and one grid plate. Figure 5 shows the mixing head that is downstream of the pin bundle.

During the test series, the apparatus required several modifications for better simulation of SNR conditions and for improved performance. A new piston track was made of aluminum with a more accurate inner diameter. Its length was 1200 mm, and the piston's weight was changed from 0.28 kg to 0.36 kg for similarity with the SNR sodium pool. To minimize the distance from the flashing fluid to the pin bundle, the spacer behind the rupture disk was reduced from 52 mm to 8 mm and was made of insulating material so heat from the core would not affect the test section.

---

*Manufactured by Fike Ind., Blue Springs, Missouri.

**Built by KWU - Erlangen, Germany.

To reduce the vapor volume in the core without changing the liquid inventory, a tightly fitting solid cylinder was inserted into the lower part of the core. This insert lifted the liquid level to 1 cm below the rupture disk, yet maintained the same propanol mass inventory. A certain vapor volume below the rupture disk was required for rapid and complete opening of the rupture-disk petals. Consecutive experiments showed, however, that corrosion had degraded performance of these inserts. Therefore, a new, smaller core was built (Fig. 6, core 2). Also, some important changes were made in its design. All pressure lines connecting the core gauges and other devices were reduced in diameter and could be closed by valves very close to the main cylindrical core vessel. In addition to the main heater, two heating elements were used at the upper and lower flanges, and the thermal insulation of the entire core was increased considerably. Two thermocouples measured the fluid temperature inside the core, and four thermometers were embedded in the wall at various axial positions to monitor temperature uniformity. All these changes led to a more accurate definition of the initial conditions in the experiments.

Another core was built for an even more accurate simulation of the prototypic case, where vapor in the center of the core expands and drives liquid fuel and steel into the upper core structure. This core (Fig. 7, cores 3 and 4) has two sections separated by a thin diaphragm; vapor is in the bottom and liquid is in the upper section. A heated pressure line with a small diameter connects the liquid and vapor. Several diaphragms of different materials and thicknesses were tested. Brass 0.025 mm thick, breaking at a pressure of 20 Pa (small compared with the initial core pressure) proved best. During the experiment, the diaphragm breaks when the pressure relief wave reaches it. Also, the explosively driven rod exerts a force on the center of the diaphragm, where an O-ring is used for a seal. To prevent any liquid from condensing in the lower section of the core, the temperature in the vapor core is kept at least $10^{\circ}C$ above the temperature of the liquid. Two different volumes of liquid in the upper core were used; core 3 with a volume of 560 cm^3 and core 4 with a volume of 360 cm^3. A further change of the test apparatus provided visual access for photography. Cylindrical view sections made of Plexiglas were inserted below and above the SNR test section. Finally, for experiments with a cooled UCS, an open metal box was installed around the UCS and filled with dry ice.

Table I lists the geometrical data of all parts necessary to define the test section in SIMMER. The component fractions (α) and the ratios of surface area to total volume were calculated with a node radius of 2.86 cm.

B. Instrumentation

In an ideal experiment the following properties should be measured:

- initial and transient pressure,
- initial and transient fluid temperature,
- initial and transient structure surface temperature,
- fluid velocity,
- liquid/vapor fractions,
- liquid drop size (flow regime),
- liquid wall film thickness, and
- velocity of piston.

Only some of these properties could be measured in this experiment.

1. Pressure Measurement. Pressures were measured with miniature pressure transducers (Kulite semiconductor, HEM-375 series), which have a metal diaphragm with a diameter of 6.35 mm. The sensor has an integrated, solid-state Wheatstone bridge. Transducers with 100, 250, and 500 psi (0.7, 1.7, and 3.5 MPa) rated differential pressures were used.

Because the transducers are sensitive to temperature changes, the transducer heads were covered loosely with rubber caps that are approximately 1 mm thick. Thus, the temperature changes were not transmitted to the metal diaphragm during the 200-ms test. However, the rubber caps introduced some uncontrollable effects. Among these were their breakage or loss and the varying stresses forced upon the transducer. The effect of the caps on the pressure measurement was investigated by experiments with helium at room temperature both with and without the caps. These results are described in Sec. II. D. 1. The transducers in the test section were mounted with the sensor flush to the inner surface. To measure the pressure in the core, it was necessary to mount the transducers in a separate cylinder above the liquid level. This cylinder was connected to the core by a small tube. The distance between inner core wall and transducer was 14 cm. This arrangement was necessary because when the transducers were installed in the wall, the rubber caps would slip off or break during the transient. The axial positions of the pressure transducers in the experimental apparatus are marked with a P in Fig. 1. In some experiments, pressures also were measured along the piston track (not shown in the schematic).

2. Temperature Measurement. Fluid temperatures were measured by thermocouples. Initially, NANMAC Pencil Probe Thermocouples (E12-2, Chromel-Alumel) were used. The wires of the thermocouples are in a thin, flat ribbon form embedded in a cylindrical insulator (4.75 mm o.d.) and insulated

from each other by a thin sheet of mica. The thermal junction is formed by abrading the sensing-tip surface. This surface protruded into the flow cross section by approximately 1 mm. The advantage of these thermocouples is their ruggedness, combined with a very short response time. We found, however, that in spite of a very fast response in the first 3 ms of the transient, they did not measure the fluid temperature in the time regime from 50 to 200 ms. Because of the finite conductivity of the insulating material, the thermal junction measures an interface temperature rather than the fluid temperature.

In later experiments, thermocouples made of thin wire (0.08 and 0.04 mm o.d.), with an exposed, bead-type junction were used. These thermocouples measured the true transient fluid temperature (see Sec. II. D. 2.), but they are extremely susceptible to mechanical failure. As for the structure, only initial temperatures were measured. The reference junctions were located in an insulated box kept at room temperature.

3. Optical Observation of the Flow. Cylindrical view sections made of Plexiglas with an i.d. of 50 mm, an o.d. of 110 mm, and a length of 60 mm were inserted below and above the UCS test section. Using four mirrors, we could film both view sections with one camera.* The films were taken at 8000 pictures/s with 16-mm Ektachrome, ASA-400 film. We used two 2400 W backlights (8 projector lamps) and two 300 W frontlights.

From the films, the times of first occurrence of vapor and liquid in both view sections can be determined. Only very rough estimates of the liquid/vapor fractions are possible, however. Velocities can be determined accurately during some periods of the transients, but at others, turbulence or the low contrast of the picture precluded precise measurements. An accurate measurement of the droplet size distribution from the films is not feasible; however, an upper limit to the size can be estimated in many cases. Although liquid films can be observed, their thicknesses cannot be determined from the pictures.

4. Measurement of Piston Motion. Three probes were positioned along the axis of the piston track (at 213, 620, and 924 mm from the lower edge of the piston track) to measure magnetically induced eddy currents. The probes change their output when the piston passes. With a signal from both the leading and the trailing edge of the piston (length is 102 mm), there are six consecutive signals. These give the position of the trailing edge of the piston at 111,

*We used the PHOTEC IV camera, manufactured by Photonic Systems, Inc.

213, 518, 620, 822, and 924 mm. Thereby, the position during the transient and its final velocity can be accurately determined.

C. Experimental Procedure and Data Acquisition

Before each test, static pressure calibrations were made by pressurizing the entire system with helium and checking each transducer against a mechanical Heise gauge. The pressure calibration data and data taken from published thermocouple calibration tables serve as insert values for the signal conditioners. A block diagram of the electronic data acquisition system is shown in Fig. 8. Fourteen data channels were on the analog tape deck, including one time channel. In most experiments six channels were devoted to pressure, four channels to temperature, and three channels to piston position.

After calibration, we filled the core with the simulant fluid and evacuated both the UCS and the core to approximately 20 Pa. A certain amount of helium was then added to the core in some tests. We then closed the lines leading to the Heise gauge and to the helium reservoir and adjusted the power of six heaters along the core axis to heat the core uniformly. Depending on the test conditions, it took between one and two hours to reach the desired pressure and temperature. Approximately 5 min before these conditions were reached, we filled the UCS with helium (2500 Pa) in some tests. Then we turned on the tape deck to record the calibration voltages corresponding to zero and full-scale pressure and temperature.

When the experimental conditions were reached, the rupture-disk-breaking mechanism was activated. In tests with photography, first we started the high-speed camera and allowed it to come to a constant speed. At a preset film footage, the camera activated the breaking mechanism. The data recorded on the analog tape were digitized and stored on the MASS storage system of the Los Alamos Central Computing Facility, where they are available for analysis.

D. Experimental Results

Forty-five different experiments have been performed. The following parameters were varied in the experiments:

- fluid (helium, propanol, ethylene glycol, methanol, heptane),
- initial pressure (0.35 - 1.80 MPa),
- initial temperature (20^{o} - 260^{o}C),
- liquid/vapor - ratio,
- vapor/noncondensible - ratio,
- core size,
- initial distribution of liquid and vapor,

- UCS - configuration (with or without pinbundle, seven-hole test, section, no UCS), and
- upper boundary (with or without piston).

Before we describe the experiments in detail, we present an overview of the documentation of the experiments and their results. Table II shows the test matrix and Table III lists the initial conditions of all successful experiments. Many experiments were repeated once or twice for a study of reproducibility. The results of the piston flight measurements are listed in Table IV. The times t_1, t_2, t_3, and t_4 refer to the positions 21.3, 62.0, 92.4, and 120.0 cm along the piston track and the trailing edge of the piston. The final velocity of the piston at z = 120 cm and its kinetic energy at this position also are given. Table V shows the quantitative results taken from the high-speed motion pictures. Figures 9 through 53 show the measured transient pressures of the 45 different experiments. The results of only one test are shown in cases where experiments were repeated. The ensuing Figs. 54 through 56 show some examples of the reproducibility of the pressure traces. Finally, results of the temperature measurements with different thermocouples are shown in Figs. 57 through 62. Some photographs of the flow leaving the UCS are shown in Figs. 63 through 68.

In all pressure and temperature plots throughout this report, the axial position of measurement is denoted by 0 through 9. The positions of the measurement locations 0 through 6 are shown in Fig. 1. The locations 7, 8, and 9 coincide with the positions of the eddy probe in the piston track.

1. Reproducibility of the Experiments. The reproducibility of an experiment was judged mainly by the similarity of the pressure traces of the repeated tests. Four separate effects have to be distinguished:

- the accuracy of the pressure transducer,
- the disturbances caused by the rubber caps,
- the initial conditions, and
- the breaking of the rupture disk.

The accuracy of the pressure transducers depends on the sensitivity and stability of the transducers, their calibration, and the quality of the data acquisition system (such as the voltage supply, signal conditioners, and amplifiers). To minimize problems with drift, the final adjustments of the amplifiers were made as late as possible before the actual experiment was started. Based on the four helium tests, the accuracy of the pressure transducers can be estimated. The experiments performed at room temperature Tests 5 and 20) were run both with and without rubber caps. In the cases

without rubber caps, the consistency of the pressure curves is best (see Figs. 13 and 28). The loss of accuracy due to the rubber caps is generally ~ 2% of the reading. In some cases, however, for one or two transducers in a test, the deviation is much greater due to slippage or breakage of the rubber caps. Such deviations usually can be identified by the inconsistency with the other pressure traces or by comparison with similar experiments. When this occurred, these pressure traces were eliminated or the experiment was repeated.

The reproducibility of the results of different tests with liquid, including all four effects mentioned above, can be judged by looking at Figs. 54 through 56. Here, the pressure traces of two or three similar experiments are plotted on one graph. Differences in the initial conditions, such as small differences in liquid volume in core 2, which result in large differences in the vapor volume (up to 100%), can have a large effect on the pressure histories. In the early runs of the experimental series (up to 16-1, all runs with the Number. X-1) small leaks in the core, which were apparent only at high temperatures, made it impossible to determine accurately the amount of helium in the core.

The performance of the rupture disk was checked by posttest inspection and by the high-speed movies. The petals were generally fully open, and from the film, the opening times were estimated as less than 0.3 ms. In cases where only one petal opened, the experiments were repeated, with the exception of the test series 35-3 through 41-1, in which only one petal out of two opened consistently.

Another proof of reproducibility is the velocity of the piston. In the series of experiments with nominally identical initial conditions (tests 26, 28, 29, 35, 43) the maximum difference in the final velocity is 12%. Therefore, the experimental system with carefully set initial conditions can accurately reproduce data. Errors in measurement either can be detected or are below the random deviation of similar runs of the same experiment.

2. Transient Temperature. Figure 57 shows two examples of the transient temperature measurements with NANMAC thermocouples. For comparison, the saturation temperatures determined from the measured transient pressures are shown. As mentioned before, the thermocouples measured a surface temperature that was neither the fluid temperature nor the UCS wall temperature because of the differing thermal conductivities between the wall and the thermocouple insulation. Except for the initial temperature, these measurements are of little value.

A comparison between the measurement with a NANMAC and a thin-wire thermocouple is shown in Fig. 58. The index "a" denotes the wire thermocouple, "b" denotes a NANMAC with a surface parallel to the flow, and "c" denotes a NANMAC angled 45° toward the flow. All three thermocouples (at T_2) were at the same axial position upstream of the pin bundle. There is little difference in the traces to 1 ms. At later times, the differences are substantial. The NANMAC thermocouple facing the flow at an angle of 45° shows a somewhat faster rise than the standard type but is still much slower than the wire thermocouple. The wire thermocouple of Fig. 58 does not reach the saturation temperature in 25 ms, but a thinner-wire thermocouple, (0.04 mm o.d.) applied in another experiment, does (Fig. 59). At times greater than 25 ms, the thermocouple in the core and the one before the pin bundle show the same temperature transient, which is the saturation temperature at these positions. For times up to 5 ms, the thermocouple in the core registers a larger temperature drop than what the saturation temperature should be according to the measured pressure (Fig. 60). This could be a local effect caused by evaporation at the tip of the thermocouple. It is also possible that the pressure at the transducer is not the pressure at the thermocouple because of the 14 cm long line between core and transducer location. The temperature at T_2 follows the saturation temperature very closely, although it is approximately 8°C lower for up to 10 ms (Fig. 61). It reaches saturation temperature at 30 ms. The measured temperature at T_6 and the saturation temperature behind the mixing head are almost identical. For comparison, the pertinent pressure traces at p_1, p_2, and p_6 are shown in Fig. 62, together with dashed lines representing the saturation pressures calculated with the measured temperatures.

An electronic compensation circuit probably would improve the response of the wire thermocouples at early times. From the current measurement, we can conclude that the two-phase mixture is in equilibrium beyond 25 ms, as it is very unlikely that a higher temperature would be determined if compensation were applied. However, it is unclear whether a temperature higher than the saturation temperature would be measured at early times if we were to apply a compensation network. Therefore, no conclusion can be drawn regarding the degree of nonequilibrium for early times.

3. Test Matrix. The pressure traces of all 45 experiments are shown in Figs. 9 through 53 in two plots each. The first 10 ms of the transient are shown in the upper plot; and the whole transient, approximately up to the time of piston impact at z = 120 cm, is shown in the lower one. The numbers at the curves denote the measuring position in Fig. 1. No signal was recorded to

indicate time zero, that is, the opening of the rupture-disk petals. Thus, time zero in the plots was chosen between 0.3 and 0.5 ms before the first response of p_2. For easy reference, the experiments are documented consecutively, although certain experiments should be grouped in view of their test conditions. We will refer to the test matrix (Table II) briefly to describe these groups of experiments and the main results.

a. Flashing Experiment (F-1). A basic experiment was performed to study the flashing of propanol using the experimental apparatus from the USD experiments. The apparatus consisted of core 2, the diaphragm, and a voided upper chamber with a volume of 260 cm^3. The ratio of the total volume to the core volume was 1.71. Both the lower (core) and the upper chamber were heated to approximately the same temperature (Table III).

The pressure histories shown in Fig. 9 suggest rapid flashing. Similar flashing experiments were performed subsequently with Freon-114 at room temperature in a Plexiglass apparatus.* The high-speed motion pictures taken in these experiments indicate that the rod triggers the flashing process when it moves in the liquid. The flashing starts at the rod and propagates radially and vertically. Experiments in which the diaphragm was broken from above with a stationary rod in the liquid showed far fewer nucleation sites and a slower flashing process. Thus, the the rod motion itself enhances the flashing process.

b. Helium Tests (5, 6, 11, 20). Four different experiments with helium as the only fluid were performed. These involved two in the original core, core 1, and two in the smaller core, core 2. In each case one test was at room temperature (tests 5 and 20) and one was at a helium temperature of 180°C (tests 6 and 20). The volume of core 1 was reduced by using a 10 cm long metal insert. The frequencies of the pressure oscillations lie between 1.2 and 1.6 kHz, the higher frequencies pertaining to the small core and the lower to the large core, with a shift to higher frequencies for the heated cases. The pressure drop is larger for the heated cases.

c. Propanol Vapor Tests (7, 12). For a comparison of similar experiments with a noncondensible fluid (helium) and a condensible vapor, tests 7 and 12 were performed. Here, the amount of liquid propanol in the core was kept very small. Test 7 should be compared with test 6 and test 12 with test 11. Because

*L. Hull; "Flashing Phenomena Experiment", Los Alamos unpublished document.

many unheated portions in core 1, (such as pressure lines where the vapor condensed), the vapor was approximately 7°C above saturation temperature. Compared with the helium tests, there were fewer pressure oscillations and the pressure drop was higher.

d. Tests with Liquid in Core 1 (1-4 and 8-10). Tests 8 and 9 were designed to have the same vapor volume as in tests 5, 6, and 7, where the liquid had the same volume as the metal inserts in these former tests. The difference between test 8 and 9 is the additional helium fraction in test 9 and a helium pressure in the UCS of 2500 Pa. The additional helium in the core leads to a lower pressure drop.

Test 10 was run with the same amount of liquid as in test 8, but with ethylene glycol instead of propanol and ,consequently, at a different initial pressure and temperature. The relative pressure drop (relative to the initial pressure) in the UCS was much larger than in test 8, although the absolute pressure drop was similar.

The first four experiments (tests 1 - 4) were performed as a continuation of former tests[1], but with only a few changes of the experimental apparatus. The ratio of liquid to vapor volume and the total core volume were varied.

e. Tests Without the Piston. Two experiments were performed with the UCS section closed at its upper end. The initial conditions in the core were the same; but in test 23 the UCS was heated to 410 K, while in test 24 the UCS was cooled to 260 K. The pressure histories show the major effect of heat transfer.

f. Test to Study the Effect of Initial Pressure and the Temperature Difference between Core and UCS (13-19, 21, 22). Experiments with propanol at three different initial pressures (0.56, 1.11, and 1.80 MPa) were performed. The UCS section was kept either at room temperature (Tests 13, 14, 15, 16) or was cooled by approximately 80 K (tests 17-19). Similar experiments were run with ethylene glycol at 0.56 MPa (tests 21, 22). Besides the effect on the pressure transients, the effect of the temperature difference on the piston energy should be noted. The kinetic energy of the piston was reduced about half in the propanol tests and by 1.5 in the ethylene glycol tests if the UCS was cooled (Table IV).

g. Tests With the Seven-Hole UCS (25, 26). Two experiments were performed with a UCS structure consisting of a seven-hole array with the equivalent flow area of the CRBR pin bundle. This UCS had also been used in the CRBR-related test series. One test each with propanol (25) and ethylene glycol (26) was run. For comparison with the SNR test section, the results should be compared with tests 13 and 21, respectively. The kinetic energy of the piston is higher by a

factor of 2 for propanol and by almost a factor of 4 for ethylene glycol, as compared with the SNR UCS. The tests with ethylene glycol were run at half the pressure of the propanol tests but at a temperature 80 K higher. Therefore, the larger area for heat transfer in the SNR UCS has a greater effect on the energy reduction.

h. Test With and without Pin Bundle (39, 42). To separate the effect of the pin bundle from that of the mixing head on the flow, Test 42 was run without the pin bundle and spacer grids. Test 39 had the same initial conditions but was run with the complete SNR UCS. The absence of the pin bundle in the UCS reduces the time of piston impact by a factor of 2, while the maximum pressure at the exit of the UCS was approximately twice as high. The kinetic energy of the piston was also twice as high. These data were obtained for an initial pressure of 0.526 MPa and a temperature difference between core and UCS of 110 K. The effect of pressure and temperature difference on the energy reduction will be discussed in Sec. III. C. 4.

i. Tests With Vapor Above or Below Liquid in the Core (28, 29, 38, 39). Experiments were performed with the liquid and vapor in chambers separated by a thin diaphragm. In these cases the vapor was below the liquid. Propanol tests 29 and 38 without noncondensible gas were performed with a large upper core chamber (core 3) and with a smaller upper core chamber (core 4). The initial pressures of tests 29 and 38 were 1.12 MPa and 0.56 MPa, respectively. The corresponding tests with the vapor above the liquid are tests 28 and 39. The differences in pressure histories and piston velocities between these two types of experiments were surprisingly small. The pressure and piston energy were somewhat higher in test 29 (large liquid core above vapor) than in test 28, while there was very little difference between tests 39 and 38, with less liquid and lower pressures.

j. Tests With Vapor/Noncondensible Mixture Below Liquid (27, 30, 38, 40, 41) With the vapor or noncondensible gas below the liquid, it is possible to perform tests with liquid at high driving pressures but low temperatures. A series of tests (34 through 38) was performed to study the effect of the amount of noncondensible gas and the initial temperature in the core. The amount of helium in the core was reduced in each test but the core pressure and liquid inventory were kept the same. Thus, helium provides all the driving pressure in tests 34 and 27 at a core temperature of 20°C, and none in tests 38 and 31 at 150°C. The pressure histories show very distinctive differences. In the case of the pure noncondensible gas, tests 27 and 34, spikes are present at the entrance of the pin bundle, but they decrease while traveling through the

bundle. There is very little pressure drop at early times during the transient, which suggests single-phase gas flow. Later, there is a clear onset of two-phase flow with higher pressure drop between consecutive pressure-measuring stations. With the higher vapor portion in tests 35 and 36, the pressure peaks decrease and the pressure drop increases at early times.

The results taken from the visual observations are listed in Table V. The time of first occurrence of both vapor and liquid decreases in tests 34 through 38 with decreasing helium pressure, and the velocities are higher for lower amounts of helium and higher core temperatures. The piston impact time has a minimum and the piston energy a maximum at 67% helium pressure (test 36). The droplets leaving the UCS were bigger in the case of helium only (test 34) and similar to the results for ethylene glycol (Fig. 66, test 41).

k. Tests With Methanol and Heptane (43, 44). One experiment each was performed with methanol and heptane in the same configuration as in test 39 with propanol. While in all tests vapor could be seen leaving the UCS before the liquid, in tests with heptane (test 44) and with ethylene glycol (test 40), no vapor could be identified in the upper view section.

III. SIMMER CALCULATIONS

A. Numerical Model

The SIMMER-II code with some modifications was run on a Control Data Corporation CDC-7600 computer. The experimental setup was divided into computational cells (r-z geometry) as shown in Fig. 1. Only one radial node was used, except for some trial runs with two radial nodes, which will be described in Sec. III. C. 7. The initial conditions of an experiment were defined as accurately as they were known from the measurements (see Table III). A sample input file is shown in Appendix B. The core region was divided into two parameter regions and into three mesh sets so we could define variable temperatures along the core axis as they were measured in most experiments. The rupture disk was modeled as a step change in the initial spatial pressure distribution. This step change is removed during the first time step of the transient calculation (0.01 ms), but the actual opening time of the rupture disk is approximately 0.3 ms. Therefore, agreement during the first few milliseconds of a test cannot be expected.

The can wall of the core was modeled as aluminum, as were the rest of the test section walls, although it was actually made of steel. No significant effect due this discrepancy was expected, however. The pin bundle was modeled with the actual material (steel), hydraulic diameter, and surface area, but the spacers were not modeled. The additional pressure drop and increase in the heat transfer coefficient from the spacers can be taken into account by the multipliers on the friction factor and the heat transfer coefficient. Two parameter sets for the pin bundle were defined to allow different multipliers at the entrance and for the rest of the bundle.

The spiral impeller and the radial ribs of the mixing head were modeled as a single component with known flow and surface areas. However, the hydraulic diameter can only be estimated using the flow and surface area information. This results in a hydraulic diameter estimate of 9.2 mm. When the hydraulic diameter was determined from steady-state single-phase pressure measurements (Ref. 11), it was found to be only 2 mm. Because we do not know how the geometry of the mixing head impacts transient two-phase flow, the hydraulic diameter must be found experimentally. A hydraulic diameter of 9.2 mm was taken as input, and was effectively modified by applying friction and heat transfer multipliers on the order of 3. These multipliers were varied in some calculations.

To define a uniform can wall thickness for the whole UCS test section, nonflow areas had to be introduced. The structure volume fractions listed in Table I were determined with a node radius of 2.86 cm. By introducing nonflow areas, these volume fractions were reduced to a value that depends on the surface area and selected wall thickness in the particular parameter region. The procedure is described in detail later (Sec. III. C. 3.). To simulate the moving piston, the plug mechanics option was used. The piston in effect represents a moving, rigid-wall boundary condition. A balance of forces is calculated at the interface, the two forces being the inertia of the piston mass and the driving pressure at the interface. No provision was made for frictional forces, but a constant back pressure and an initial breakaway force can be defined in the input. The velocity and the displacement of the plug were obtained through time integrals of the acceleration and the velocity. The moving interface was simulated by the opening of a nonflow area to the flow area.

Other modifications of SIMMER-II were the correction for the case of a staggered mesh; modifications for the analytic equation of state, which allowed temperature-dependent liquid densities; and smaller changes that will be described at the time they had any effect on the calculations. Other aspects of the model are discussed in the relevant sections of this report.

B. Physical Properties

Table VI lists the properties used for the five simulant fluids employed in this study. Of all the liquid properties, the current version of SIMMER allows only the liquid density to be a function of temperature. A constant value for the other properties in the liquid state had to be chosen. Tables VII through X list the values of the density, specific heat, thermal conductivity, surface tension, and kinematic viscosity of the saturated liquids in the relevant temperature ranges (from Refs. 12 through 15).

The variable liquid densities are defined in SIMMER by the correlations given in Table XI. For the specific heat, a value typical of the respective core temperatures was chosen. The values of the other three properties were chosen at approximately 20 to 40 K below the core temperature. The input for the energy at the critical point (e_{crit}) was set to zero, in which case SIMMER uses a default value. Some of the properties for the vapor state are estimates or extrapolations because exact values were not available.

C. Results

1. Helium Tests. In these experiments there was no phase change but heat transfer occurred between the structure and the gas. Also, there were no liquid components. Thus, an update file was made* to allow helium as "fission gas" to transfer heat, as well as to nullify large sections of the XCHANJ overlay that pertain to phase change. In addition, the liquid/gas drag term, KIJ, was zeroed out and the liquid velocities equated with the gas velocities. The latter was done because SIMMER sometimes has trace amounts of liquid components 4 and 8. A copy of this update file is in Appendix C. The model that dumps all of the dissipation energy, HFIGJ, created by the wall friction into the gas was retained. Thus, friction heats the gas, which in turn can transfer some of this energy to the structure and vice versa via the heat transfer model.

Test 5 was taken as a sample case. In the very early phase of the transient, at t≃0.2 ms, large flow speeds (t≃1.4 m/s) and high gas temperatures (≃ 820 K) were computed for cell 32 by the SIMMER code. For a crude comparison, an independent calculation of the analytical solution of a pure shock tube was made.* A comparison of the two calculations for this cell at 0.2 ms is as follows:

VARIABLE	SIMMER	ANALYTIC
p (MPa)	2.0×10^{-1}	3.1×10^{-2}
ρ (kg/m^3)	1.2×10^{-2}	1.3×10^{-3}
T (K)	8.2×10^{-2}	1.1×10^{3}
U (m/ms)	1.4×10^{0}	2.1×10^{0}

Certainly a shock front would be destroyed by the pin bundle, so at best the above comparison is largely qualitative. However, it does show that high temperatures can occur in the very early phases of the transient when the highly rarified, initially low-pressure gas is compressed. The initial pressure discontinuity produces a shock with a pressure ratio of ≃12.0 and a density ratio of ≃3.0. Thus, a shock temperature ratio of ≃4 is realized.

To separate the effects of dissipation and heat transfer, four SIMMER runs were performed. One run had both friction and heat transfer off, one had only friction on, one had only heat transfer on, and one had both on. Figure 69 shows the effect of heat transfer and friction on the pressures before the bundle (A) and in the upper space (B). Calculations without heat transfer and

*P. J. Blewett, Q-8, Los Alamos National Laboratory.

friction provide pressures that are too low. The introduction of friction raises the pressure initially, but there is almost no effect after 20 ms. The addition of heat transfer raises the pressure curves in the entire transient to the level measured. These curves are not shown as they are too close to the measured one.

Figure 70 presents a comparison of the measured and calculated pressures during the first 10 ms of the transient for p_2 (before the pin bundle). The frequencies of the oscillations are almost identical. The shift to earlier times of the calculated oscillations is probably due to inadequate modeling of the rupture disk.

The effects of the various parameters, such as friction and heat transfer coefficients, were not studied for the helium tests. The multipliers for friction and heat transfer were set to 1, except for the pin bundle entrance (= 8), the pin bundle (= 2), and the mixing head (= 1.8). The structure-side heat transfer coefficient was set to 1000 $W \cdot m^{-2} \cdot K^{-1}$.

The two graphs (Figs. 71 and 72) show the effect of friction and heat transfer on energy conservation and the kinetic energy of the piston, respectively. Figure 71 shows total energy E of the gas-structure system as a function of time. Thus, E equals the sum of the gas internal energy, gas kinetic energy, piston kinetic energy, and the change of the structure internal energy. This method of calculating E is equivalent to taking zero as the reference energy for the structure. Very little difference in E was discernible between the case with heat transfer only and the case with neither heat transfer nor friction. Thus, heat transfer has a negligible effect on total energy conservation. However, with friction on, total energy is more nearly conserved; albeit there is some question as to how to calculate the dissipation term in the internal energy equation. SIMMER may more nearly conserve energy with friction because friction slows the flow; thus, the overall calculation of the dynamics is more accurate. Without friction, SIMMER loses 14% of the system's energy in the early part of the transient and at the end of the calculation the loss is about 11%. With friction, the corresponding losses are 8.6% and 7%.

The second graph (Fig. 72) depicts the sum of the gas kinetic energy and the piston kinetic energy as a function of time. After 2 ms almost all the kinetic energy is due to piston motion. From this graph we conclude that friction has a very small effect on kinetic energy, about 2% at late times; heat transfer has a late time effect of about 10%.

2. Flashing Experiment (F-1). The main parameter governing the flashing process in SIMMER is the droplet size of the liquid in the core. The SIMMER code has five criteria for the determination of the droplet size (fluid dynamics breakup based on Weber number criterion, hydraulic diameter, liquid mass in each cell, flashing breakup and liquid coalescence). Flashing breakup leads to very small droplets in the first few time steps, restricted only by the speed of the pressure-relief wave traveling through the core from the top to the bottom. The speed of this wave depends on the initial vapor fraction in the liquid, according to the sound velocity in a two-phase medium. Because of the very high vapor velocities (around 100 m/s) at early times, the Weber number criterion leads to even smaller droplets in the upper nodes of the core (around 10^{-7} m).

SIMMER provides the option to define a minimum and maximum droplet size. A series of SIMMER runs were performed to study the effect of the minimum droplet size in the core (r_{pmin}), the vapor fraction in the liquid, and the maximum droplet size in the upper chamber. The parameters we varied are listed in Table A. The noding was as follows: node 1-10, liquid core; node 11-12, vapor core: node 13-20, upper chamber.

TABLE A
PARAMETRIC VARIATION

	Core		Upper Chamber		Vapor Fraction
Run	r_{pmin} $x10^4$m	r_{pmax} $x10^4$m	r_{pmin} $x10^4$m	r_{pmax} $x10^4$m	In Core (%)
1	1	1	0.01	1	2.88
2	1	1	1	1	2.88
3	1	100	0.01	100	2.88
4	0.5	100	0.01	100	2.88
5	2	100	0.01	100	2.88
6	1	100	0.01	100	0.36
10/11	0.01	100	0.01	100	2.88

The effect of the minimum droplet size in the core is demonstrated in Fig. 73. The calculated pressures in the upper and lower chamber are shown together with the measured pressure in the lower chamber (core). In runs 5, 3, and 4, the minimum droplet size was set to $2x10^{-4}$, $1x10^{-4}$, and $0.5x10^{-4}$ m, respectively. The droplet size as a function of time is shown for node 5 (center of liquid core), for node 12 (vapor space in core just below the rupture

disk), and for node 15 (upper chamber). The optimal droplet radius for this set of parameters lies between $1x10^{-2}$ and $2x10^{-4}$ m.

The effect of the minimum drop size in the upper chamber can be seen by comparing runs 1 and 2 in Fig. 74. In run 2 the droplet radius is set to $1x10^{-4}$ m by making the input minimum and maximum identical. In run 1 the minimum in the upper chamber is 10^{-5} m.

The effect of the maximum drop size in the lower and upper chamber is shown in runs 1 and 3. Note that the scale of the droplet-size plot for run 3 is different from the others. Also shown for the same runs are the liquid velocity, the liquid volume fraction, the energy transfer to the liquid, and the liquid temperature in Figs. 74b and 74c. Comparing runs 1 and 3, we note little difference in the velocities for the entire transient. The same is true for pressures for about the first 10 ms. Later, however, the pressure and temperature are higher for increasing maximum drop size. In this latter case, there is no (or only very small) energy transfer to and from the liquid once the liquid droplet radius is above 0.5 mm. For agreement with the measured pressure transients, a fine tuning of the droplet sizes in both the lower and upper chamber is necessary.

Figure 75 shows the effect of the initial vapor fraction in the liquid during the first 10 ms of the transient. There was no difference in the pressures after 20 ms. To study the different criteria for the determination of the droplet size, a SIMMER version was created that does not contain the flashing breakup criterion. The only mechanism that leads to droplet breakup in this case is the fluid-dynamic breakup based on the Weber number criterion. The critical Weber number for these runs was reduced from 15 to 3. Figure 76 shows the resulting pressure transients and droplet sizes. The pressures in run 10 are much too low. To increase the pressure, the surface area of the liquid droplets was artificially increased by a factor of 5 in run 11.

In all calculations for the flashing experiment, the parameter COAL, which governs the coalescence of droplets, was set to 1. A change of this parameter would change the droplet growth and thereby the pressure transient. Because the models applied in SIMMER for flashing breakup, fluid-dynamic breakup, and coalescence are crude and do not describe observed physical processes accurately, we could not expect that a set of parameters describing the present flashing experiment correctly will do the same for other flashing experiments.

3. Tests With No Piston. Tests 23 and 24 served as a study of heat transfer and condensation in SIMMER. Without the moving piston, the upper

boundary condition is defined more precisely and the computing times are shorter.

For a better understanding of the following calculations, some aspects of the SIMMER-II heat transfer model should be discussed. SIMMER defines a single temperature for each structure material in each mesh cell. A structure-side heat transfer coefficient is defined by dividing the thermal conductivity by half the thickness of a wall. This assumed "thin-wall behavior" is correct only for slow transients. For rapid transients in which the thermal penetration distance into the wall is less than the thickness of the wall, this method underestimates the heat flux. Also, the structure-side heat transfer coefficient sets an upper limit to the fluid-side heat transfer coefficient. A method to improve the heat transfer calculation is to estimate the duration of the transient and define a penetration thickness (δ) and heat transfer coefficient (h) accordingly.

A structure can be considered thin with respect to the transient heat flux for sufficiently small values of the Biot number ($Bi = h\delta/k$). The heat transfer coefficient h, however, can vary by more than an order of magnitude during a transient because of the occurance of different regimes of two-phase flow. For example, droplet condensation may occur at the beginning of the transient and film condensation at later times. This makes it difficult to estimate a wall thickness that will give reasonable results during all periods of the transient. However, the ratio of effective wall thicknesses for different materials subjected to the same transient flow can be easily determined. The governing parameter is the Fourier number ($Fo = \alpha\Theta/\delta^2$). Therefore, $\delta \propto (\alpha\Theta)^{1/2}$, and using the thermal diffusivities α for aluminum and steel, the thicknesses have a ratio of 5 ($\delta_{AL}/\delta_{St} = 5$). The conductivities have a ratio of 15 ($k_{Al}/k_{St} = 15$), so the heat transfer coefficients should have a ratio of 3 ($h_{Al}/h_{St} = 3$).

As a base case, we assumed that the entire pin mass acts as a heat sink ($r_{pin} = 1.2$ mm). When we take into consideration the different geometries of a pin and the can wall and apply the above ratios, the effective thickness of the can wall becomes 3.6 mm and the heat transfer coefficients are 4.1×10^4 and 12.3×10^4 $W \cdot m^{-2} \cdot K^{-1}$, respectively. By introducing a nonflow area, the proper structure mass volume fractions are obtained. Table XII shows the input parameters that were varied for the runs described below.

TABLE XII
PARAMETRIC VARIATIONS

Run	h_{pin} $x10^{-4}$	h_{can} $x10^{-4}$	Fraction of Pin Mass	Can Wall Thickness
	$W \cdot m^{-2} \cdot K^{-1}$			mm
24-1	4.1	12.4	1.0	3.6
24-2	8.1	25.0	0.5	1.8
24-3	6.2	18.7	0.75	2.7
23-18	4.1	12.4	1.0	3.6
23-15	4.1	12.4	1.0	1.8
Minimum droplet size in core			$7x10^{-5}$ m	
Minimum droplet size in UCS			$5x10^{-7}$ m	

Figure 77 (run 24-1) shows the calculated pressure histories at the six pressure measuring stations together with the measured pressures p_1 and p_6. Also shown are the liquid velocities (Fig. 77a), the fluid temperatures (Fig. 77b), and the structure temperatures (Fig. 77c). It is obvious that too much heat is transferred to the structure and the pressure drop is too low. For the next run only half the mass was taken to act as a heat sink; and, accordingly, the heat transfer coefficients are twice as high. Now in the second run (run 24-2), the final pressure is too high, and insufficient heat is transferred to the structure. In the third run (run 24-3) 75% of the mass was taken, and here the final pressure is similar to the measured, although it is reached too soon. A somewhat better result (not shown) was obtained by taking the heat transfer coefficients of the first run but (inconsistently) using only half the mass as a heat sink.

Other calculations were performed with variations of the droplet size and the heat transfer multipliers in the core and UCS. These variations had little effect on the pressure transients and such other variables as fluid velocities and temperatures.

At the downstream end of the test section, SIMMER has difficulties in calculating the correct pressure and temperature. The velocity and vapor volume fraction both drop to zero. No heat is transferred and the temperatures are constant. The can wall temperature of node 32 does not rise above 250 K. A

turbulence model would be necessary to simulate the liquid motion and provide for heat transfer.

Figure 78 shows the results of two calculations for test 23 in which the UCS was heated. Run 23-18 had identical input parameters as run 24-1 except for the UCS temperatures. As in run 24-1, the pressure drops are too low in run 23-18. In run 23-15, the structure-side heat transfer coefficients are the same but the can wall mass was reduced by a factor of 2. The calculated pressure in node 32 is not shown because of its large oscillations starting at 45 ms.

In conclusion, with proper structure-side heat transfer input, SIMMER-II calculates about the right pressure histories and final pressures for two transients with quite different structure temperatures. Some model deficiencies became obvious in this study. The lack of a heat conduction model inside the structure requires that the amount of structure that will act as a heat sink has to be estimated. The resulting "structure-side heat transfer coefficient" cannot describe the heat transfer correctly throughout the transient. For better results it might be necessary to change this parameter inconsistently with the amount of structural mass. Discrepancies remain at early times in the transient when high-speed condensing flow and drop-wise condensation lead to very high heat transfer rates, which SIMMER cannot calculate. Also, it is difficult to simulate the low heat transfer rates once a liquid film has formed at the structure.

4. Reduction of Kinetic Energy by the UCS. An important result from the experiments is the piston kinetic energy data. These data are compared with the maximum kinetic energy of the piston as calculated by SIMMER. The maximum energy was calculated with the proper initial conditions for the test, no pin bundle or mixing head in the UCS, zero friction and heat transfer at the can wall, and the droplet radius set to 10^{-8} m to achieve maximum flashing rates.

TABLE XIII

COMPARISON OF KINETIC ENERGY AND TIME OF PISTON IMPACT IN EXPERIMENTS AND CALCULATED WITH MAXIMUM FLASHING AND WITHOUT FRICTION AND HEAT TRANSFER IN UCS

	INITIAL CONDITIONS		MEASURED VALUES		CALCULATED VALUES		RATIO
TEST	p (MPa)	ΔT (K)	t_{imp} (ms)	E_{exp} (J)	T_{imp} (ms)	E_o (J)	E_{exp}/E_o
15	0.56	117	101	136	36	762	0.177
18	0.56	190	141	76	36	762	0.100
13	1.11	133	65	340	27	1353	0.251
17	1.11	200	98	172	27	1353	0.127
16	1.80	163	50	549	25	1600	0.343
21	0.56	200	133	61	37	6940	0.088
22	0.56	257	174	41	37	694	0.059
43	0.97	100	61	373	28	1361	0.274
44	0.35	116	114	114	43	573	0.199
39	0.53	115	94	194	--	818	0.237
42	0.53	115	51	407	--	818	0.498
12	1.11	133	76	56	32	665	0.084
25	1.11	150	37	696	27	1353	0.514
26	0.43	202	60	235	37	694	0.339

In Table XIII the results for the 14 most important experiments are listed, and Fig. 79 shows some of the results in graphic form. The kinetic energy from the experiments is E, and E_o is the maximum energy calculated with SIMMER. The solid lines are the interpolated results of the propanol tests (tests 13 through 18). As indicated in the Fig. 79, the kinetic energy reduction is very sensitive to the temperature difference between the core and UCS. Tests with and without the pin bundle (tests 39 and 42) gave reduction factors of 1/4.2 and 1/2, indicating that the pin bundle has a large effect on the energy reduction factors.

5. Effect of Parameter Variations. Test 17 (propanol, 1.11 MPa, $\Delta T = T_{core} - T_{UCS} = 200$ K) was chosen to study the effect of some parameters on the pressure and kinetic energy of the piston. An input parameter set was established with which SIMMER calculated the pressures and piston movement in

reasonable agreement with the experimental results. Some of the more important parameters had the following values:

minimum drop size in core	node 1 - 4	2×10^{-4} m
minimum drop size in core	node 5 - 12	5×10^{-5} m
minimum drop size in UCS	node 13 - 32	5×10^{-7} m
maximum drop size in lower space	node 13 - 17	1×10^{-5} m
maximum drop size in UCS	node 18 - 32	5×10^{-4} m
structure-side heat transfer coefficient, pins		4.1×10^{4} $W \cdot m^{-2} \cdot K^{-1}$
structure-side heat transfer coefficient, can walls		12.3×10^{4} $W \cdot m^{-2} \cdot K^{-1}$
fraction of pin mass involved		1
wall thickness of can wall		1.8 mm

Table XIV shows the varied parameters and the amount of their variation. Also listed are the calculated impact times and kinetic energies of the piston. The last row shows the change of the kinetic energy compared with the base case. The corresponding pressure plots are shown in Fig. 80.

TABLE XIV

EFFECT OF PARAMETER VARIATIONS ON KINETIC ENERGY OF PISTON
EXPERIMENT NO.17, BASIS OF VARIATIONS IS RUN 3

Run	Parameter Varied	by Factor	Impact Time (ms)	Kinetic Energy (J)	Factor
3	Base case	1.0	82	200	1.00
5	Minimum drop size in core	0.5	76	218	1.09
6	Structure wall thickness	1.6	88	153	0.77
7	Heat transfer multiplier	5.0	81	170	0.85
8	Friction multiplier	5.0	117	128	0.64
9	Heat transfer vapor structure	10.0	82	200	1.00
10	Friction liquid structure	10.0	122	140	0.70
Experimental Values			98	170	0.85

The kinetic energy changed from the base case by factors lying between 0.64 and 1.09. The use of a heat transfer multiplier of five (Run 7) produced the best agreement with the experimental data. Variation of the coefficient in the Nusselt number relation for the heat transfer between the vapor and structure did not have any effect. Thus the structure-side heat transfer coefficient sets an upper limit to the vapor-side heat transfer in SIMMER. Variations of other

parameters, such as liquid coalescence, liquid droplet size distribution, maximum droplet size, and Weber number had minor effects on pressure and piston movement.

6. Calculation With a Fixed Set of Input Parameters. Because of the deficiencies in the modeling of flashing processes, flow regimes, and heat transfer in SIMMER, a fixed set of input parameters cannot produce correct results for different experiments. Thus, different initial pressures and temperatures, liquid inventories, or different fluids require different parameter sets. Rather than adjust each parameter for all of the tests and look at the variance of the parameters, we tried to find a parameter set that results in the least overall deviation in the pressures and piston energies of the most important tests. Except for test 42, these were the same tests as used for the study of the reduction of kinetic energy. A parameter set that produced good results for tests 13 and 17 was used as the starting point. The complete input file (run 17-14) is listed in Appendix B.

TABLE XV

INPUT PARAMETERS

PARAMETER	RUN 1	RUN 2	RUN 3
r_{pmin}, core (m)	5×10^{-5}	5×10^{-5}	1×10^{-4}
r_{pmax}, lower space (m)	1×10^{-5}	1×10^{-5}	3×10^{-4}
Friction factor multiplier, core	2	2	1×10^{1}
Heat transfer multiplier, UCS	1	0.5	0.5
Pin mass	1	1	0.5
Structure-side heat transfer Coefficient in piston track	1.2×10^{4}	0.6×10^{4}	0.6×10^{4}

Three series of runs have been performed; the parameters varied are listed in Table XV. The results are shown in Table XVI in terms of the ratio E_s/E, E being the kinetic energy of the piston from the experiments and E_s being the energy calculated by SIMMER. The corresponding pressure plots are shown in Fig. 81a-81g.

TABLE XVI

VARIATION OF PISTON KINETIC ENERGY RATIO

Test	RUN 1	RUN 2	RUN 3
13	0.97	1.22	1.16
17	1.15	1.50	1.51
15	1.00	1.22	1.27
18	0.87	1.19	1.30
16	0.74	0.91	0.92
39	0.72	0.80	0.84
43	0.59	0.81	0.76
44	0.77	1.16	1.15
12	1.25	2.40	1.86
21	0.85	1.00	1.11
22	0.73	0.62	0.93
25	0.66	0.89	0.79
26	0.48	0.53	0.49

The average deviation was not improved when we changed the parameters. For the propanol test series 13 through 18, the first parameter set gave the least deviation, the maximum being -26% (test 16). If we exclude tests 25 and 26, which were run with the seven-hole UCS and test 12 which was run with only propanol vapor, the maximum deviations in series 1 were +15%, -41%. They are somewhat higher for the other two series. The least deviation for all 13 tests was also obtained in series 1, (+25% and -52%). Thus, although we could not improve all of the calculated results by changing parameters, for certain tests the agreement with the experimental results was better. A more detailed study of these results, including the pressures, and more calculations would reveal the way that droplet sizes and heat transfer characteristics should be adjusted as a function of the initial conditions and fluids.

Regarding the pressure plots, three measured pressure traces are generally shown (p_2, p_3 and p_6), together with the calculated pressures at all six measuring stations. In test 39 the pressure in the upper part of the piston track is also shown (p_9).

There seems to be a discrepancy in some cases between the calculated pressure at the exit of the UCS compared with the measured one and the kinetic energy of the piston. In run 21-3, for instance, the calculated pressure was below the measured pressure, but the calculated piston energy was above the experimental piston energy. It should, however, be noted that condensation

occurred in the piston track, so this was probably modeled incorrectly. The mass of the wall in the piston track could not be modeled correctly, and therefore the heat transfer coefficient was set to a small number.

The sudden drop in pressure in tests 21, 22, 15, 18, and 44 is probably due to the absence of liquid at these times. Figure 82a shows the fraction of liquid and the liquid velocities for runs 21-2 and 44-2, and Fig. 82b shows the temperatures of the liquid and can walls. At the time the liquid volume fraction reaches zero, the wall temperature remains constant and the liquid and vapor temperatures decrease sharply, which in turn decreases the pressure. (The constant pressure at the end of runs 18-1 and 18-2 is due to an input error regarding the plot data output.) This indicates that the liquid is leaving the core and the UCS too quickly. The comparison of the velocities as they were observed in test 44 with the calculated velocities indicates somewhat higher velocities in the calculation (see Table V), but the differences are small. However, no liquid was observed at the exit of the UCS up to 32 ms, while SIMMER calculates a gradual increase of the liquid volume fraction in node 31, starting at 5 ms. The discrepancies in the pressure histories make improved modeling in SIMMER desirable, while the maximum deviation of the piston energy by a factor of approximately two seems tolerable.

7. Tests With Vapor Below Liquid in the Core. Calculations were performed for the test series in which the vapor was below the liquid in the core (tests 34-38). The input parameters were the same as in the previous test series (series 1), as shown in the input file in Appendix B, except for some parameters for the core and lower space. These parameters are listed in Table XVII.

TABLE XVII

INPUT PARAMETERS FOR TESTS 34-38

Parameter	Vapor Core	Liquid Core	Vapor Space	Lower Space
Node	1 - 5	6 - 11	12	13 - 17
Maximum droplet radius ($x10^{-4}$m)	500	500	50	50
Minimum droplet radius ($x10^{-4}$m)	50	1(500)	0.5(50)	50
Friction factor multiplier	1(10)	10	2(10)	2
Heat transfer multiplier	1(10)	10	2(10)	2

Each test was run twice. The parameters changed for the second run are shown in parentheses in Table XVII.

Figure 83 a-e shows the calculated pressures, liquid volume fractions and liquid velocities of the two runs. The results regarding the piston movement are listed in Table XVIII.

TABLE XVIII

PISTON IMPACT TIME AND KINETIC ENERGY

	Experiment		Run 1			Run 2		
Test	t	E	t	E_s	E/E_s	t	E_s	E/E_s
34	96	64	98	81	1.27	76	117	1.83
35	80	122	105	124	1.02	84	135	1.11
36	65	196	98	115	0.59	90	102	0.52
37	71	181	119	115	0.64	120	106	0.59
38	97	172	87	199	1.16	93	187	1.09

The calculated results agree reasonably well with the experimental data for test 34 (helium pressure only) and test 38 (vapor pressure only). The agreement for the other tests is rather poor. SIMMER does not reproduce the early pressure rise in the UCS as was measured in tests 35 through 37. The liquid velocities at the exit of the UCS are always too low (compare with Table V). The decrease of the piston impact time to a minimum for test 36 and the corresponding maximum of the piston energy are not calculated by SIMMER.

The changed input parameters for run 2 do not improve the overall picture. Other changes in the input data and the modeling were tested, including calculations with two radial nodes and a modification of the model for two-phase momentum exchange.* No substantial improvement of the calculated results was achieved by any of these modifications. A more thorough study of these tests is necessary. Again, the agreement between experiment and calculation is rather poor for the pressure histories and other transient properties, while the piston kinetic energy is 50% to low.

*Supplied by J. F. Dearing, Q-7, Los Alamos National Laboratory, unpublished data.

IV. SUMMARY AND CONCLUSIONS

A series of experiments has been completed that simulates the flow dynamics in the SNR Upper Core Structure (UCS) postulated to occur during the expansion phase of an LMFBR core-disruptive accident. The experiments were designed to verify some of the thermal-hydraulics models in SIMMER-II. Four different liquids were used to simulate the flashing UO_2 and numerous parameter variations were made regarding initial pressure, temperature, and configurations of the test apparatus.

The experimental data consist of pressure histories at up to seven locations along the test section, the piston velocity, and for some tests, high-speed motion pictures of the flow entering and leaving the UCS. The analysis of the film provides a rough estimate of the liquid/vapor fractions, the fluid velocities, and an upper limit of the liquid droplet size.

The experiments showed the large effect of the heat transfer in the UCS and the relatively small effect of friction. The reduction in final kinetic energy by the presence of the UCS is a function of the initial pressure and the temperature difference between core and UCS. Kinetic energy reduction factors of up to 16 have been determined.

Calculations with SIMMER-II have been performed for most of the tests. With proper tuning of the input parameters, SIMMER can reproduce correct results for all experiments except for those where a mixture of vapor and noncondensible gas is below the liquid initially in the core. No single set of the crucial input parameters can, however, produce correct results for all of the experiments. The use of such a fixed set for different experiments results in deviations by factors up to two in the kinetic energy of the piston, compared with the experimental results.

Three major modeling deficiencies have been identified:

- the flashing process and the associated droplet size distributions;
- the distinction between flow regimes, in particular, the lack of liquid films on the structure; and
- the transient heat conduction in the structure.

Because of these model deficiencies, the application of the input parameters from the present experiments to the prototypic case is questionable. A calculation of a case with prototypic materials and scaled pressure, temperature, and geometry should be compared with a corresponding simulant experiment.

More calculations for the present series of experiments would probably yield better insight as to how the input parameters have to be changed as a function of fluid properties, inventory, and initial pressure and temperatures. This might render the application to the prototypic case justifiable. Preference should be given to the implementation of new models in SIMMER, which could be tested with the present experimental data. In that case, perhaps a few additional experiments would be useful with measurements of the structure temperature at different distances from the surface and with a better determination of the flow regime.

Acknowledgement

The USD experimental program for SNR typical geometry was funded by the Kernforschungszentrum Karlsruhe (KfK) and performed at the Los Alamos National Laboratory (LANL). The author acknowledges the assistance of the following LANL personnel: R. Rochester and G. Gray, Group WX-7, for their help with the explosives; R. Baca and E. Montoya, Group Q8, for their help in the fabrication of experimental hardware; A.Salazar, Group WX-10, for the digitiza tion of the data; P. Blewett, E.J. Chapyak (Q8) and W. Bohl (Q7) for their assistance in the handling of the SIMMER-code; and L. Hull (Q8), for reviewing this report.

REFERENCES

1. D. Wilhelm, V. S. Starkovich and E. J. Chapyak, "A Simulant-Material Investigation of Flow Dynamics in the CRBR Upper Core Structure," Los Alamos National Laboratory report LA-9478-MS, NUREG/CR-2866 (September 1982).

2. L. L. Smith, "SIMMER-II, A Computer Program for LMFBR Disrupted Core Analysis," Los Alamos National Laboratory report LA-7515-M, NUREG/CR-0453 (October 1978).

3. E. J. Chapyak and V. S. Starkovich, "The Role of Similitude in the Design of LMFBR Safety-Related Simulation Experiments," International Meeting on Fast Reactor Safety Technology, Seattle, Washington, USA, (1979).

4. C. R. Bell, R. D. Burns, and L. B. Luck, "Impact of SIMMER-II Model Uncertainties on Predicted Postdisassembly Dynamics," Los Alamos National Laboratory report LA-8053-MS (October 1979).

5. M. G. Stevenson, Compiler, "Nuclear Reactor Safety, October 1 - December 31, 1981," Los Alamos National Laboratory report LA-9305-PR, NUREG/CR-2281, Vol. 4 (May 1982), pp. 29-38.

6. M. G. Stevenson, Compiler, "Nuclear Reactor Safety, January 1 - March 31, 1982," Los Alamos National Laboratory report LA-9442-PR, NUREG/CR-2814, Vol. 1 (August 1982), pp. 17-23.

7. M. G. Stevenson, Compiler, "Nuclear Reactor Safety, April 1 - June 30, 1982," Los Alamos National Laboratory report LA-9556-PR, NUREG/CR-2814, Vol. 2 (December 1982).

8. M. G. Stevenson, Compiler, "Nuclear Reactor Safety, July 1 - October 31, 1982," Los Alamos National Laboratory report LA-9649-PR, NUREG/CR-2814, Vol. 3 (April 1983), pp. 19-22.

9. N. N. Sheheen and M. G. Stevenson, Compilers, "Nuclear Reactor Safety, October 1 - December 31, 1982," Los Alamos National Laboratory report LA-9740-PR, NUREG/CR-2814 (July 1983).

10. M. G. Stevenson, Compiler, "Nuclear Reactor Safety, April 1 - June 30, 1983," Los Alamos National Laboratory report (in preparation). (1983).

11. A. Benemann, "Cavitation Problems in Mixing Devices of SNR-300 Fuel Elements," IAEA International Working Group on Fast Reactors, Specialists Meeting on Cavitation in Sodium and Studies of Analogy with Water as Comparred to Sodium, Cadarache, France, April 12 - 16, 1976.

12. N. B. Vargaftik, Tables on the Thermophysical Properties of Liquids and Gases, Hemisphere Public Corp., Washington, D.C., (1975).

13. R. W. Gallant, "Physical Properties of Hydrocarbons," Hydrocarbon Processing 46 (4), 183-196 (April 1967).

14. A. J. Kubicek and P. T. Eubank, "Thermodynamic Properties of n-Propanol," J. of Chem. and Eng. Data 17 (2), 232-235 (1972).

15. C. L. Yaws and J. R. Hopper, "Methanol, Ethanol, Propanol and Butanol," Chem. Eng. 119-127 (June 7, 1976).

TABLE I GEOMETRICAL DATA OF TEST SECTION

Section	Length (mm)	Hydraulic Diameter (mm)	Void Volume (cm^3)	Volume Fraction α Void	α Aluminum	α Steel	Aluminum Surface Area per Unit Volume (m^{-1})	Steel Surface Area per Unit Volume (m^{-1})
Core 1	374	41	865	0.90	–	0.10	–	83
Lower Space	82	48	186	0.88	0.12	–	60	–
Pin Bundle	172	2	115	0.26	0.42	0.32	57	496
Middle Space	12	44	18	0.59	0.41	57	–	
Mixing Head	82	9.2	67	0.32	0.68	–	94	–
Upper Space	127.3	40	190	0.52	0.48	–	50	–
Core 2	176	41	365	0.81	–	0.19	–	83
Core 3 4, Vapor Core	130	41	260	0.78	–	0.22	–	83
Core 3 Liquid Core	280	41	560	0.78	–	0.22	–	83
Core 4 Liquid Core	166	41	340	0.80	–	0.20	–	83
Lower Space (F, F2)	142	48	304	0.83	0.17	–	63	–
Upper Space (F2)	182	40	278	0.59	0.41	–	54	–
7-Hole Test Section	494	12.7	438	0.35	0.65	–	109	–
Lower Space for 7-H-T	34	48	60	0.68	0.32	–	60	–

TABLE II TEST MATRIX

FLUID		PRESS.	TEMP.	CORE 1	CORE 2				CORE 3	CORE 4	
LIQUID	GAS	(MPa)	(°C)			UCS C	NPT UCS C/H	UCS-7-H	VBL	VBL F2	VAL F2
	HELIUM	1.25	20	5	20						
			180	6	11						
	PROPANOL VAPOR	1.25	185	7							
		1.12	180		12						
PROPANOL	VAPOR	0.56	150		15	18,19	23[H]	25	31[F]	38	39,42[MPB]
		1.12	180	8	13	17	24[C]		28[VAL],29		
		1.80	200		16						
PROPANOL	VAPOR + HELIUM	0.56	20						27	34	
			80							35	
			100							36	
			130							37	
		1.12	150						32[F]		
			170	1-4, 9	14					33[F]	
ETHYLENE GLYCOL	VAPOR	0.42	250						30	40	
		0.56	260	10	21	22		26			
ETHYLENE GLYCOL	VAPOR + HELIUM	0.42	180							41	
METHANOL	VAPOR	0.97	137								43
HEPTANE	VAPOR	0.35	147								44

NPT NO PISTON TRACK
NPB NO PIN BUNDLE IN UCS
7-H 7-HOLE UCS
C UCS COOLED
H UCS HEATED

VBL VAPOR BELOW LIQUID IN CORE
VAL VAPOR ABOVE LIQUID IN CORE
F FILM TAKEN AT UCS ENTRANCE
F2 FILM TAKEN AT UCS ENTRANCE AND EXIT

TABLE III INITIAL CONDITIONS OF TESTS

Test No.	Core No.	Core Volume [cm^3]	Liquid Volume In Core [cm^3]	Vapor Pressure In Core [MPa]	Helium Pressure In Core [MPa]	Core Temperature [K]	Helium Pressure In UCS [Pa]	Temperature In UCS [K] T_2	T_4	T_6
1-1	1	865	377 P	0.980	0.132	447	2500	309	301	296
2-1	1	865	637 P	0.871	0.240	442	2500	308	300	295
3-1	1	430	228 P	0.957	0.041	446	2500	306	298	293
4-1	1	430	344 P	0.906	0.206	444	2500	305	297	292
5-1	1	630	-	-	1.250	289	20	289	289	289
5-2	1	630	-	-	1.250	290	20	290	290	290
6-1	1	630	-	-	1.250	463	20	303	295	290
6-2	1	630	-	-	1.250	463	20	305	297	292
6-3	1	630	-	-	1.112	456	20	305	297	292
7-1	1	630	0 P	1.250	-	458	20	303	295	290
7-2	1	630	4 P	1.250	-	458	20	317	309	303
8-2	1	865	235 P	1.112	-	453	20	311	302	296
9-1	1	865	235 P	0.987	0.125	447	2500	310	302	297
10-1	1	865	235 E	0.561	-	537	20	332	318	308
11-1	2	365	-	-	1.112	451	20	320	309	303
11-2	2	365	-	-	1.112	456	20	318	308	301
12-1	2	365	7 P	1.112	-	453	20	332	318	309
12-2	2	365	21 P	1.112	-	453	20	331	320	310
12-3	2	365	14 P	1.112	-	453	25	335	323	313
13-1	2	365	317 P	1.112	-	453	20	331	321	312
13-2	2	365	341 P	1.112	-	453	20	330	319	310
13-3	2	365	334 P	1.112	-	453	20	336	325	315
14-1	2	365	313 P	0.982	0.130	447	20	334	324	315
14-2	2	365	330 P	1.012	0.100	448	2500	332	322	313
15-1	2	365	302 P	0.561	-	425	20	323	314	307
15-2	2	365	314 P	0.561	-	425	2500	315	305	299
16-1	2	365	330 P	1.702	0.100	472	2500	337	326	316
16-2	2	365	330 P	1.802	-	475	2500	321	309	300
17-1	2	365	334 P	1.112	-	453	20	260	254	252
18-1	2	365	330 P	0.561	-	425	20	240	235	232
19-2	2	365	330 P	0.561	-	425	2500	258	251	248
20-1	2	365	-	-	1.112	295	20	295	295	295
20-2	2	365	-	-	1.112	296	20	296	296	296

TABLE III cont.

INITIAL CONDITIONS OF TESTS

Test No.	Core No.	Core Volume [cm^3]	Liquid Volume In Core [cm^3]		Vapor Pressure In Core [MPa]	Helium Pressure In Core [MPa]	Core Temperature [K]	Helium Pressure In UCS [Pa]	Temperature In UCS [K] T_2	T_3	T_4	
21-3	2	365	330	E	0.526	-	531	2500	341	326	311	
22-1	2	365	330	E	0.561	-	535	2500	293	278	271	
23-1	2	365	334	P	1.112	-	453	20	410	407	401	NPT
24-1	2	365	334	P	1.112	-	453	20	261	244	231	NPT
25-1	2	365	334	P	1.112	-	453	20	317	305	298	7-H
26-2	2	365	318	E	0.431	0.095	523	20	334	316	305	7-H
26-3	2	365	318	E	0.431	0.095	523	20	334	316	305	7-H
27-1	3	820	500	P	0.002	0.629	290	20	290	290	290	VBL
27-1	3	820	500	P	0.002	0.698	293	20	293	293	293	VBL
27-3	3	820	480	P	0.002	0.664	293	20	293	293	293	VBL
28-1	3	820	500	P	1.112	-	453	2500	320	311	304	
28-2	3	820	500	P	1.112	-	453	2500	321	312	305	
28-3	3	820	500	P	1.112	-	453	2500	320	311	304	
29-1	3	820	500	P	1.112	-	453	2500	324	315	307	VBL
29-2	3	820	500	P	1.112	-	453	2500	331	320	310	VBL
29-3	3	820	520	P	1.112	-	453	2500	328	323	308	VBL
30-1	3	820	510	E	0.423	-	523	2500	354	334	317	VBL*
31-1	3	820	500	P	0.560	-	424	2500	303	299	298	VBL/F*
31-2	3	820	500	P	0.595	-	426	2500	305	301	298	VBL/F
32-1	3	820	490	P	0.556	0.556	424	2500	306	303	300	VBL/F
33-1	4	600	280	P	0.838	0.274	441	2500	312	311	304	VBL/F
34-1	4	600	280	P	0.002	0.524	294	2500	294	294	294	VBL/F2
35-1	4	600	281	P	0.061	0.557	354	2500	298	297	296	VBL
35-2	4	600	278	P	0.040	0.450	343	2500	298	297	296	VBL
35-3	4	600	281	P	0.053	0.473	350	2500	298	298	297	VBL/F2*
36-1	4	600	282	P	0.175	0.351	384	2500	306	304	302	VBL/F2*
37-1	4	600	285	P	0.328	0.198	405	2500	308	305	302	VBL/F2*
38-1	4	600	283	P	0.526	-	422	2500	309	305	303	VBL/F2*
39-1	4	600	283	P	0.526	-	422	2500	312	308	306	F2*

TABLE III cont.

INITIAL CONDITIONS OF TESTS

Test No.	Core No.	Core Volume [cm^3]	Liquid Volume In Core [cm^3]		Vapor Pressure In Core [MPa]	Helium Pressure In Core [MPa]	Core Temperature [K]	Helium Pressure In UCS [Pa]	Temperature In UCS [K] T_2	T_4	T_6	
40-1	4	600	278	E	0.423	-	523	2500	328	322	318	VBL/F2*
41-1	4	600	272	E	0.066	0.357	458	2500	317	313	309	VBL/F2*
42-1	4	600	289	P	0.526	-	422	2500	312	307	304	NPB/F2
43-1	4	600	471	M	0.974	-	410	2500	308	305	303	F2
43-2	4	600	471	M	0.974	-	410	2500	311	310	309	
43-3	4	600	471	M	0.974	-	410	2500	313	305	300	
44-1	4	600	484	H	0.354	-	420	2500	307	304	302	F2
F-1	2	365	300	P	0.390	-	411	-	-	416	-	

P Propanol
E Ethylene Glycol
M Methanol
H Heptane

NPT No Piston Track
NPB No Pin Bundle
VBL Vapor Below Liquid
7-H 7-Hole UCS

F Film taken below UCS
F2 Film taken below and above UCS
* One half of rupture disk closed

TABLE IV PISTON FLIGHT DATA

Test	t1 (ms)	t2 (ms)	t3 (ms)	t4 (ms)	v (m/s)	Ekin (J)	
1 - 1	26.5	52.4	67.3	76.3	34.4	166	*#
2 - 1	24.8	40.0	48.0	54.1	48.0	322	#
3 - 1	31.7	50.9	60.9	68.5	38.5	266	
4 - 1	51.8	66.7	75.0	81.4	45.4	368	
5 - 1	12.2	22.3	27.9	32.2	67.3	812	
5 - 2	12.2	22.3	27.9	32.2	67.3	812	
6 - 1	12.3	23.9	29.9	34.5	64.4	742	
6 - 2	12.3	23.9	29.9	34.5	64.4	742	
6 - 3	14.8	26.4	33.0	38.2	56.6	572	
7 - 1	15.6	28.1	35.2	40.8	52.6	495	
7 - 2	15.1	26.8	33.2	38.1	59.2	628	
8 - 2	34.3	58.2	71.5	81.8	28.3	143	
9 - 1	22.5	40.0	50.5	58.9	34.7	215	
10 - 1	63.0	118.5	142.5	160.3	16.7	50	
11 - 1	17.8	32.2	40.5	47.0	44.7	358	
11 - 2	17.5	31.1	39.1	45.4	46.0	378	
12 - 1	38.5	65.8	83.2	97.4	20.2	73	
12 - 2	36.4	65.0	82.1	95.7	21.3	81	
12 - 3	27.1	45.9	61.2	76.2	17.7	56	
13 - 1	31.8	50.0	59.6	67.0	40.0	286	
13 - 2	32.9	50.0	58.8	65.5	44.0	346	
13 - 3	32.3	48.8	57.6	64.4	43.5	338	
14 - 1	28.2	45.5	54.7	61.8	41.6	310	
14 - 2	32.8	48.8	57.7	64.6	42.3	32p	
15 - 2	52.3	76.4	90.0	100.6	27.5	136	
16 - 1	25.0	37.9	44.8	50.1	55.4	549	
16 - 2	28.3	41.9	49.1	54.6	53.2	508	
17 - 1	53.6	76.5	88.8	98.3	31.0	172	
18 - 1	74.1	108.2	126.7	141.0	20.6	76	
19 - 2	66.6	99.3	116.3	129.3	22.3	92	
20 - 1	16.2	28.8	35.8	41.2	53.8	519	
20 - 2	15.8	28.0	34.9	40.3	54.2	526	
21 - 3	74.0	112.1	132.7	148.6	18.5	61	
22 - 1	84.9	130.0	155.0	174.4	15.1	41	
25 - 1	15.3	25.9	31.9	36.6	62.3	696	
26 - 2	24.3	41.8	52.0	60.0	36.2	235	
26 - 3	24.3	41.8	52.0	60.0	36.2	235	
27 - 1	28.8	51.7	66.5	78.7	23.6	99	
27 - 2	28.0	50.0	63.5	74.4	26.7	127	
27 - 3	27.1	47.5	59.8	69.6	29.5	156	
28 - 1	27.5	42.5	51.0	57.6	44.0	346	
28 - 2	30.2	45.7	53.9	60.2	46.8	392	
28 - 3	31.8	47.8	55.7	61.7	49.6	440	
29 - 1	31.8	46.0	53.3	58.9	53.0	503	
29 - 2	30.9	44.9	52.2	57.8	52.8	499	
29 - 3	31.1	45.1	52.2	57.6	54.7	536	
30 - 1	70.6	112.5	132.2	146.9	20.1	72	
31 - 1	53.6	75.2	86.4	94.9	34.5	213	
31 - 2	45.0	66.5	77.4	85.7	35.6	227	
32 - 1	17.7	30.4	37.7	43.4	50.9	464	
33 - 1	21.0	36.0	44.3	50.7	45.5	370	
34 - 1	35.0	63.0	81.2	96.4	18.9	64	
35 - 1	27.8	48.9	61.9	72.4	27.6	137	
35 - 2	29.0	50.0	63.7	75.0	25.3	114	
35 - 3	30.8	54.8	68.9	80.0	26.1	122	
36 - 1	26.5	45.3	56.4	65.2	33.1	196	
37 - 1	29.0	50.0	61.8	71.0	31.8	181	
38 - 1	52.7	75.5	87.7	97.3	31.0	172	
39 - 1	51.5	73.1	84.7	93.6	32.9	194	
40 - 1	77.7	122.4	144.2	160.6	18.0	58	
41 - 1	34.8	62.8	79.9	93.6	21.0	80	
42 - 1	22.8	37.0	44.9	51.0	47.7	407	
43 - 1	32.0	47.5	55.7	62.0	46.8	392	
43 - 2	33.2	50.8	59.9	66.8	42.4	323	
43 - 3	30.7	46.6	55.0	61.4	45.7	373	
44 - 1	56.9	86.5	101.8	113.5	25.3	114	

z1 = 0.2132 m
z2 = 0.6196 m
z3 = 0.9244 m
z4 = 1.2000 m
piston mass = 0.36 kg

* old piston track
z1 = 0.1300 m
z2 = 0.5250 m
z3 = 0.9150 m
z4 = 1.2000 m

\# piston mass = 0.28 kg

TABLE V DATA FROM OPTICAL OBSERVATION

TEST	FLUID	PRESS. (MPa)	TEMP. (°C)	P-HE (%)	P-VAP (%)	VAP. IN UPP. SP. (ms)	LIQ. IN UPP. SP. (ms)	PISTON IMPACT (ms)	APPROXIMATE VELOCITY IN LOWER SPACE (m /s)	APPROXIMATE VELOCITY IN UPPER SPACE (m /s)
34 B	PROPANOL	.526	21	100	0	26	52	96	30 → 0	9 → 14
35 B	PROPANOL	.526	77	90	10	23	45	80	30	12 → 20
36 B	PROPANOL	.526	111	67	33	16	40	65	110 → 30	30
37 B	PROPANOL	.526	132	38	62	18	35	71	110 → 30	18 → 25
38 B	PROPANOL	.526	150	0	100	14	23	97		35 → 60
39 A	PROPANOL	.526	150	0	100	13	21	94	30 → 10	35 → 60
42 A°	PROPANOL	.526	150	0	100	7	12	51	30 → 10	30
40 B	ETHY.GL.	.423	250	0	100	–	44	160	100 → 10	10
41 B	ETHY.GL.	.423	185	84	16	15	60	94	30 → 10	15
43 A	METHANOL	.974	137	0	100	6	16	62	10 → 10	30
44 A	HEPTANE	.354	147	0	100	–	32	113	10	15

A VAPOR ABOVE LIQUID IN CORE
B VAPOR BELOW LIQUID IN CORE
° UCS WITHOUT PIN BUNDLE

TABLE VI

PROPERTIES USED AS INPUT FOR SIMMER

		Helium	Propanol	Methanol	Ethylene Glycol	Heptane
		H_2	C_3H_8O	C_3H_3OH	$C_2H_4(OH)_2$	C_7H_{16}
ρ_{sol}	$kg\ m^{-3}$	125	800	887	1140	773
C_{vsol}	$Jkg^{-1}K^{-1}$	125	1800	2300	2100	2000
T_{melt}	K	1.0	147	175	260.2	182.56
$h_{fus}\ 10^3$	$J\ kg^{-1}$	25.8	86.5	100.4	181	
λ_{sol}	$Wm^{-1}K^{-1}$	0.026	0.176	0.181	0.200	0.156
ρ_{liq}	kgm^{-3}	125	628	668	912	563
C_{vliq}	$J\ kg^{-1}K^{-1}$	125	5120	3770	3430	2820
λ_{liq}	$W\ m^{-1}K^{-1}$	0.026	0.129	0.174	0.10	0.098
$\sigma_{liq}10^3$	$N\ m^{-1}$	77.7	10.6	11.8	27.0	8.28
$\eta_{liq}\ 10^3$	Pa s	0.018	0.148	0.141	0.15	0.140
$P^*\ 10^{-10}$	-	0.0002	3.62412	5.16413	23.1488	0.589765
$T^*\ 10^{-3}$	-	0.001375	4.7027	4.45489	6.904	4.08593
$h^*\ 10^{-6}$	Jkg^{-1}	0.029	1.0602	1.65781	1.41726	0.48825
T_{crit}	K	5	536.8	513	647	549
	-	0.3305	0.3713	0.37067	0.41102	0.3798
C_{vvap}	$Jkg^{-1}K^{-1}$	3197.85	1806.33	1410	1884	2107
γ	-	1.65	1.043	1.184	1.043	1.0394
d_{Atom}	A	2.56	4.549	3.626	5.13	6.1
$e_{crit}10^{-6}$	$J\ kg^{-1}$	-	1.287	-	3.52	-
M	kg/Mol	4	60.0	32.043	62.069	100.198
ε/k	K	10.02	577.0	481.8	378	500
ρ_{crit}	$kg\ m^{-3}$	-	275	275	333	235
ρ_{satvap}	$kg\ m^{-3}$	-	76.92	74.4	60.88	-

TABLE VII

PROPERTIES OF SATURATED LIQUID PROPANOL

T	ρ	C_p	λ	$\sigma\ 10^3$	$\eta\ 10^3$
^oC	kg m^{-3}	$Jkg^{-1}K^{-1}$	$W\ m^{-1}K^{-1}$	$N\ m^{-1}$	Pa s
0	819.3	2243	0.156	25.4	3.85
20	803.5	2375	0.153	23.9	2.20
40	787.5	2533	0.150	22.5	1.38
60	770.0	2750	0.148	20.7	0.920
80	752.0	2952	0.146	19.0	0.630
100	732.5	3200	0.144	17.3	0.447
120	711.0	3510	0.141	15.8	0.337
140	687.5	3944	0.138	14.2	0.250
160	660.0	4414	0.134	12.5	0.188
180	628.5	5123	0.129	10.6	0.148
200	592.0	5862	0.122	8.6	0.119

TABLE VIII

PROPERTIES OF SATURATED LIQUID ETHYLENE GLYCOL

T	ρ	C_p	λ	$\sigma\ 10^3$	$\eta\ 10^3$
^oC	kg m^{-3}	$Jkg^{-1}K^{-1}$	$W\ m^{-1}K^{-1}$	$N\ m^{-1}$	Pa s
0	1130	2294	0.301	50.3	65.1
20	1116	2382	0.285	48.4	21.4
40	1101	2445	0.273	46.7	9.58
60	1087	2537	0.258	44.9	5.17
80	1077	2629	0.243	43.1	3.22
100	1058	2721	0.228	41.3	2.15
120	1040	2822	0.213	39.5	1.5
140	1022	2923	0.198	37.7	1.11
160	1005	3015	0.183	35.9	0.84
180	988	3098	0.167	34.2	0.67
200	975	3182		32.4	
220	955	(3265)			
240	934	(3350)			
260	912	(3430)			
374	333				

TABLE IX

PROPERTIES OF SATURATED LIQUID METHANOL

T	ρ	C_p	λ	$\sigma\ 10^3$	$\eta\ 10^3$
^oC	kg m^{-3}	$Jkg^{-1}K^{-1}$	$W\ m^{-1}K^{-1}$	$N\ m^{-1}$	Pa s
0	810.0	2420	0.210	24.5	0.817
20	791.5	2460	0.203	22.6	0.578
40	774.0	2520	0.196	20.9	0.446
60	755.5	2900	0.190	19.3	0.346
80	735.5	3070	0.185	17.5	0.271
100	714.0	3300	0.181	15.7	0.214
120	690.0	3580	0.177	13.6	0.170
140	664.0	3810	0.174	11.5	0.136
160	634.0	4180	0.171	9.3	0.109

TABLE X

PROPERTIES OF SATURATED LIQUID n-HEPTANE

T	ρ	C_p	λ	$\sigma\ 10^3$	$\eta\ 10^3$
°C	kg m^{-3}	$Jkg^{-1}K^{-1}$	$W\ m^{-1}K^{-1}$	$N\ m^{-1}$	Pa s
0	700.5	2160	0.134		0.526
20	683.6	2226	0.129	20.86	0.414
40	666.5	2301	0.123	18.47	0.338
60	649.1	2390	0.118	16.39	0.281
80	631.1	2470	0.113	14.35	0.239
100	612.4	2570	0.108	12.47	0.198
120	592.6	2670	0.104	10.63	0.167
140	571.1	2780	0.100	8.87	0.143
160	548.1	2890	0.096	7.19	0.122
266	234.1				0.027

TABLE XI

VARIABLE LIQUID DENSITY

	A_1	A_2	A_3	B_1	B_2
Propanol	1064.07	-0.8862	0.0	2.5904	0.3759
Methanol	994.561	-0.4960	$-6.667\ 10^{-4}$	2.5503	0.36047
Ethylene Glycol	1242.37	-0.1800	$-8.39\ 10^{-4}$	2.7263	0.2719
Heptane	878.43	-0.4825	$-6.2\ 10^{-4}$	2.6771	0.4492

$T \leq 2/3\ T_{crit}$: $\rho = A_1 + A_2\ T + A_3\ T^2$

$T > 2/3\ T_{crit}$: $\rho = \rho_{crit}\ [1 + B_1(1 - T/T_{crit})^{B_2}]$

$B_3 = 0$

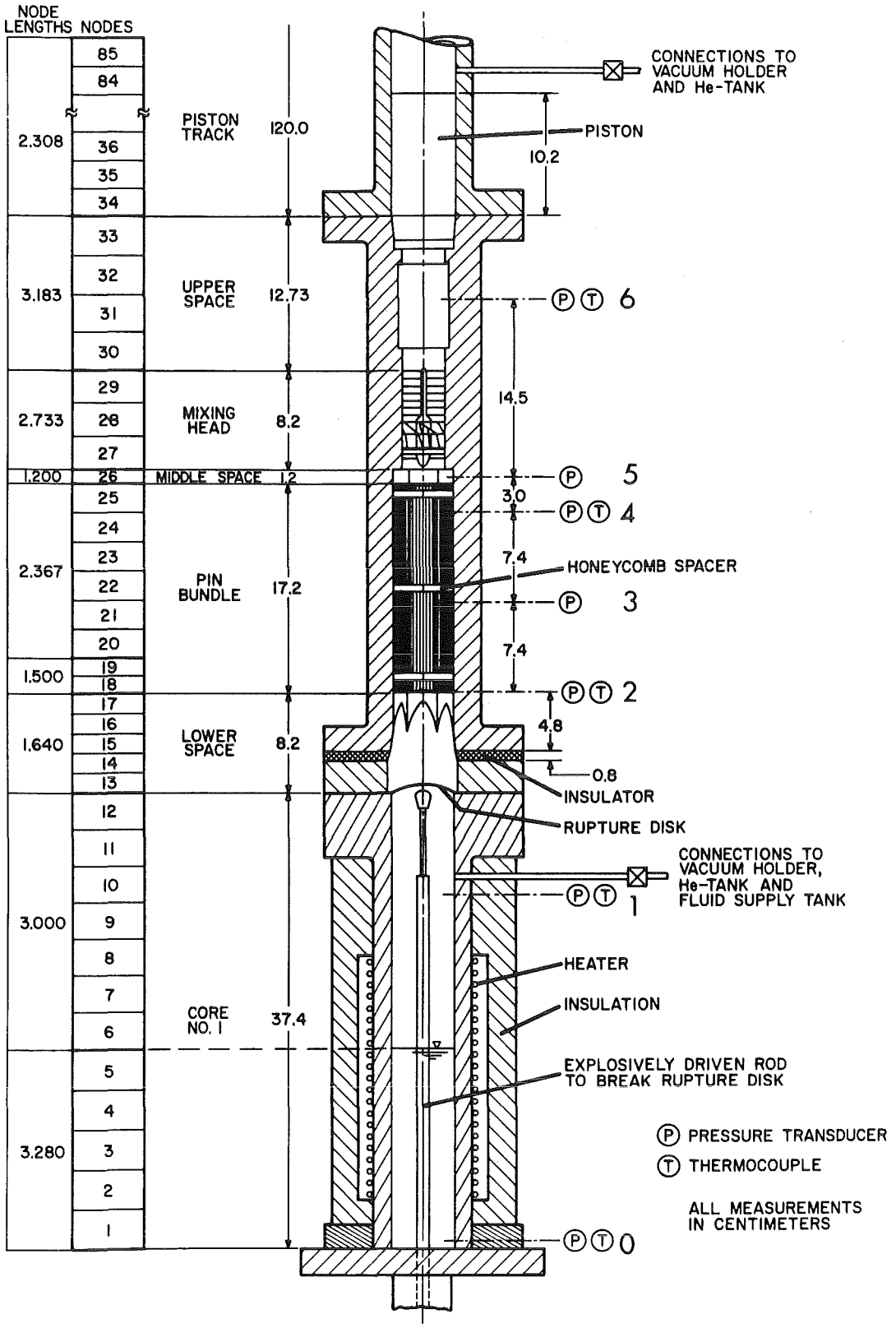

Fig. 1. Schematic of experimental apparatus.

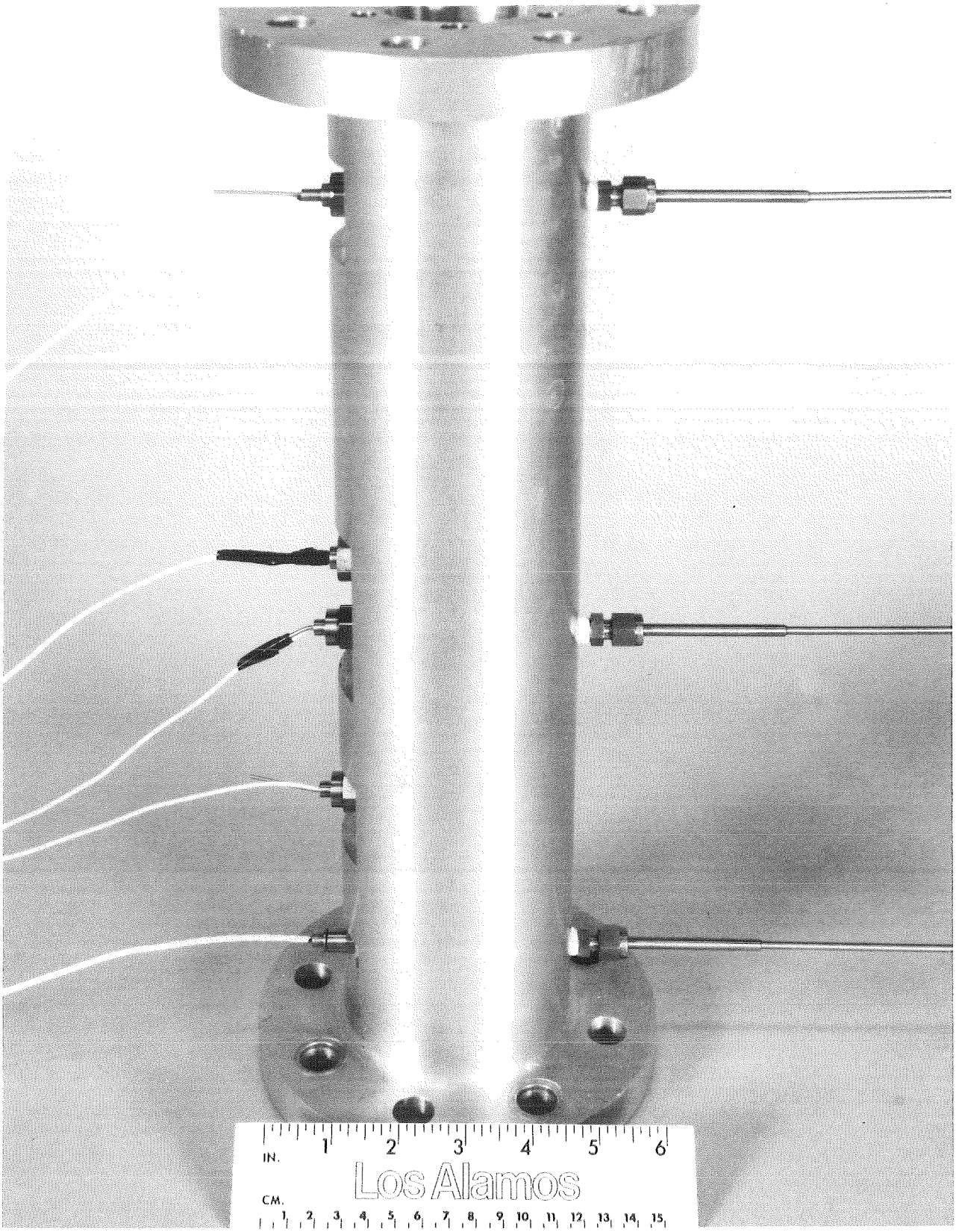

Fig. 2: UCS-test section

Fig. 3: Pin bundle

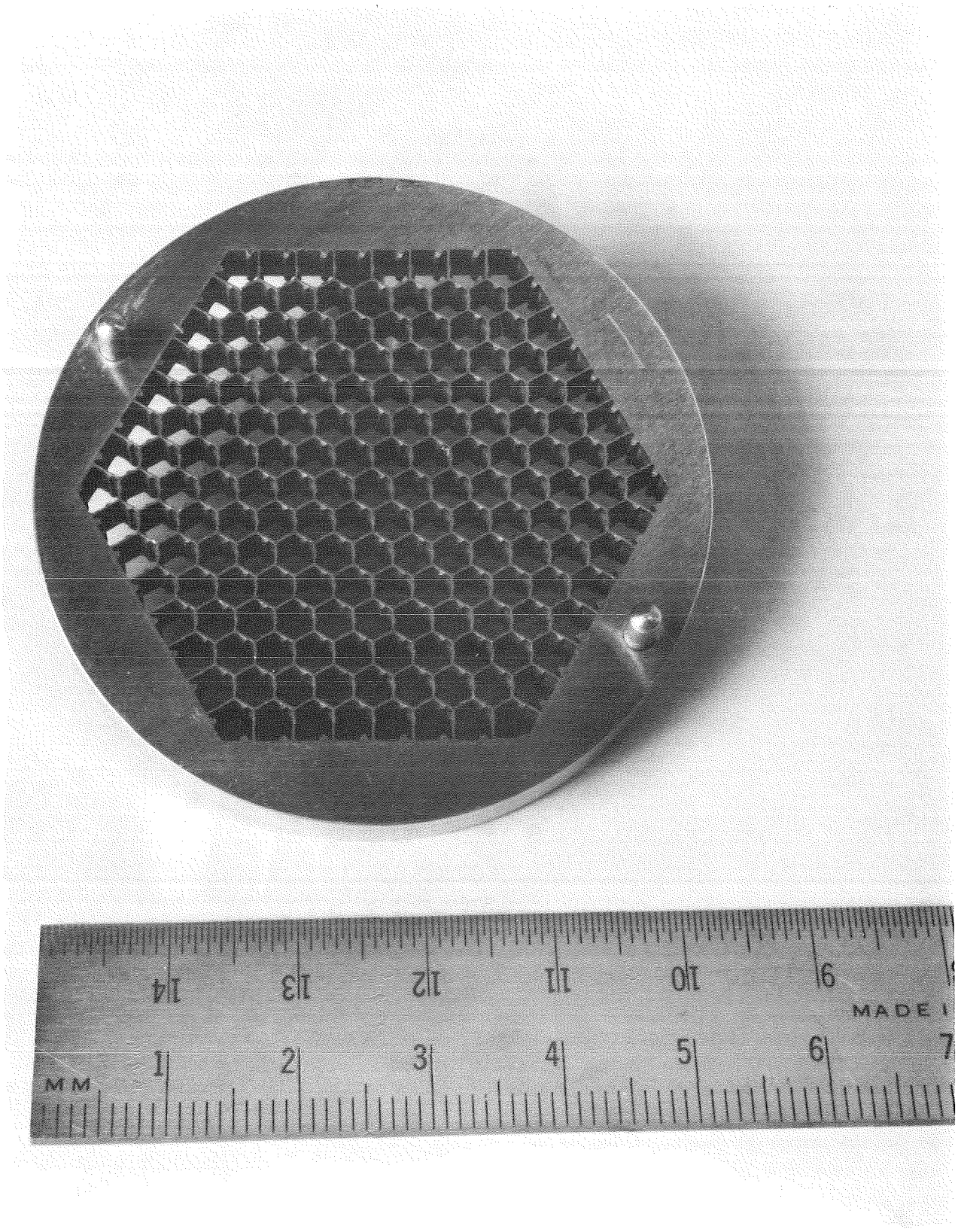

Fig. 4: Spacer grid

Fig. 5 Mixing head

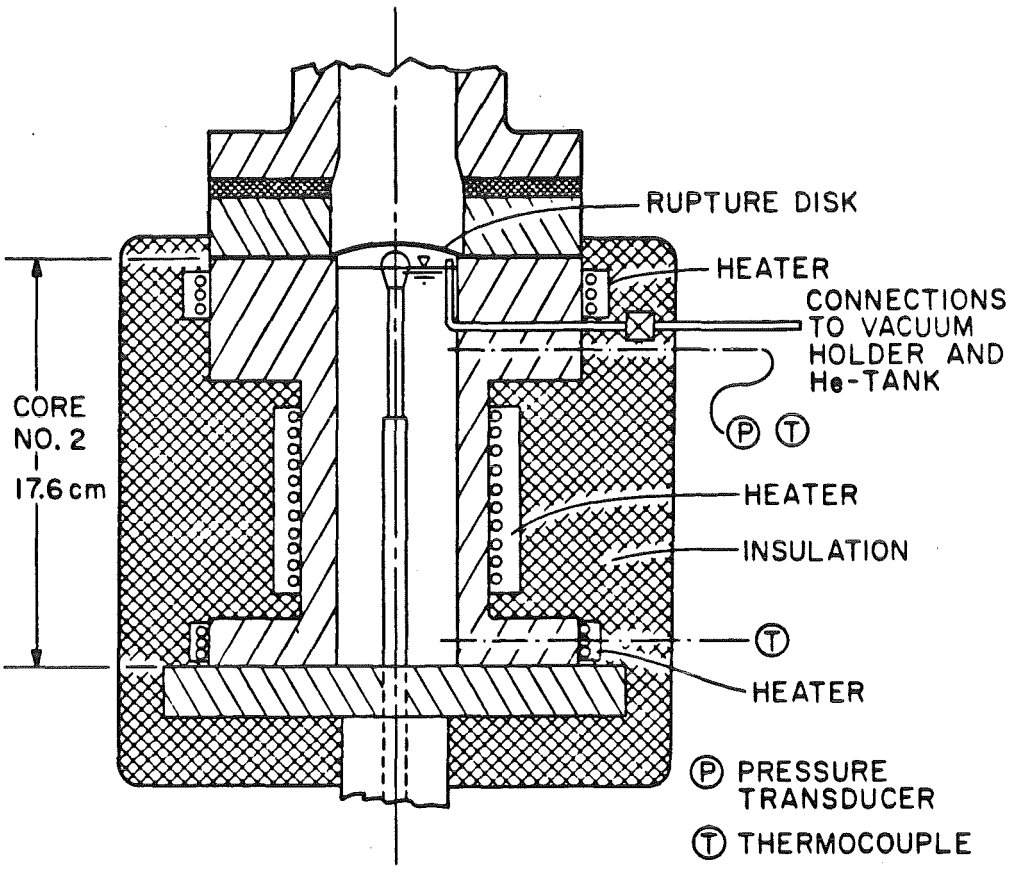

Fig. 6. Schematic of Core No.2.

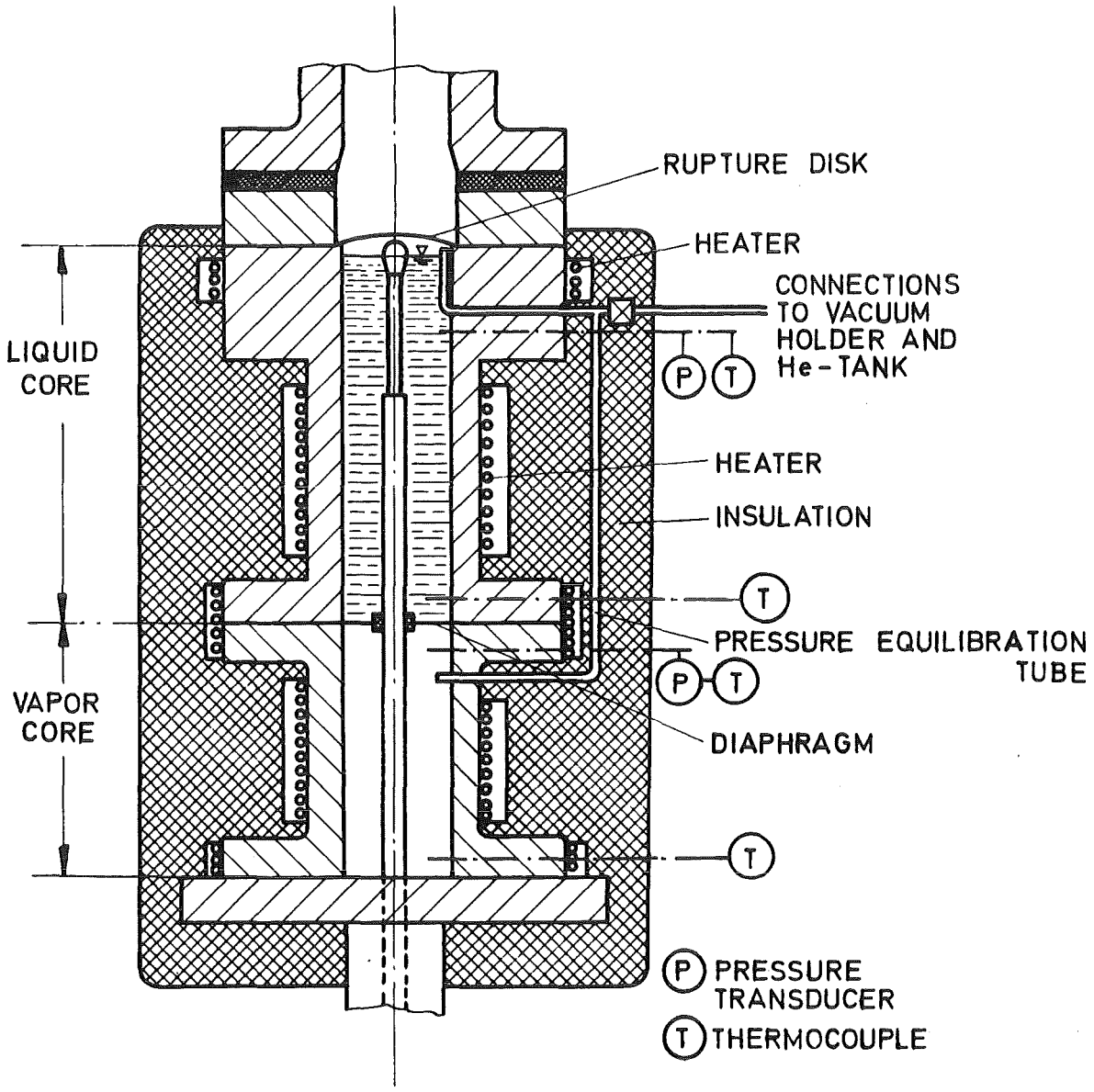

Fig. 7. Schematic of Core No.3 and No.4.

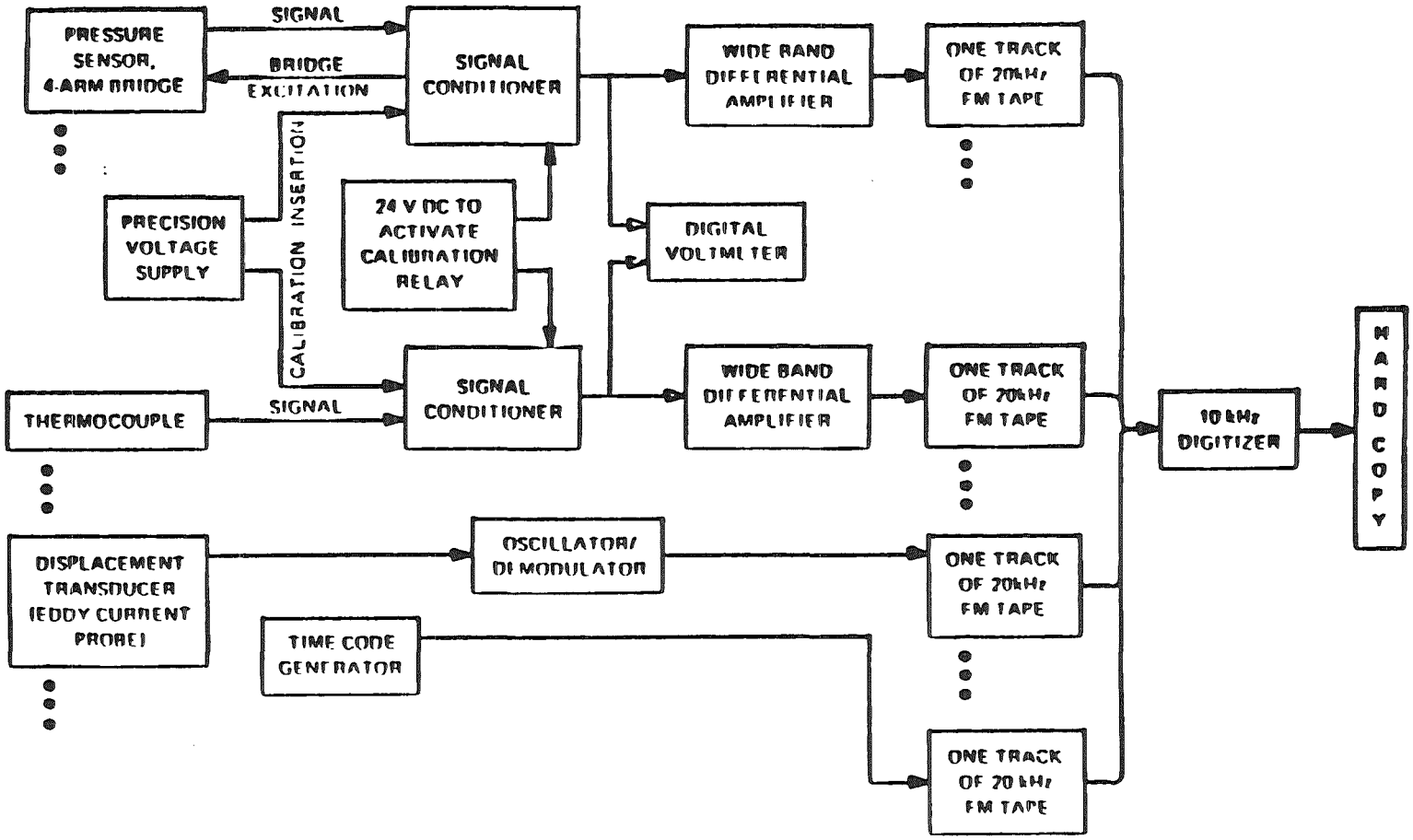

Fig. 8. Block diagram of data aquisition system.

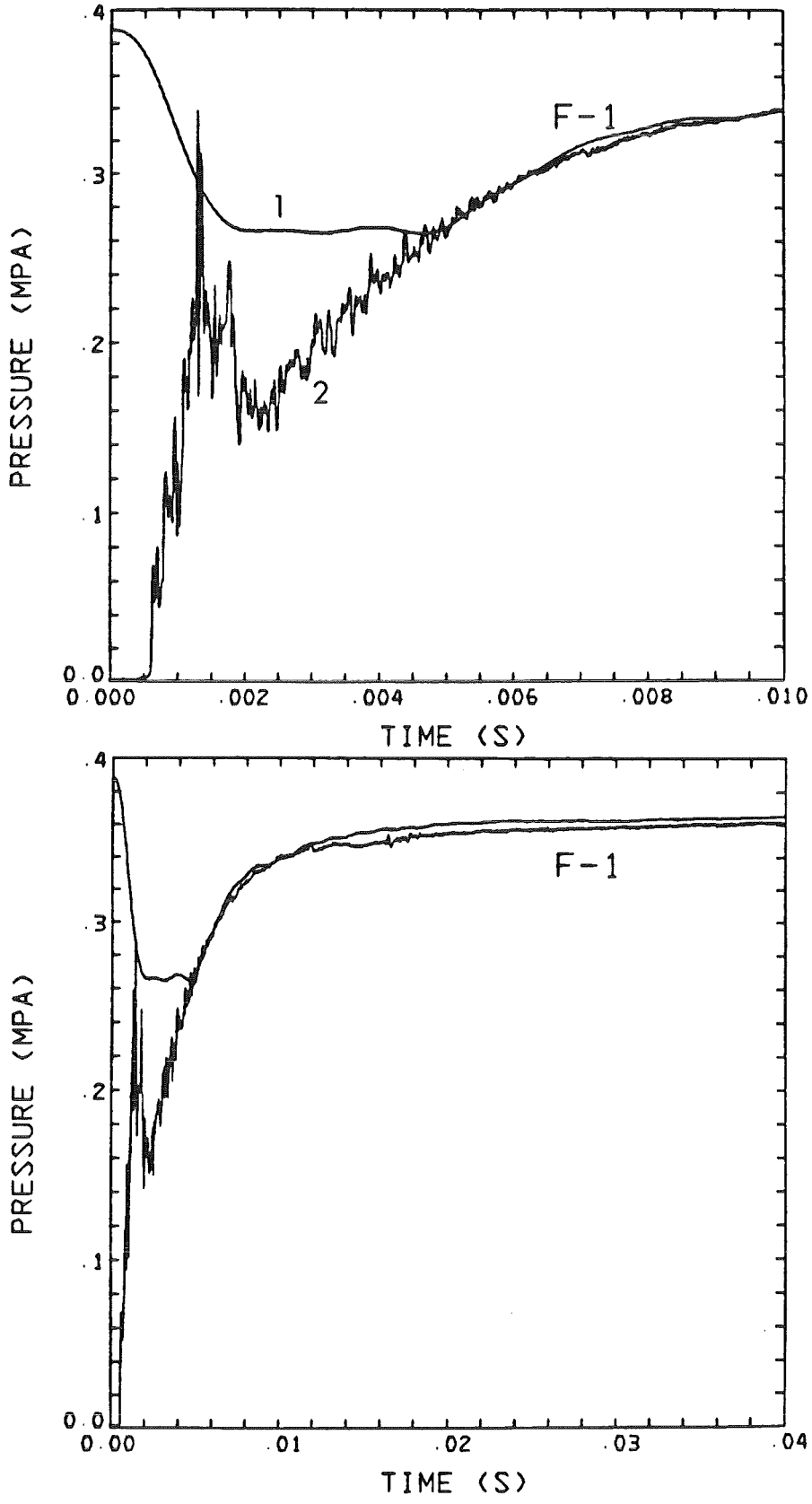

Fig. 9. Pressure in lower (1) and upper (2) chamber in flashing experiment.

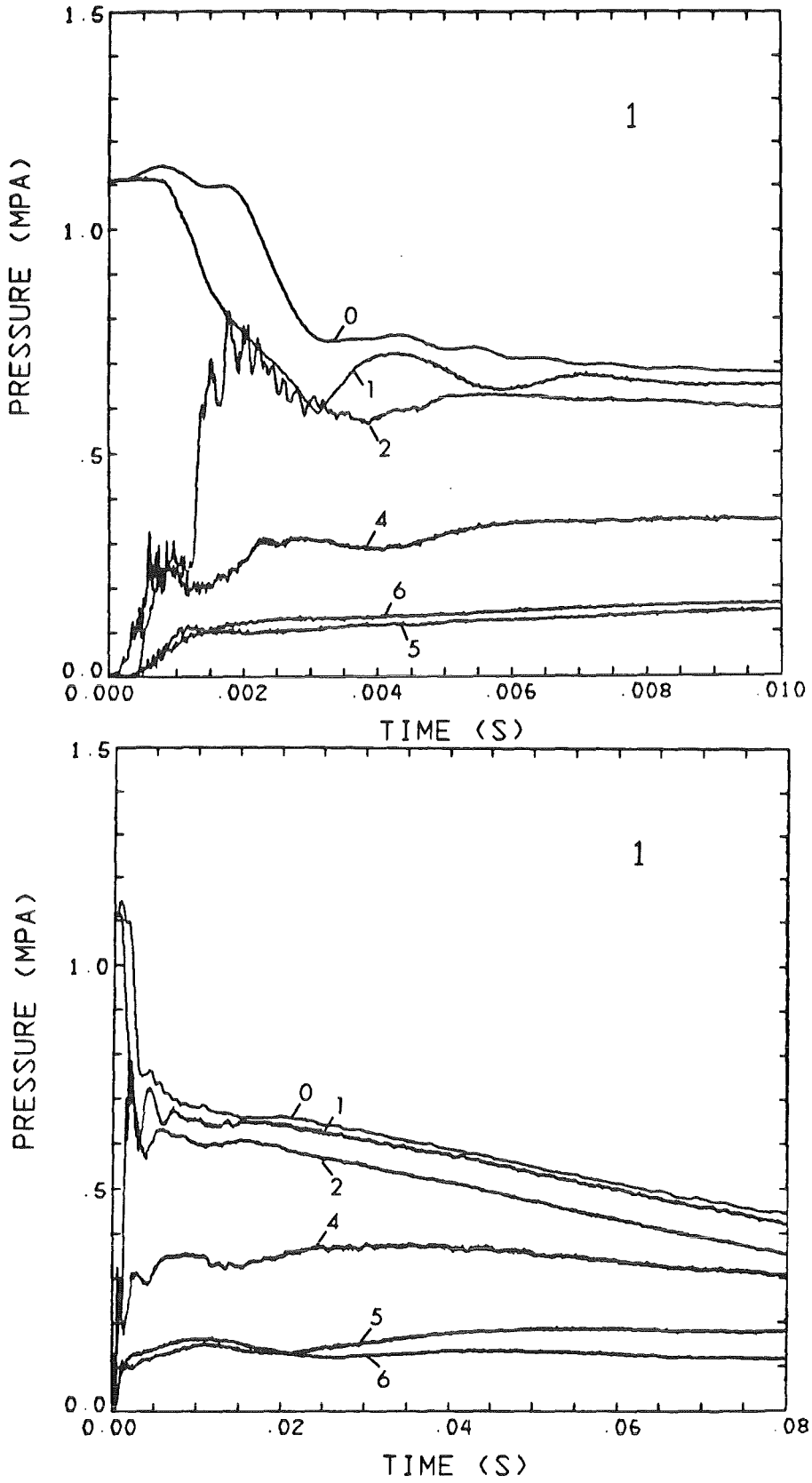

Fig. 10. Pressures in Test 1.
(measuring positions 1-6 are denoted in Fig.1 and positions 7, 8 and 9 coincide with Z1, Z2 and Z3 in Table IV; applies to figures 10 through 62).

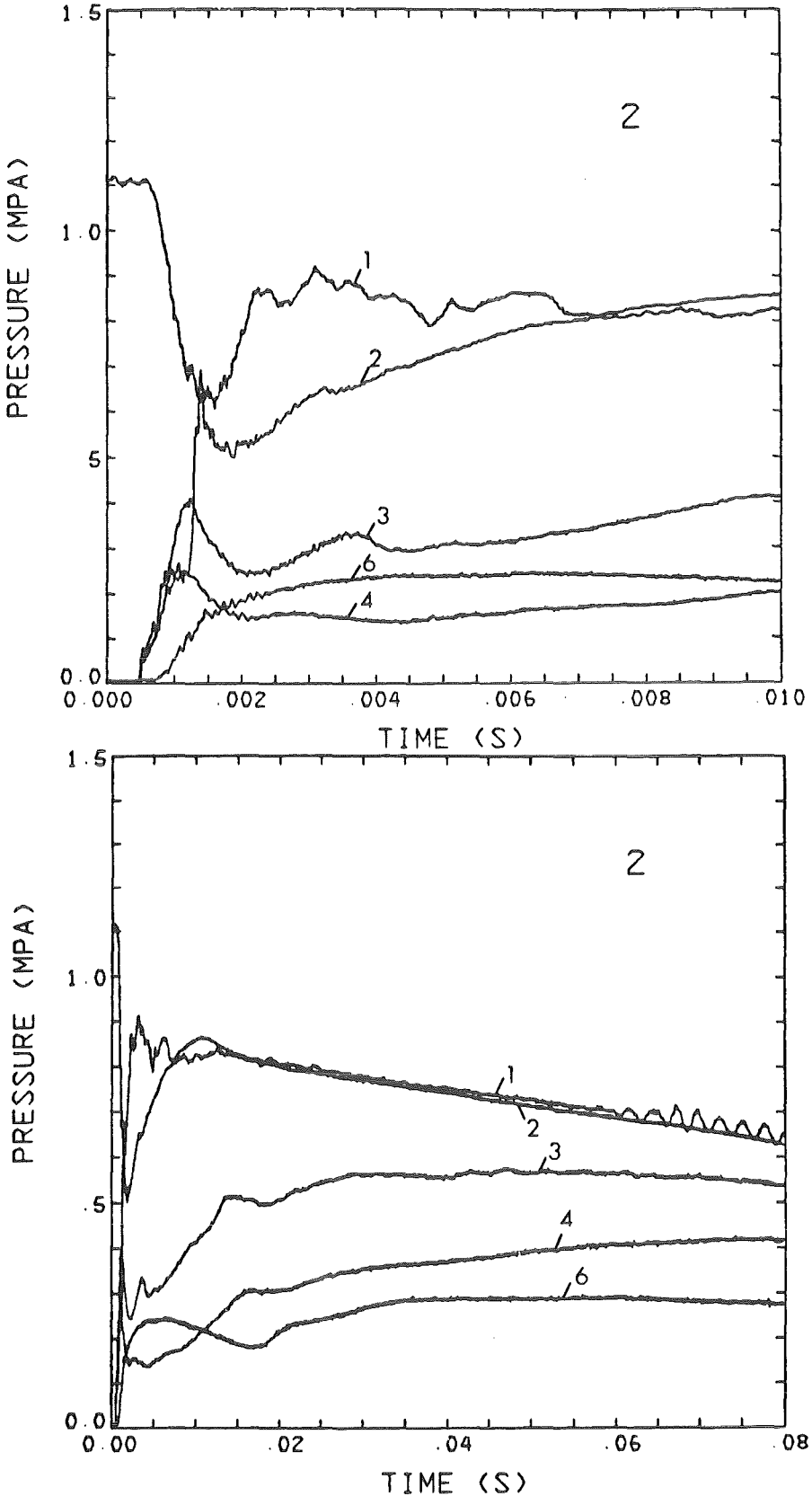

Fig. 11. Pressures in Test 2.

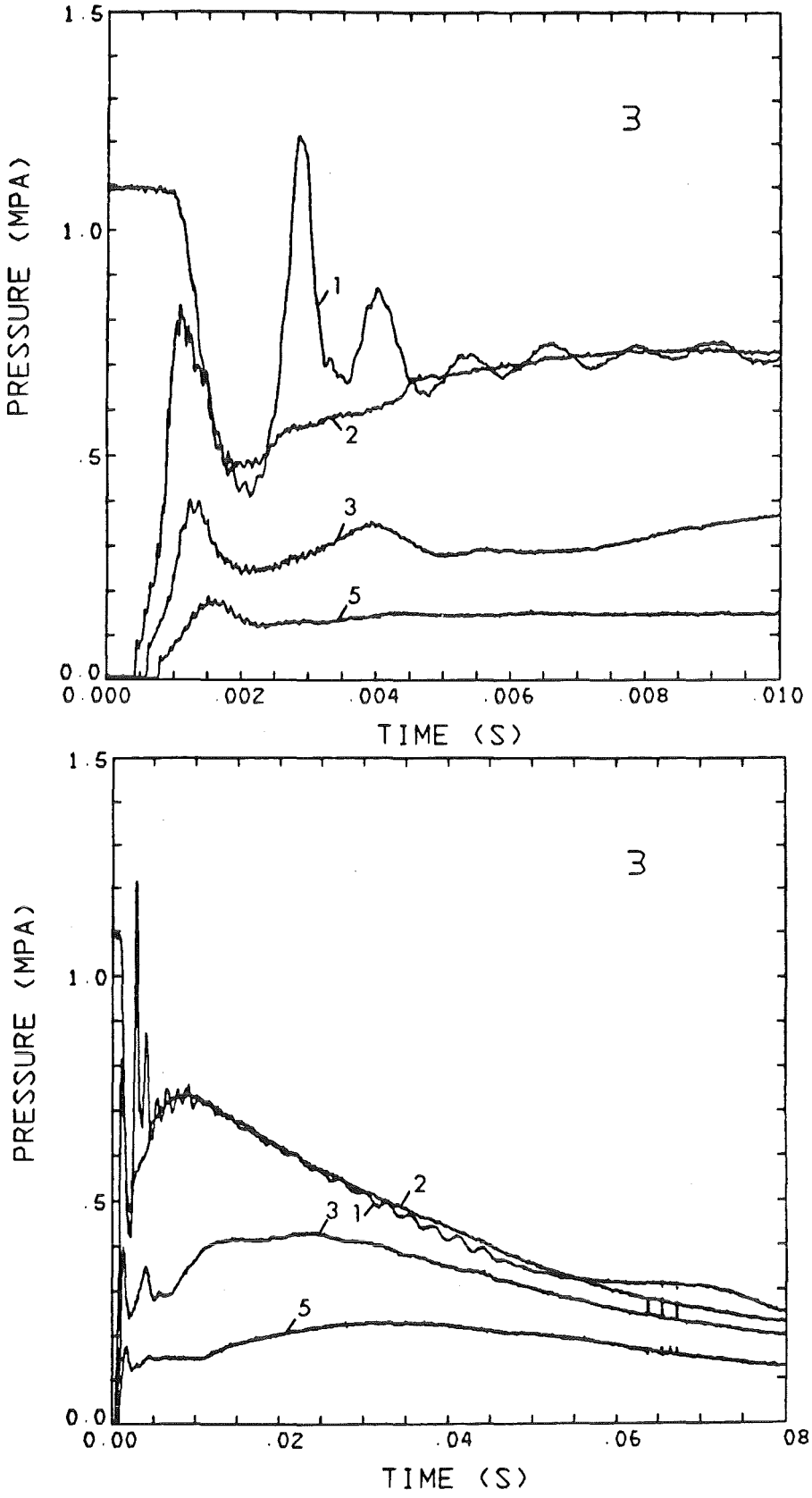

Fig. 12. Pressures in Test 3.

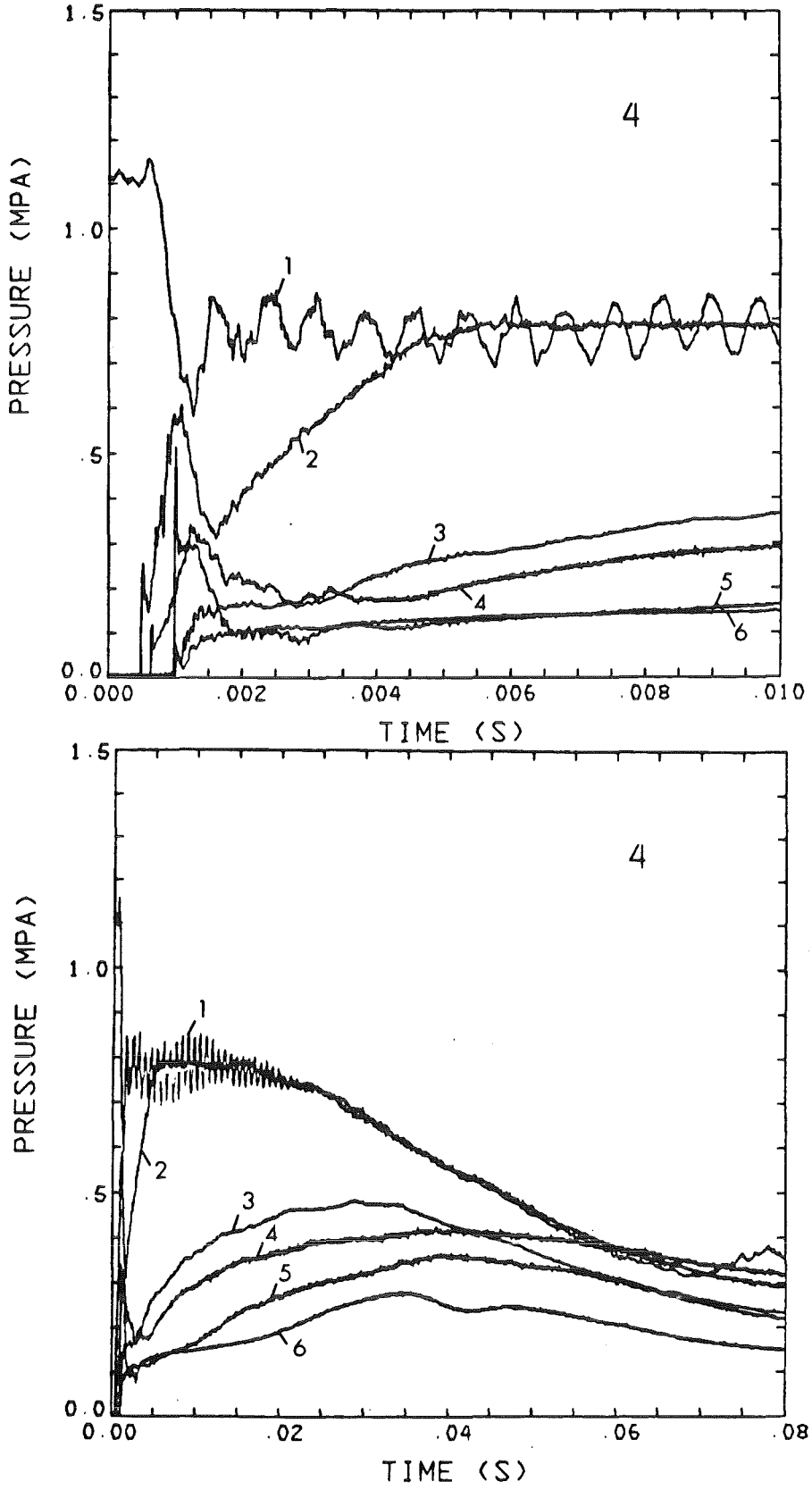

Fig. 13. Pressures in Test 4.

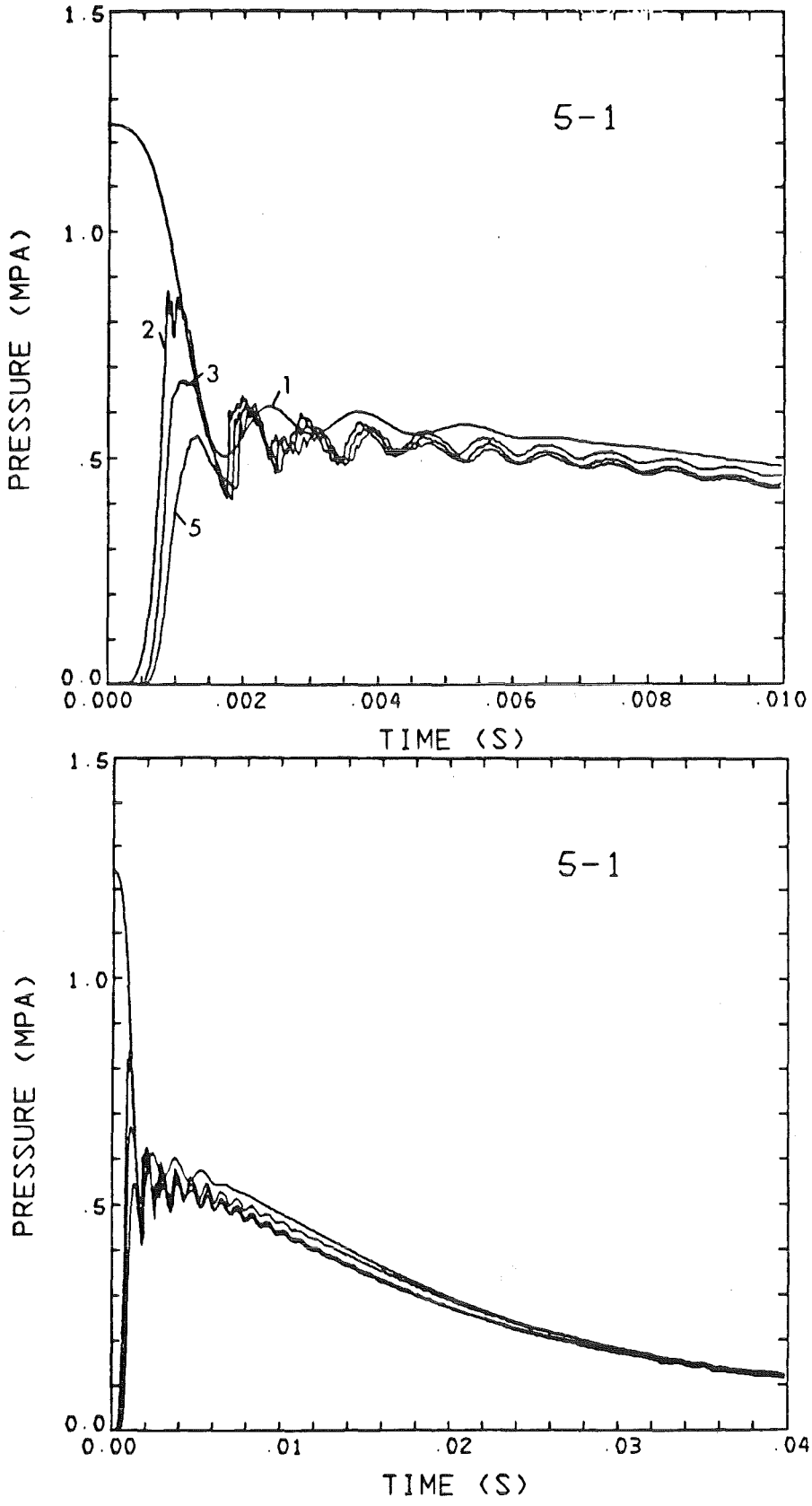

Fig. 14. Pressures in Test 5.

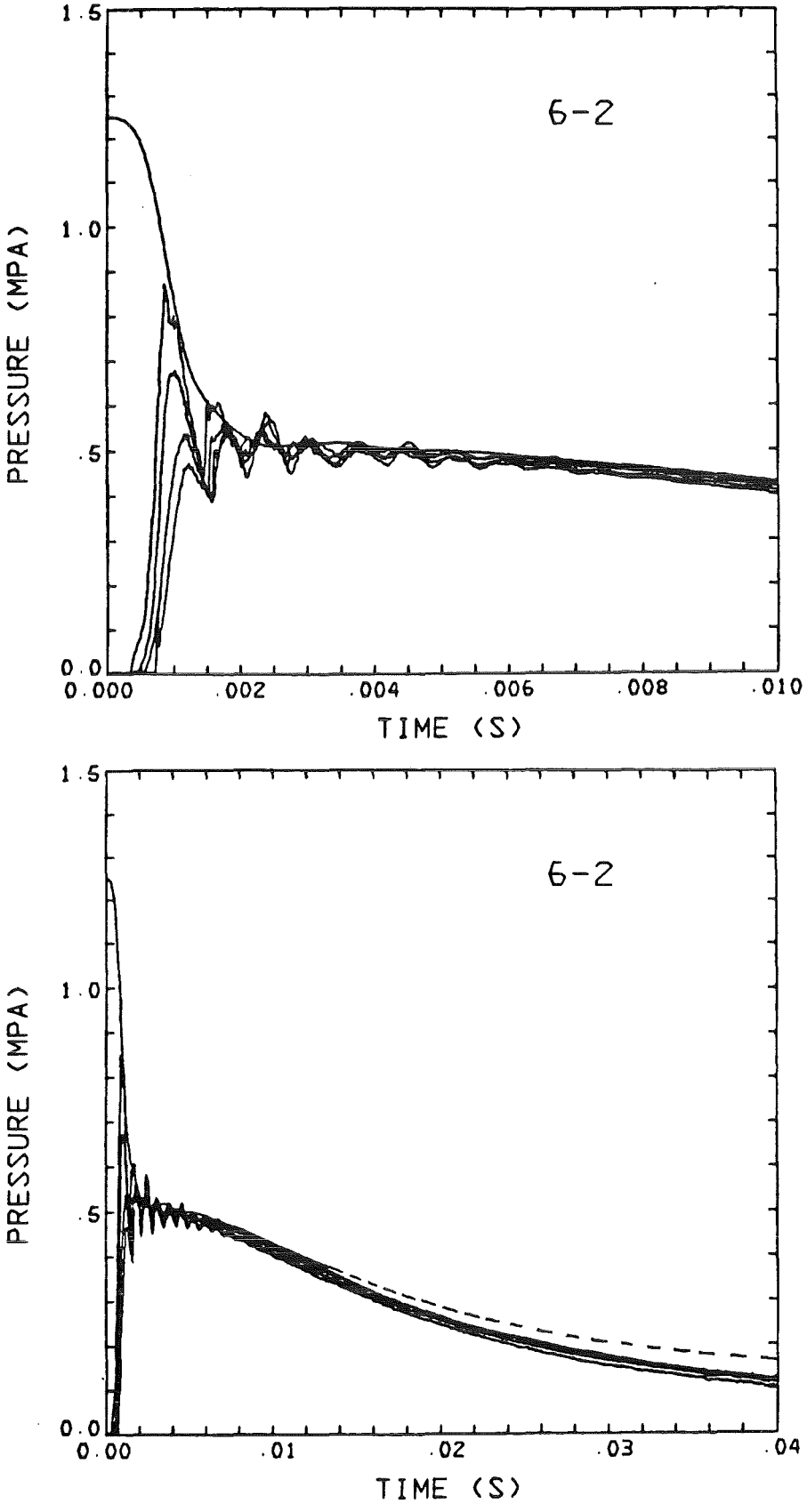

Fig. 15. Pressures in Test 6.

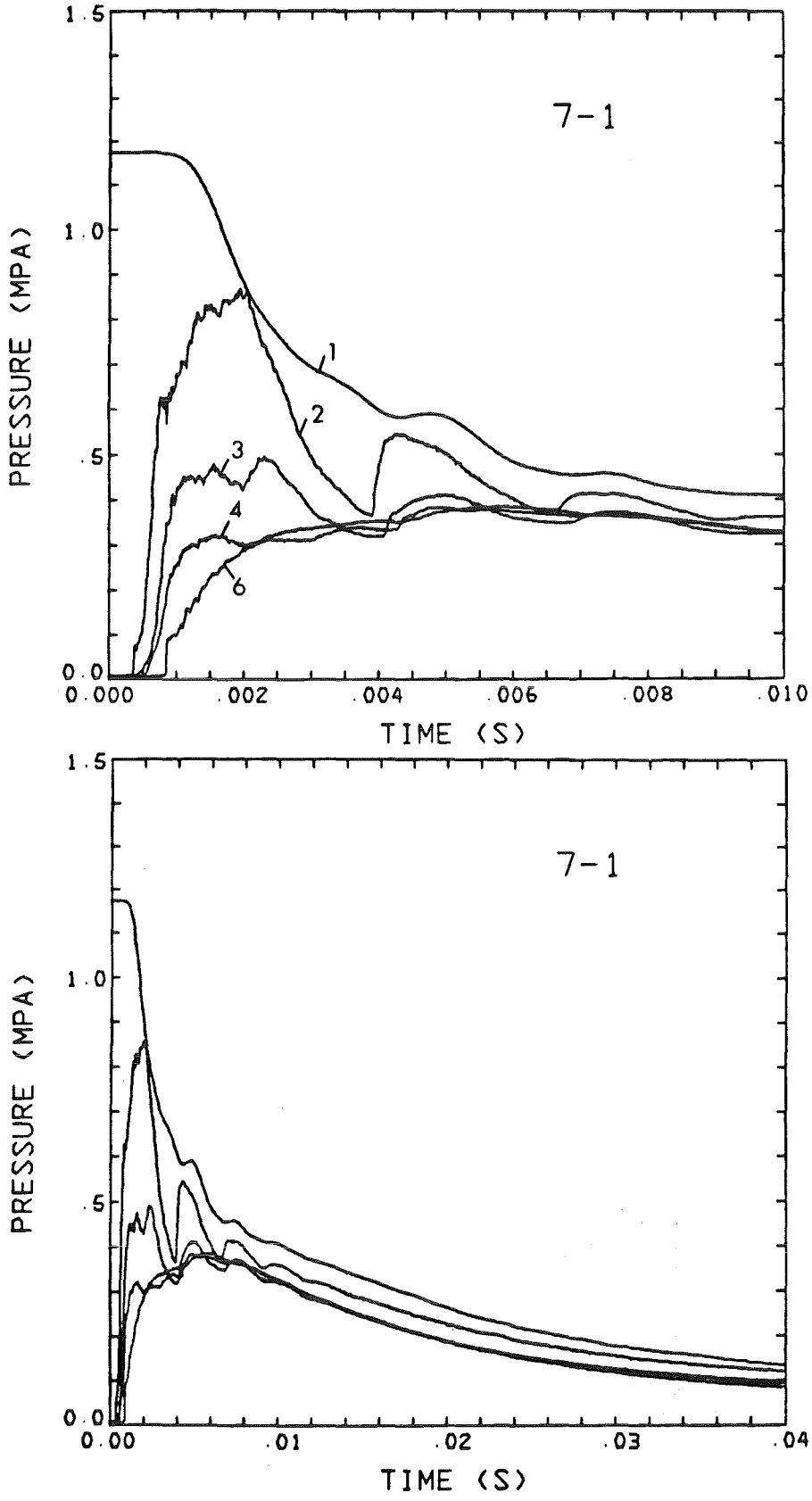

Fig. 16. Pressures in Test 7.

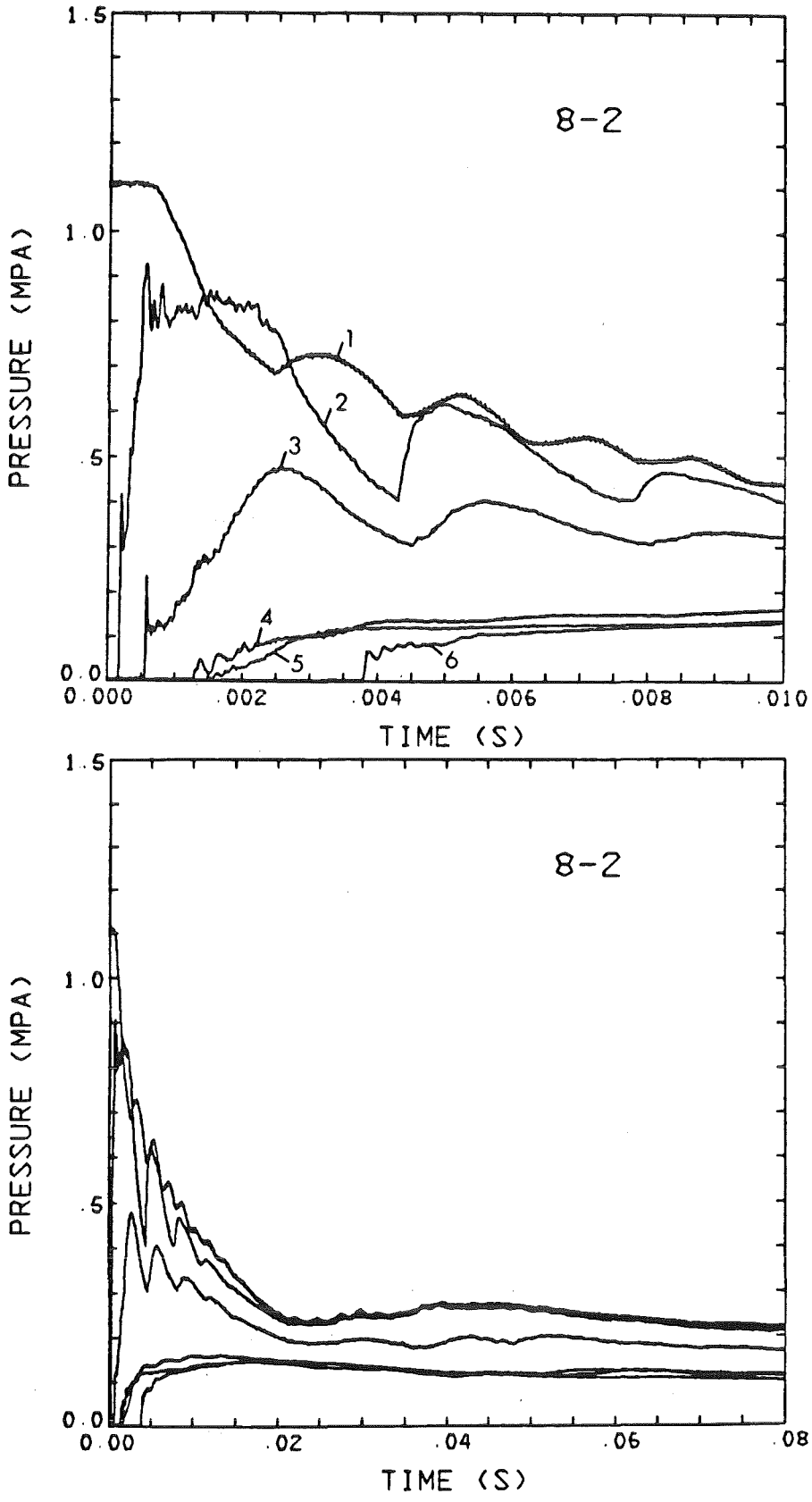

Fig. 17. Pressures in Test 8.

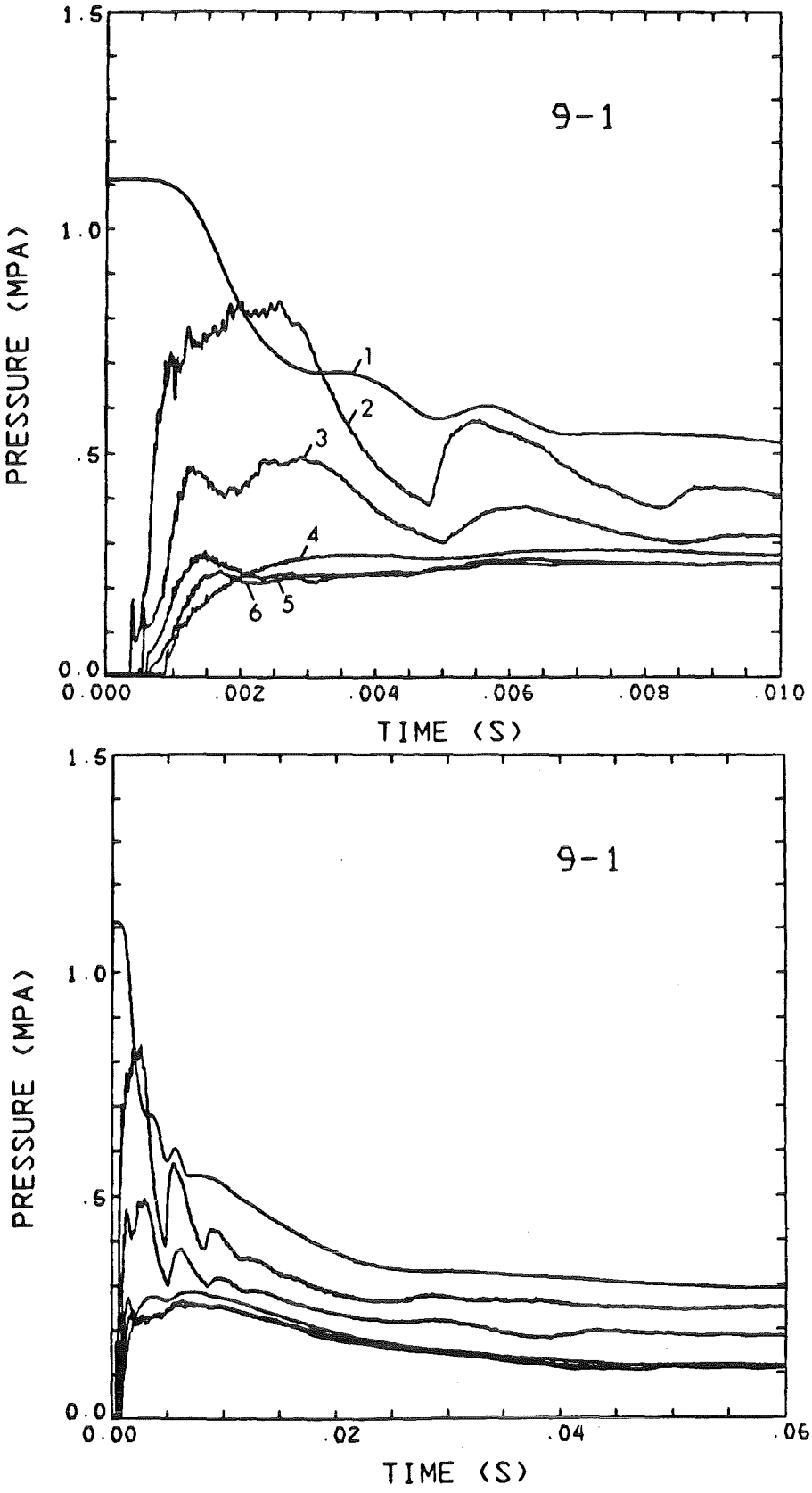

Fig. 18. Pressures in Test 9.

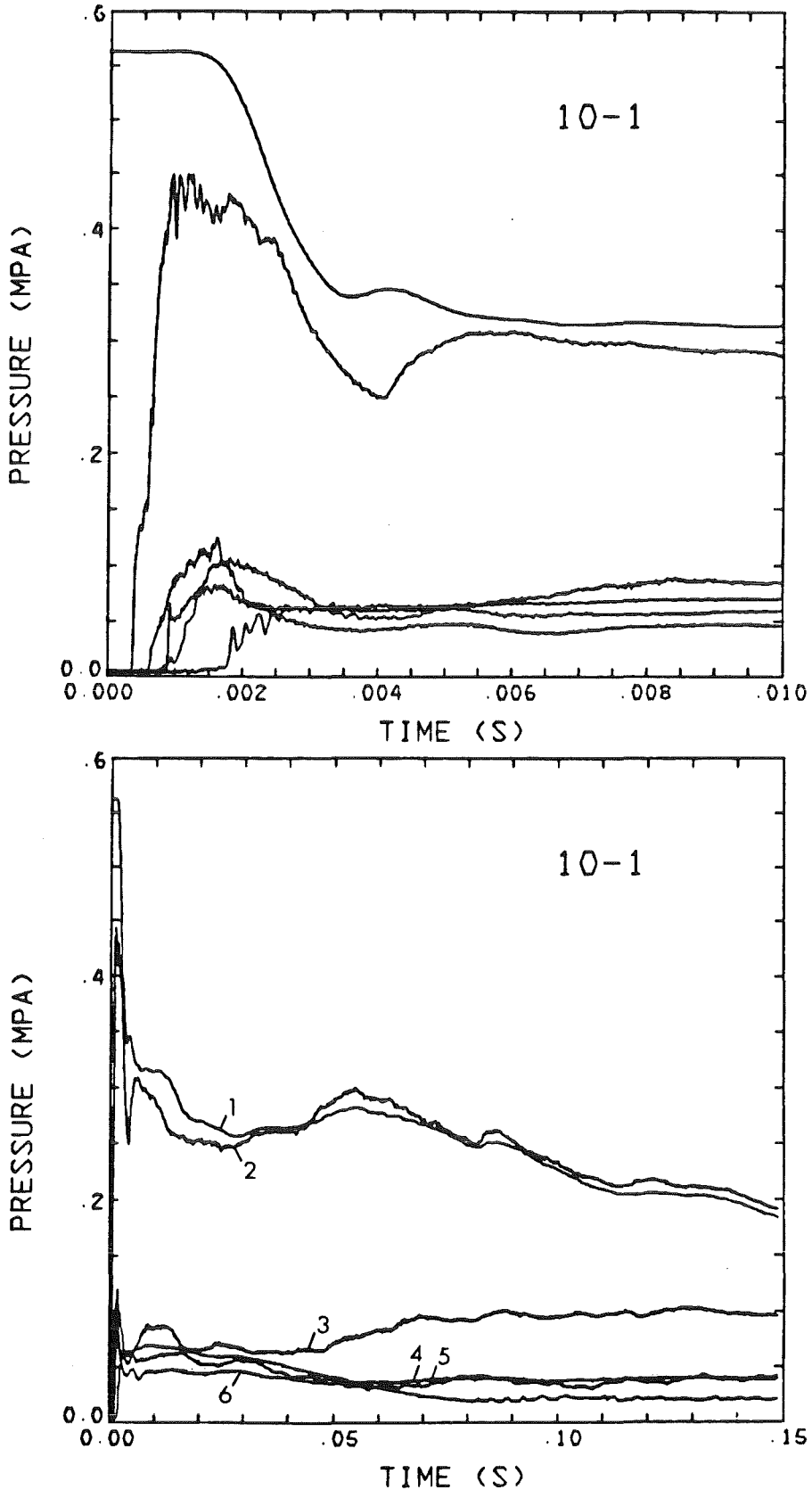

Fig. 19. Pressures in Test 10.

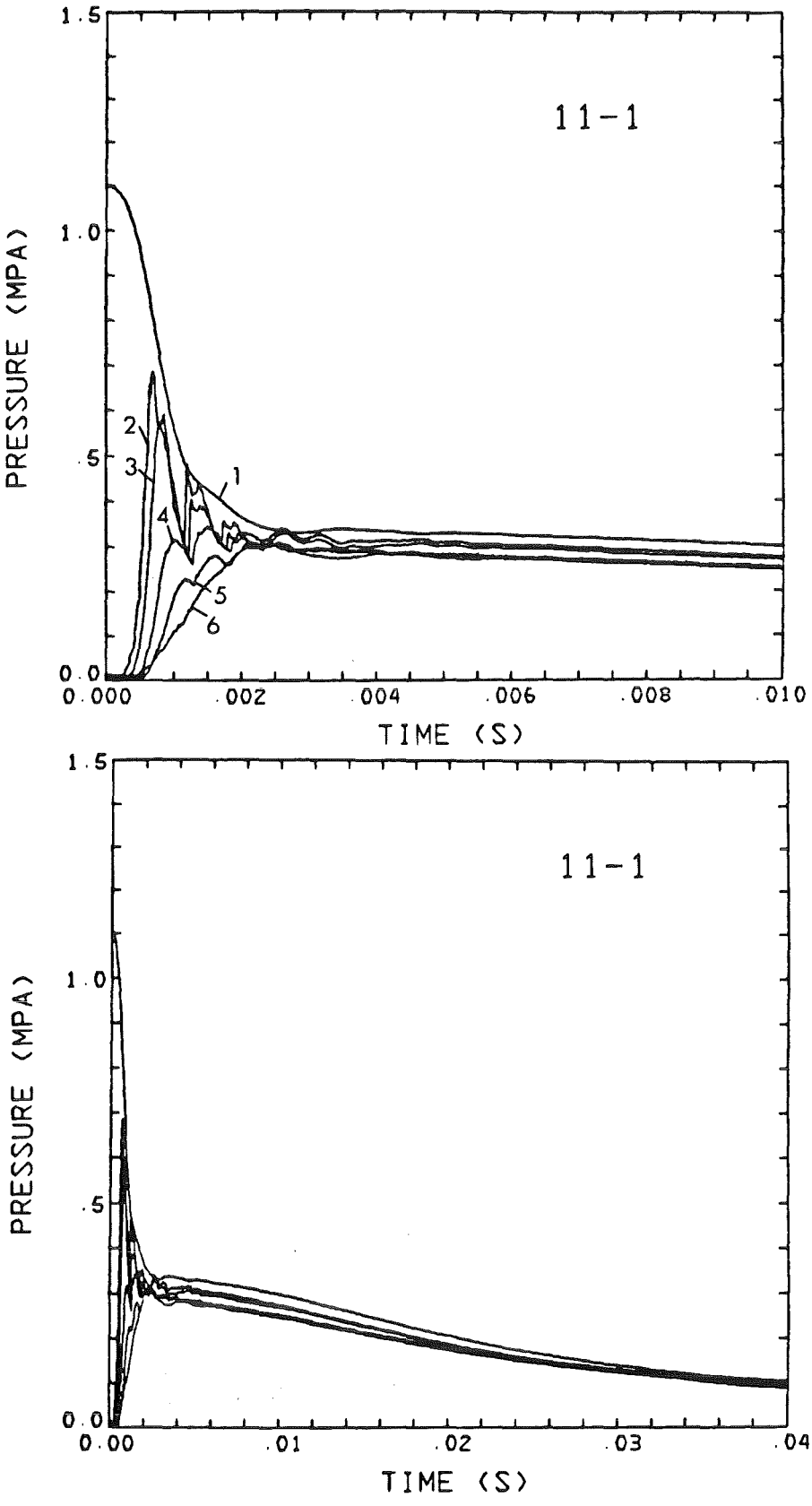

Fig. 20. Pressures in Test 11.

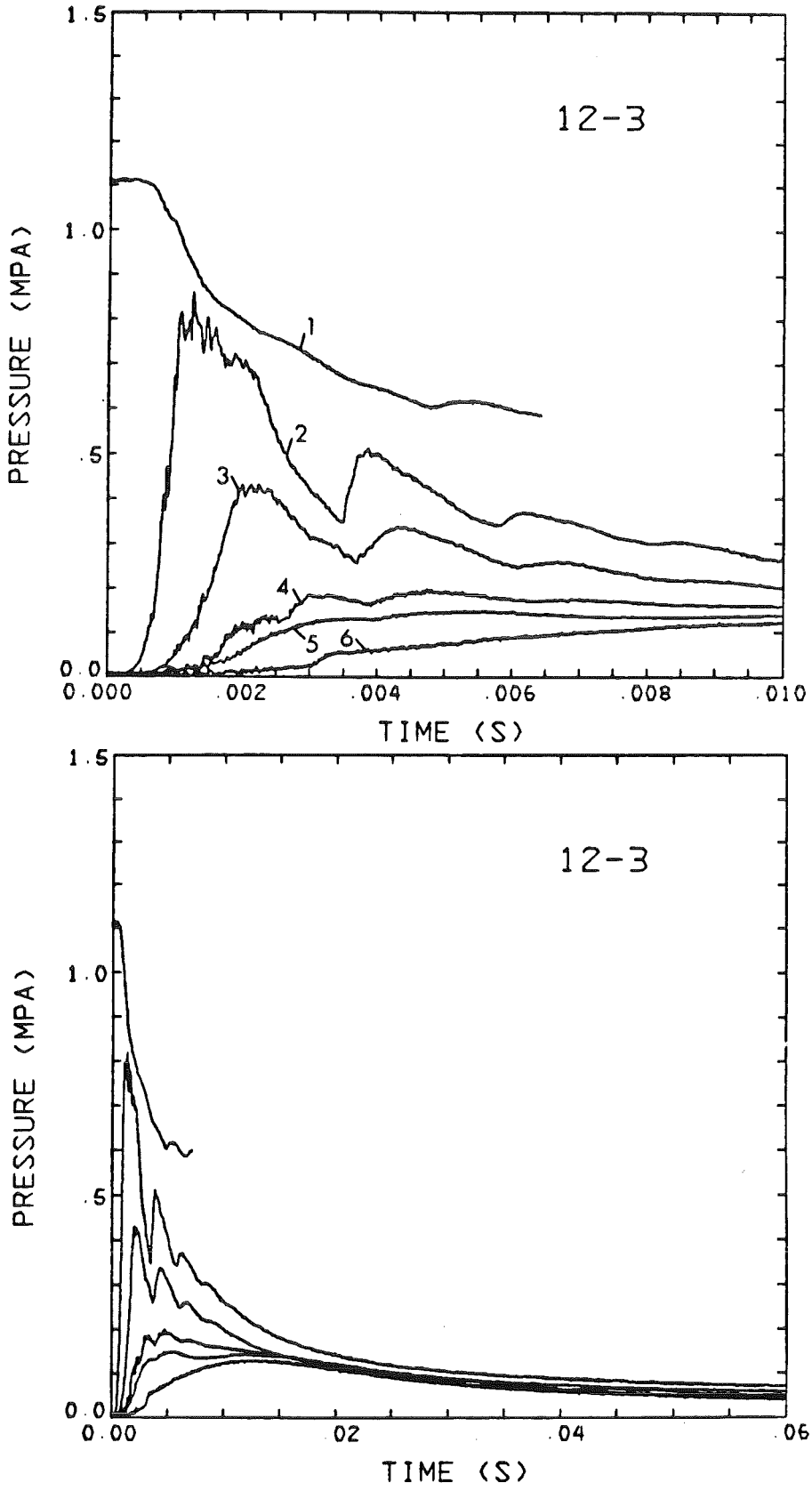

Fig. 21. Pressures in Test 12.

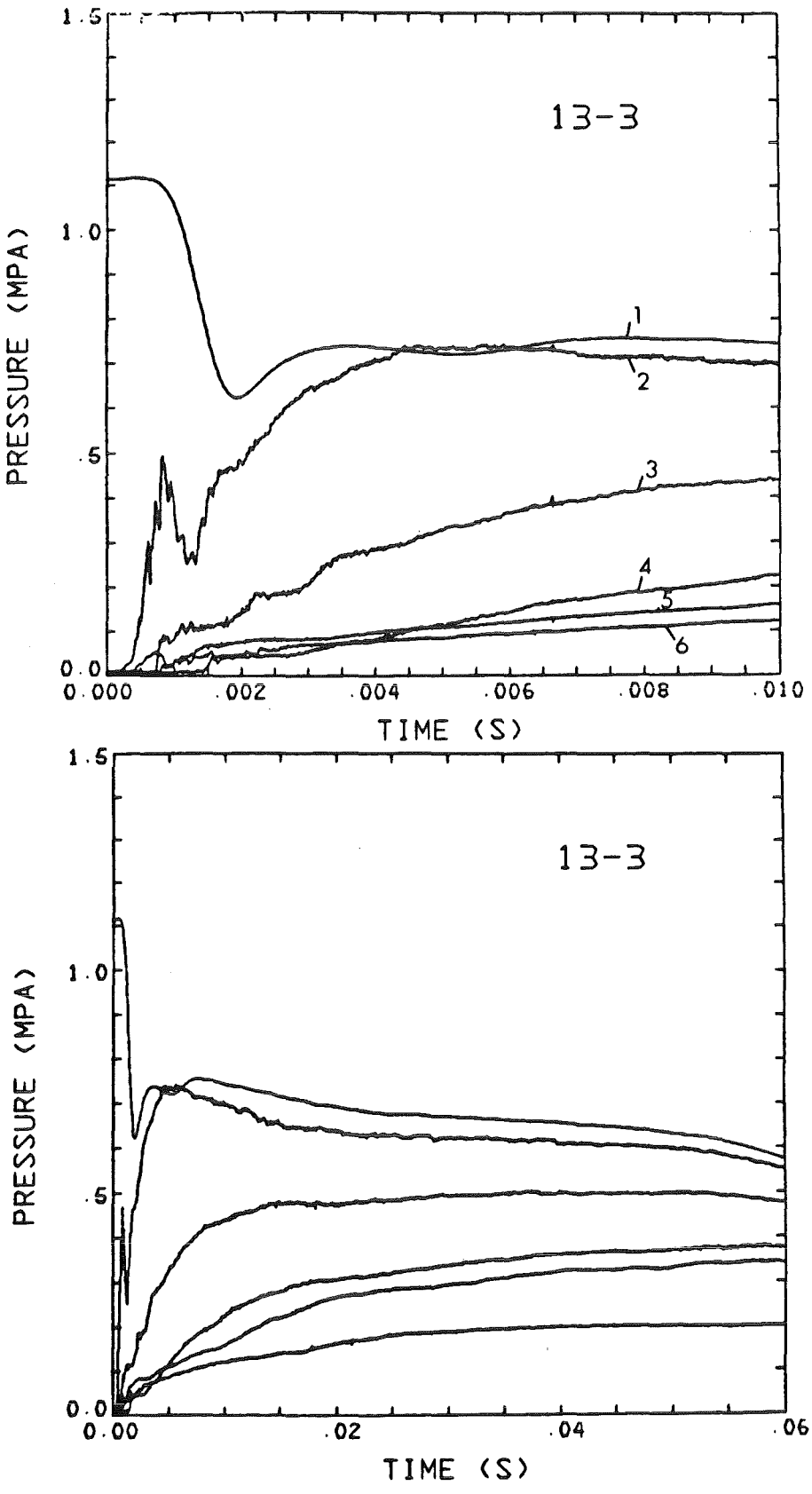

Fig. 22. Pressures in Test 13.

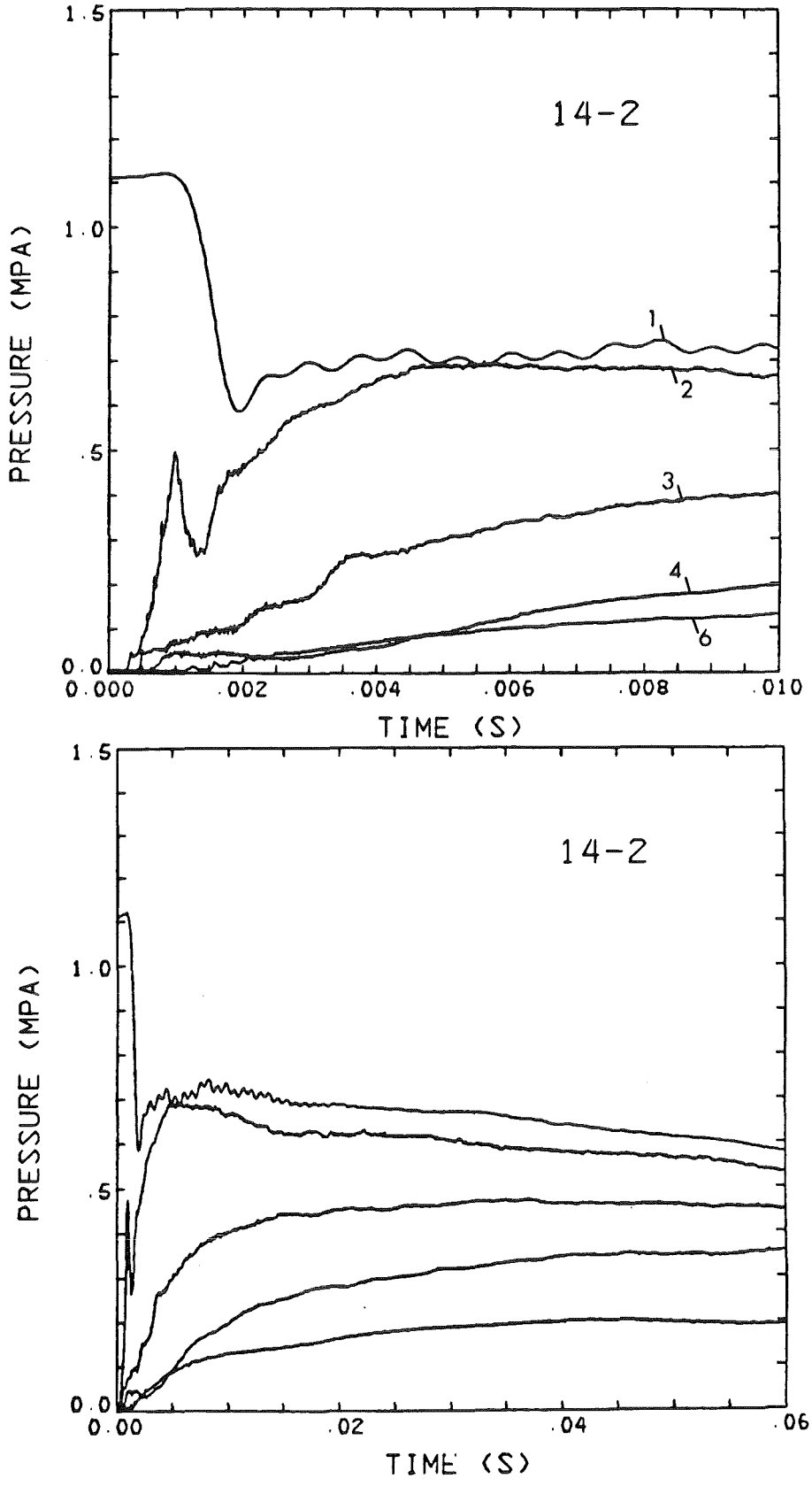

Fig. 23. Pressures in Test 14.

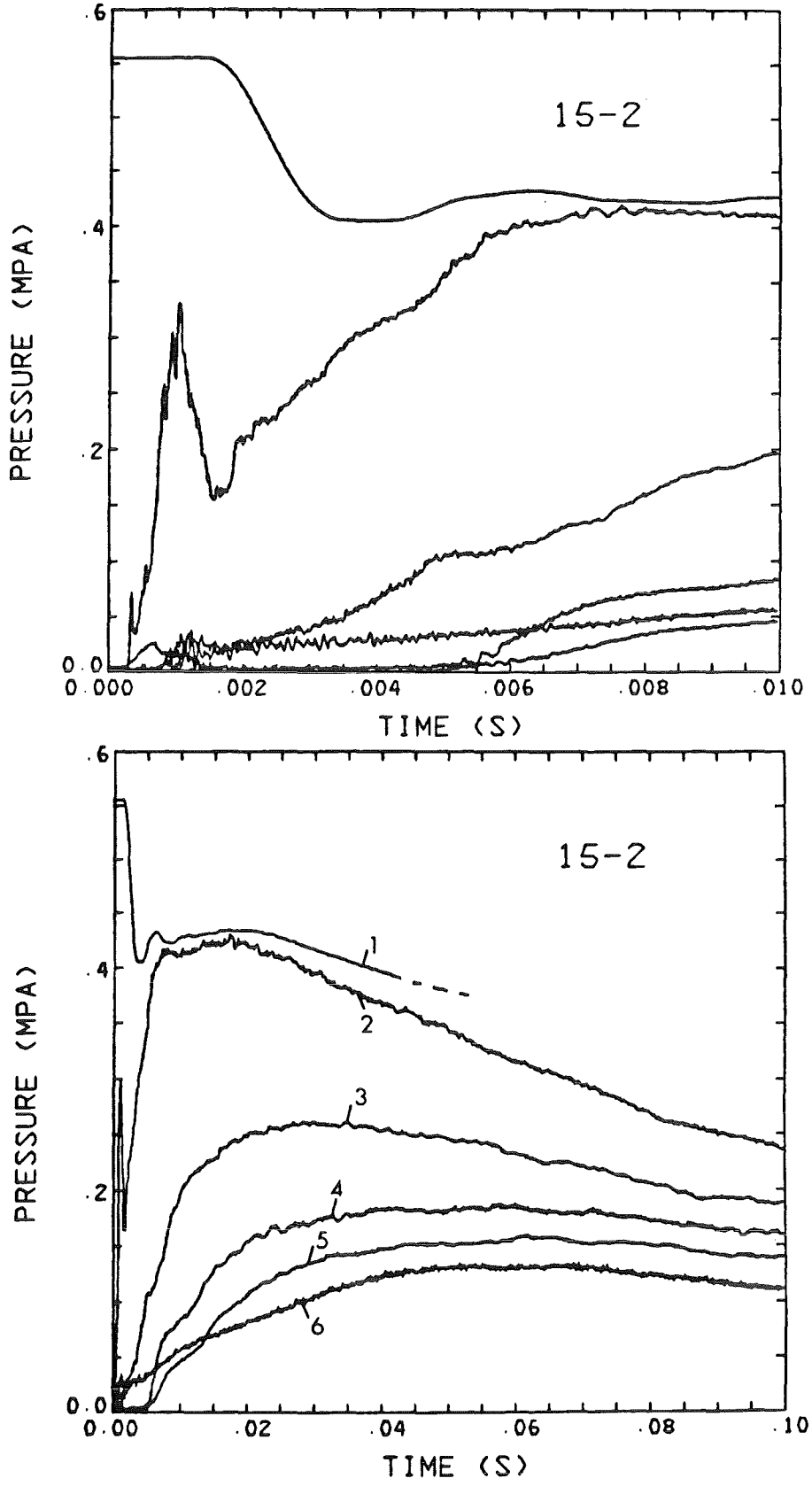

Fig. 24. Pressures in Test 15.

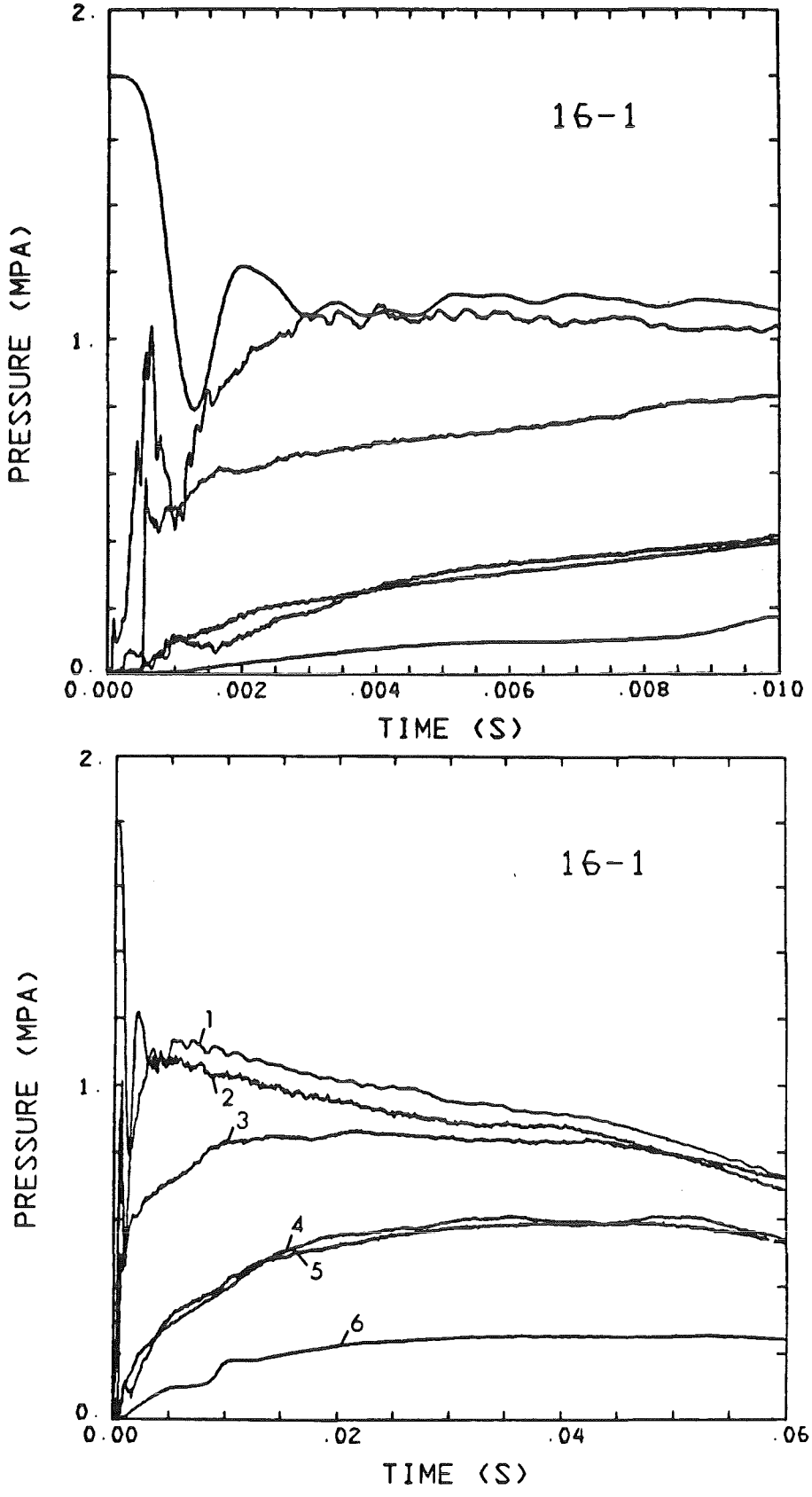

Fig. 25. Pressures in Test 16.

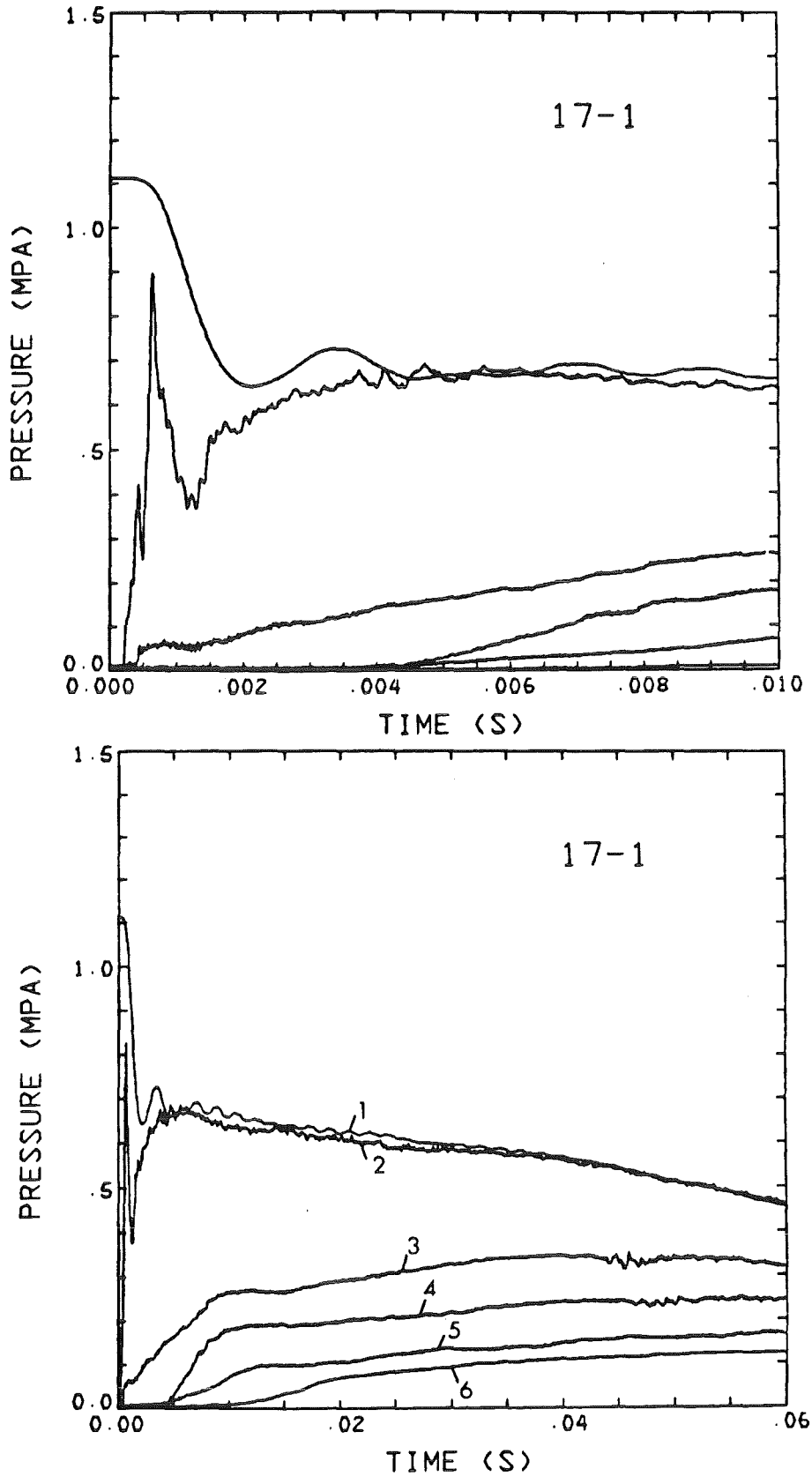

Fig. 26. Pressures in Test 17.

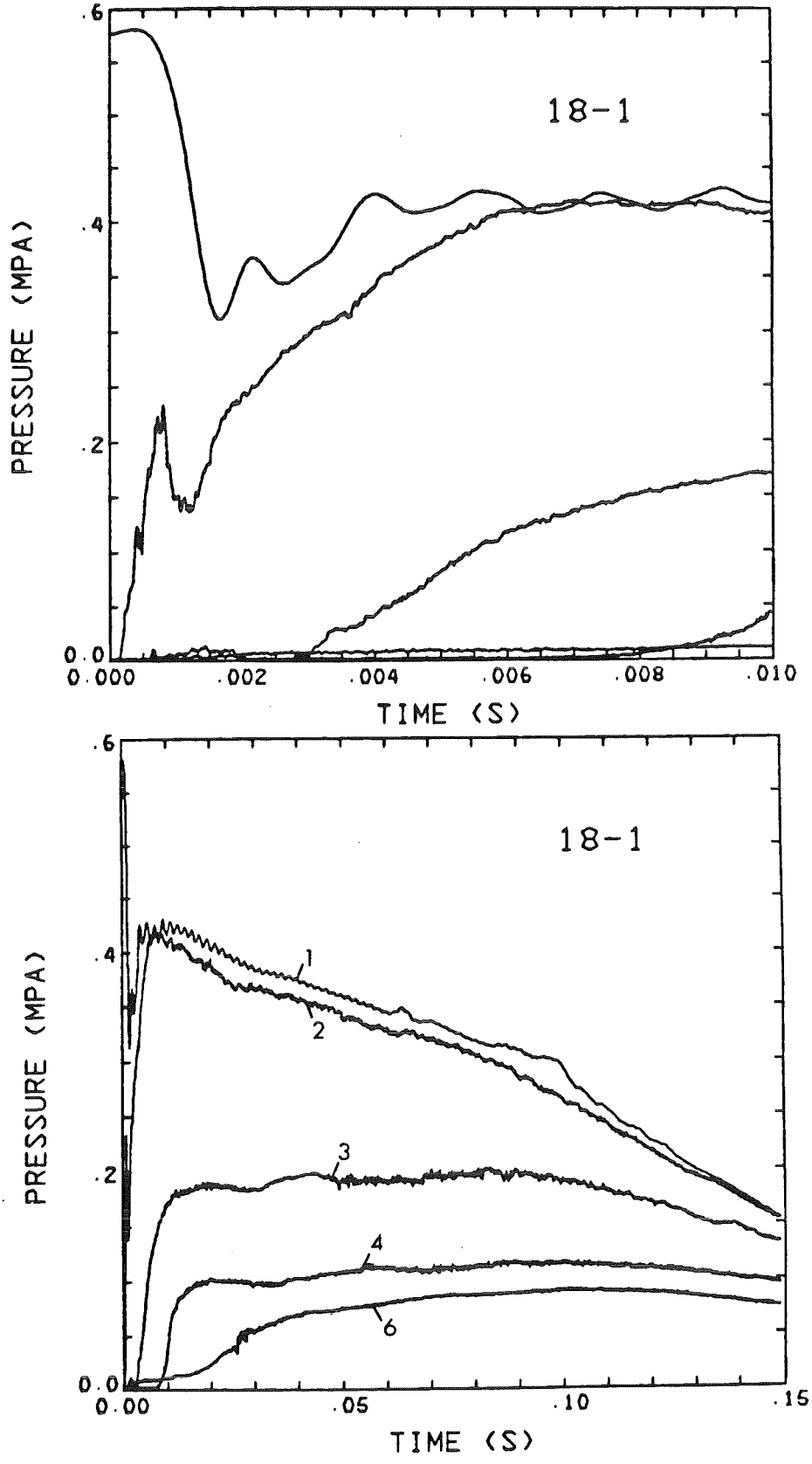

Fig. 27. Pressures in Test 18.

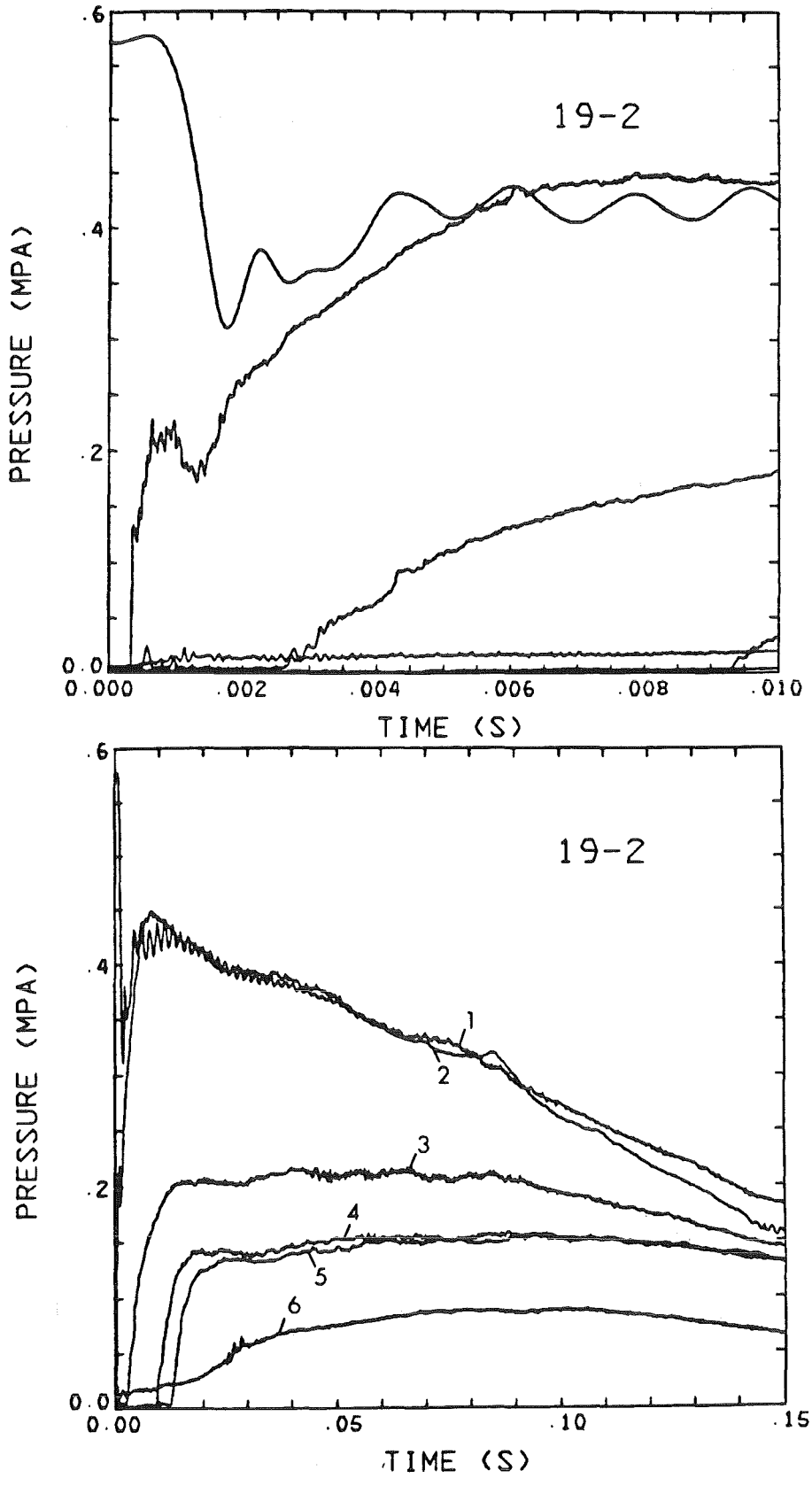

Fig. 28. Pressures in Test 19.

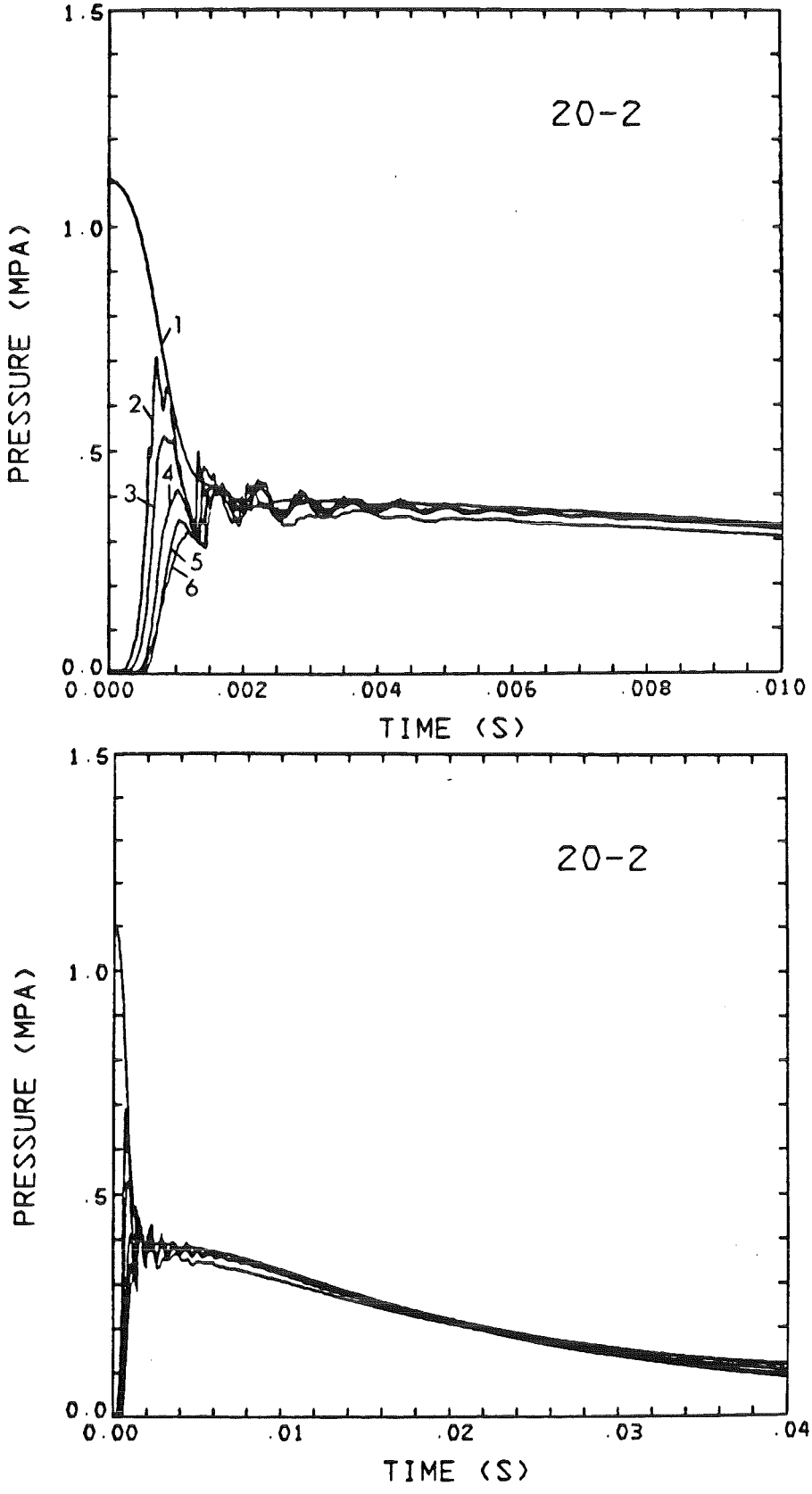

Fig. 29. Pressures in Test 20.

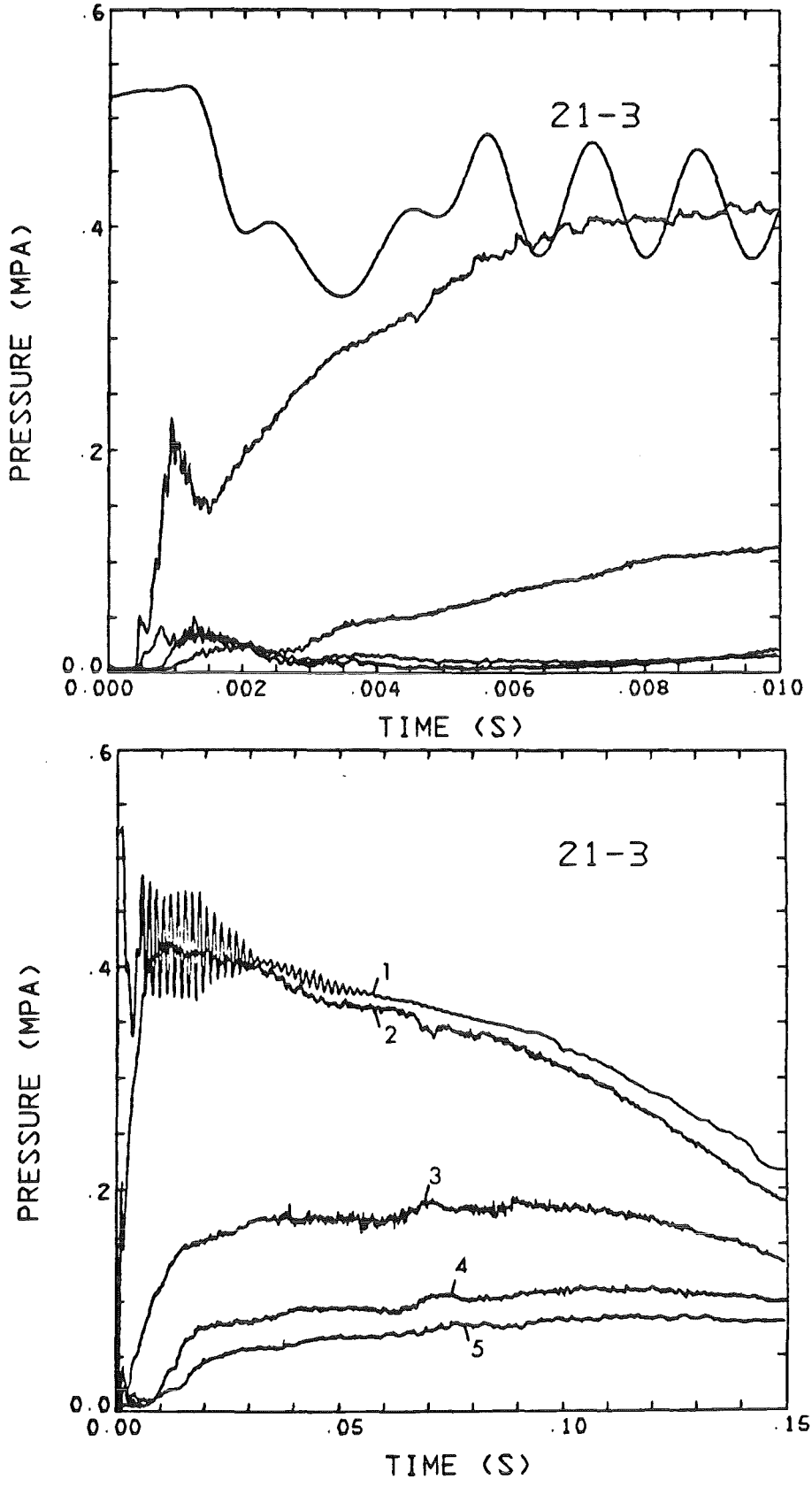

Fig. 30. Pressures in Test 21.

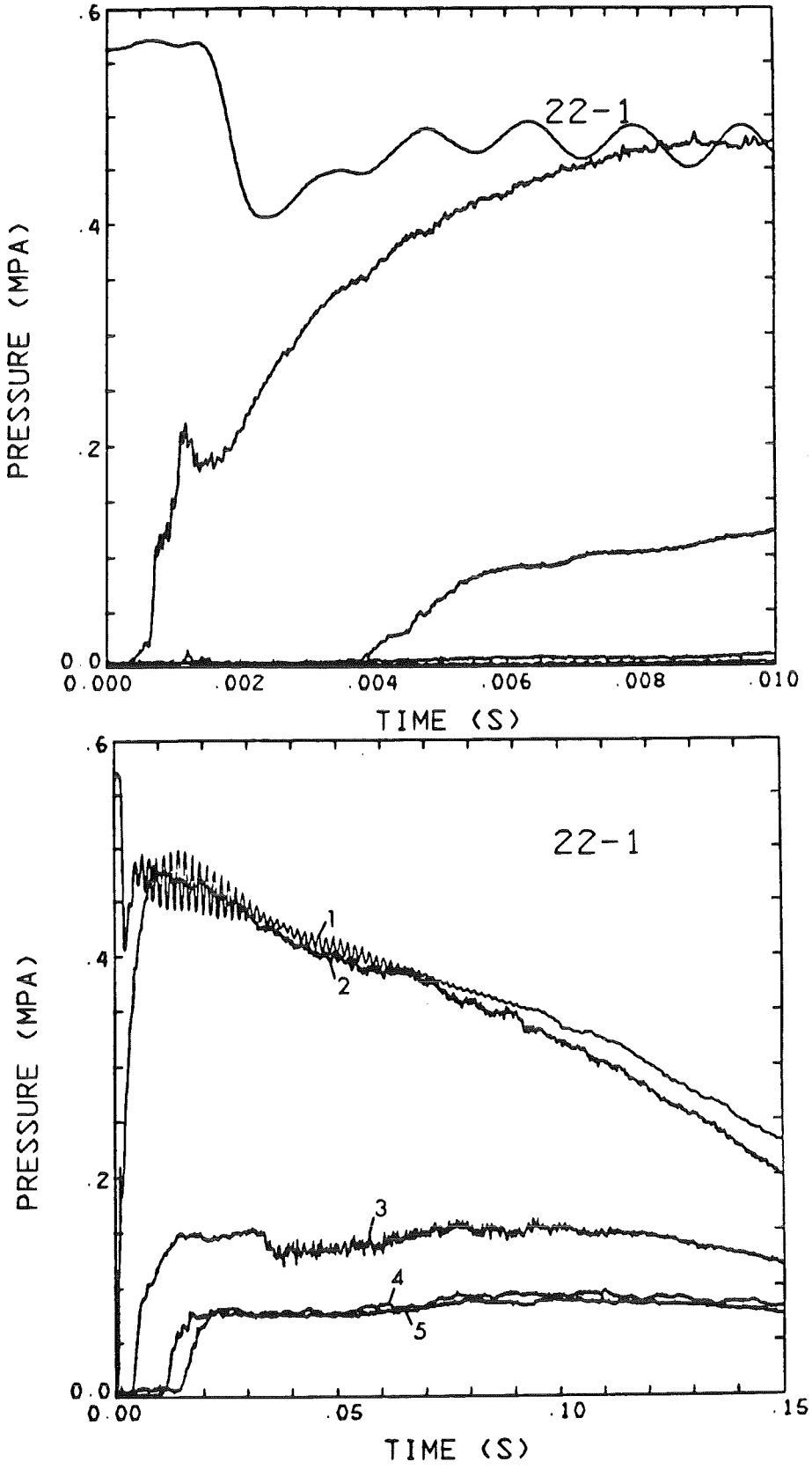

Fig. 31. Pressures in Test 22.

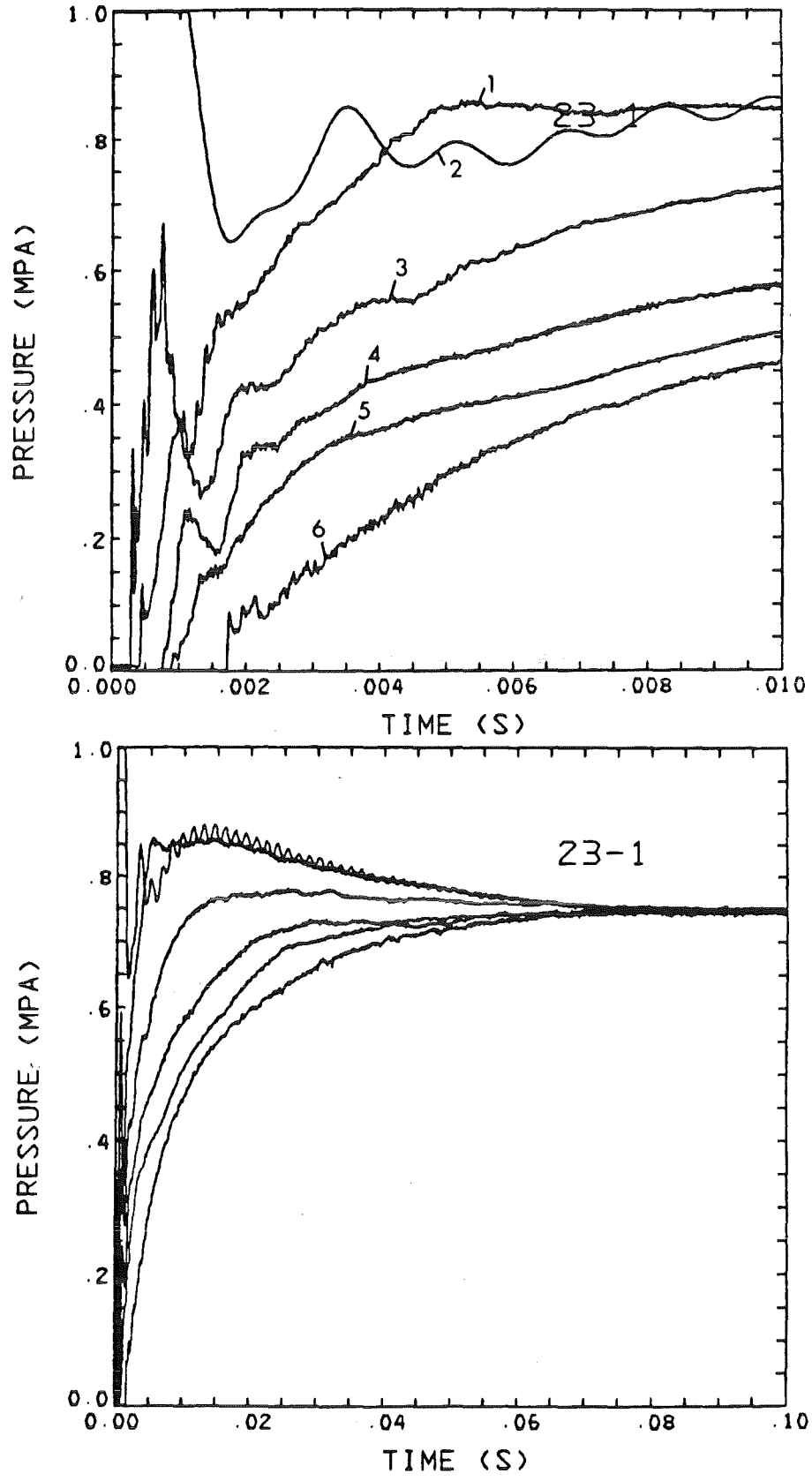

Fig. 32. Pressures in Test 23.

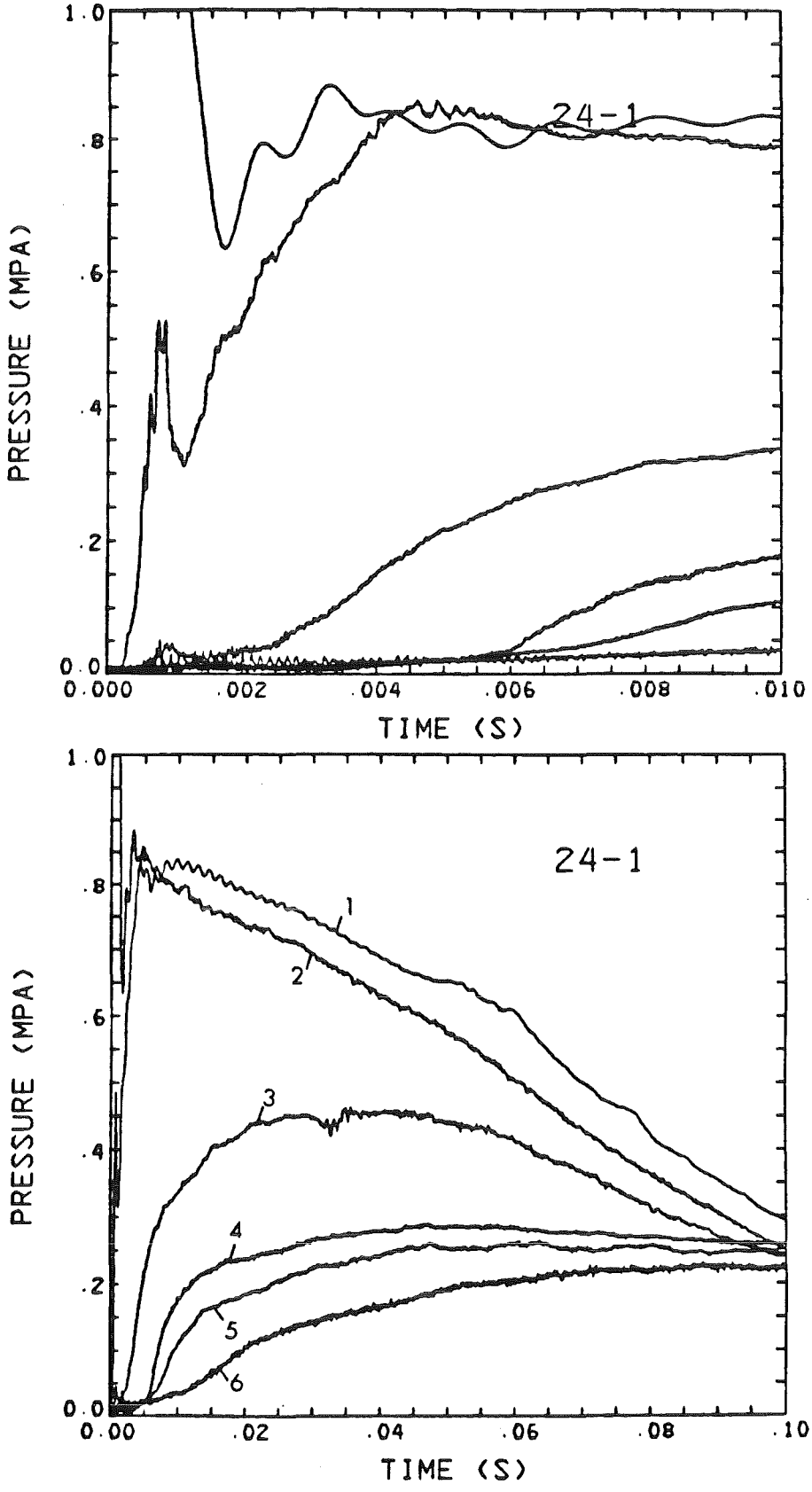

Fig. 33. Pressures in Test 24.

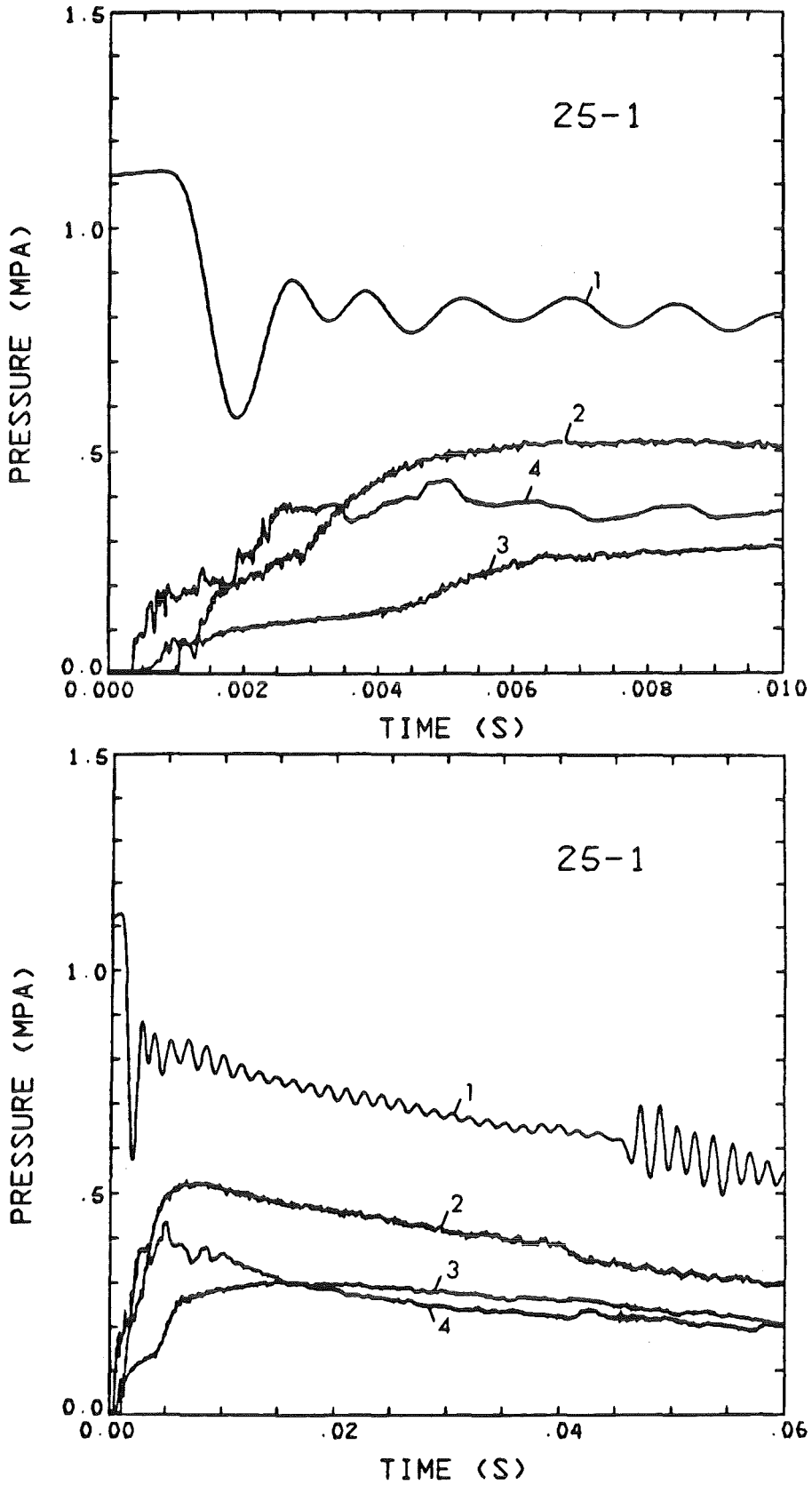

Fig. 34. Pressures in Test 25.

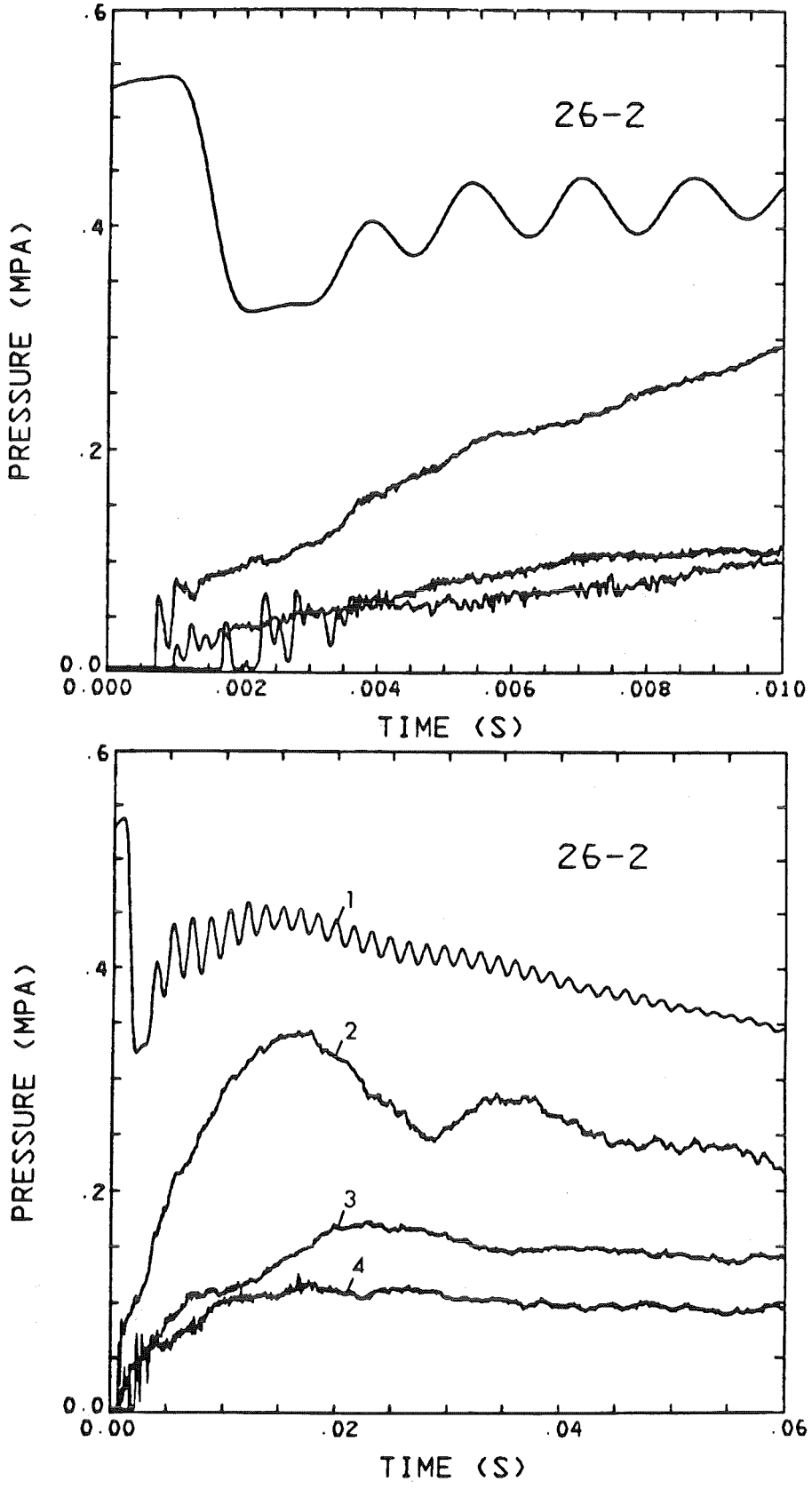

Fig. 35. Pressures in Test 26.

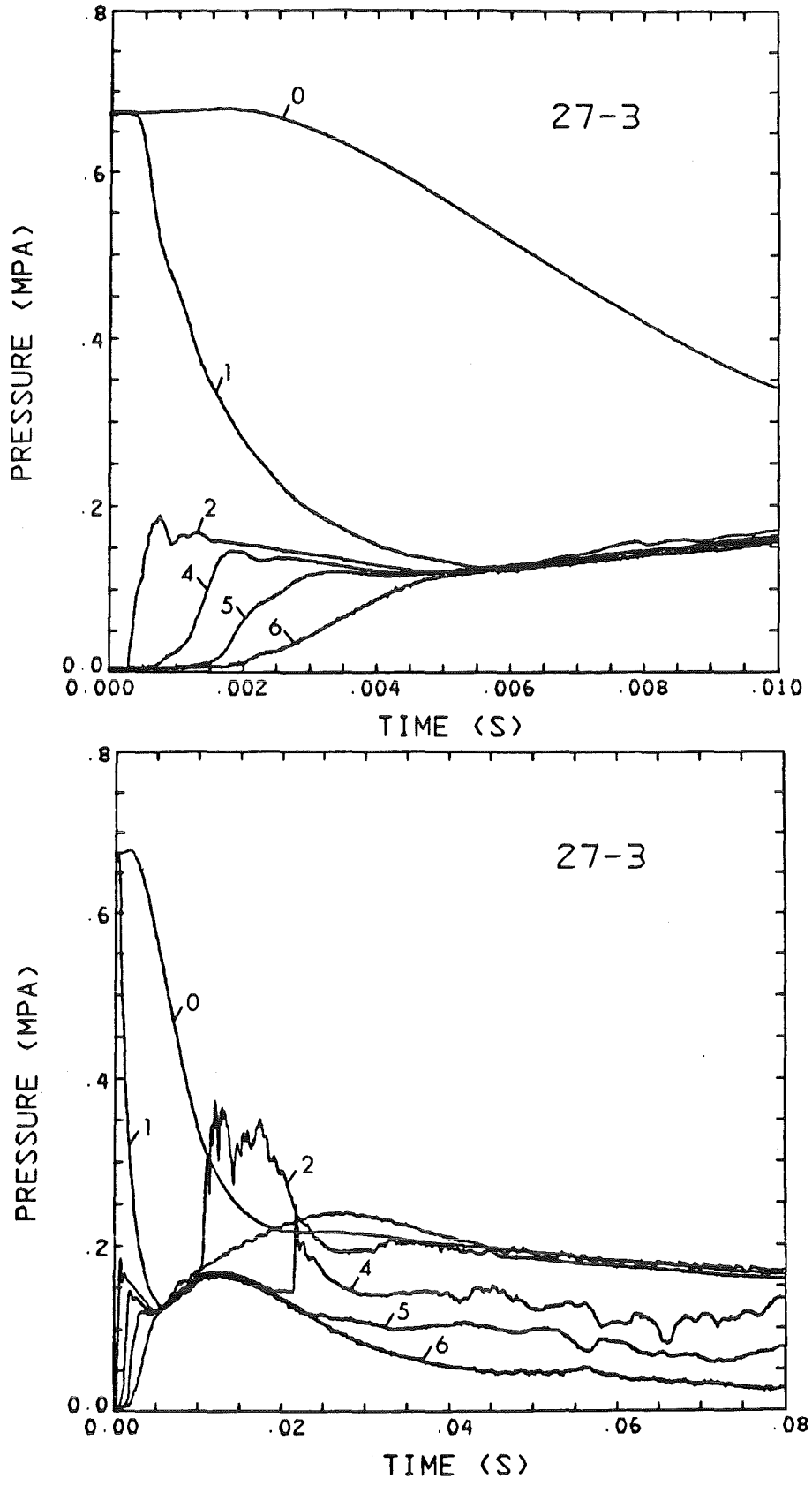

Fig. 36. Pressures in Test 27.

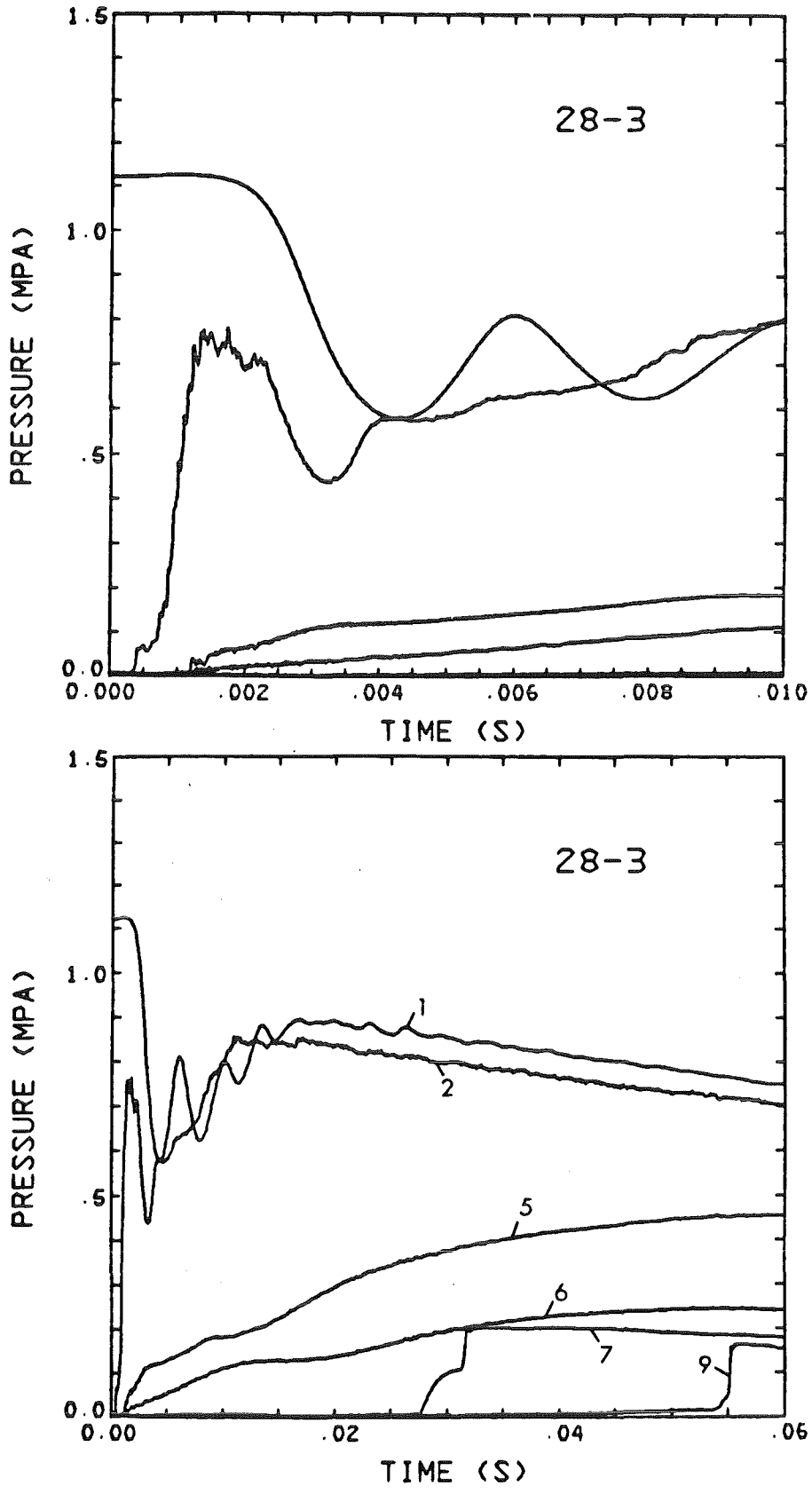

Fig. 37. Pressures in Test 28.

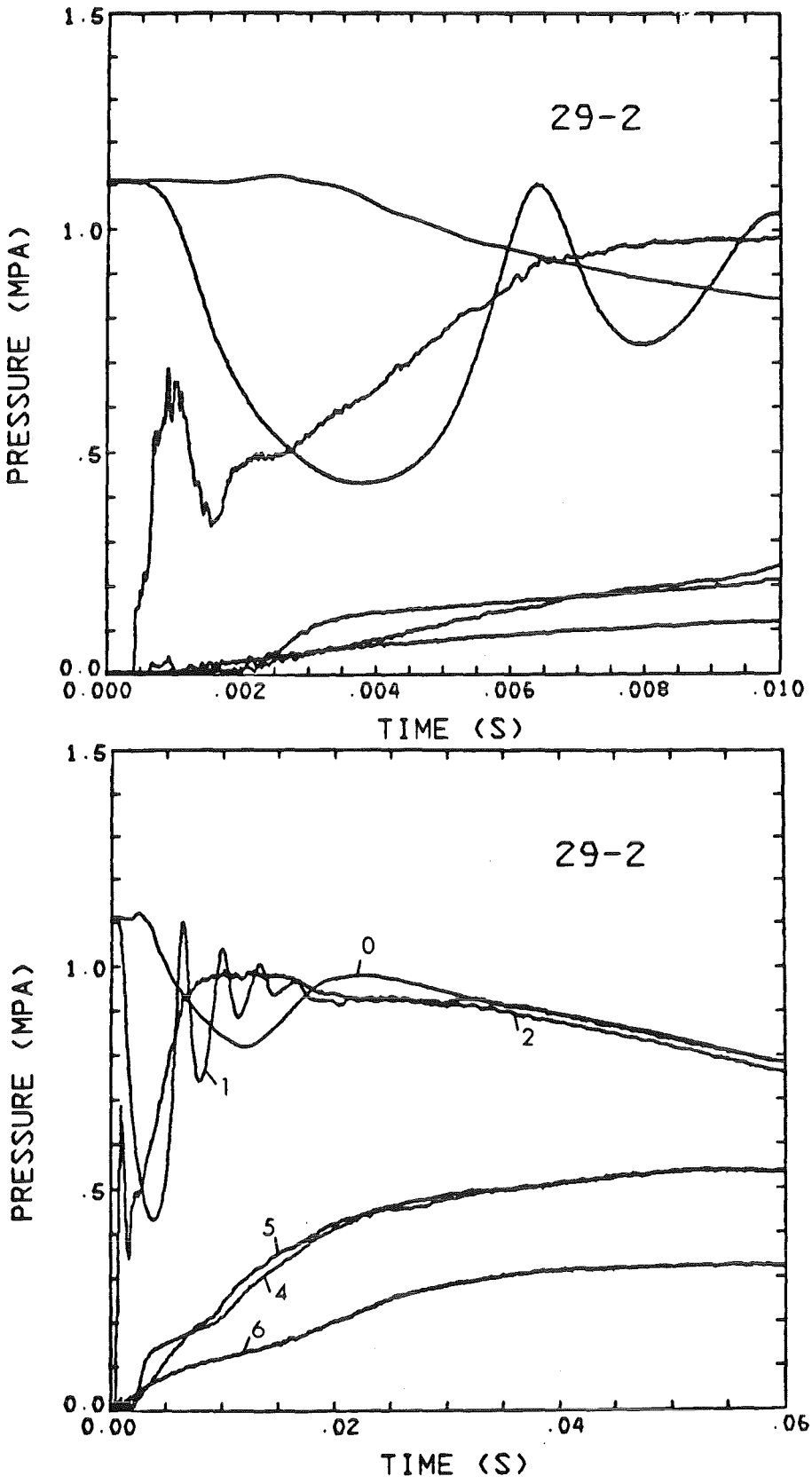

Fig. 38. Pressures in Test 29.

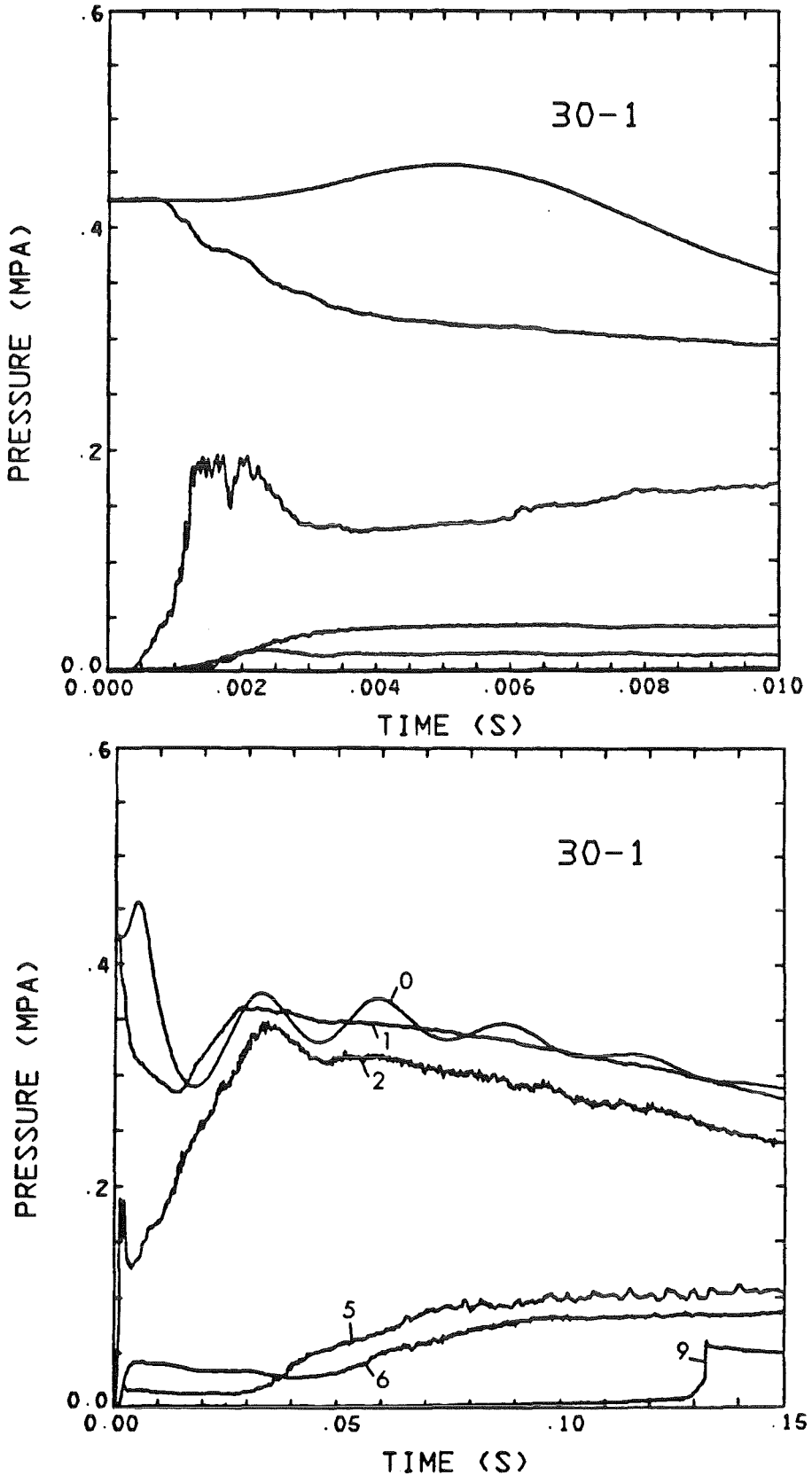

Fig. 39. Pressures in Test 30.

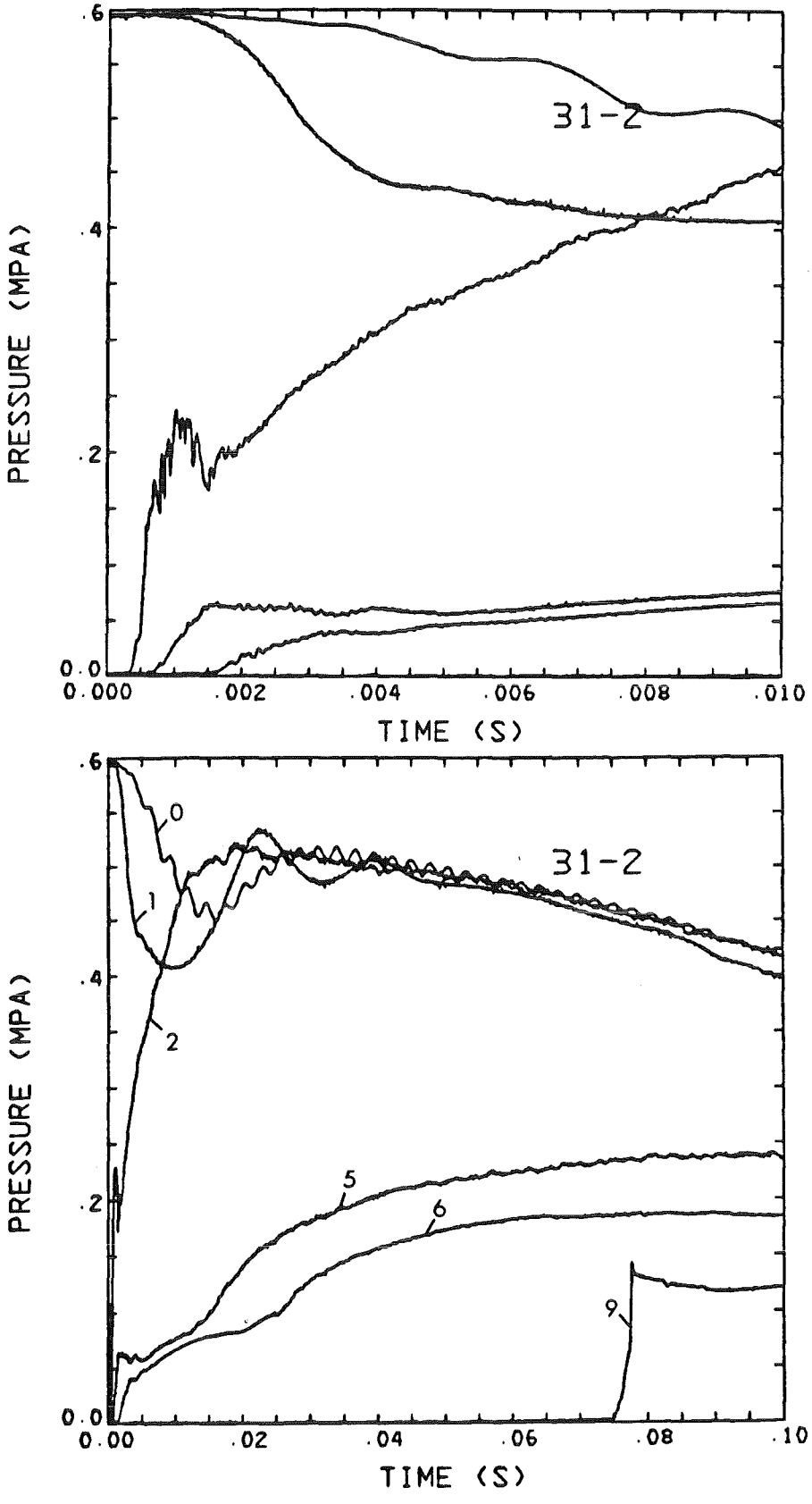

Fig. 40. Pressures in Test 31.

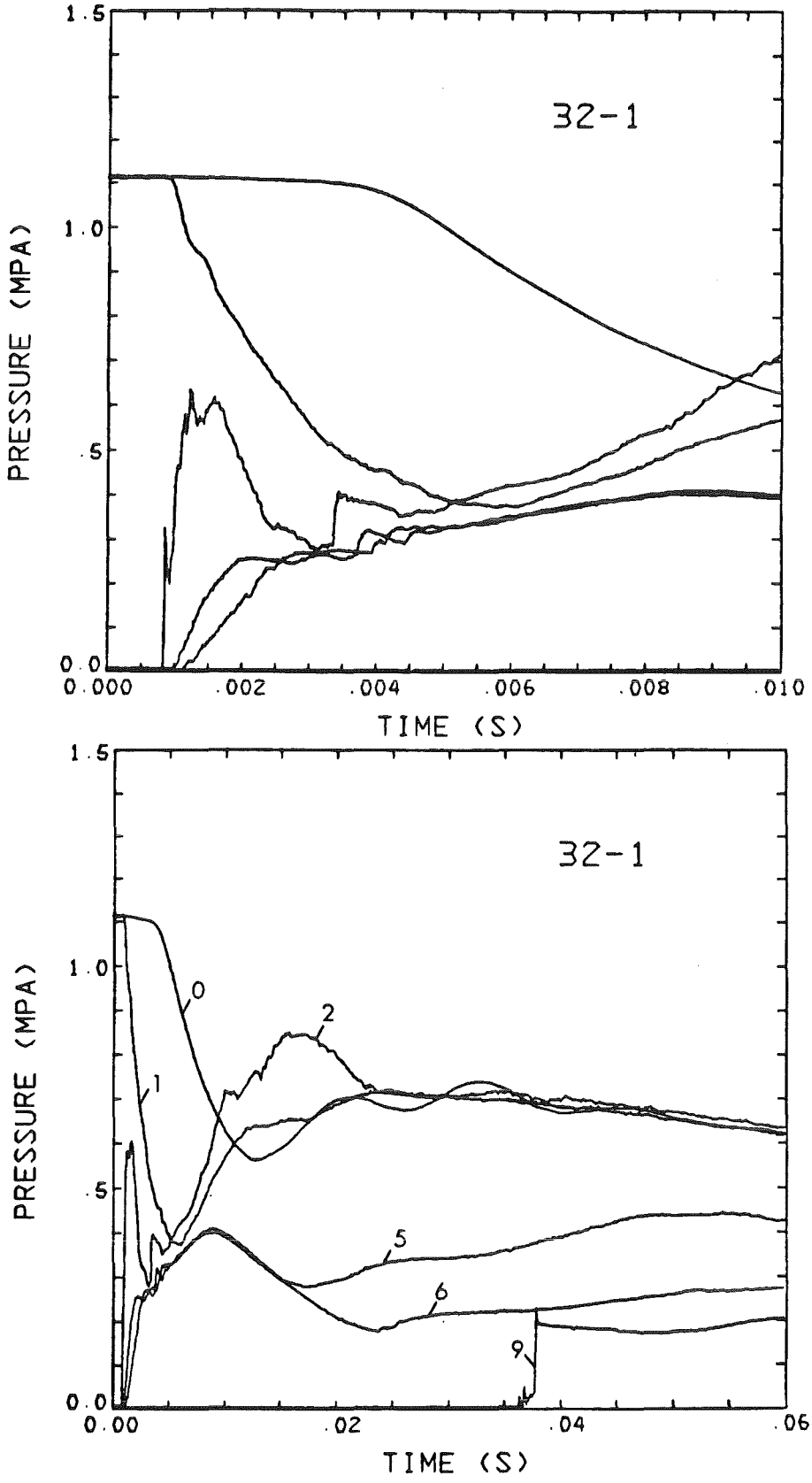

Fig. 41. Pressures in Test 32.

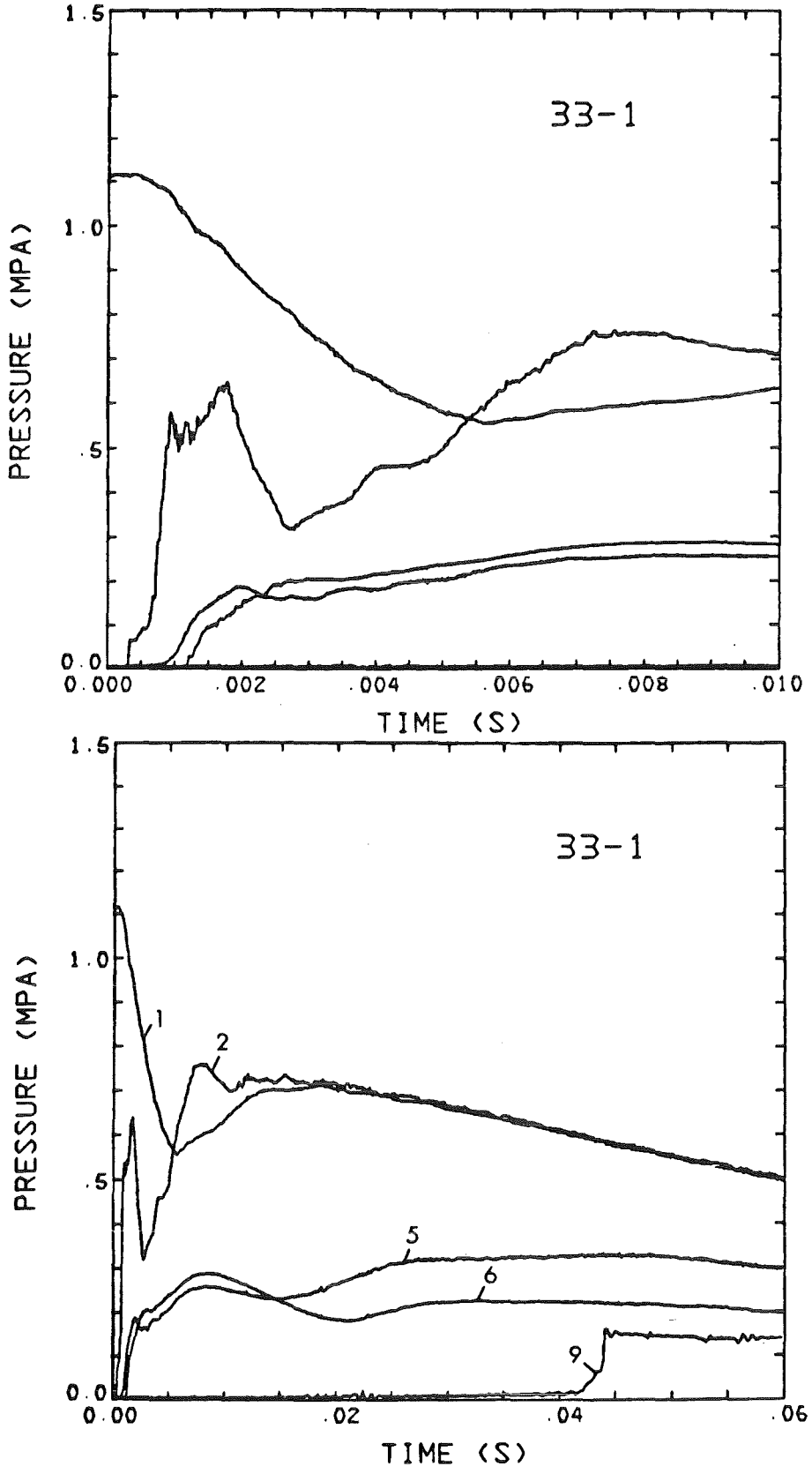

Fig. 42. Pressures in Test 33.

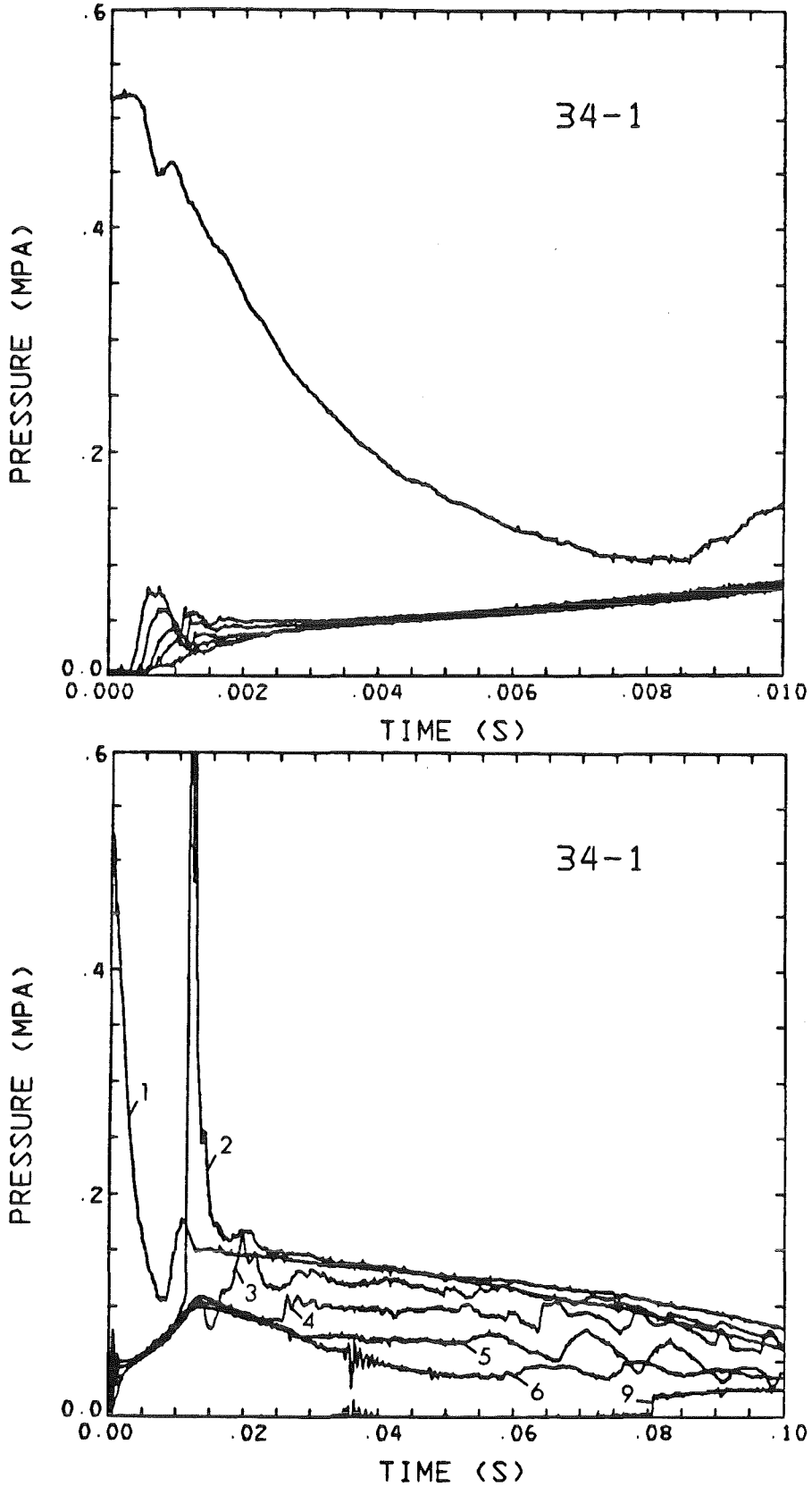

Fig. 43. Pressures in Test 34.

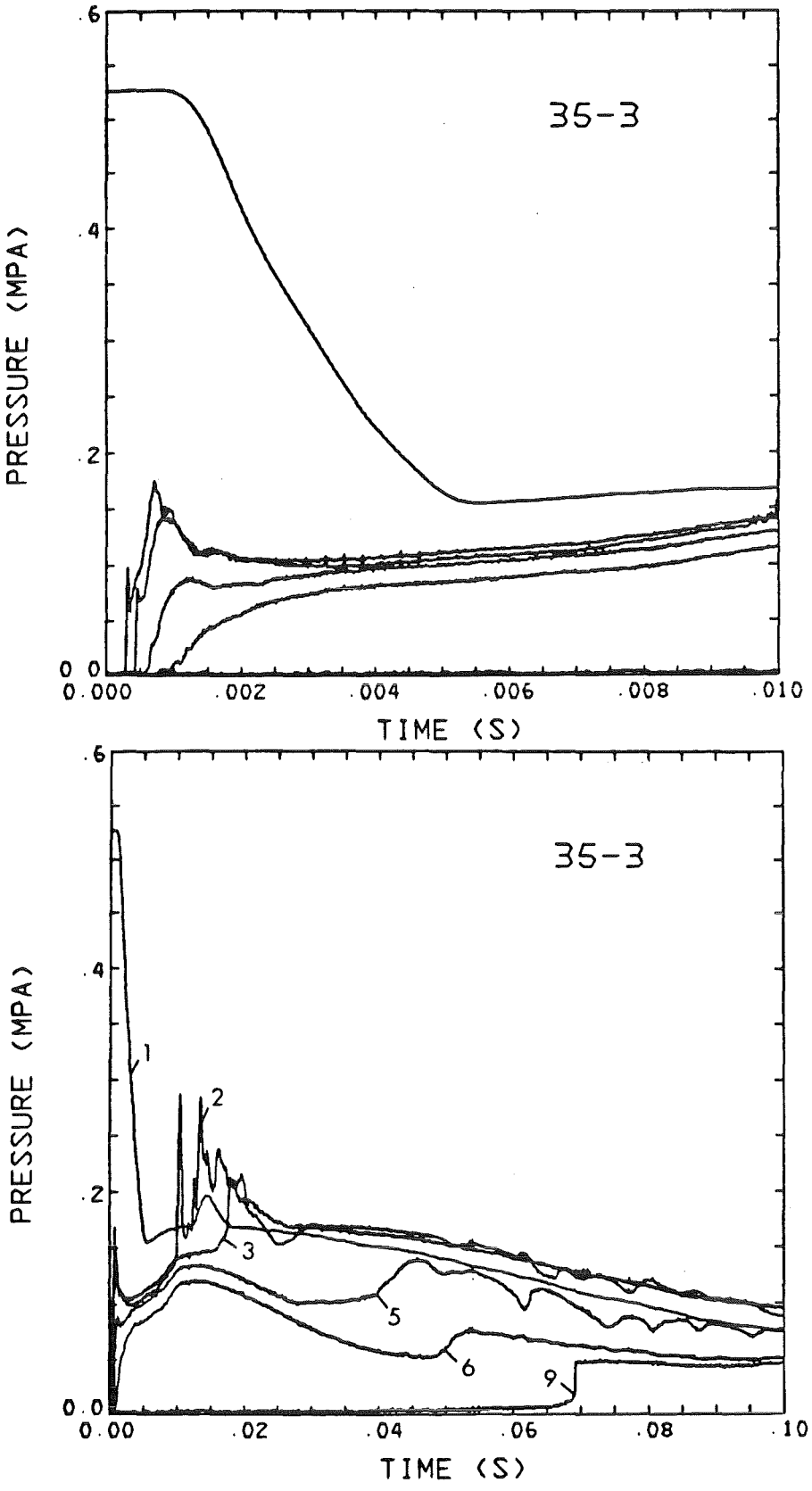

Fig. 44. Pressures in Test 35.

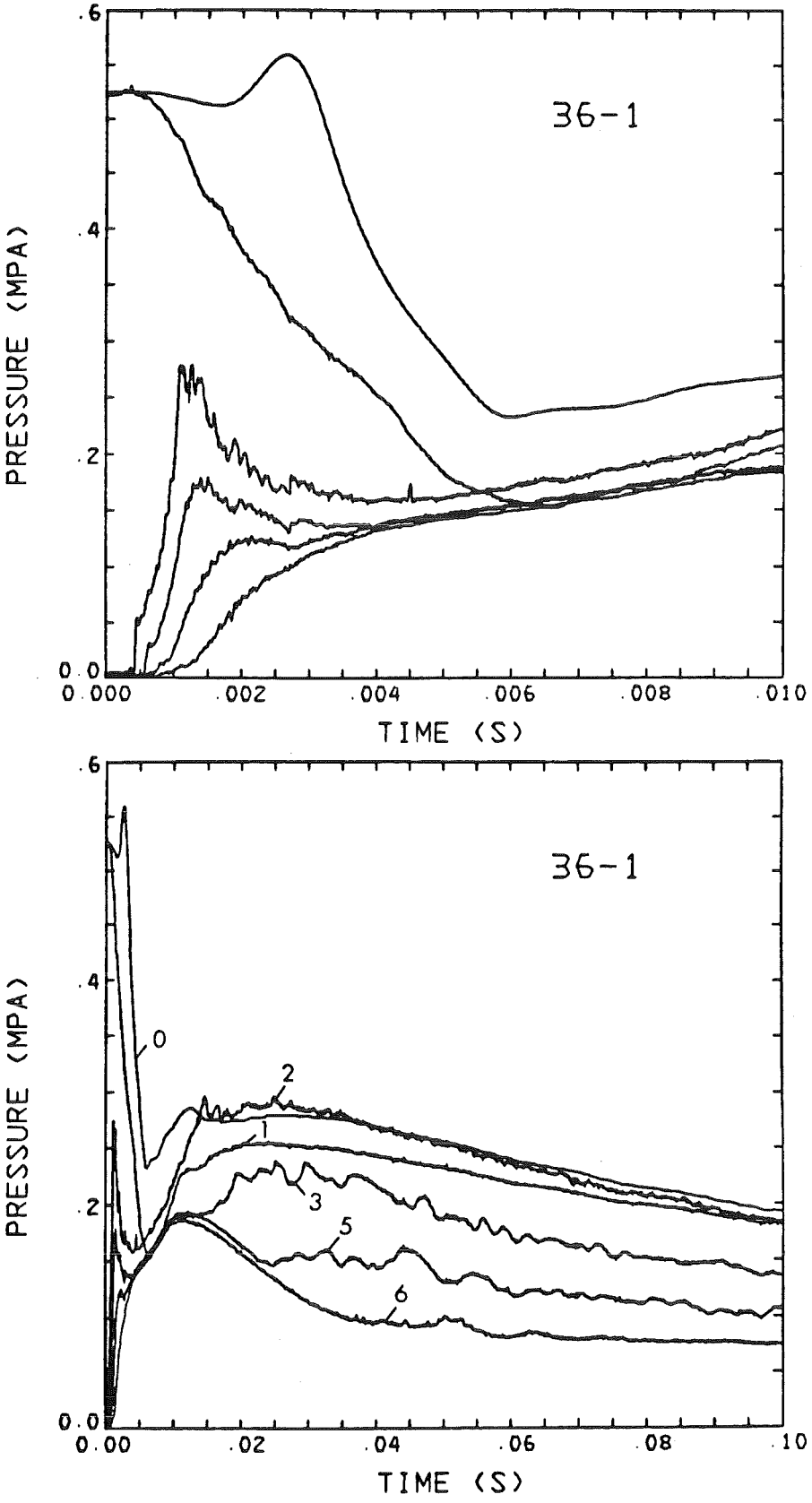

Fig. 45. Pressures in Test 36.

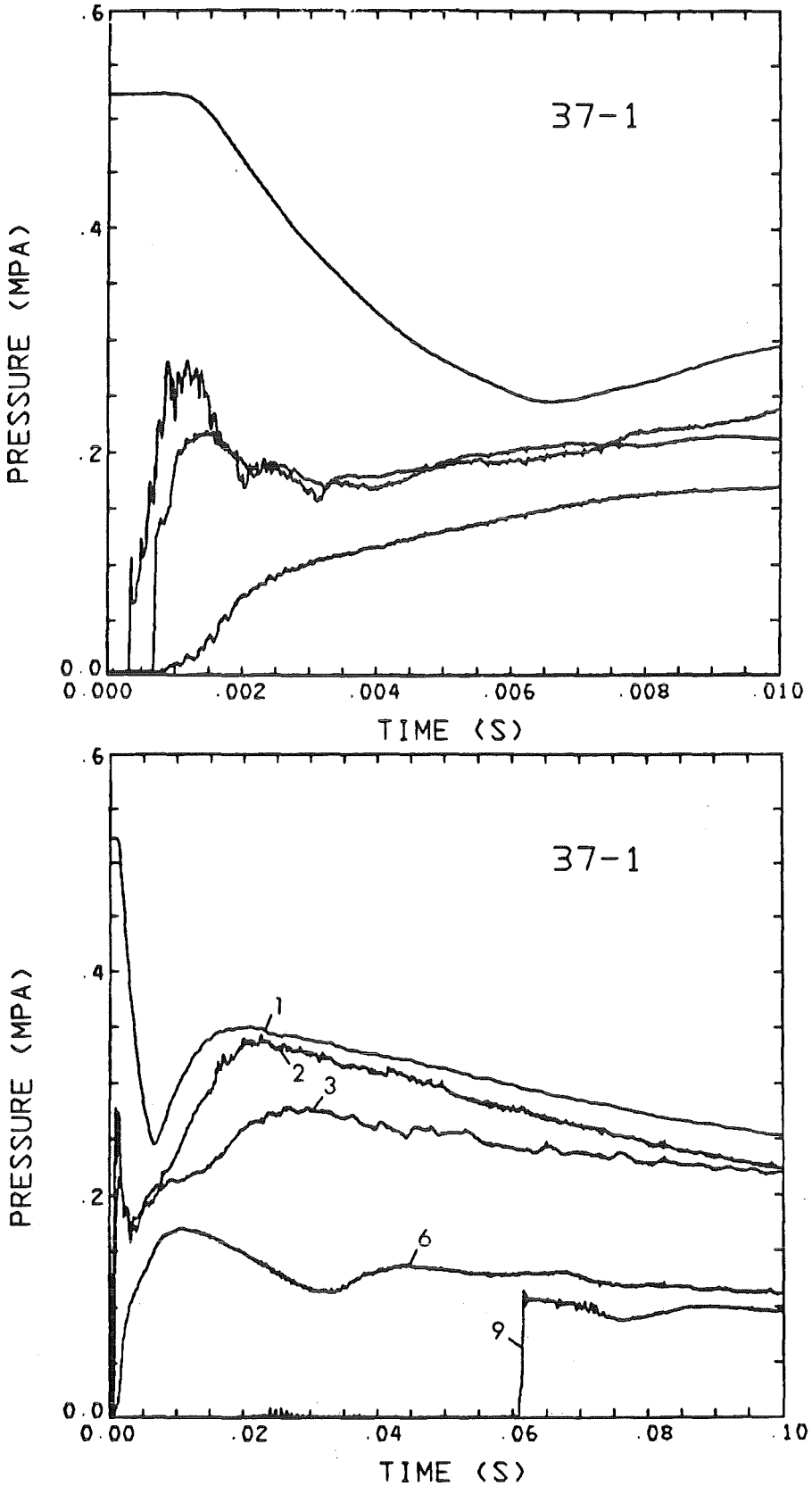

Fig. 46. Pressures in Test 37.

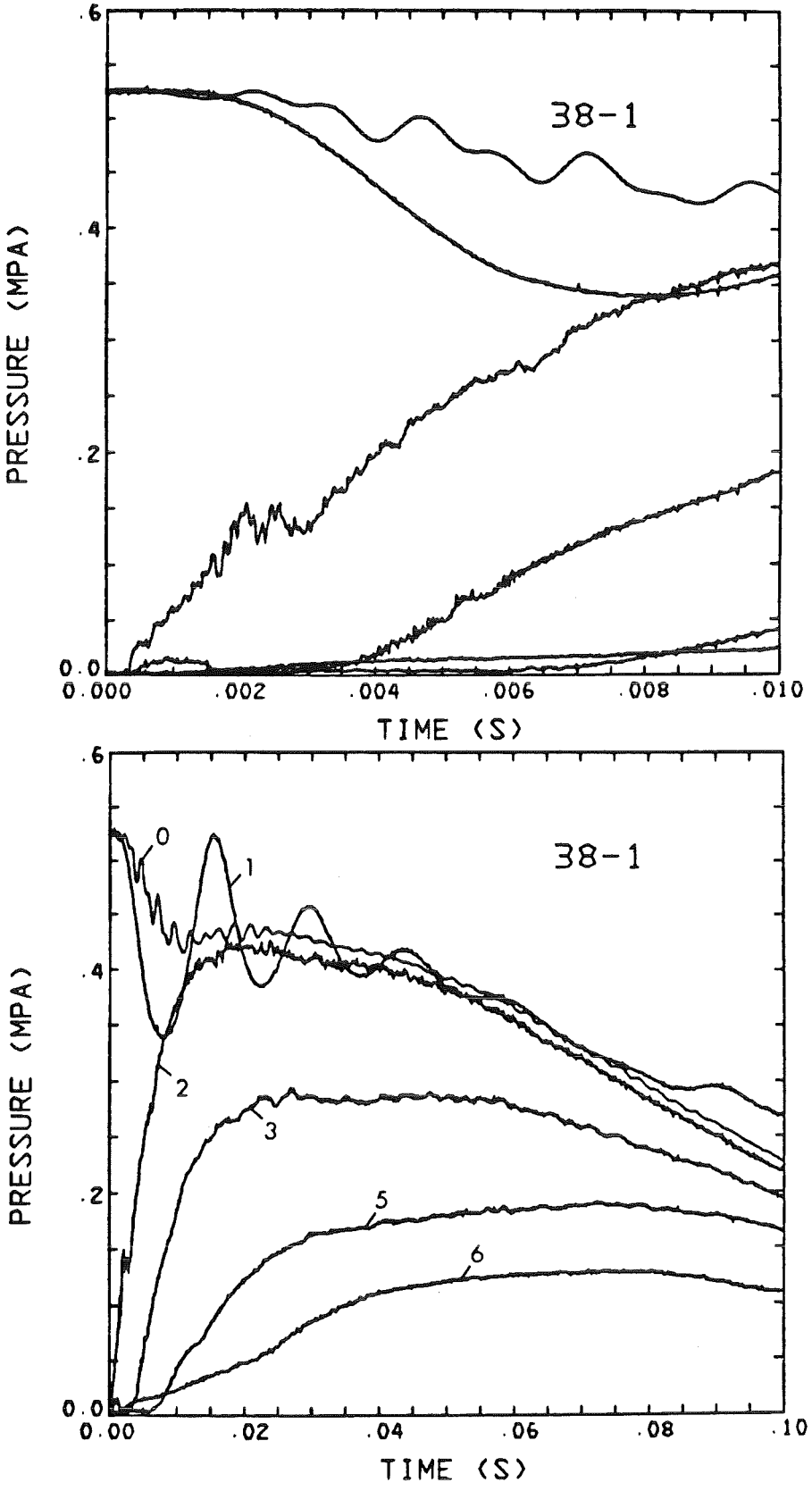

Fig. 47. Pressures in Test 38.

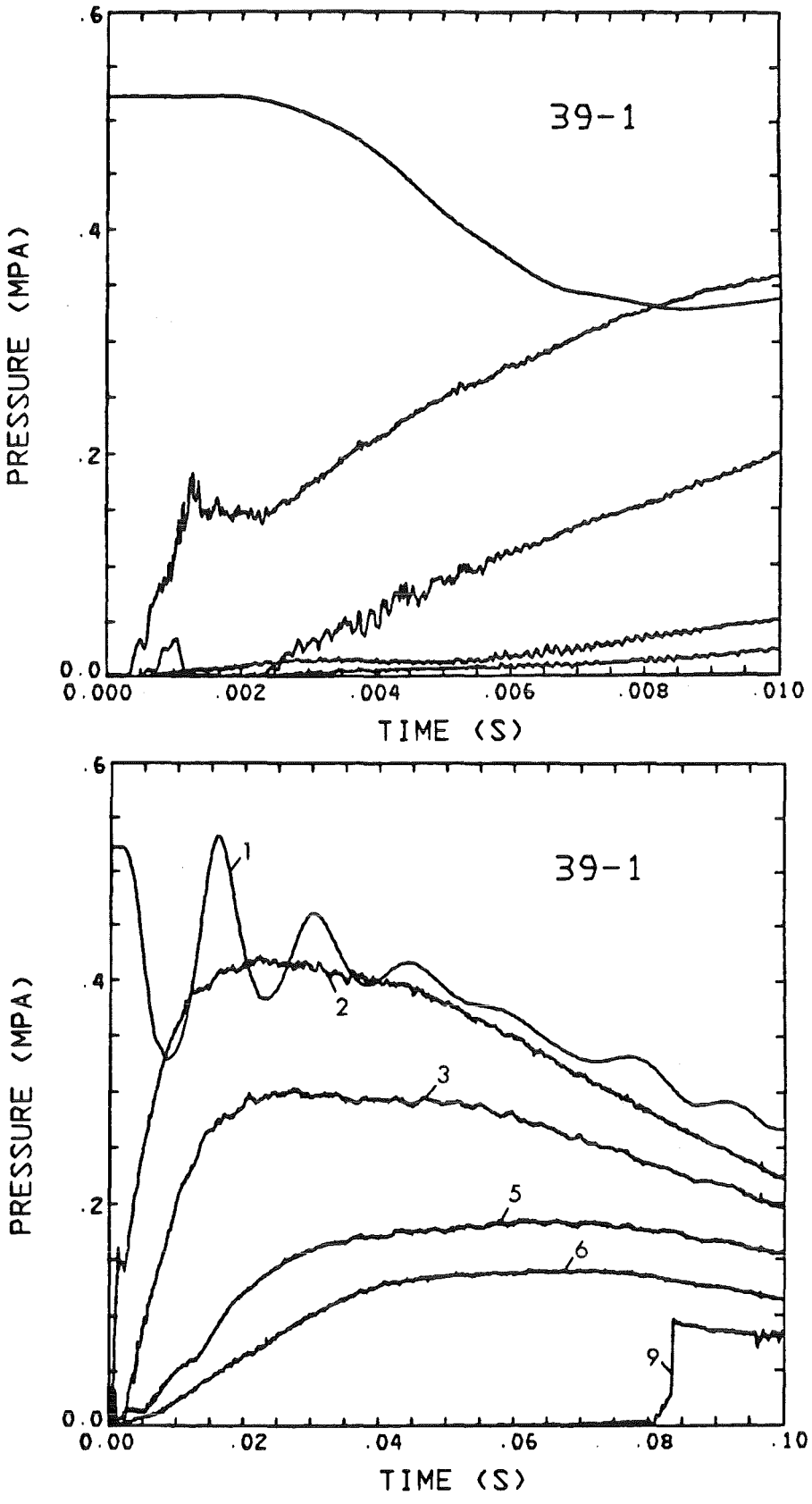

Fig. 48. Pressures in Test 39.

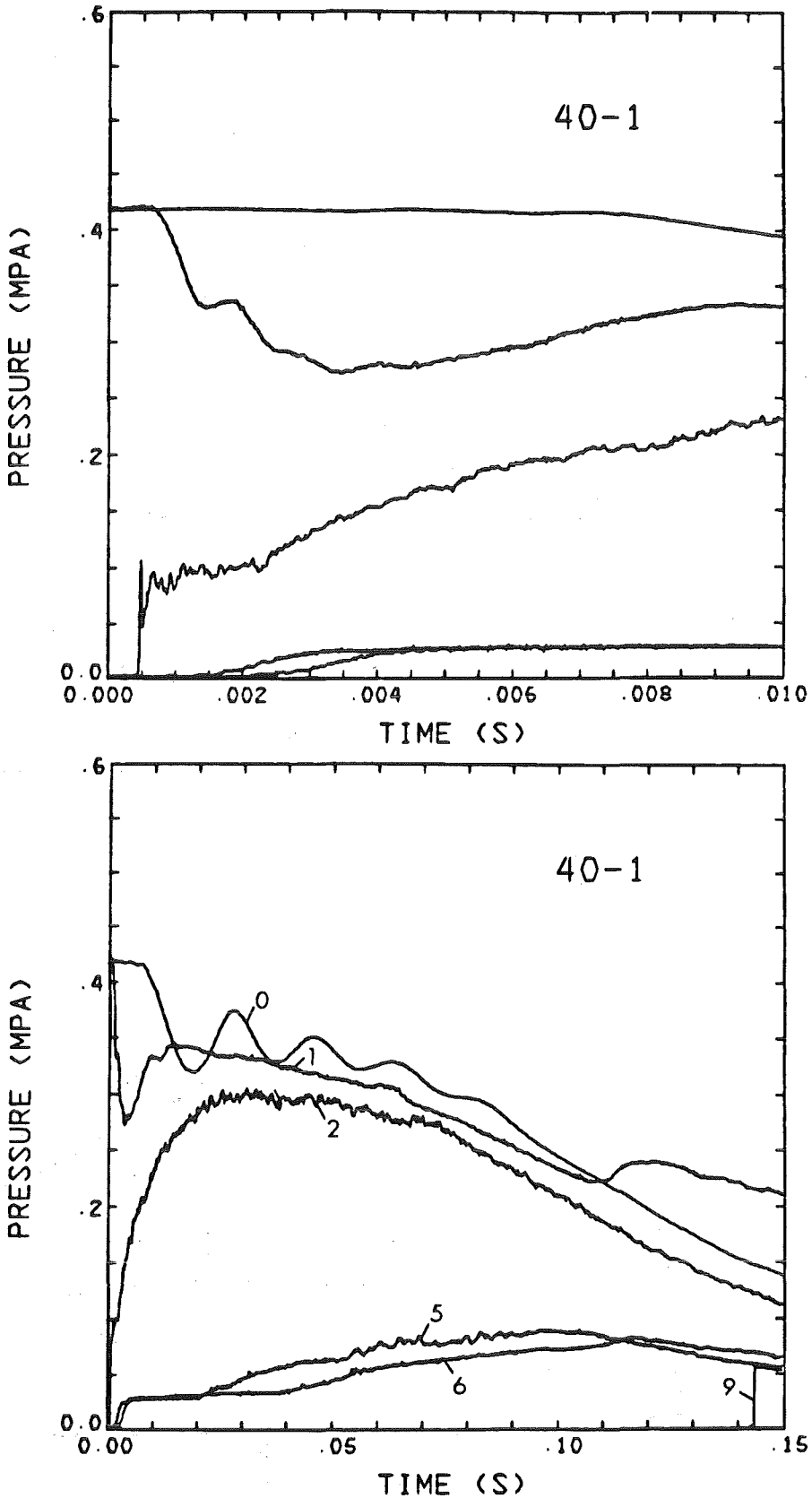

Fig. 49. Pressures in Test 40.

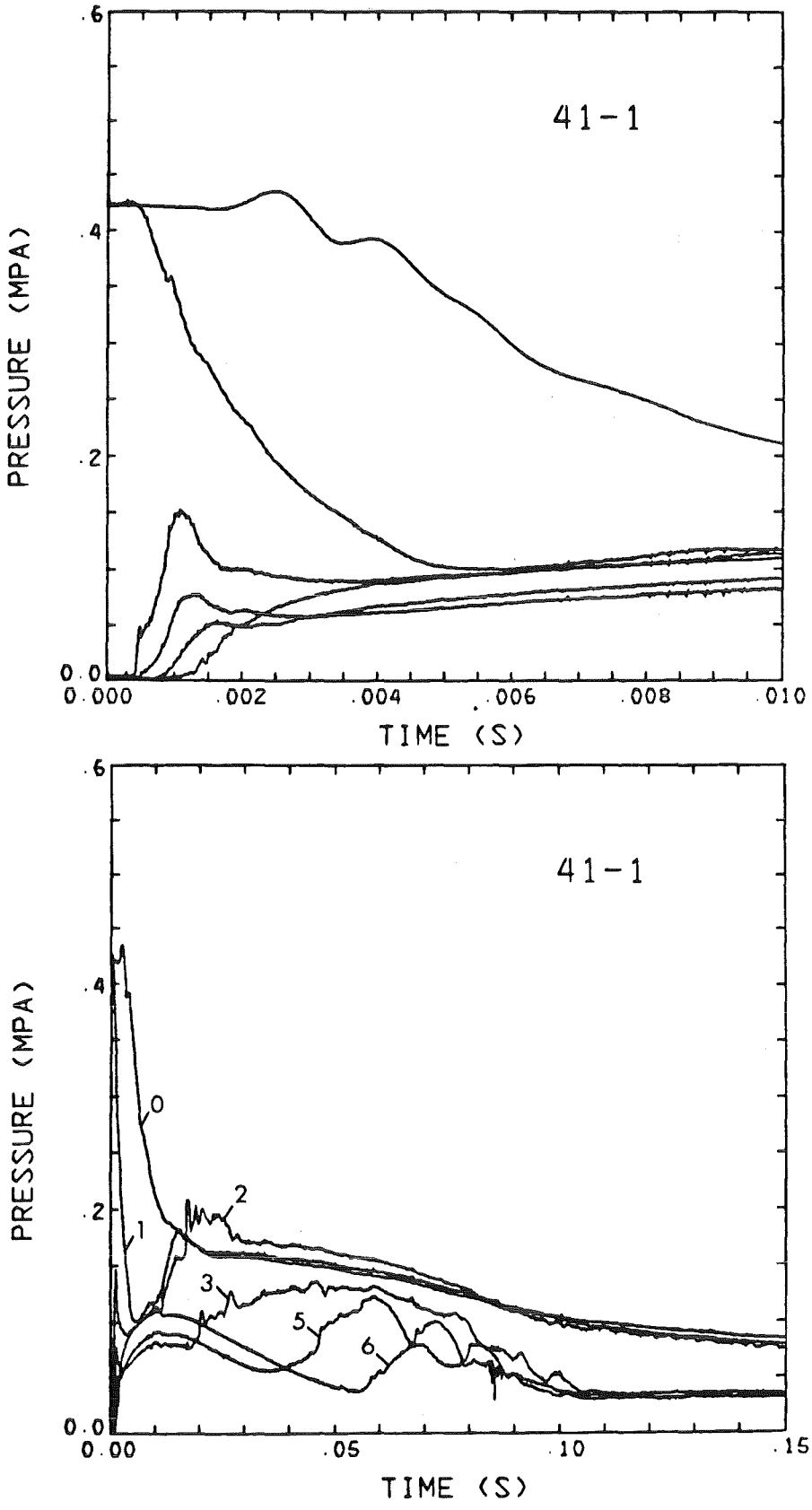

Fig. 50. Pressures in Test 41.

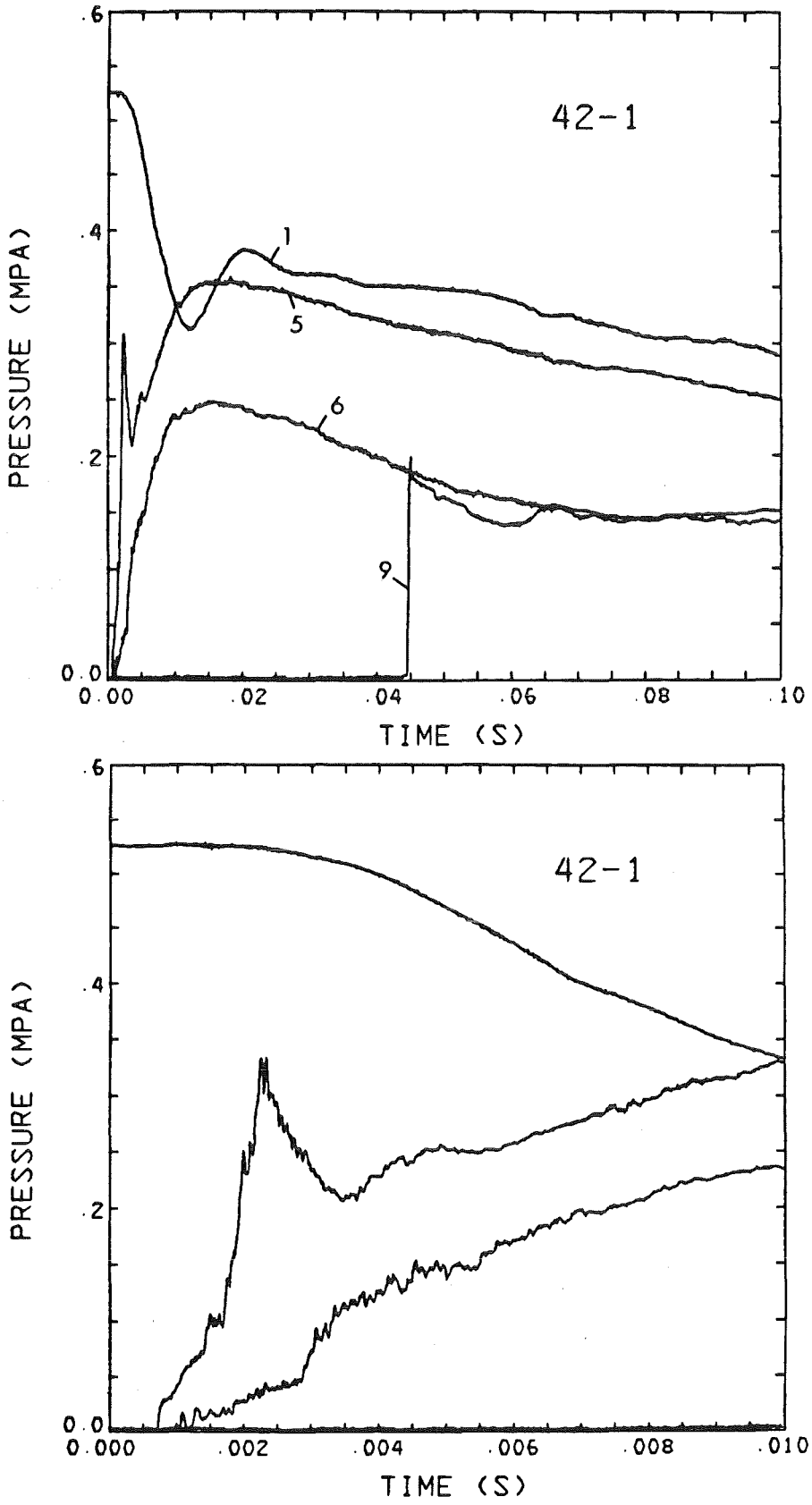

Fig. 51. Pressures in Test 42.

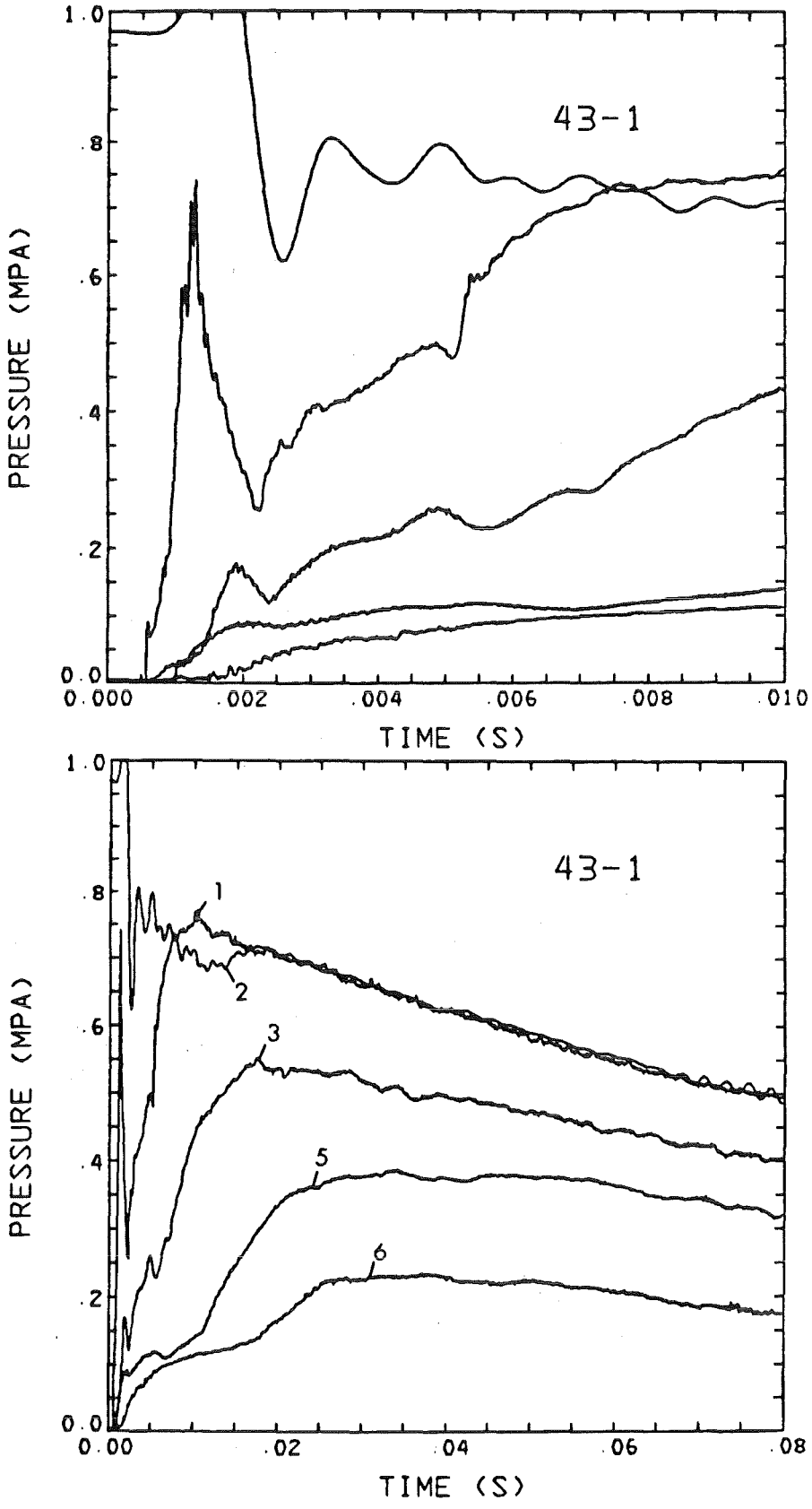

Fig. 52. Pressures in Test 43.

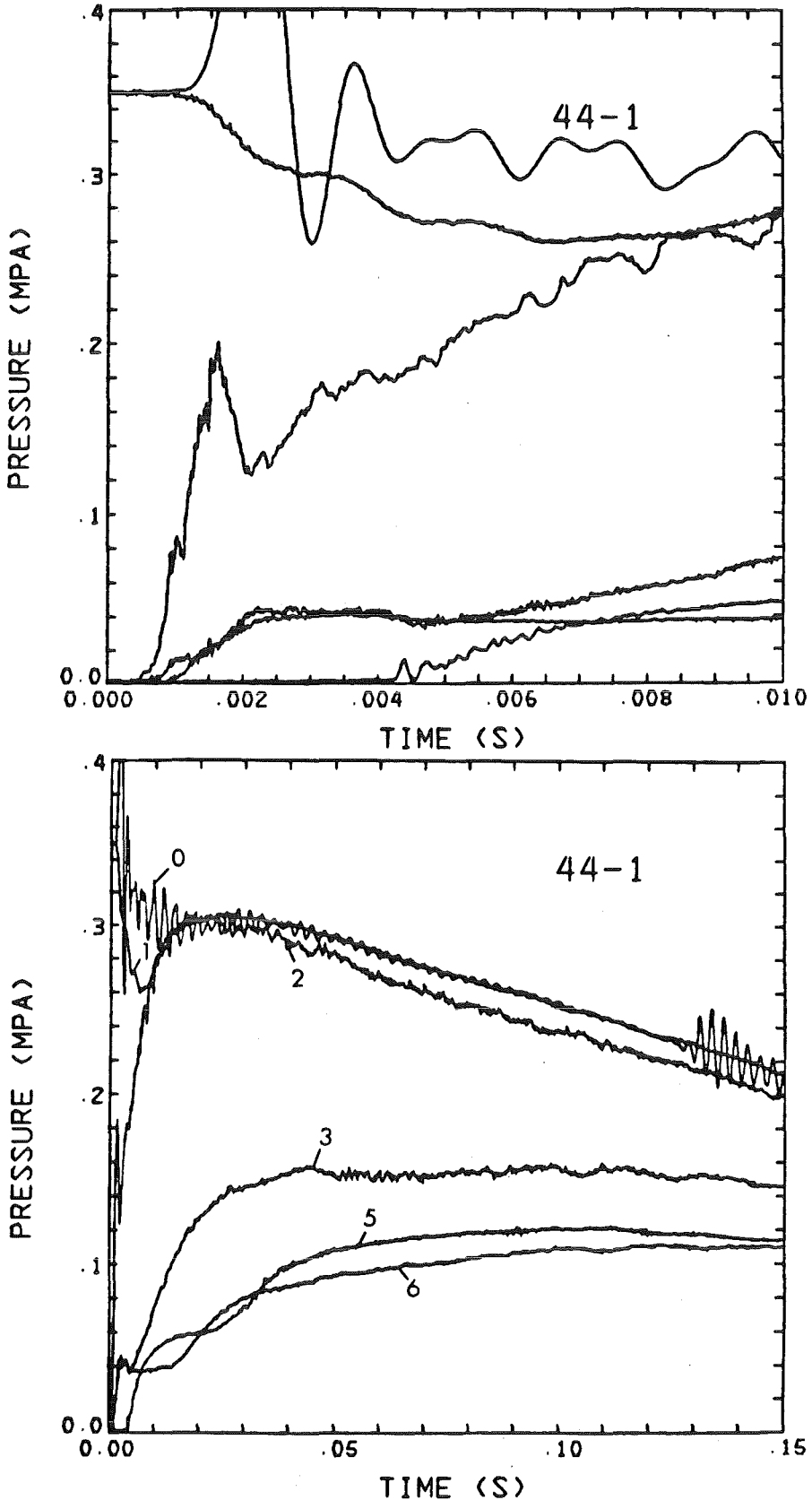

Fig. 53. Pressures in Test 44.

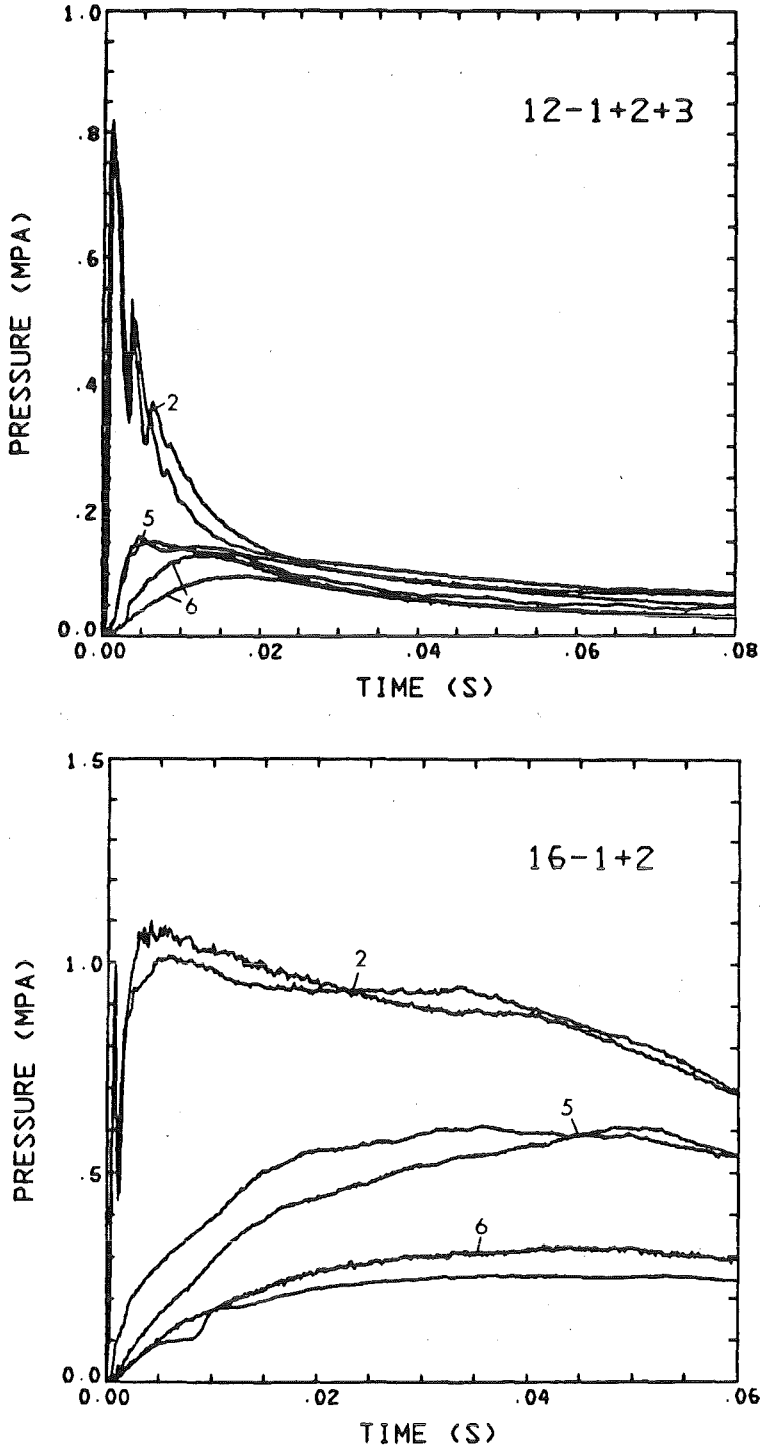

Fig. 54. Reproducibility of pressures in Test 12 (3 runs) and Test 16 (2 runs).

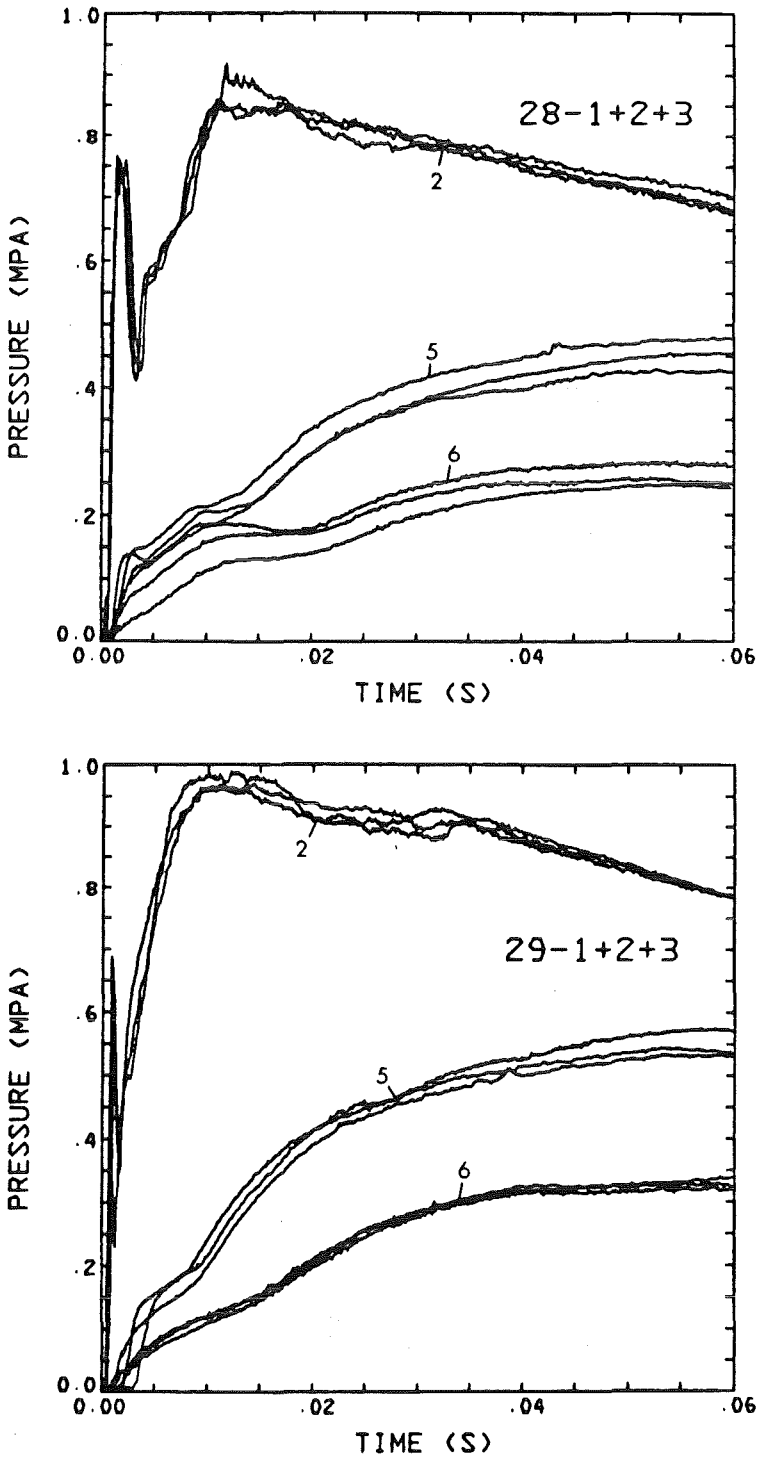

Fig. 55. Reproducibility of pressures in Test 28 and 29 (3 runs each).

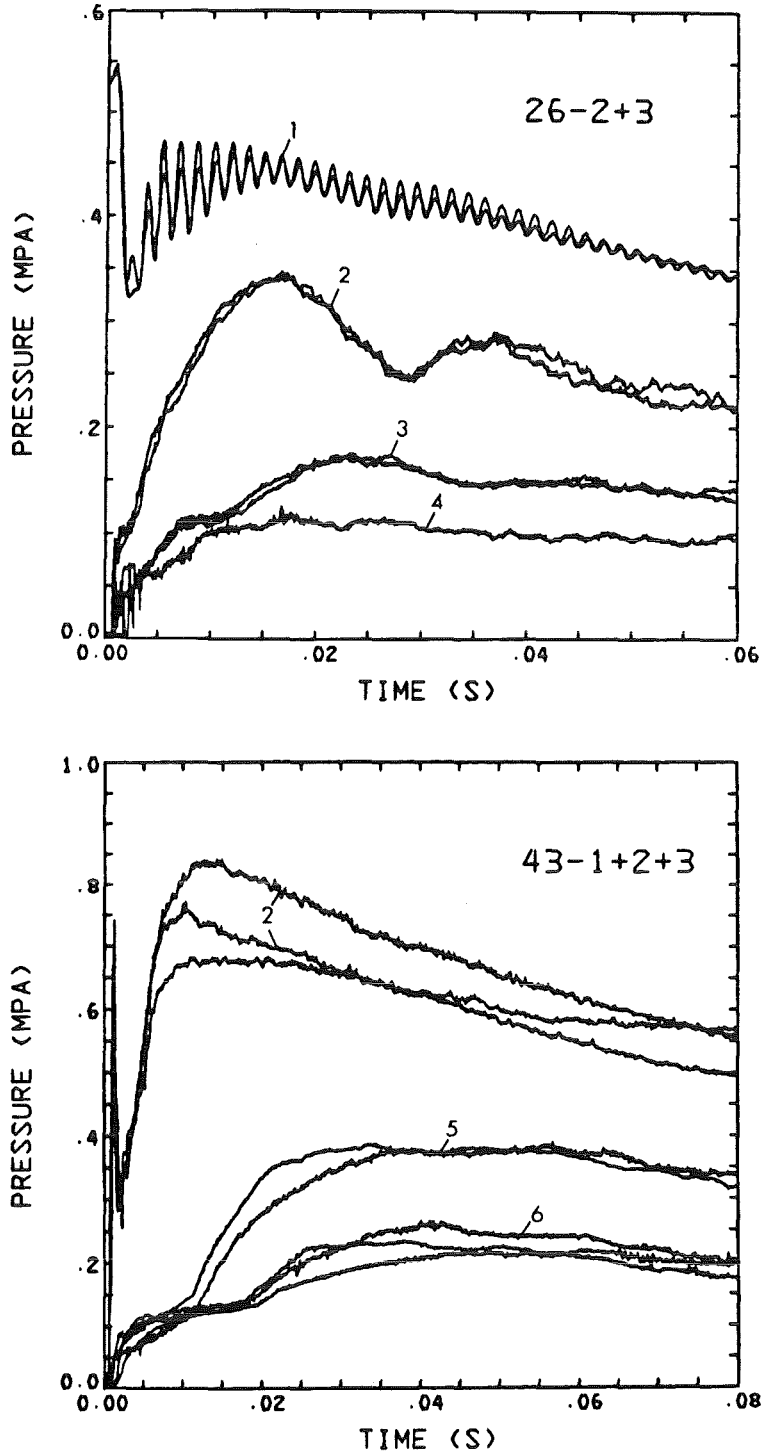

Fig. 56. Reproducibility of pressures in Test 26 (2 runs) and Test 43 (3 runs).

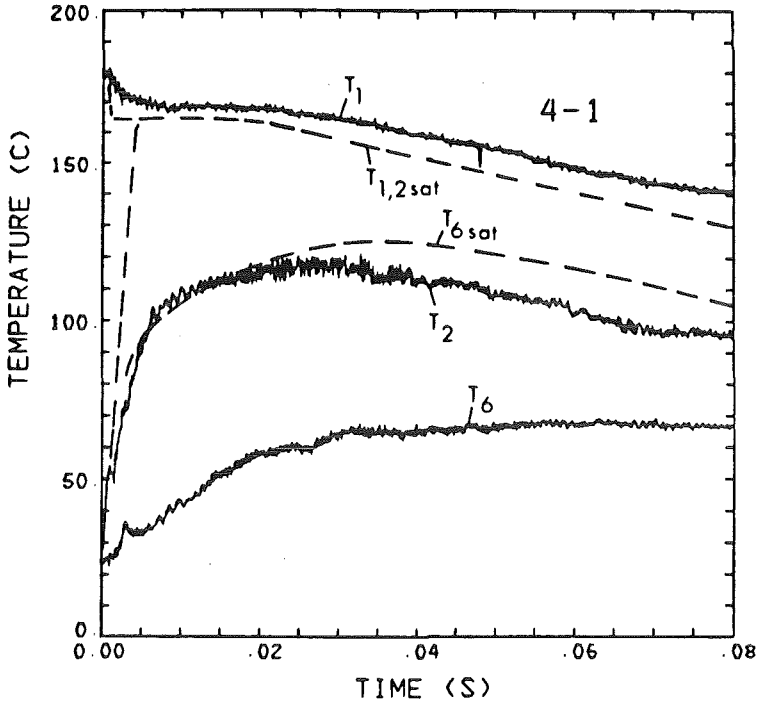

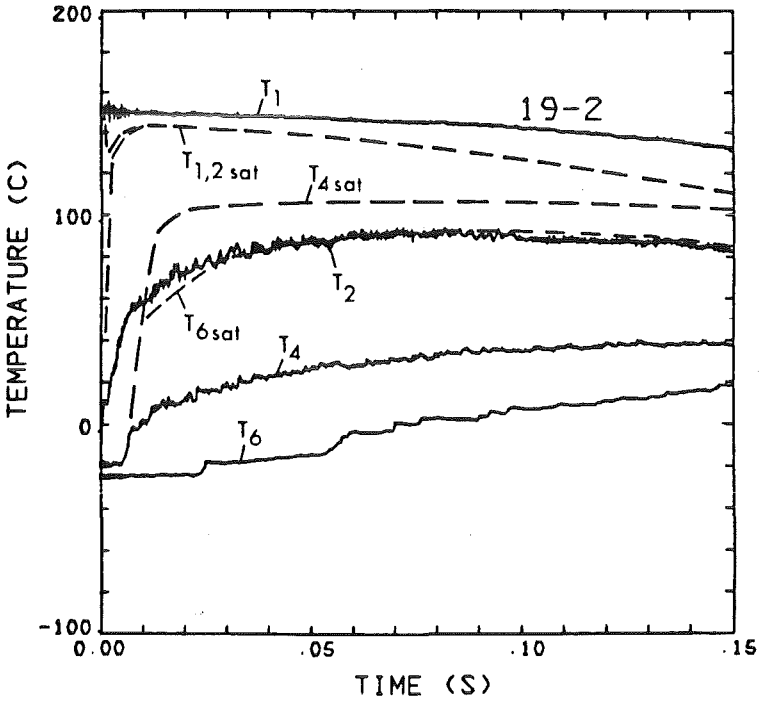

Fig. 57. Comparison of temperatures measured with NANMAC thermocouples and saturation temperatures.

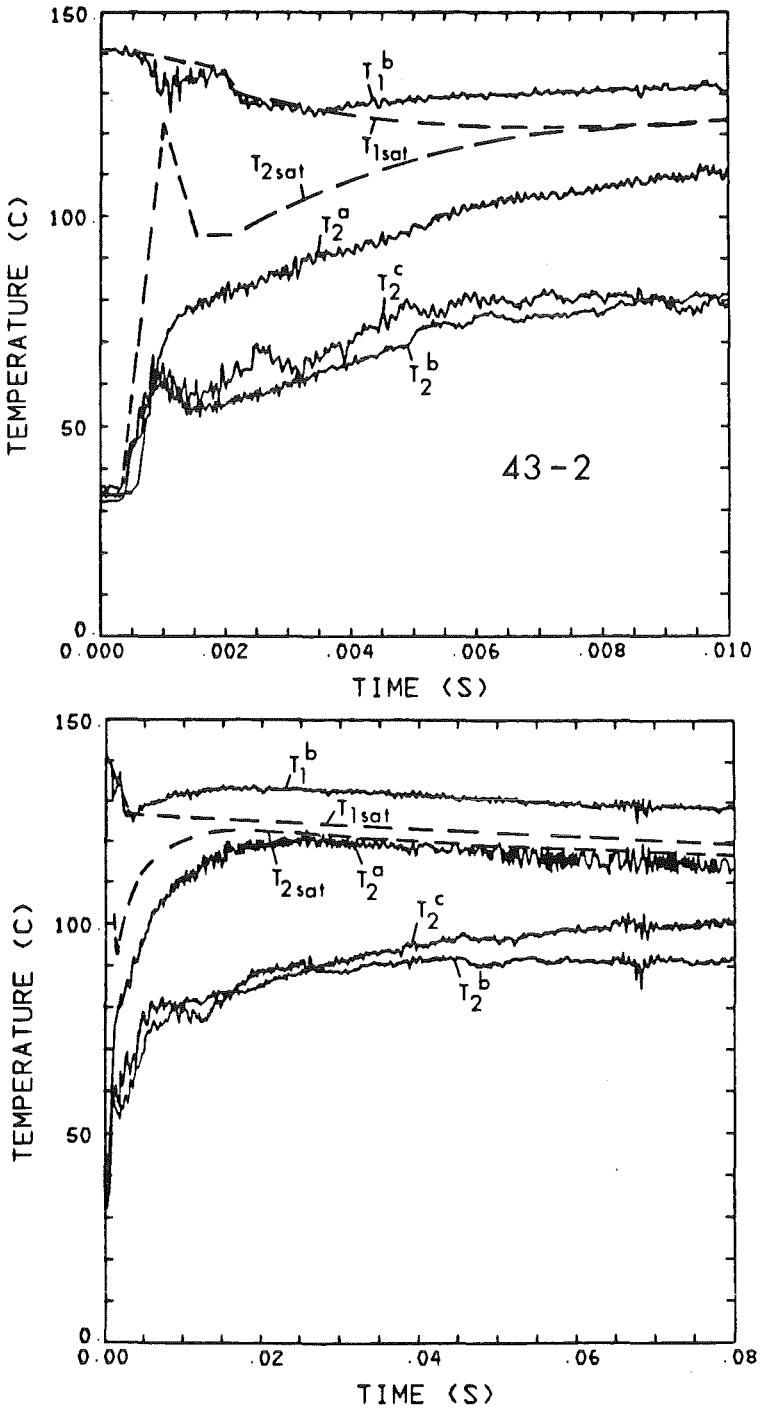

Fig. 58. Comparison of temperatures measured with thin wire thermocouple (a), NANMAC thermocouple, surface parallel with flow (b) and NANMAC thermocouple, surface 45° to flow (c)

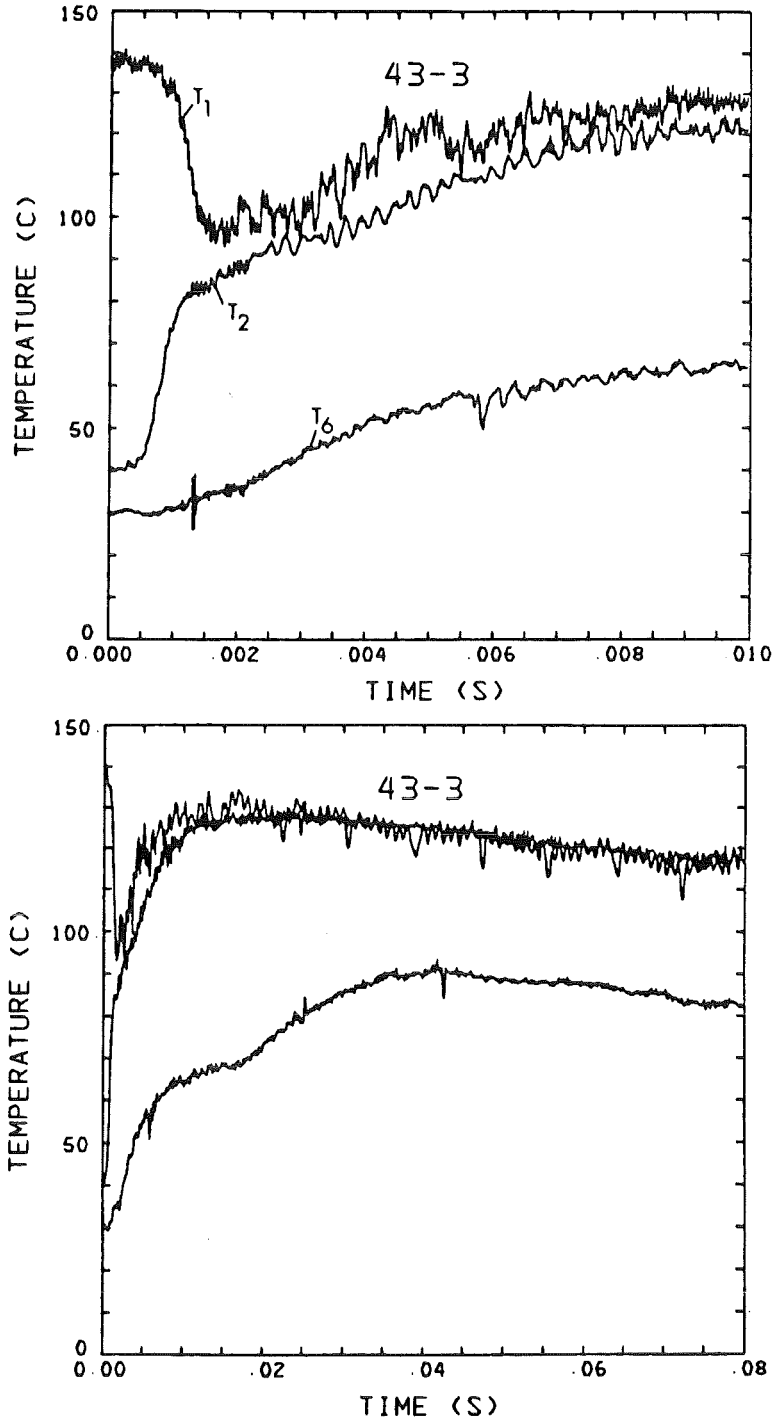

Fig. 59. Temperatures measured with thin wire thermocouple for 10 ms and 80 ms.

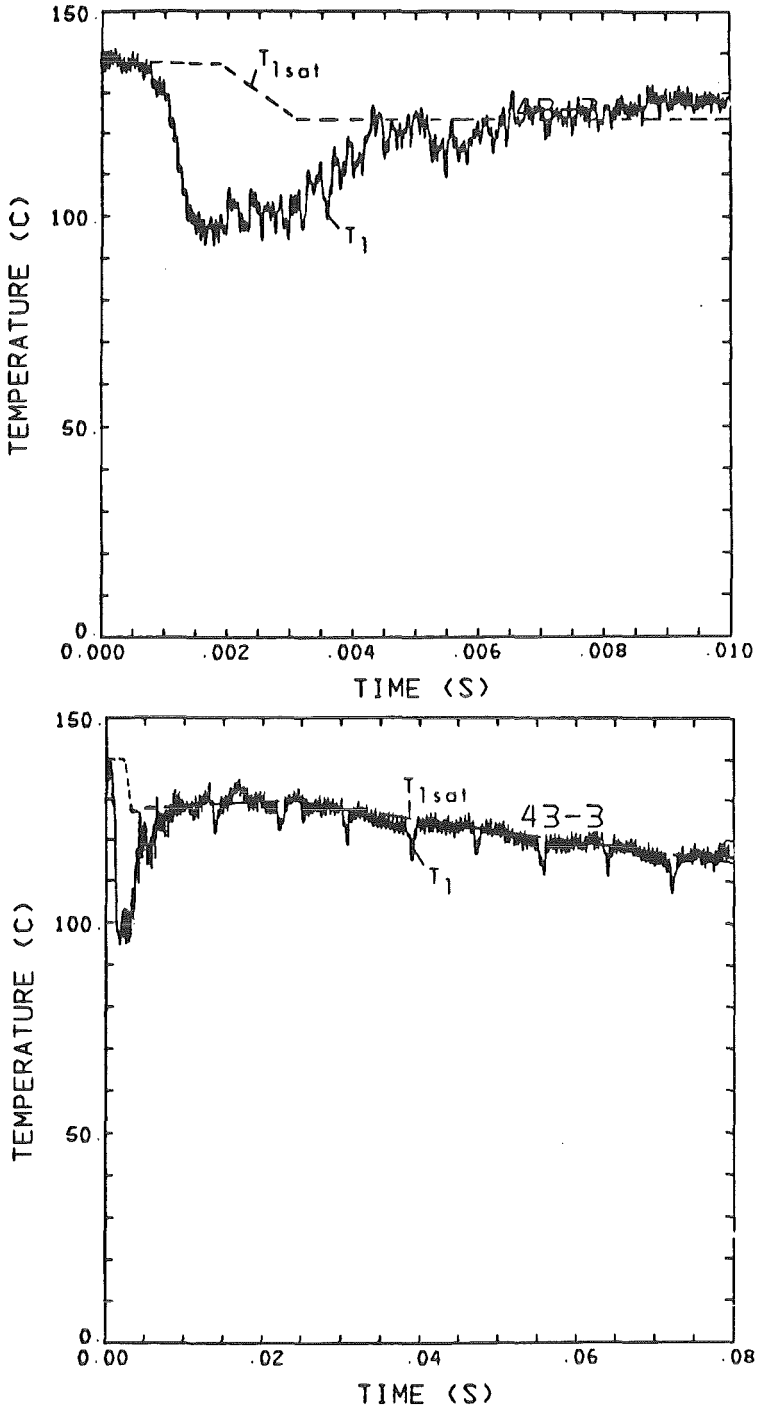

Fig. 60. Comparison of measured temperature and saturation temperature in the core.

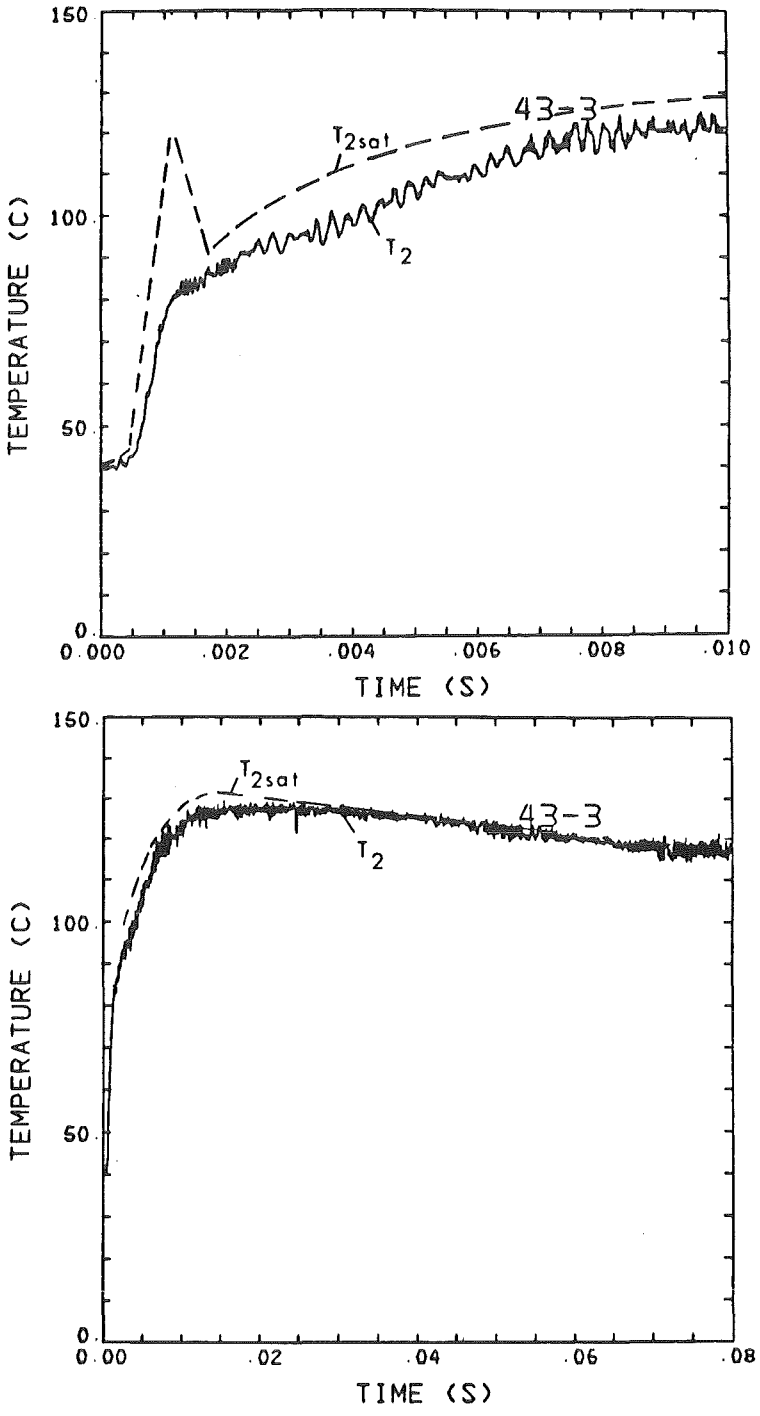

Fig. 61. Comparison of measured temperature and saturation temperature in the lower space.

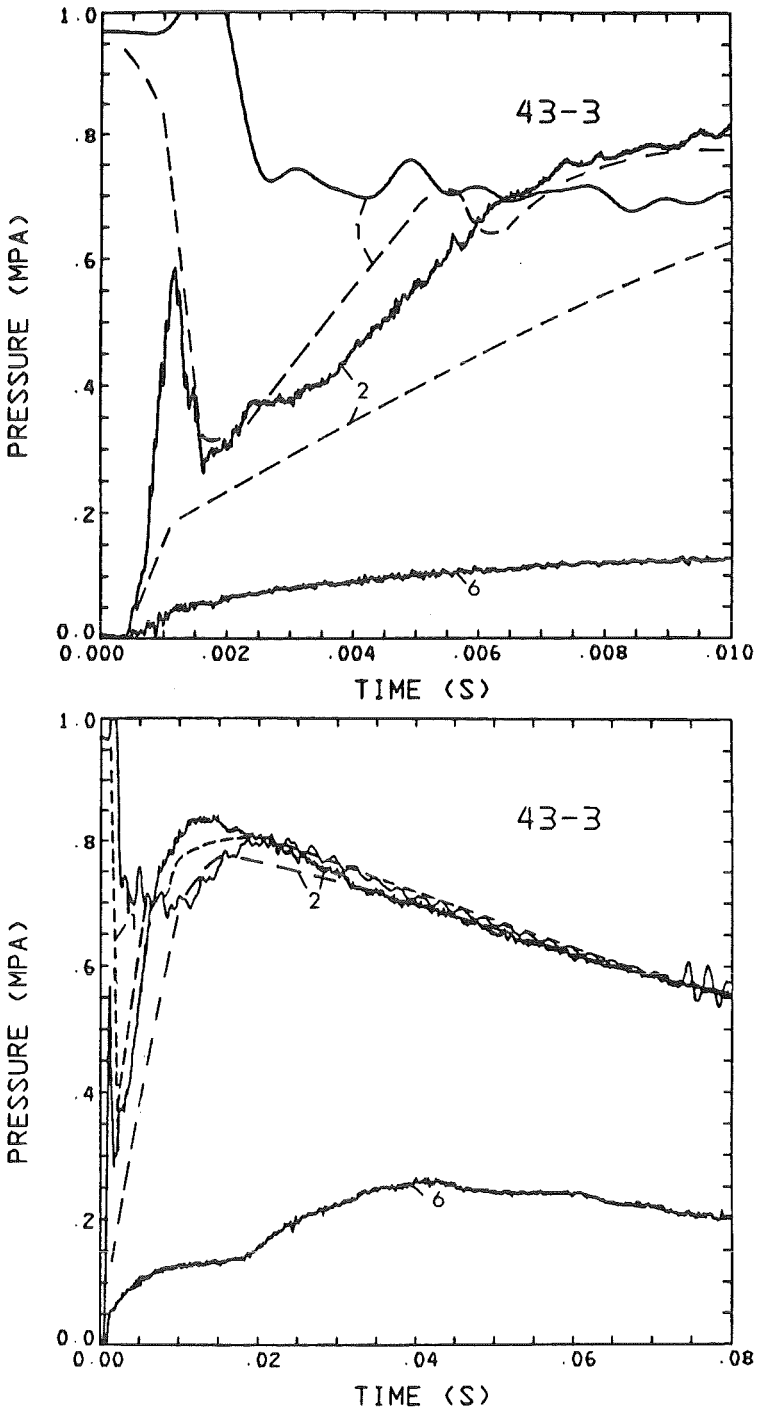

Fig. 62. Comparison of measured pressures and saturation pressures and saturation pressures determined from measured temperatures.

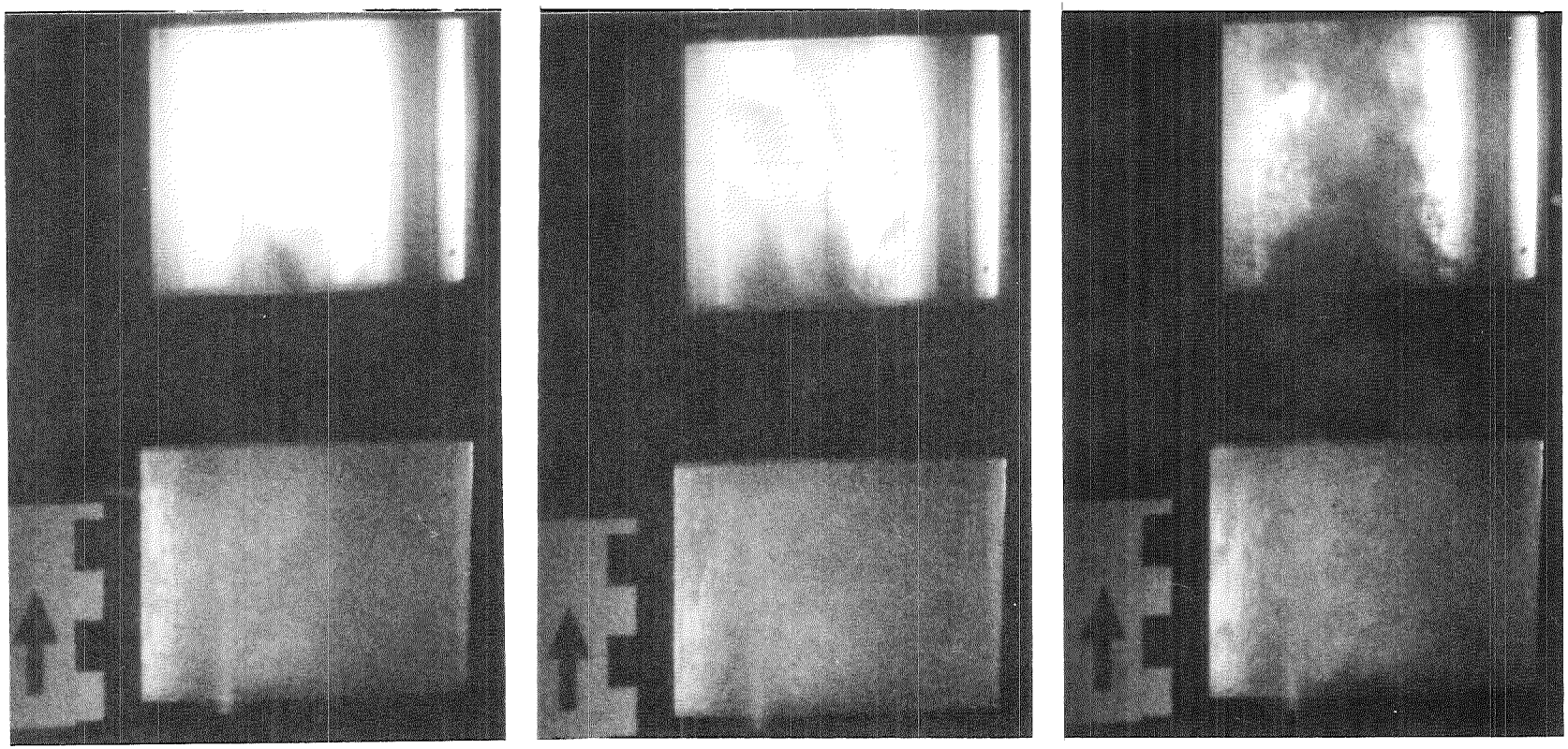

t = 20 ms

t = 22 ms

t = 25 ms

Fig. 63. Photographs of upper and lower view section in Test 39 (Propanol).

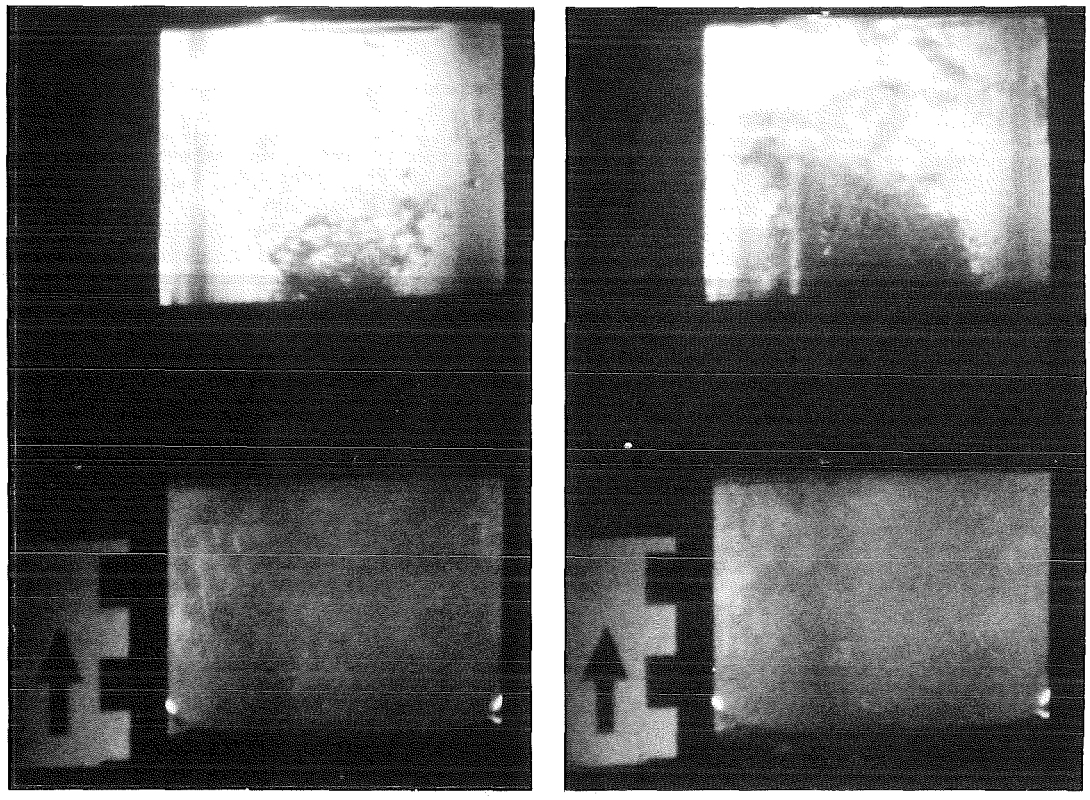

t = 50 ms

t = 57 ms

Fig. 64. Photographs of upper and lower view section in Test 40 (Ethylene Glycol).

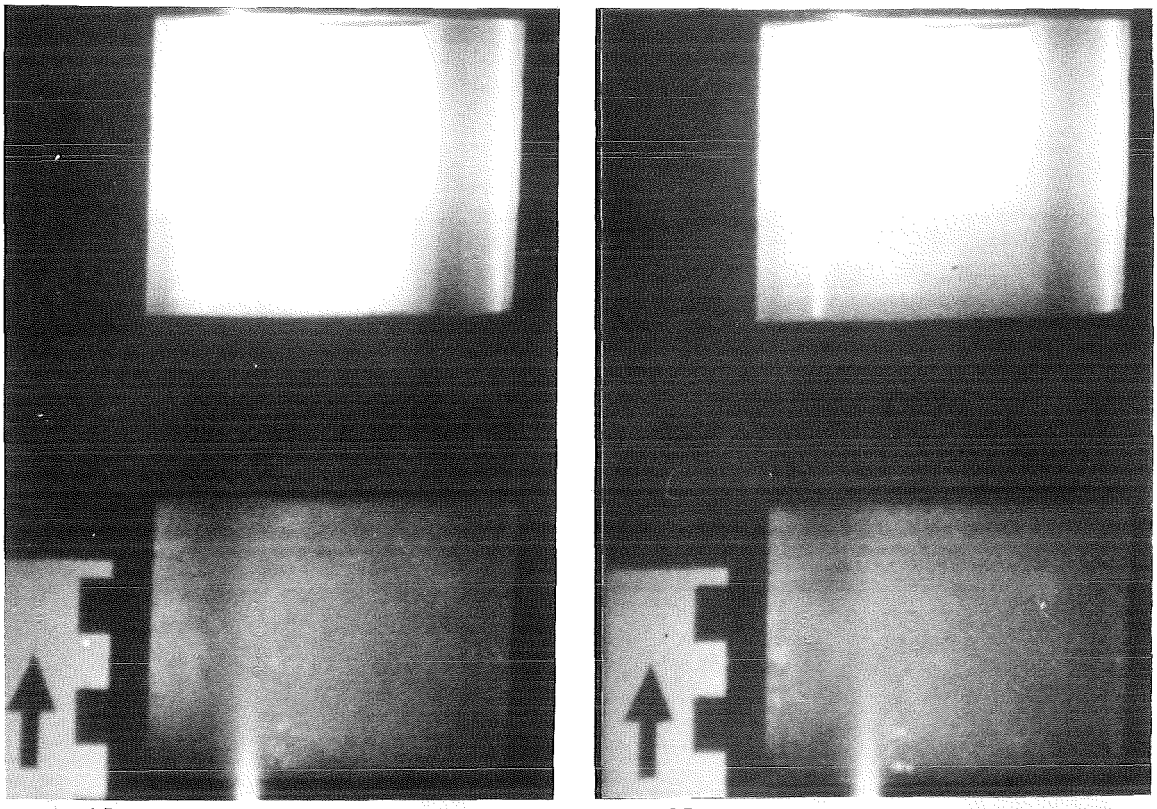

t = 15 ms

t = 25 ms

t = 62 ms

t = 65 ms

Fig. 65. Photographs of upper and lower view section in Test 41 (Ethylene Glycol + Helium).

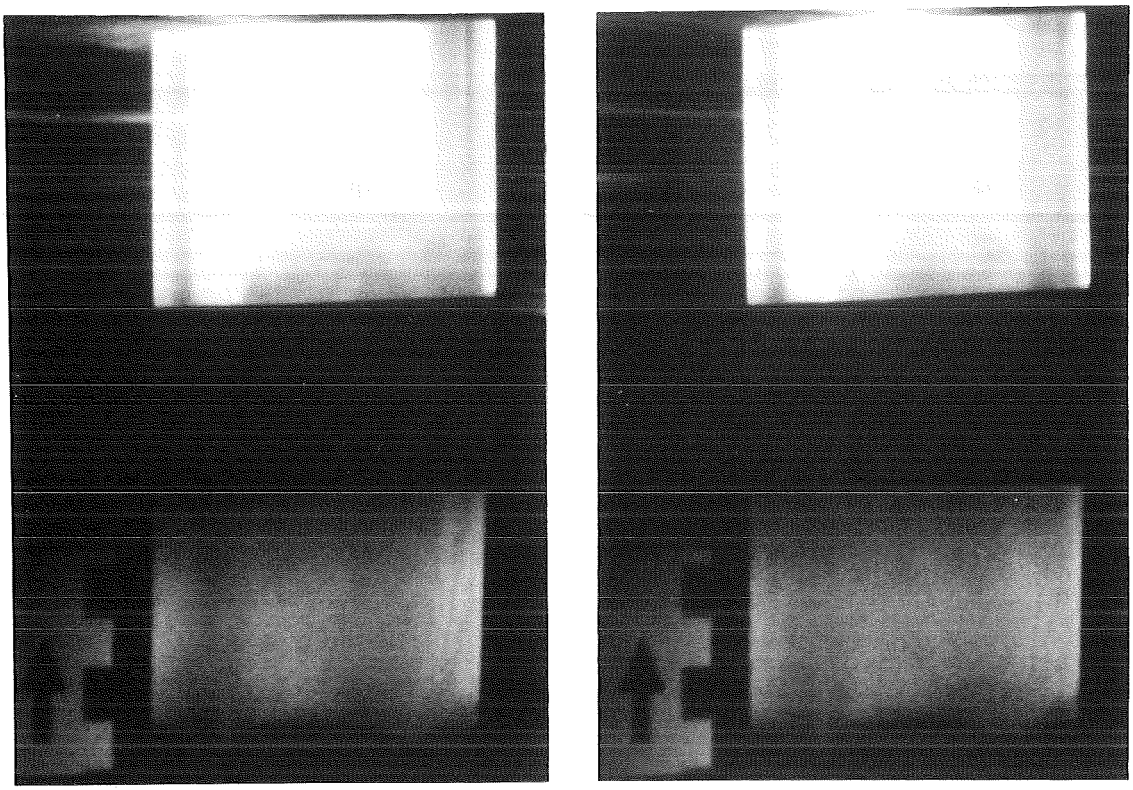

t = 13 ms

t = 15 ms

Fig. 66. Photographs of upper and lower view section in Test 42 (Propanol, no pinbundle).

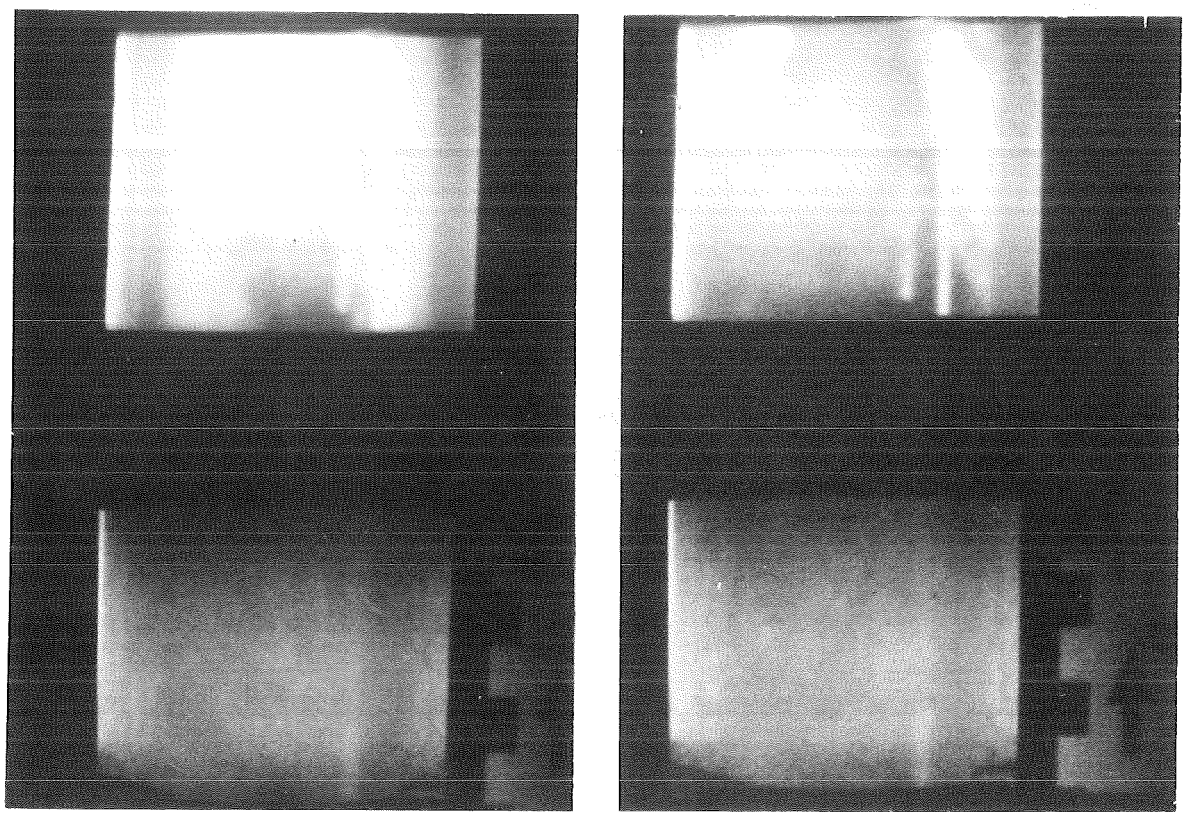

t = 18 ms t = 20 ms

Fig. 67. Photographs of upper and lower view section in Test 43 (Methanol).

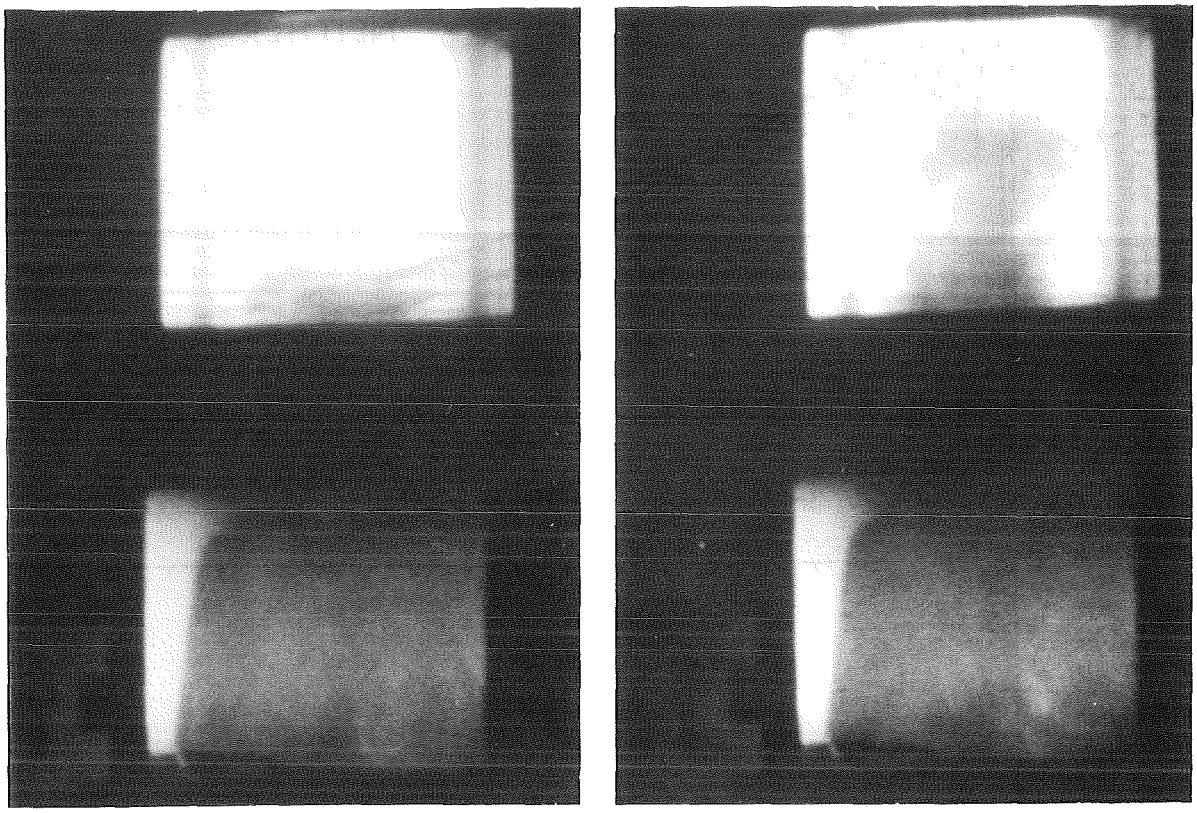

t = 23 ms

t = 25 ms

Fig. 68. Photographs of upper and lower view section in Test 44 (Heptane).

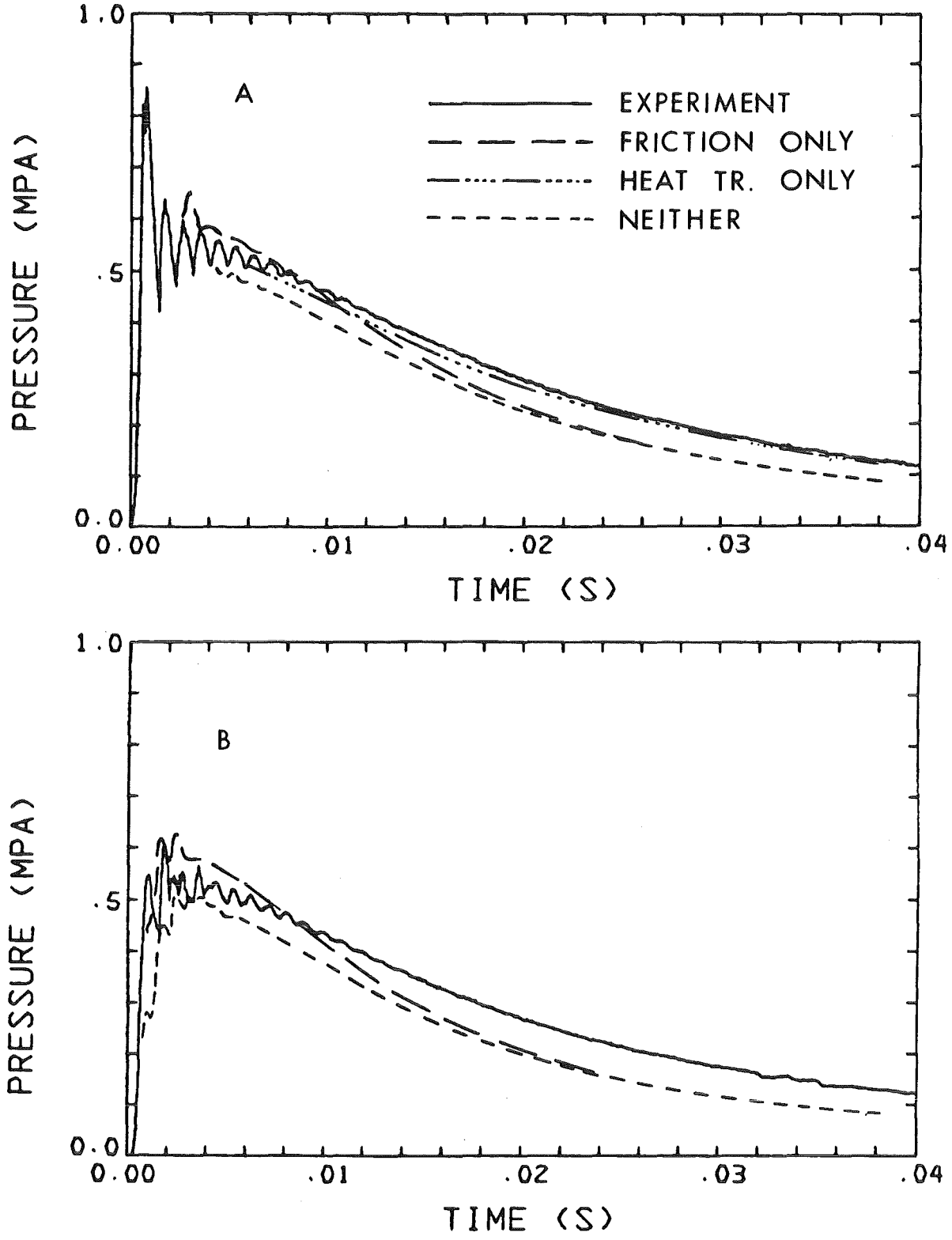

Fig. 69. Calculations for Test 5 (Helium); effect of heat transfer and friction on the pressure before the bundle (A), and in the upper space (B).

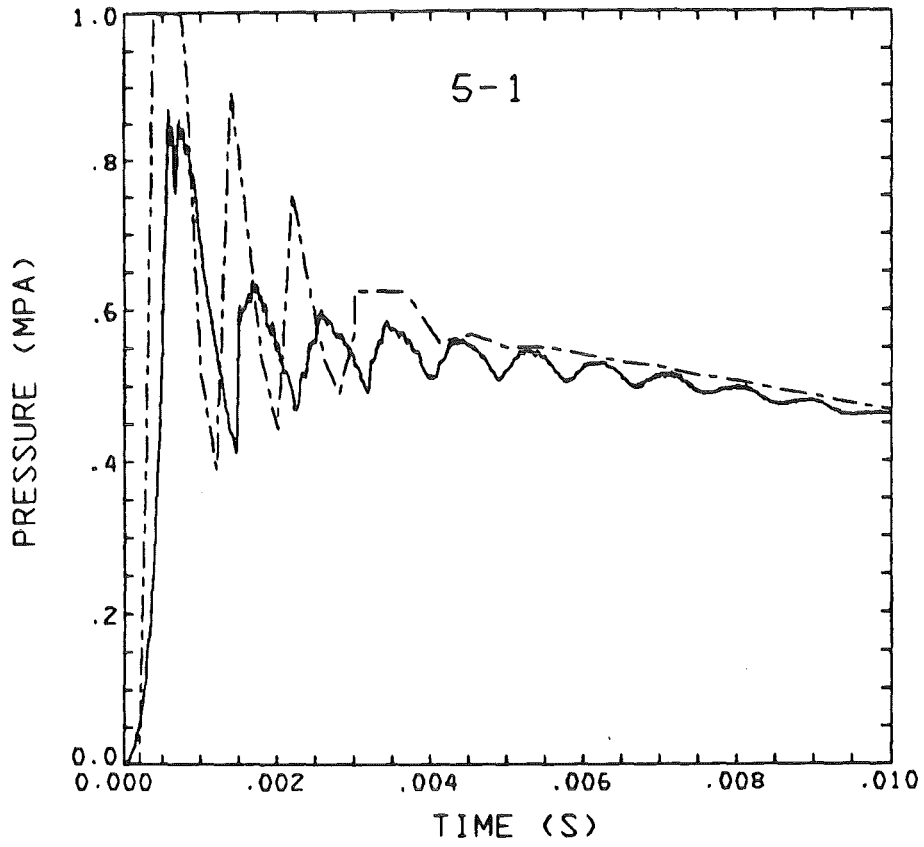

Fig. 70. Comparison of measured and calculated pressure in lower space in Test 5.
(full line: measurement, dashed line: calculation)

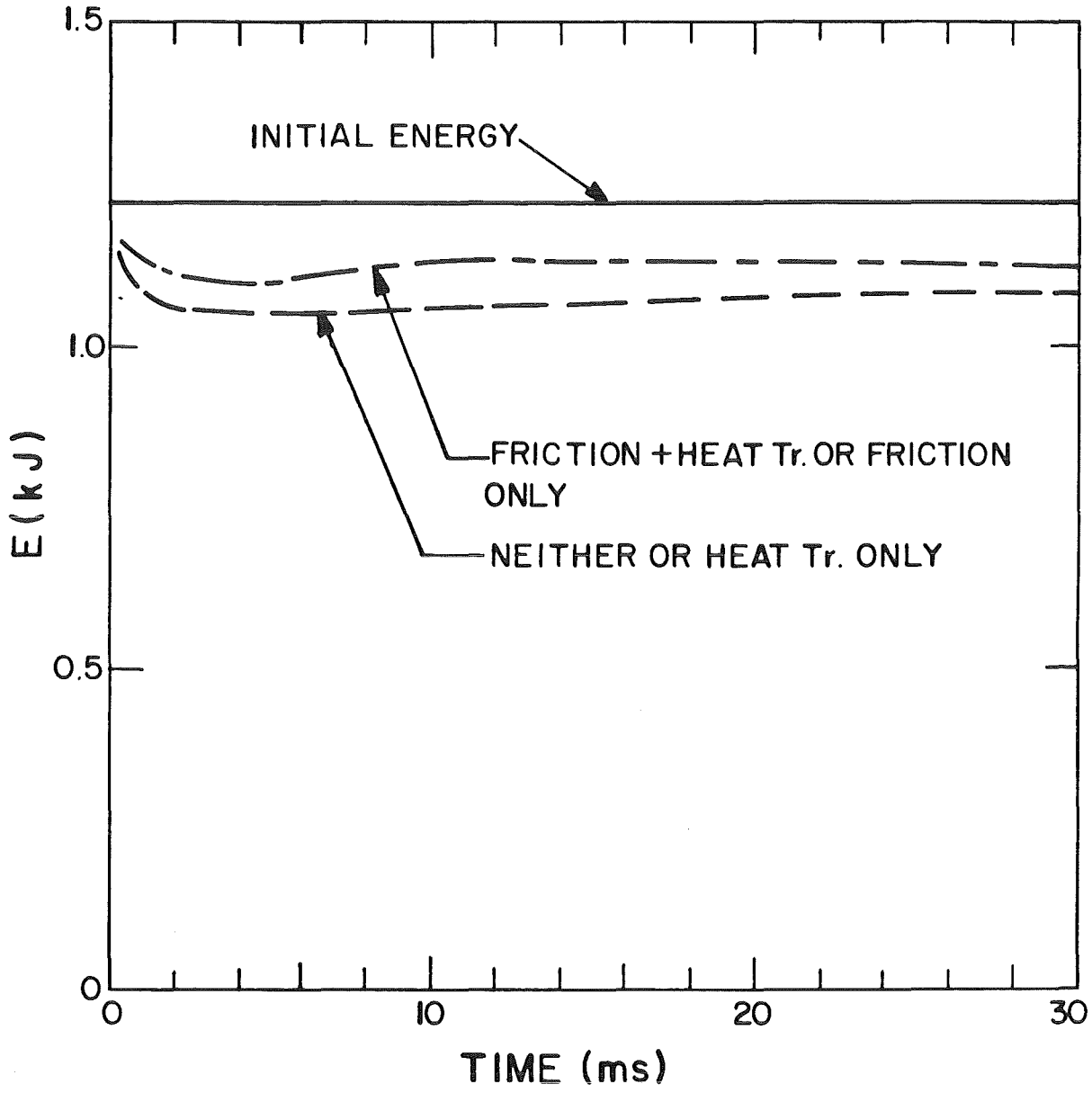

Fig. 71. Calculations for Test 5 (Helium); effect of heat transfer and friction on the energy conservation of the system.

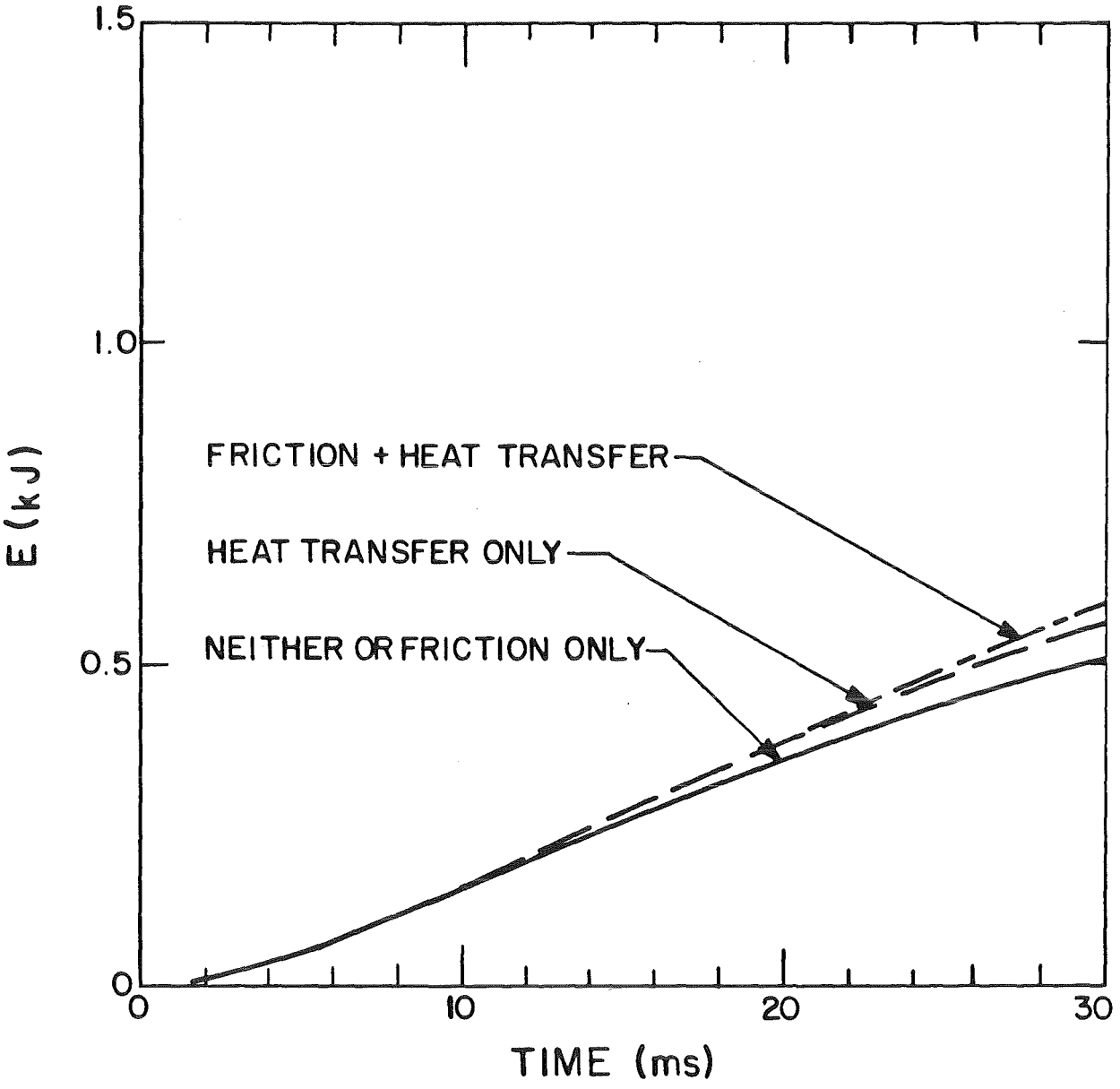

Fig. 72. Calculations for Test 5 (Helium); effect of heat transfer and friction on the kinetic energy of the system.

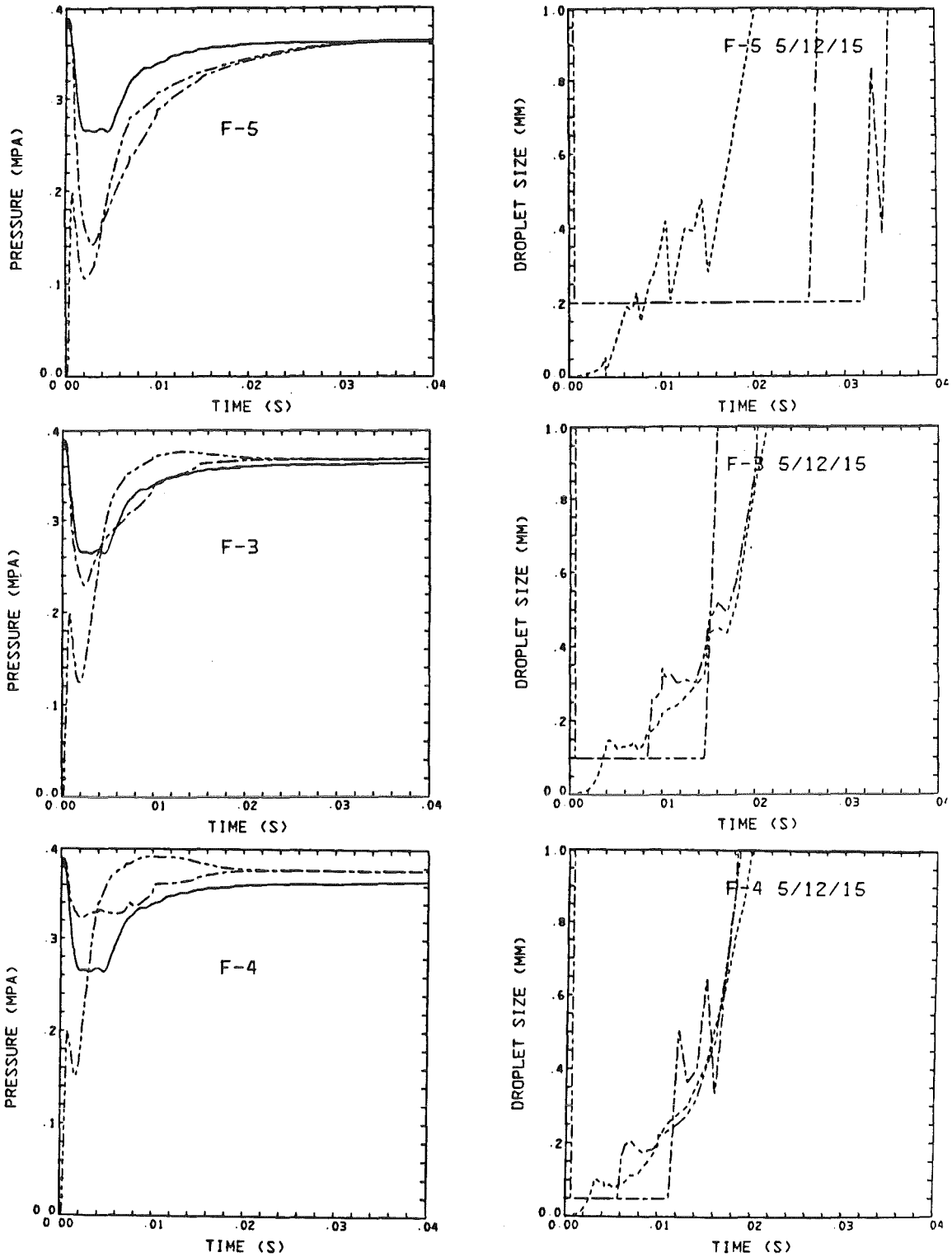

Fig. 73. Calculation for the Flashing Experiment; effect of minimum droplet size on pressure.
full line: measured pressure in lower chamber
dashed lines: calculated: ——— in lower chamber
——·—·— in upper chamber
calculated droplet size: ——·——node 5, ——··——node 12, ----- node 15

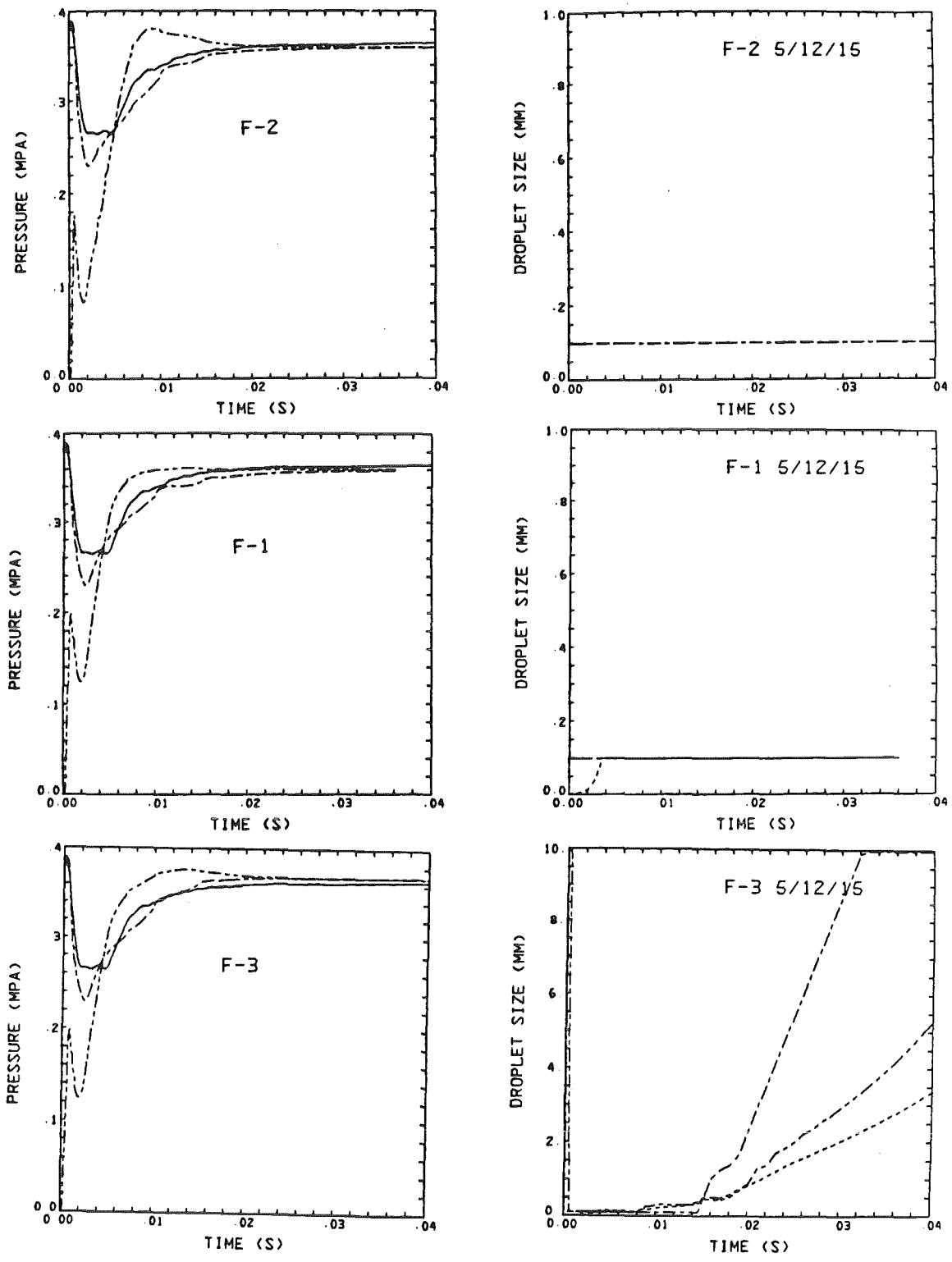

Fig. 74a. Calculation for the Flashing Experiment; effect of maximum droplet size on pressure (notation see Fig. 73.).

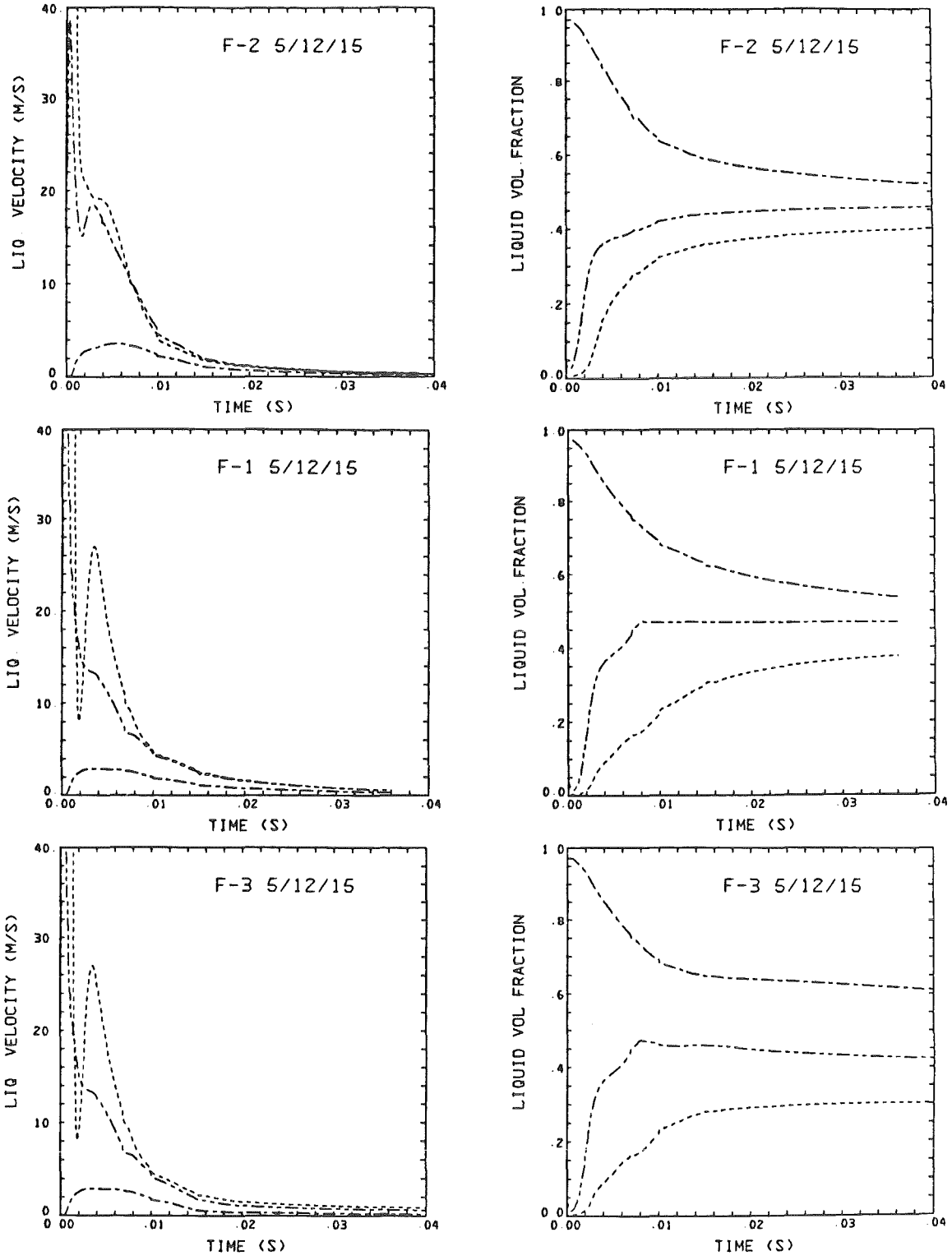

Fig. 74b. Liquid velocity and liquid volume fraction in nodes 5, 12 and 15.

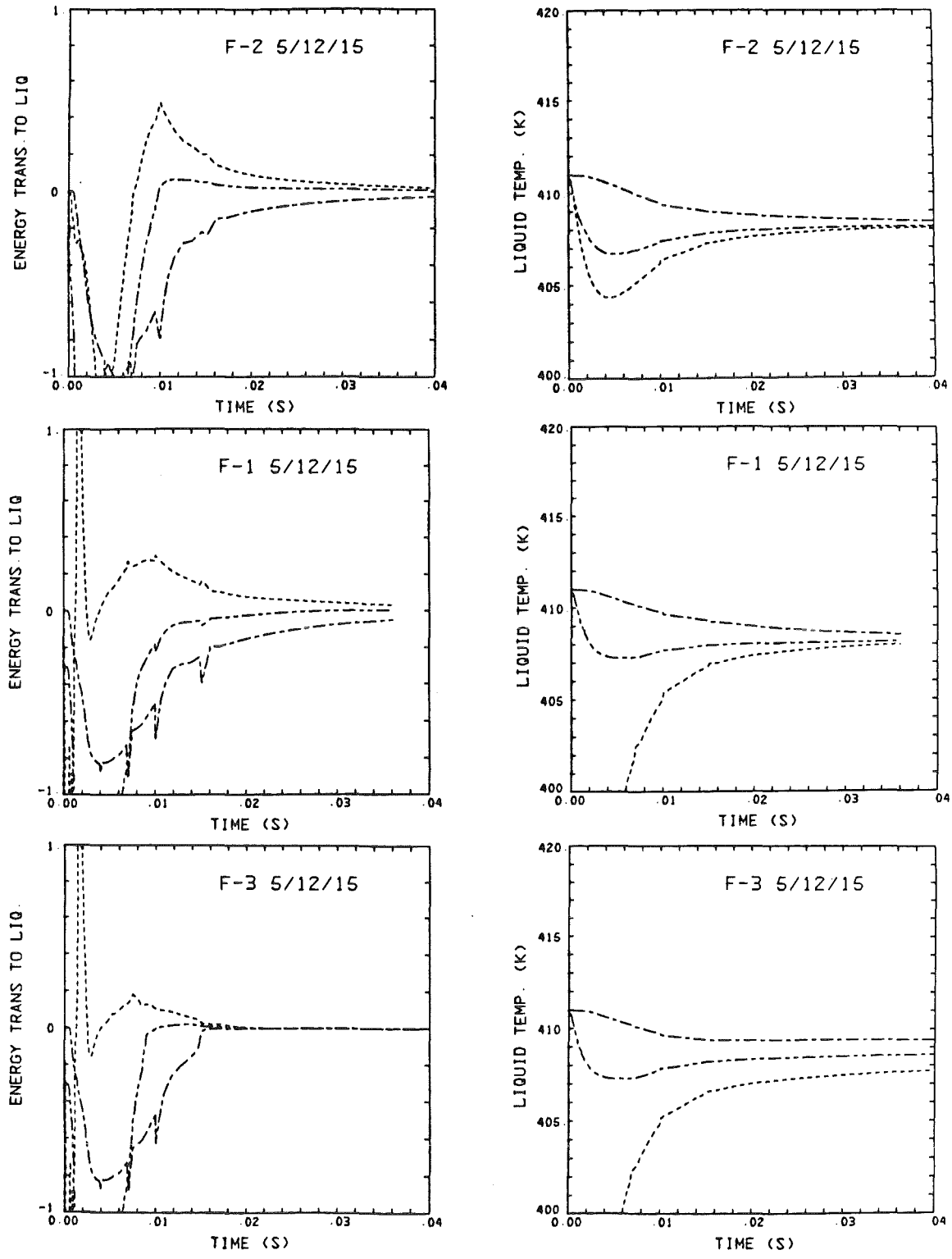

Fig. 74c. Energy transfer to liquid and liquid temperature.

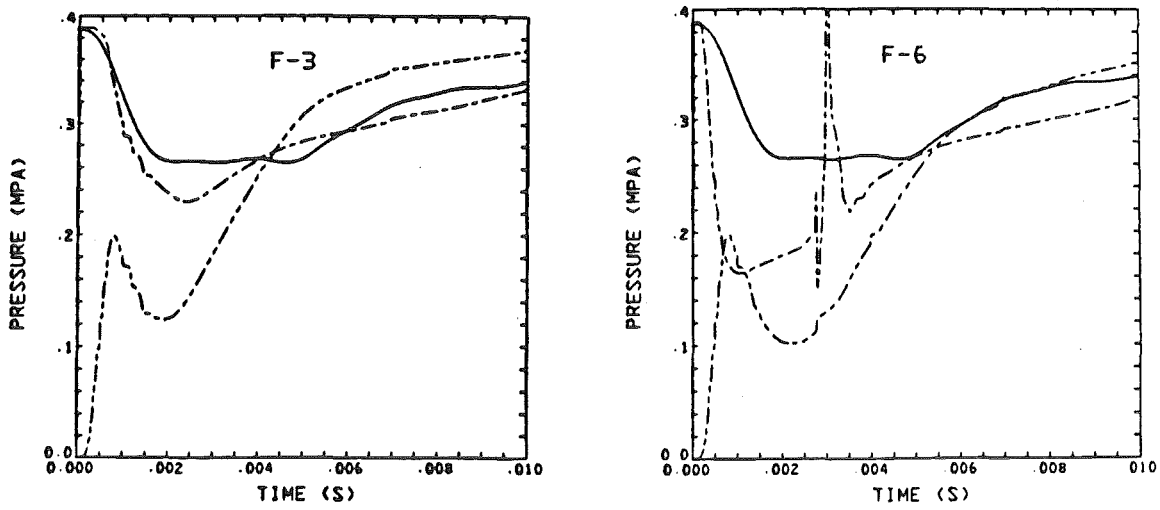

Fig. 75. Calculation for the Flashing Experiment;
effect of initial vapor fraction in the liquid
on pressure during 10 ms.
F-3: vapor fraction = 2.88 %
F-6: vapor fraction = 0.36 %
full line: measured pressure in lower chamber
dashed lines: calculated: —·— in lower chamber
—·—·— in upper chamber

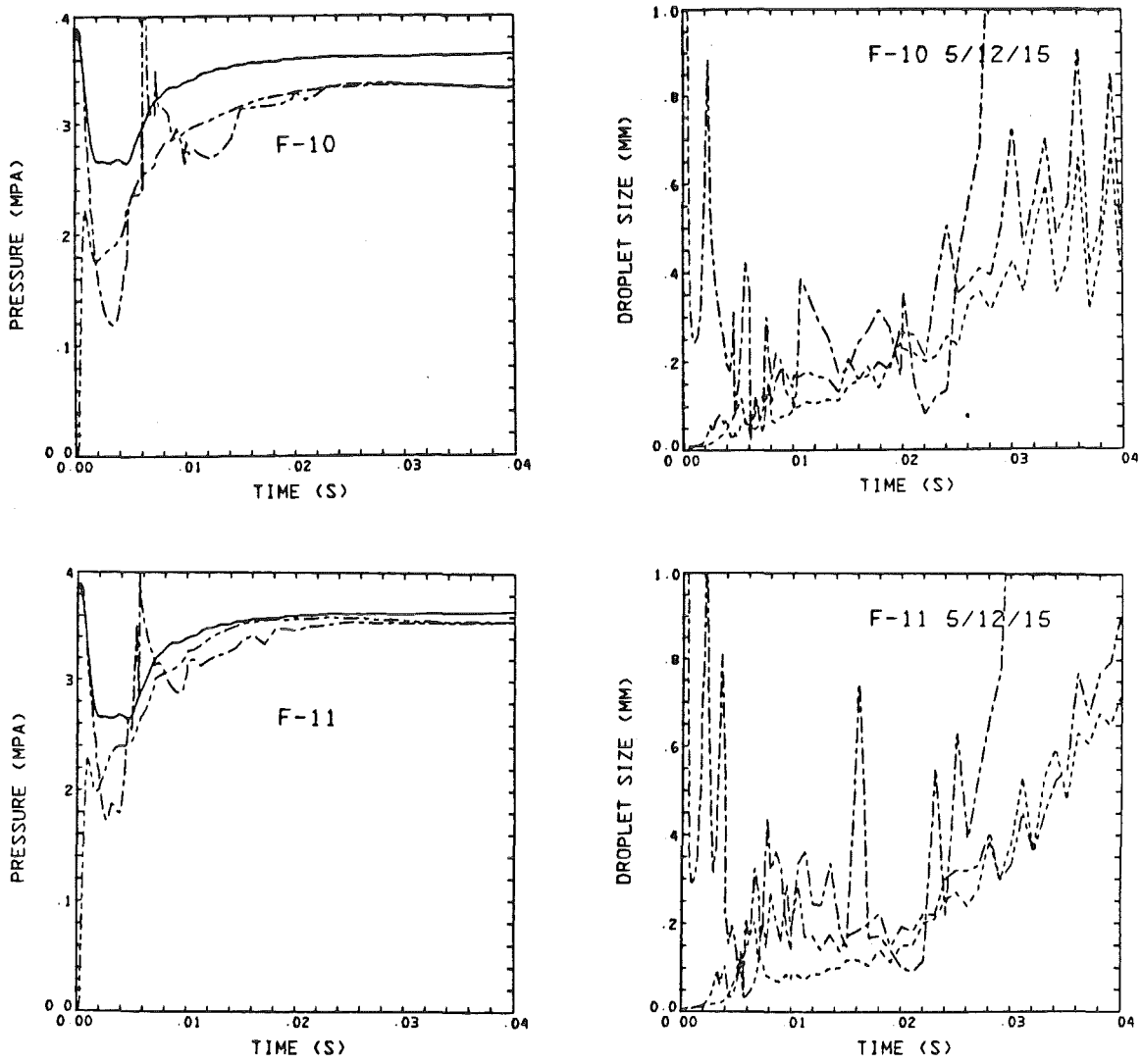

Fig. 76. Calculation for the Flashing Experiment without flashing break-up criterion for droplet size (notation see Fig. 74.).

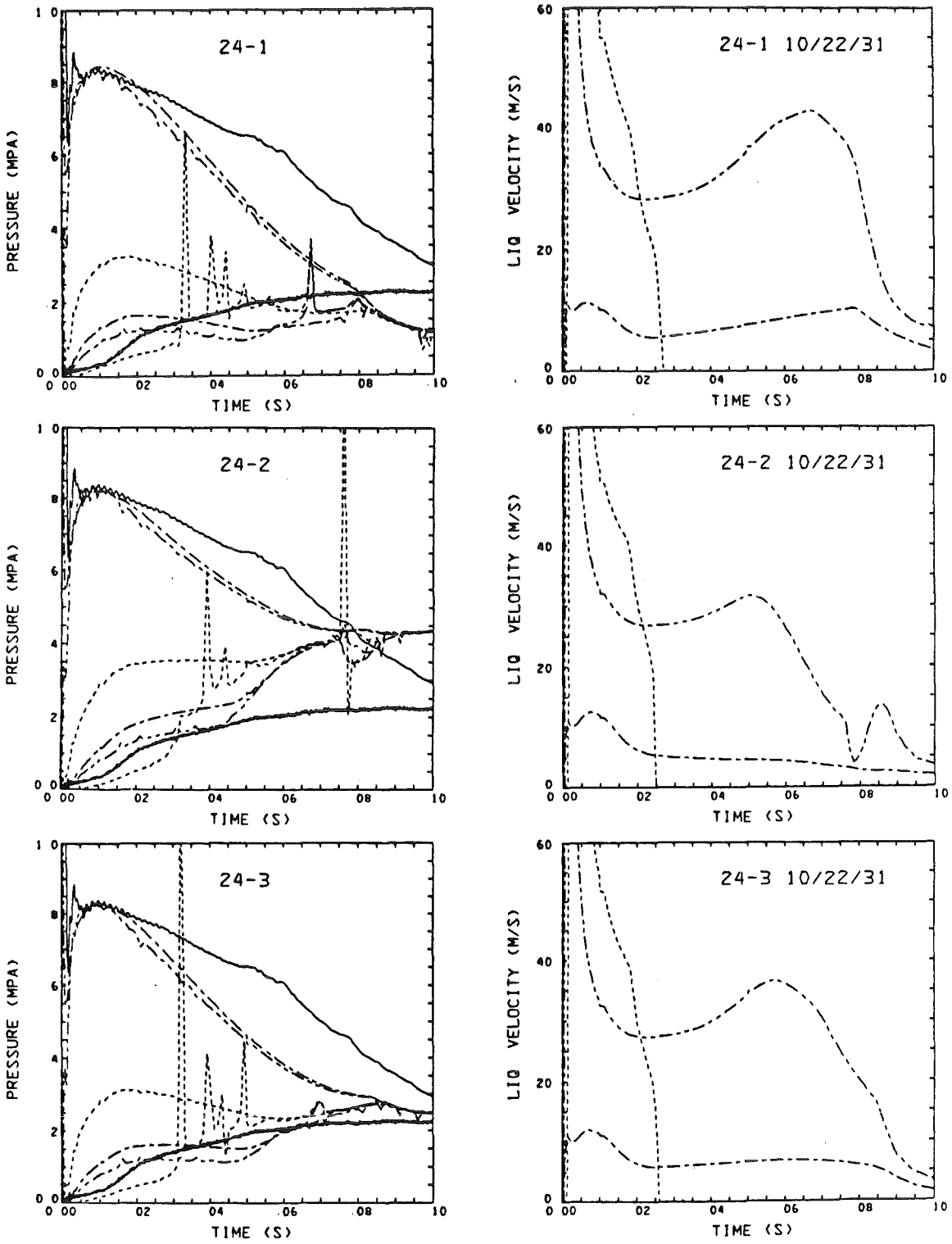

Fig. 77a. Calculations for Test 24 (no piston); effect of structure mass volume fraction on pressure;
full lines: measured pressures p_1 and p_6
dashed lines calculated p_1 through p_6
calculated parameters: —·— node 10
— - — node 22
------- node 31

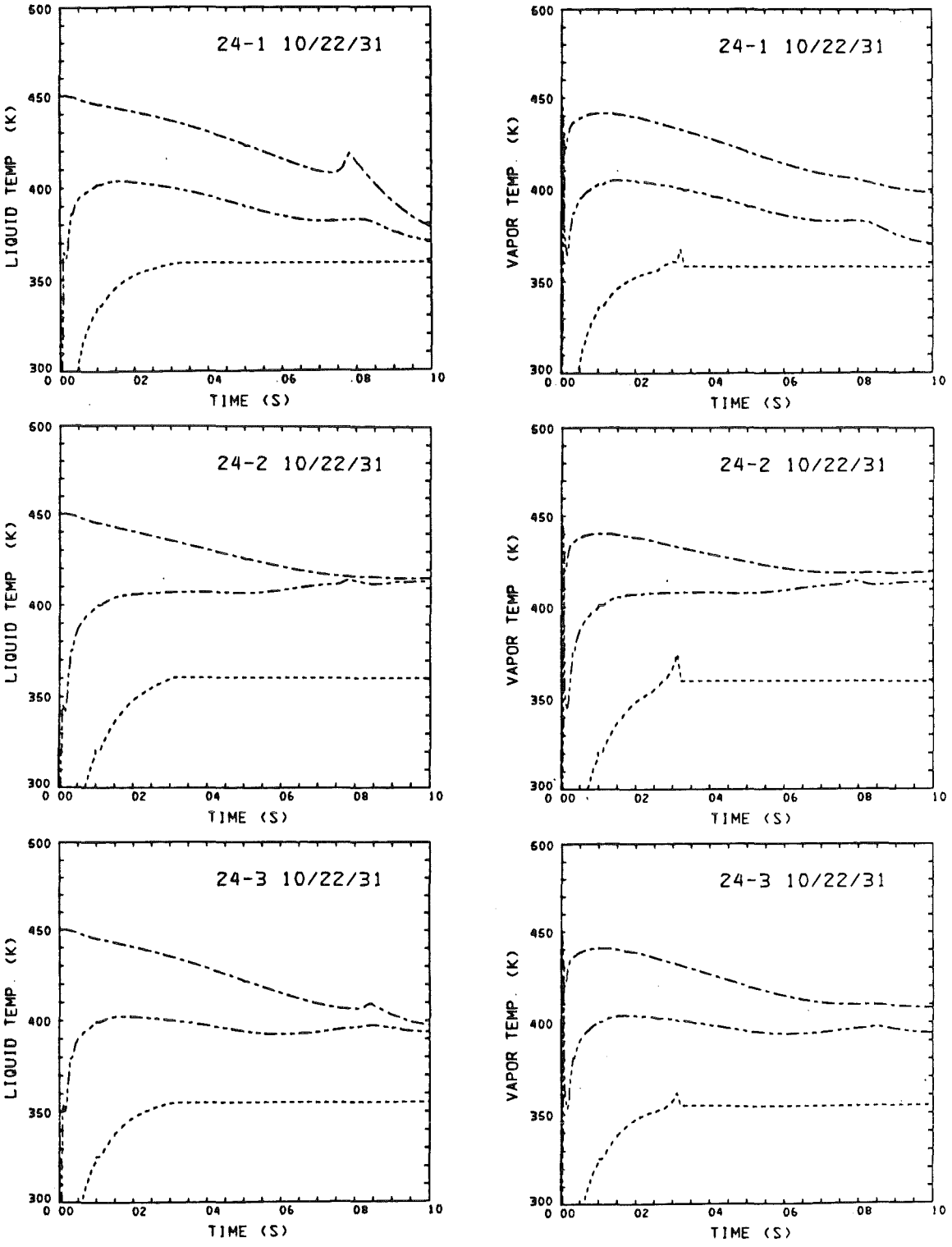

Fig. 77b. Calculated fluid temperatures for Test 24.

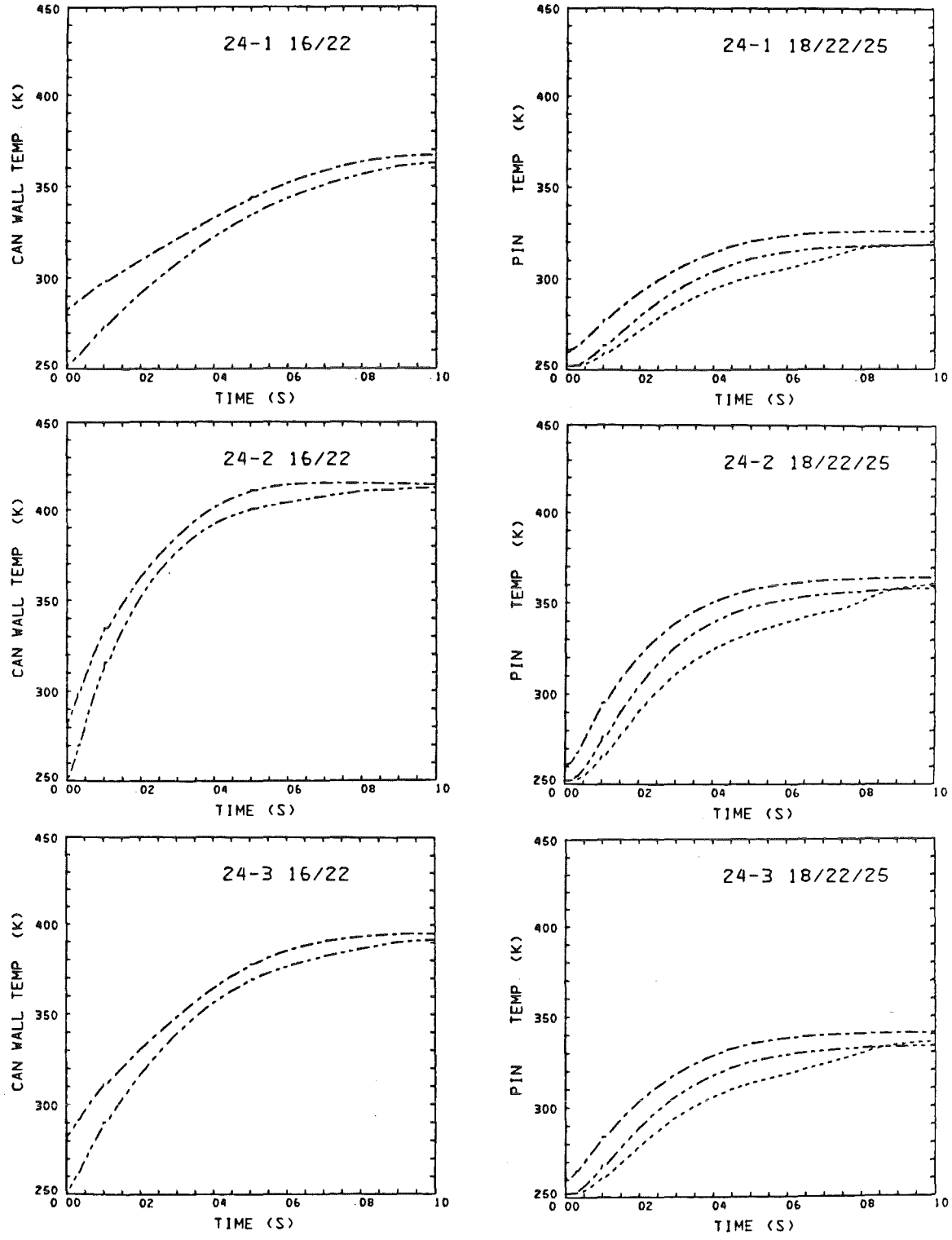

Fig. 77c. Calculated structure temperatures for Test 24.

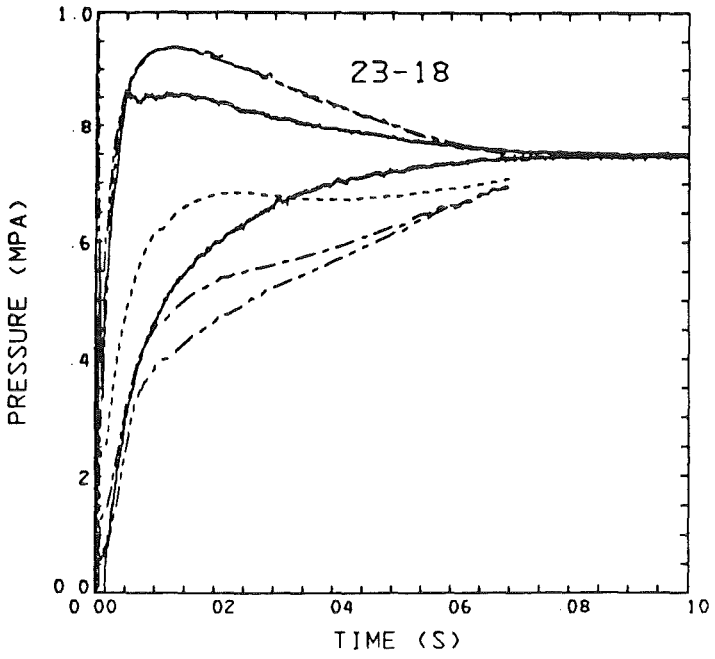

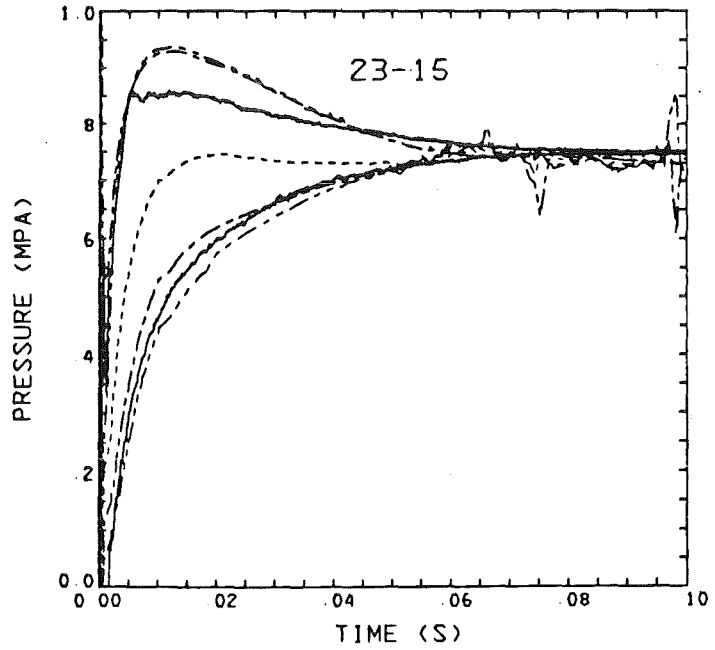

Fig. 78. Calculations for Test 23; effect of can wall mass on pressure (notation see Fig. 77a.).

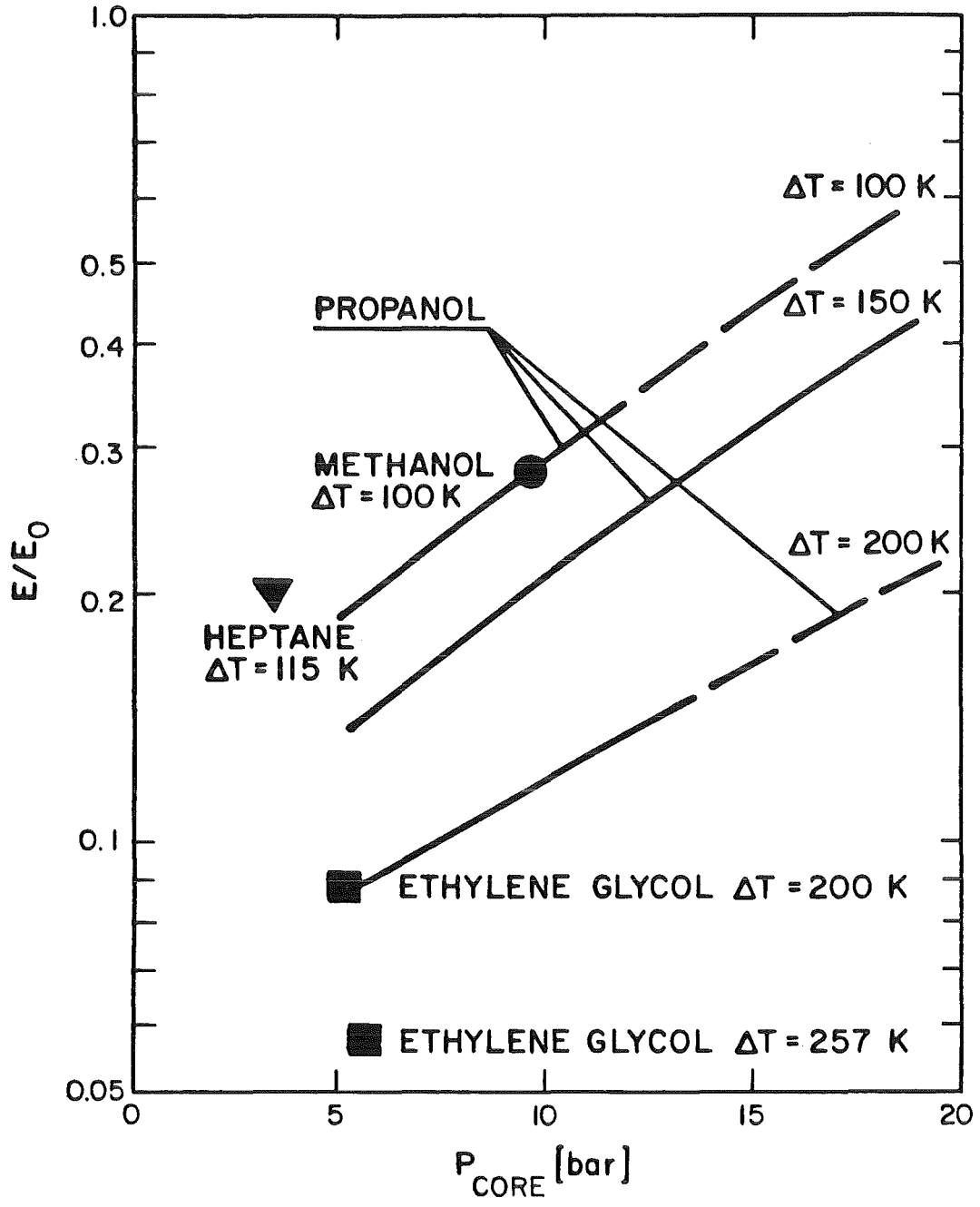

Fig. 79. Reduction of the kinetic energy of the piston as a function of the initial core pressure and the temperature difference between core and UCS.

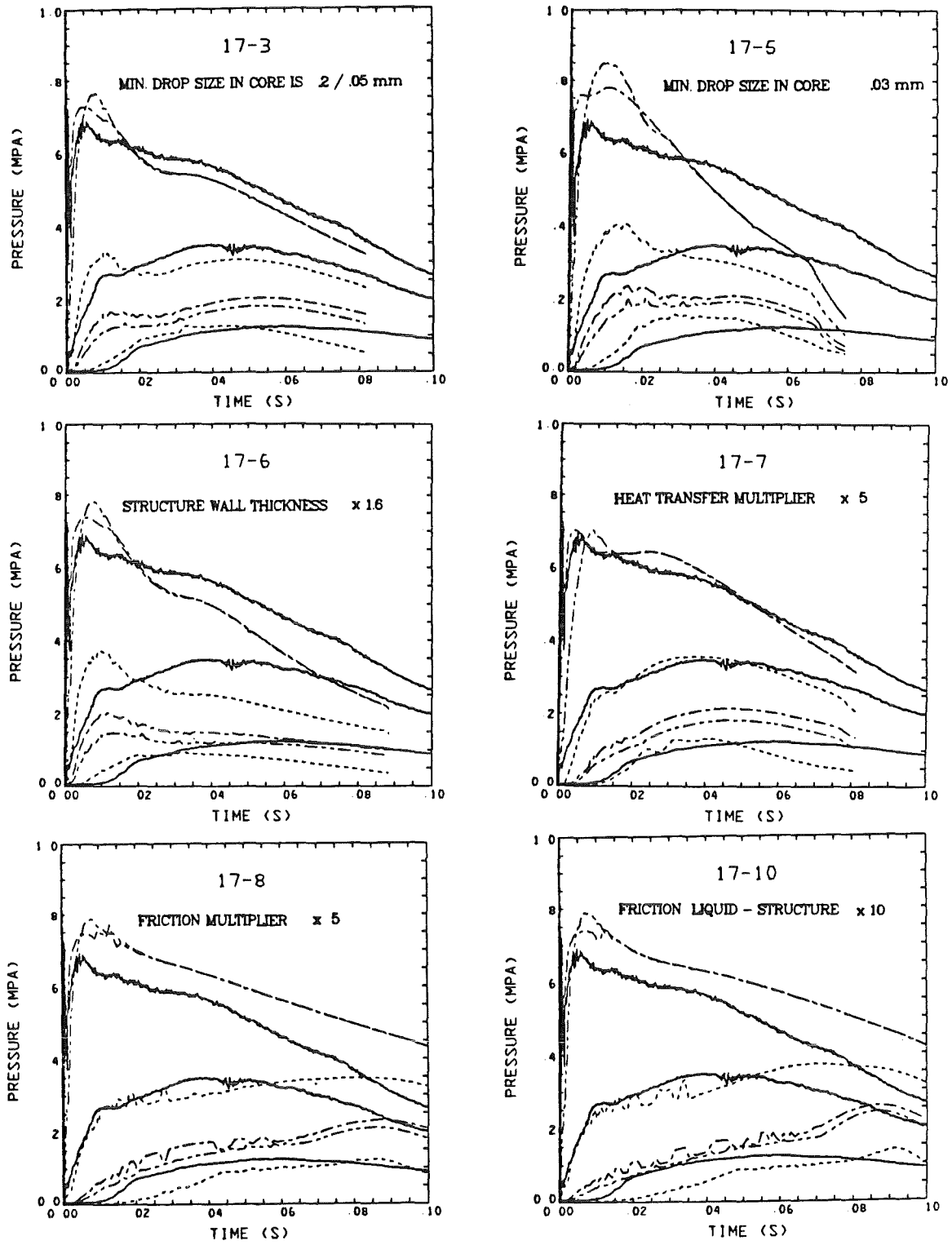

Fig. 80. Calculations for Test 17; effect of parameter variations on pressures;
full lines: measured pressures p_1, p_3 and p_6,
dashed lines: calculated pressures p_1 through p_6.

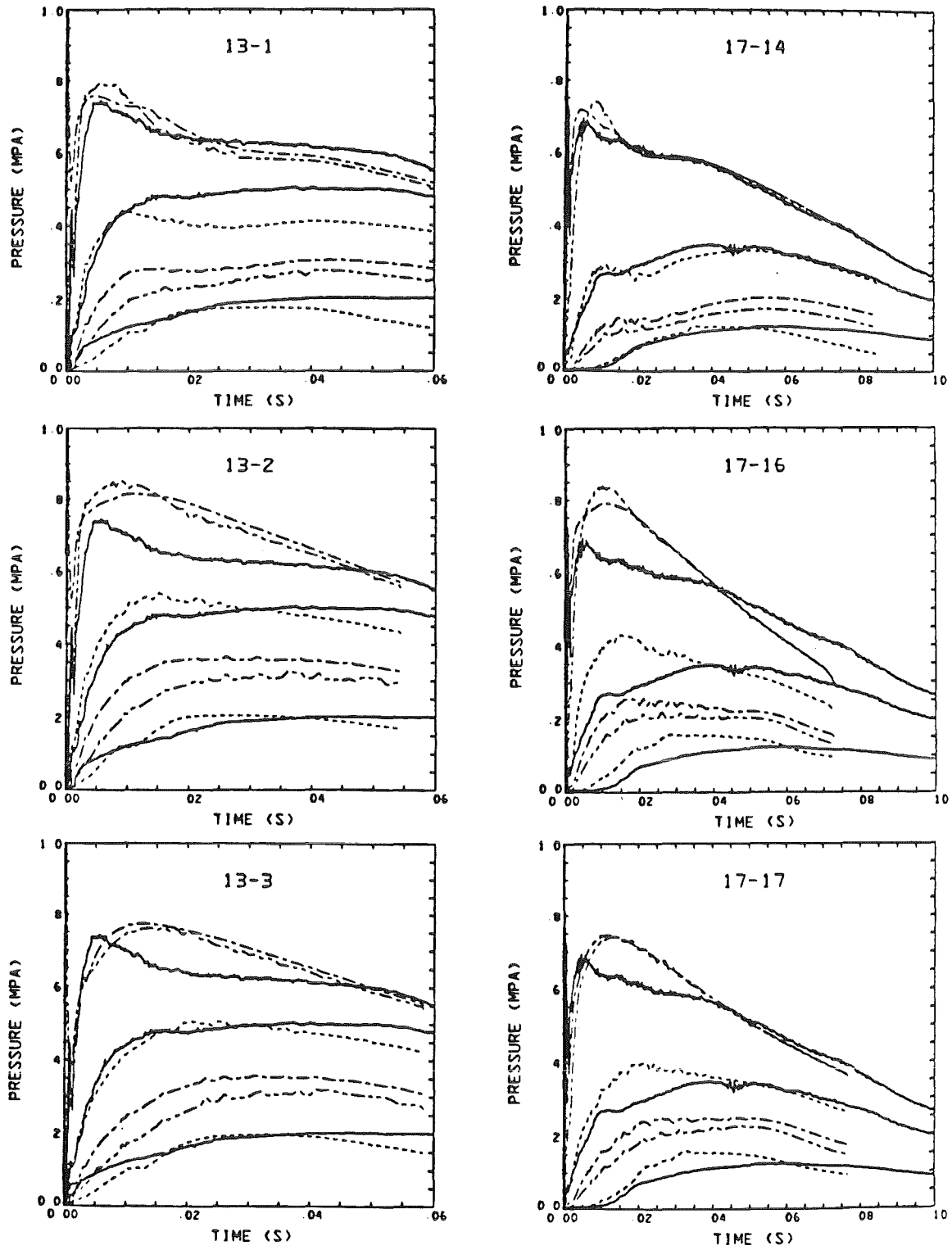

Fig. 81a. Calculations with fixed set of input parameters;
full lines: measured pressures p_1, p_3 and p_6
dashed lines: calculated pressures p_1 through p_6.

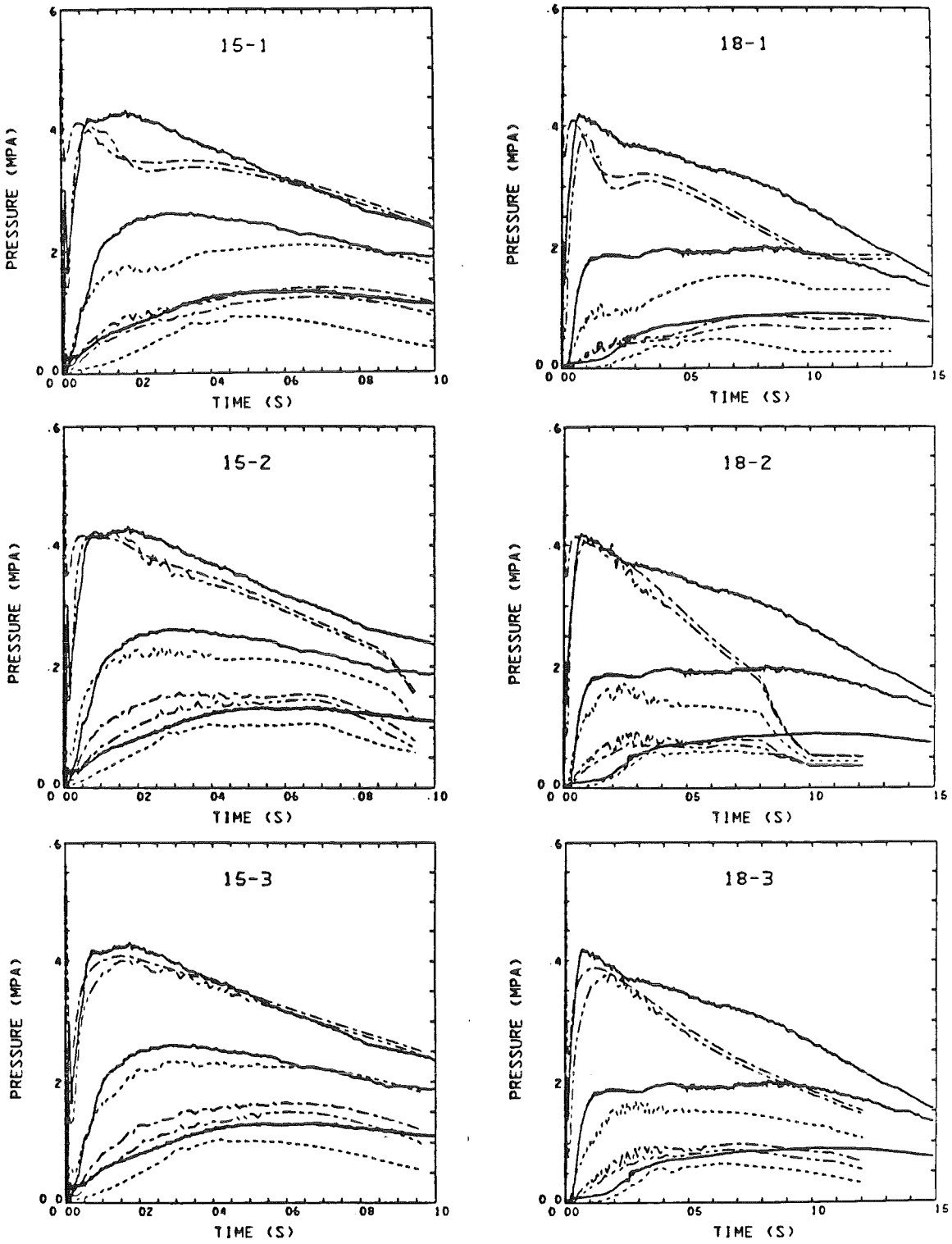

Fig. 81b. Calculations with fixed set of input parameters.

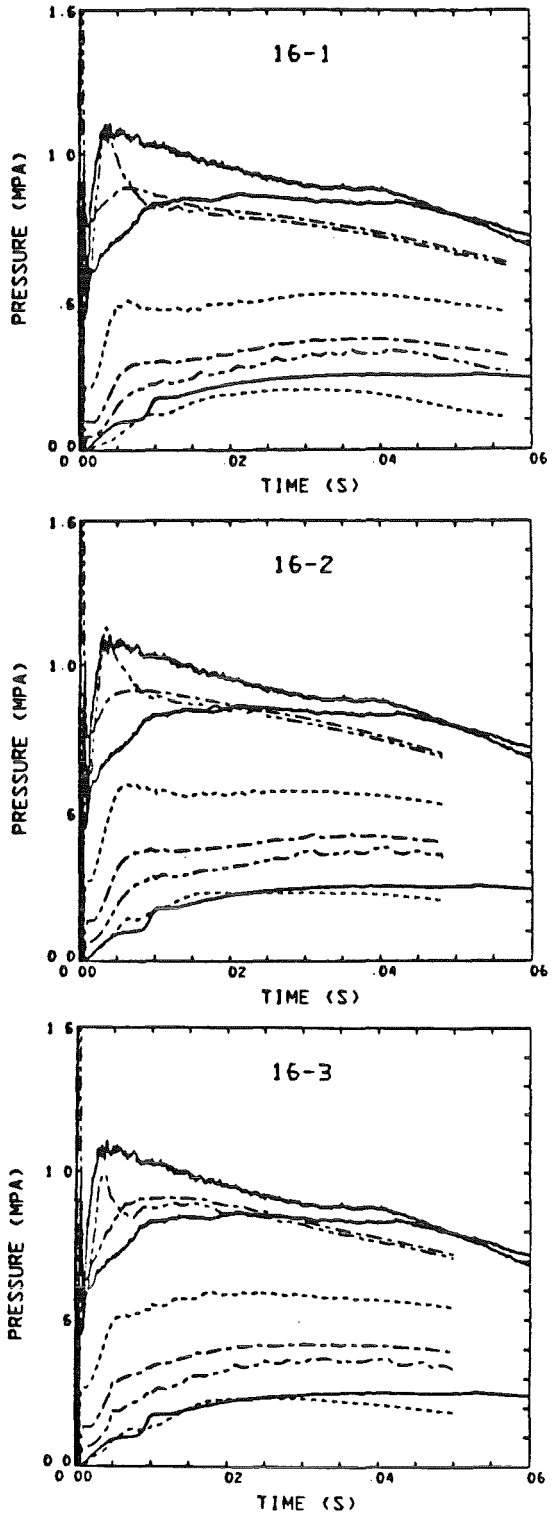

Fig. 81c. Calculations with fixed set of input parameters.

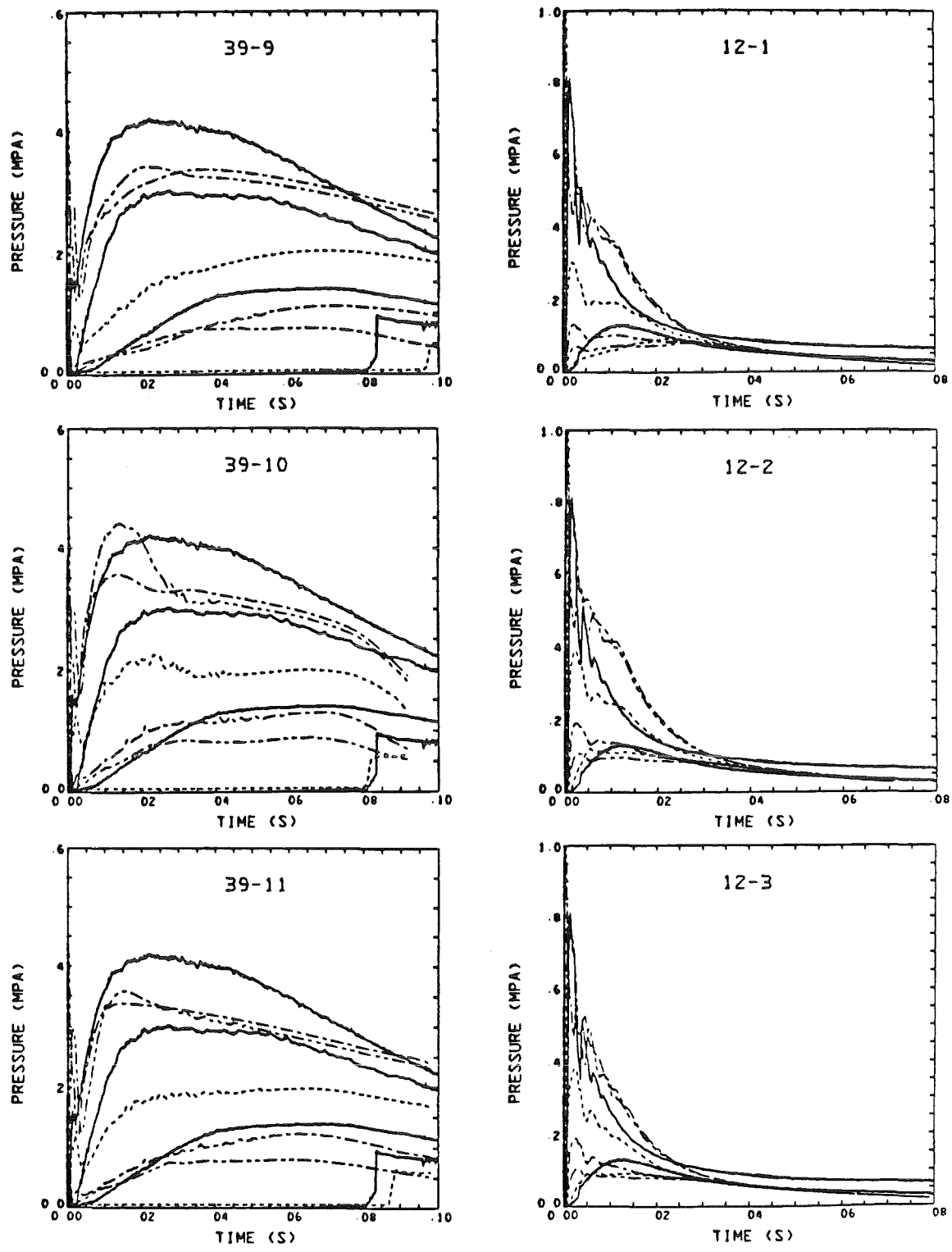

Fig. 81d. Calculations with fixed set of input parameters.

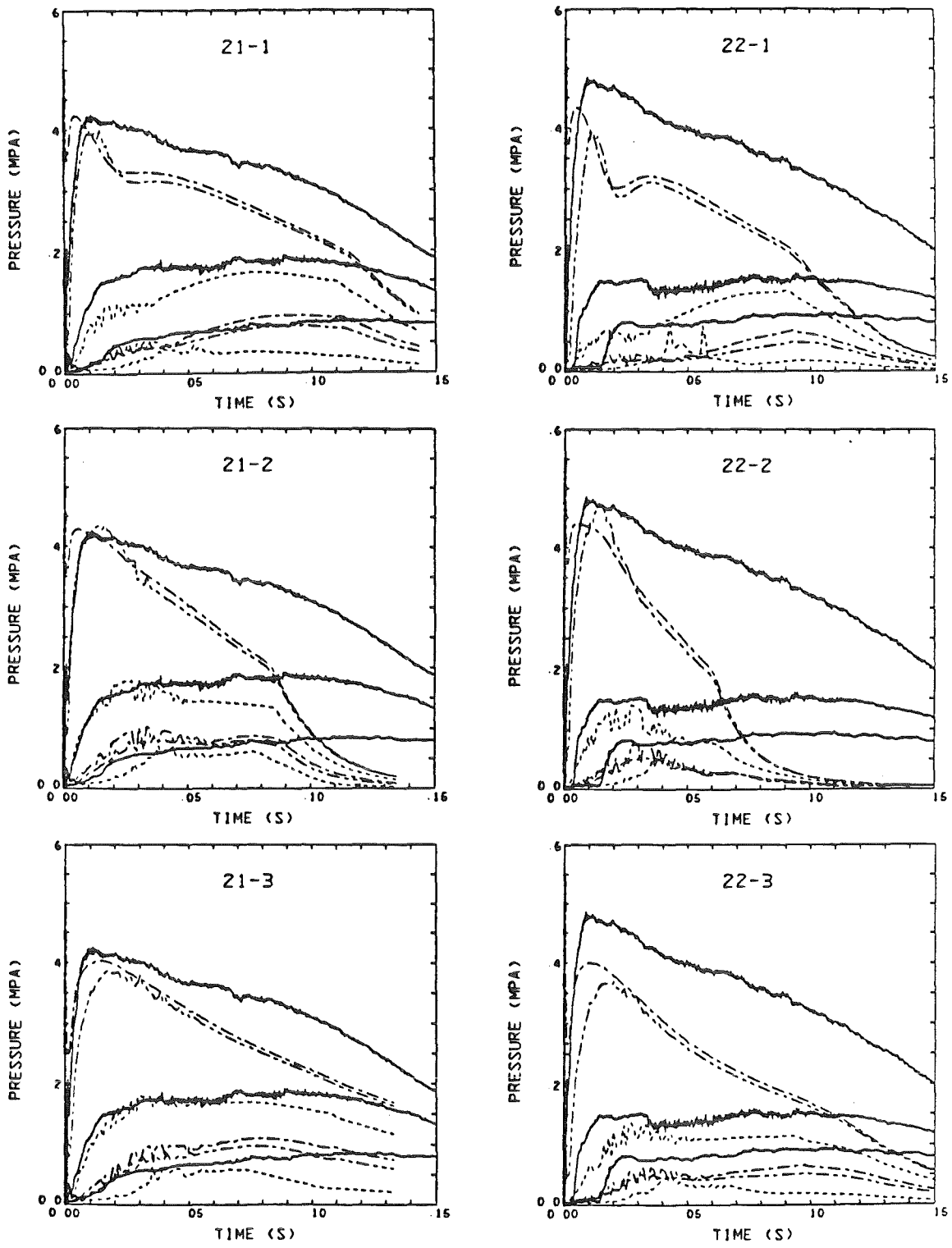

Fig. 81e. Calculations with fixed set of input parameters.

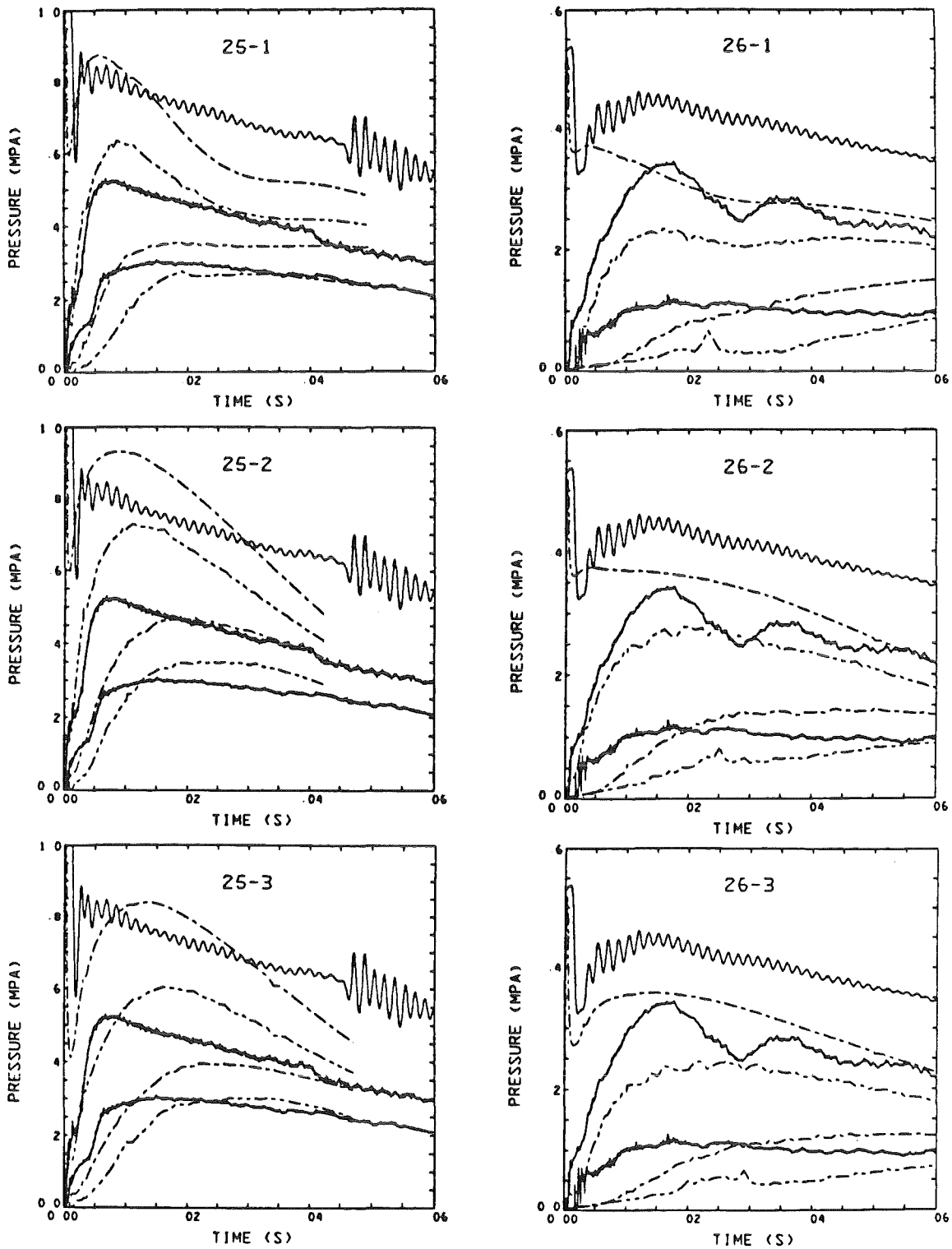

Fig. 81f. Calculations with fixed set of input parameters.

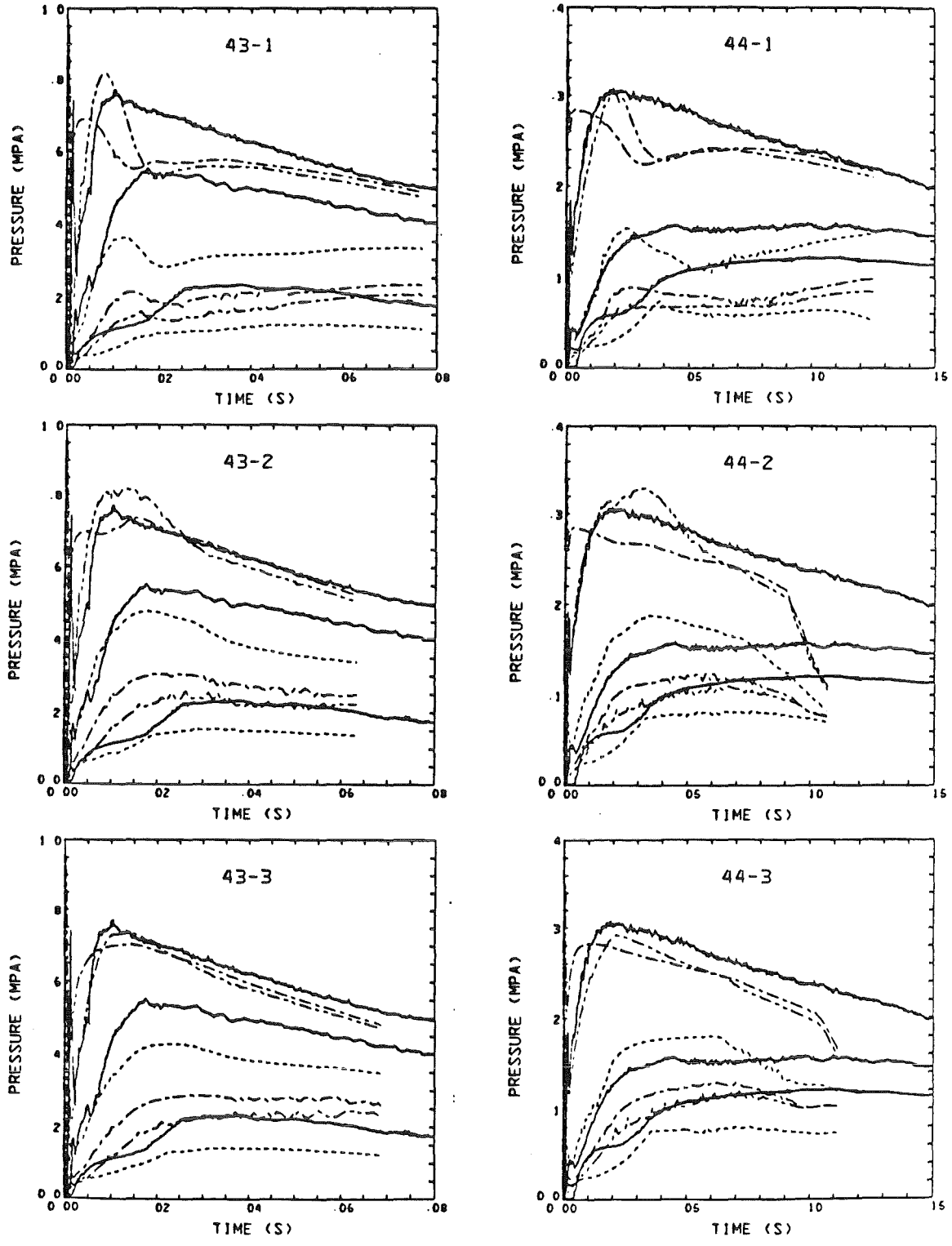

Fig. 81g. Calculations with fixed set of input parameters.

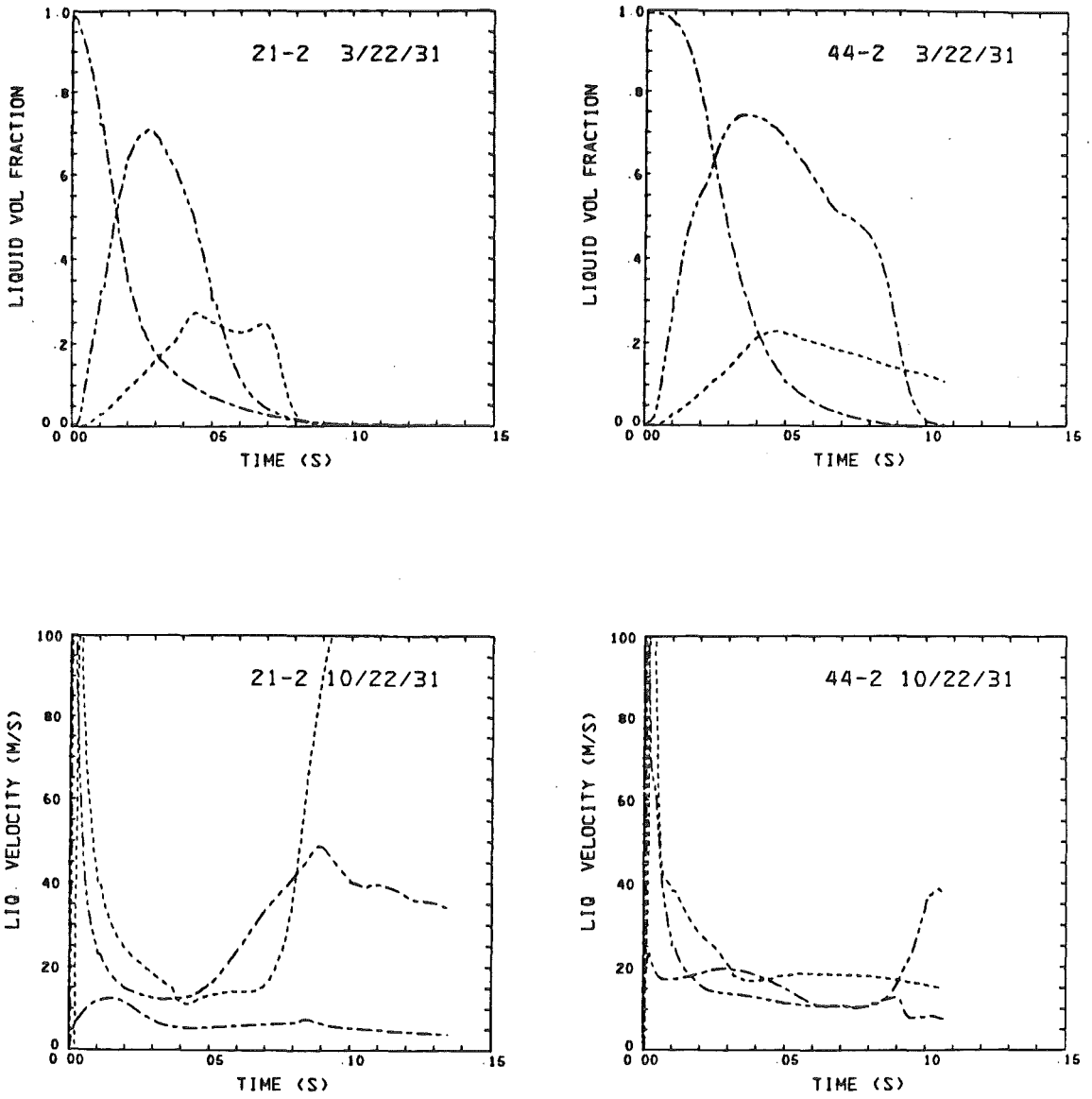

Fig. 82a. Calculated liquid volume fraction and velocity for Test 22 and 44 (Run 2)
sequence of lines with regard to nodes: —·— /—··— /----- .

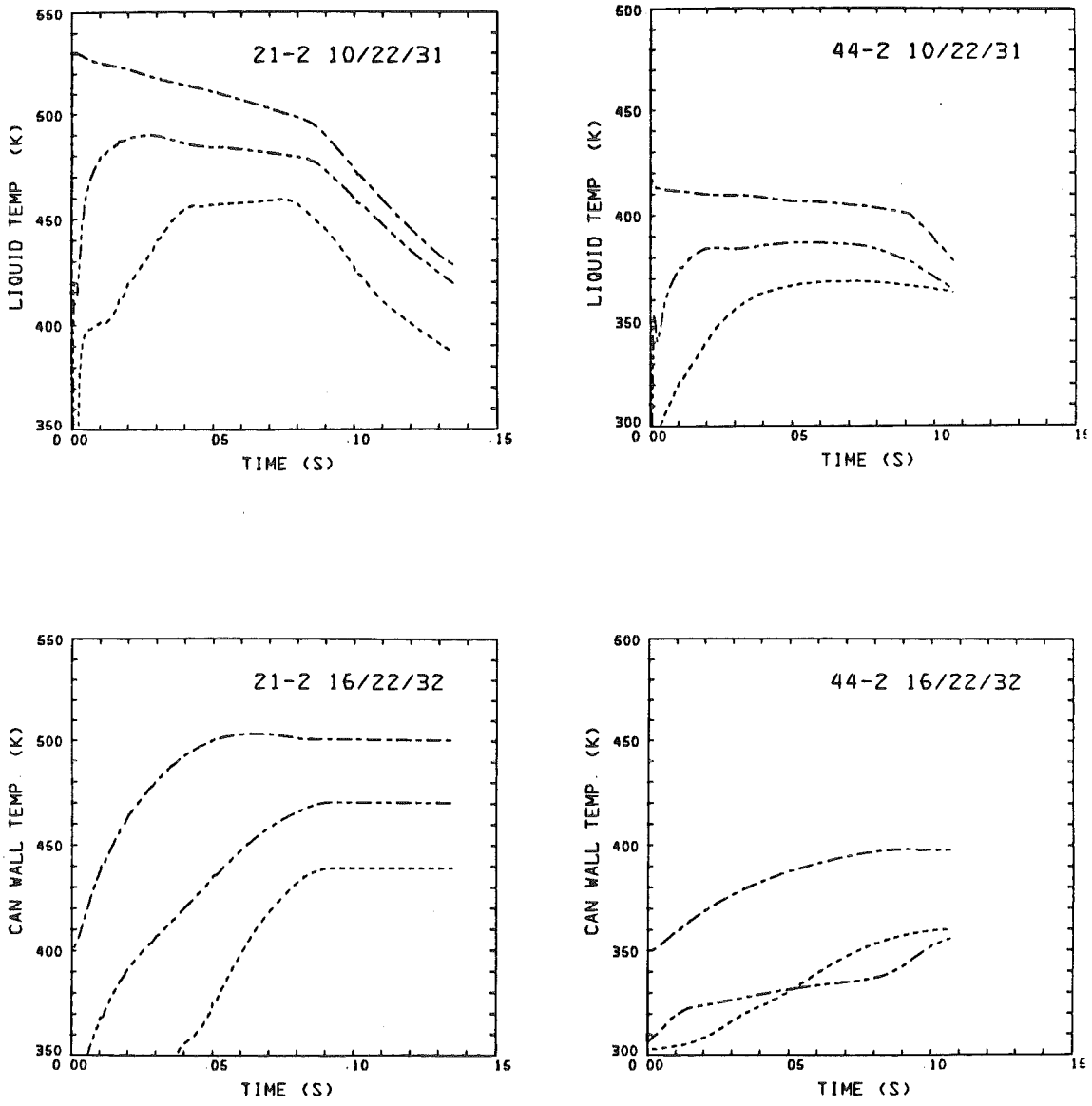

Fig. 82b. Calculated temperatures for Test 22 and 44 (Run 2); notation as before.

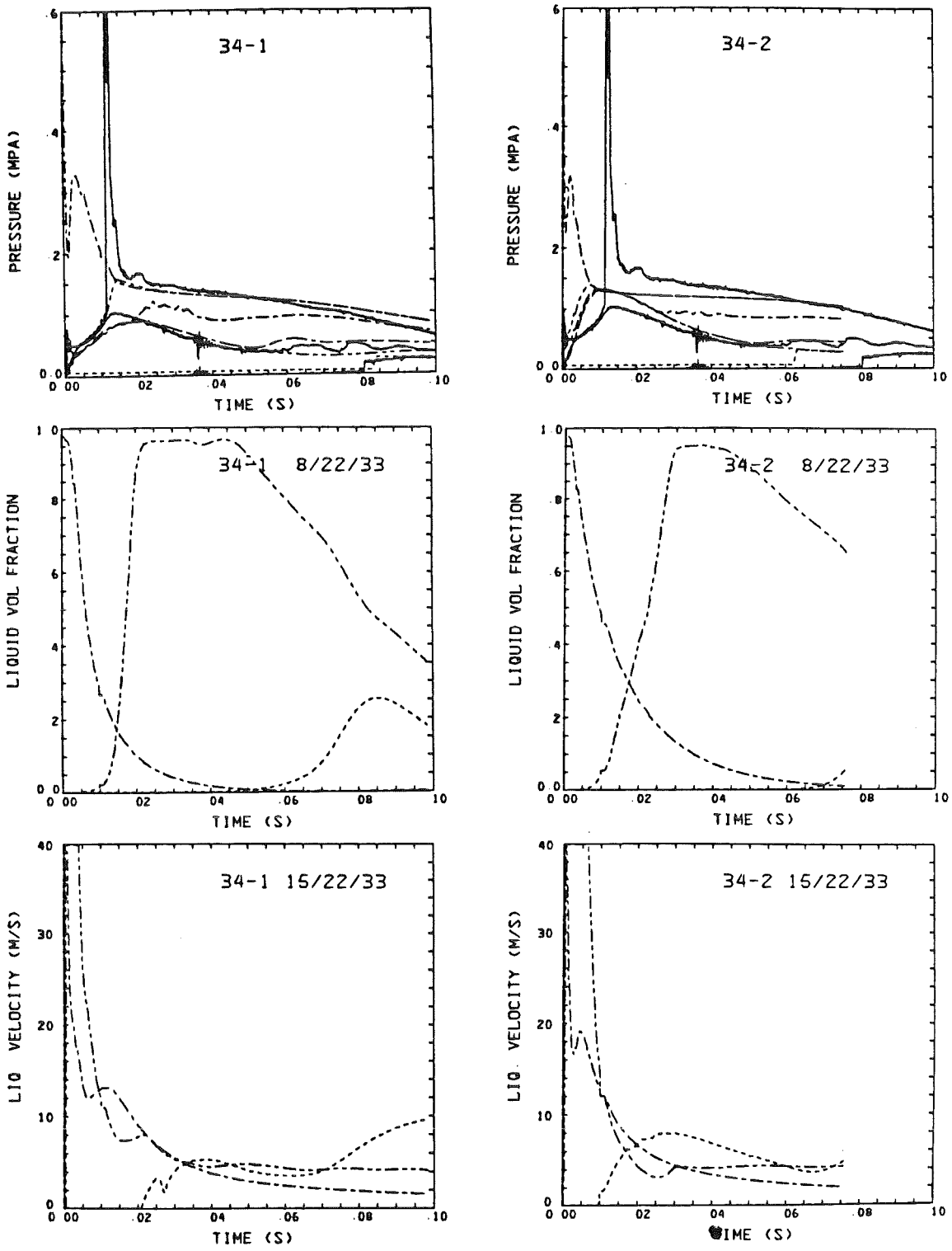

Fig. 83a. Calculations for Test 34;
full lines: measured pressures p_2, p_6 and p_9
sequence of dashed lines with regard to nodes: ——-/——-—/------.

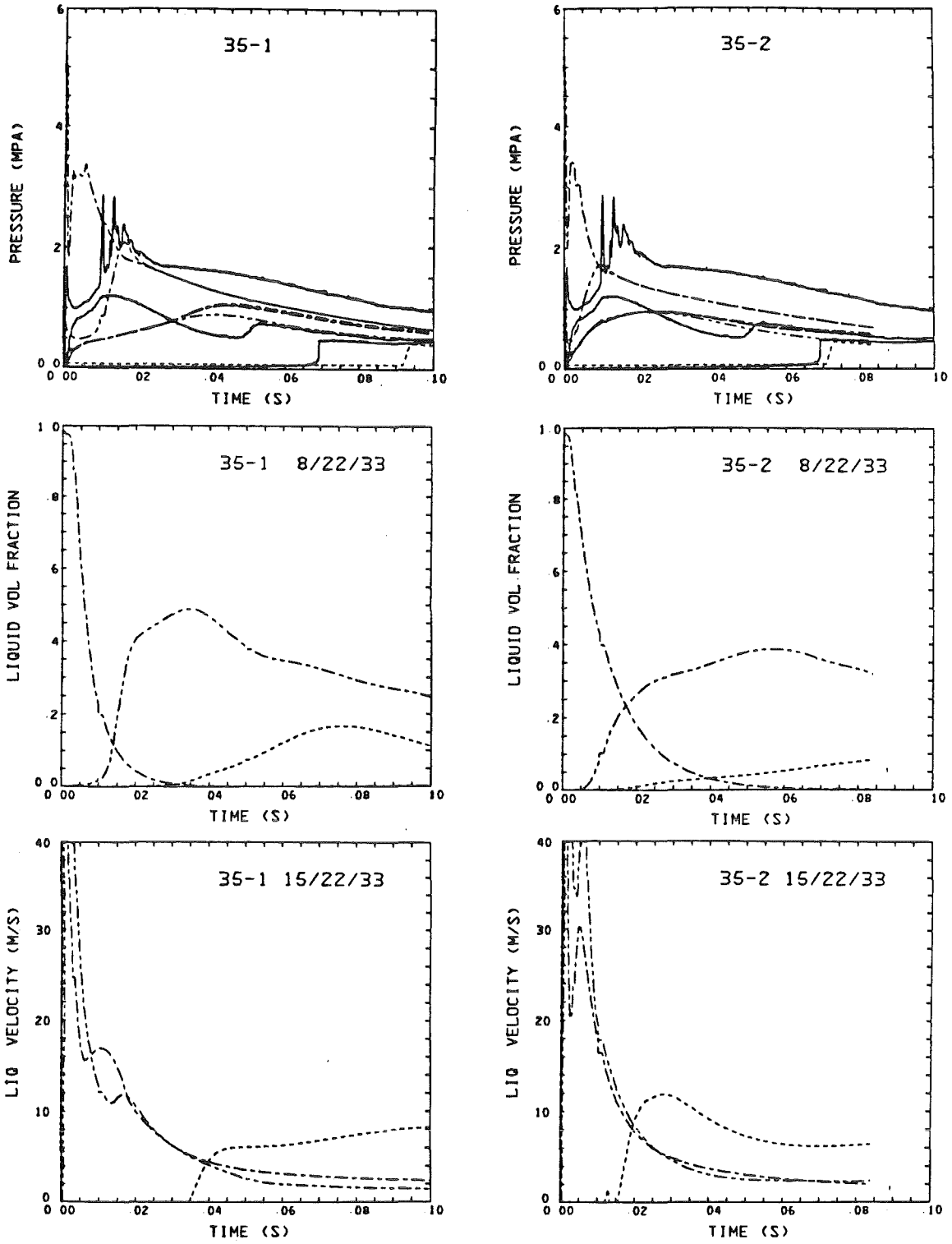

Fig. 83b. Calculations for Test 35; notation see Fig. 83a.

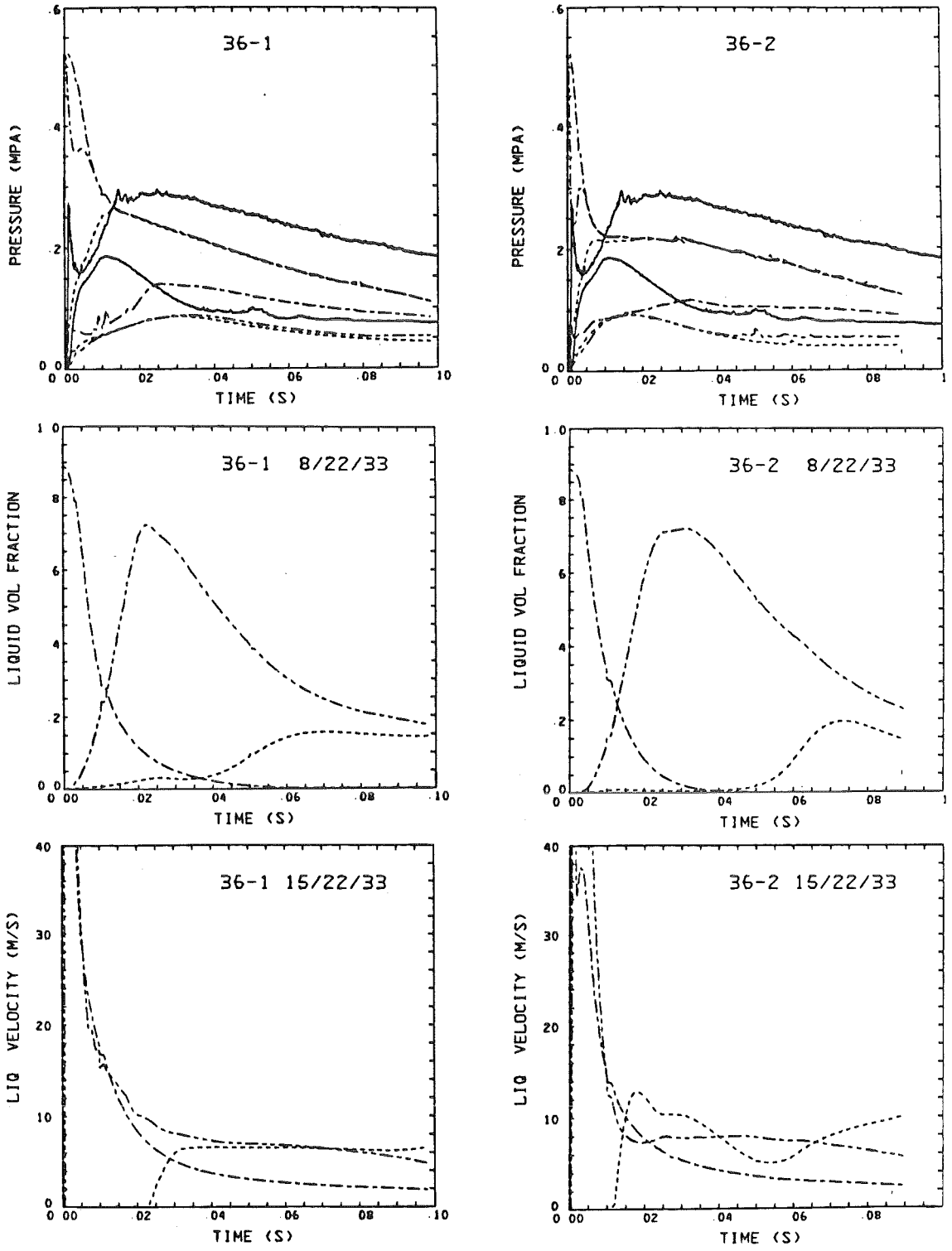

Fig. 83c. Calculations for Test 36; notation see Fig. 83a.

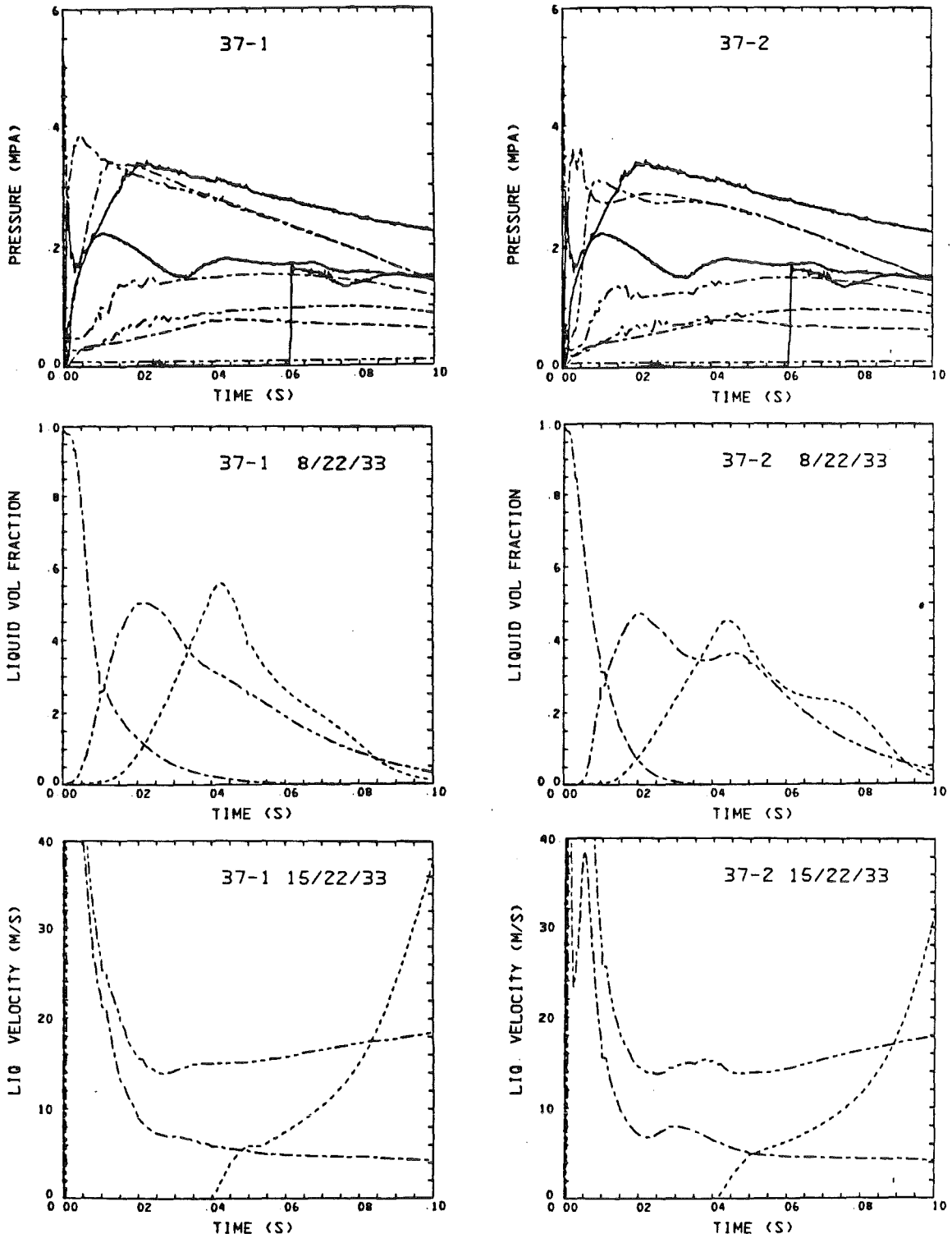

Fig. 83d. Calculations for Test 37; notation see Fig. 83a.

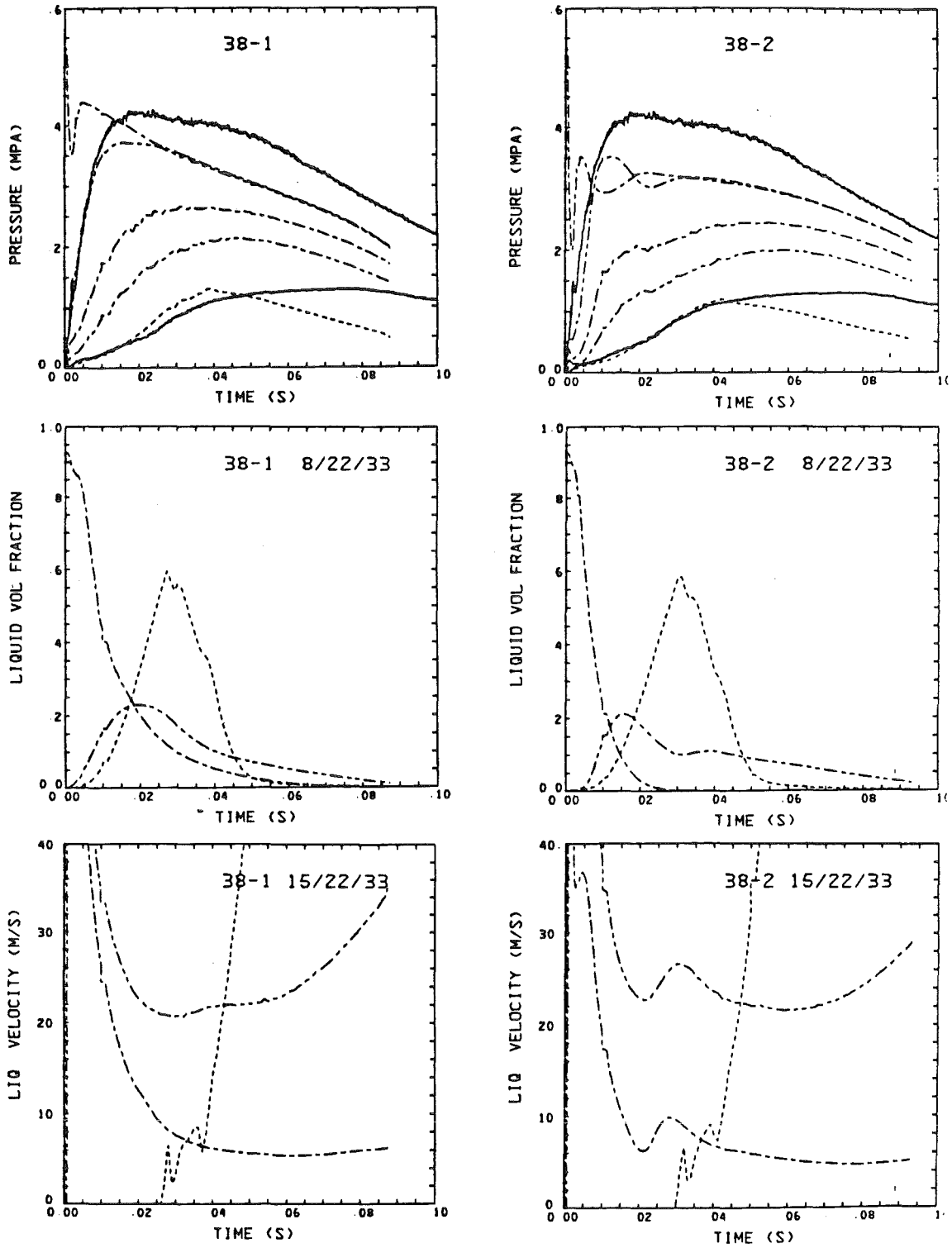

Fig. 83e: Calculations for Test 38; notation see Fig. 83a.

APPENDIX A

DESIGN CONSIDERATIONS FOR THE PISTON AND PISTON TRACK

The mass of the piston and the length of the flight path have to be modeled considering the simulation of the three-dimensional expansion of the fuel vapor bubble in the sodium pool by a one-dimensional movement of a solid cylinder. Because the design considerations related to the USD/CRBR experiments were not contained in Ref. 1, they will be given here, together with the considerations for the SNR-related experiments.

Without any structures above the UCS, the bubble emerging from the UCS has a roughly spherical shape. Further, the SIMMER results show that we can assume a coherent, uniform movement of the upper pool interface toward the vessel head. Thus, the top of the bubble will expand in the axial direction a much longer distance than will the flat sodium pool/cover gas interface (see Fig. A-1). By comparing this bubble volume and the cover-gas volume, we derive the maximum axial distance z that the bubble interface travels in the axial direction by $z = 2r - h$, where r is the bubble radius with the bubble center already emerged from the UCS exit plane and h is the height of that part of the bubble that hypothetically still is hidden in the UCS. When we assign a as the height and D the diameter of the cylindrical cover-gas volume and the sodium pool, we have

$$\frac{1}{4}\pi D^2 a = \frac{4}{3}\pi r^3 - \frac{1}{3}\pi h^2 (3r-h), \text{ with } h \leq r \quad .$$

To simplify calculations, the bubble surface always is supposed to coincide with the upper end of the core periphery. With this assumption, only minor effects of the bubble growth in the vicinity of the radial blanket are neglected. Thus,

$$2rh - h^2 = \frac{1}{4}c^2 \quad ,$$

where c is the diameter of the cylindrical periphery of the core. By assuming $h \leq r$, we obtain

$$h = r - (r^2 - \frac{1}{4}c^2)^{1/2} \quad .$$

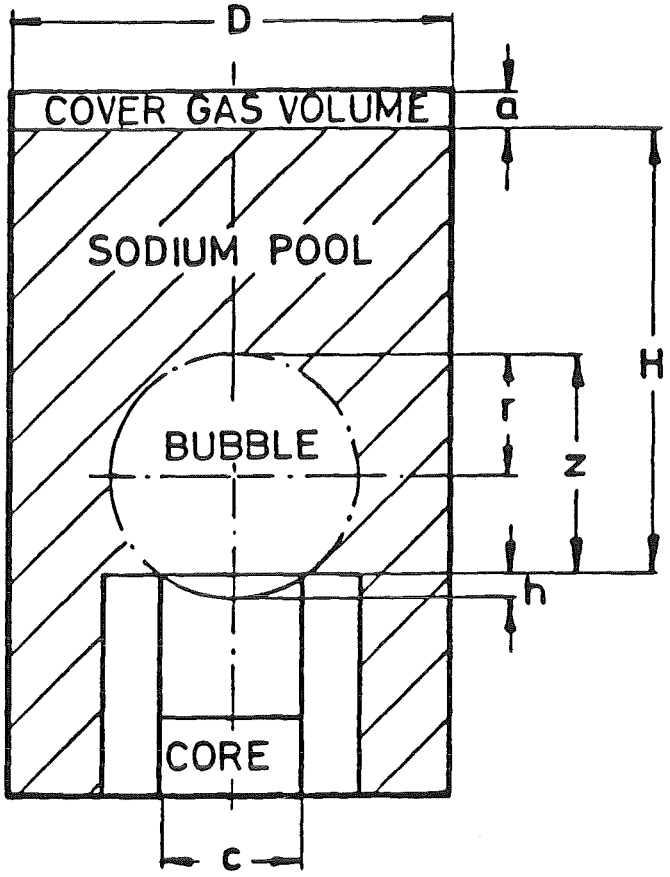

Fig. A-1. Model of the HCDA bubble emerging from the UCS (no Upper Internal Structure, UIS) of a CRBR.

Combination of this formula with the volume equation yields r as a function of D, C, and a such that

$$\frac{2}{3}r^3 + \left(\frac{2}{3}r^2 + \frac{1}{12}c^2\right)\left(r^2 - \frac{1}{4}c^2\right)^{1/2} - \frac{1}{4}D^2a = 0 \quad .$$

If we take D = 6 m, c = 2 m, and a = 0.5 m, the radius of the bubble will be

r = 1.27 m and z = 2.04 m. Thus, the spherical bubble can emerge into the sodium pool and develop to a maximum height that is approximately four times higher than the displacement of the upper surface of the pool. Because length scales in the USD experiment are reduced to 40% of prototypic lengths, this result implies that a piston flight distance of 0.82 m would be necessary to model the anticipated maximum displacement of the CRBR sodium pool.

In the case of an SNR-type reactor, 300 MWe (see Fig. A-2), the cover gas volume is larger and the above-core pool depth H smaller than in CRBR-type reactor. If we take D = 6.7 m, a = 1.6 m, c = 1.7 m, the spherical bubble would emerge into the cover gas plenum before slug impact. It is therefore necessary to anticipate the doming of the sodium surface and the slug impact occurring at a smaller bubble radius than has been calculated with the analytical equation. Moreover, the pool depth changes drastically, impeding an easy assessment of the piston mass. As a compromise, we assume the lower sodium interface to move 3 m upward and the piston mass according to the weight of the initial pool depth. The one-dimensional movement of the piston is only a very rough model of the complex retention of the expanding bubble due to three-dimensional pool movement. Any difference in the scaling calculations below is dominated by this fact.

The flight distance is scaled down by the length scale factor to 1.2 m. The mass of a pool column can be scaled by using the equivalence of the forces acting on the column and its acceleration. Consequently, the mass of a simulant column is scaled down using pressure, area, and acceleration scaling factors, yielding a piston mass of 0.2 kg. Because of a previous analysis, the density and volume of the pool column were used to scale the mass. For a first approximation, the density of all moving fluids was scaled down by a factor of 4.4, which was derived from the ratio of molecular masses of UO_2 and its simulants. Therefore, the resulting mass of 0.35 kg yields a high retention of the working fluid. This also sets an upper limit on the calculation of 0.2 kg, which may be influenced by scaling uncertainties of the acceleration.

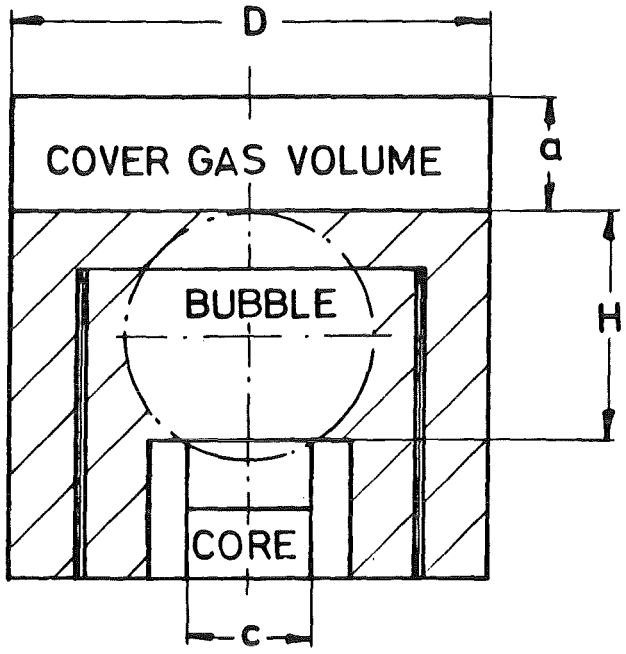

Fig. A-2. Model of the HCDA bubble emerging from the UCS of a SNR.

APPENDIX B

SAMPLE INPUT FILE

```
  1       0  -105Q08LMY USD-17-1 SNR PROPANOL , CORE #2 150 PSI, LMY
  2       2      0      0      0      0      3      1      1    500      0
  3    USD-SNR-17-1, SIMMER ANALYSIS, CORE # 2,150 PSI,PROPANOL
  4    USD-SNR-17-1, SIMMER ANALYSIS, CORE # 2,150 PSI,PROPANOL
  5   1.50000E-01   1.0          0.9
  6       1     85
  7    FLUID DYNAMICS INPUT
  8      10     85      0      0      5      0      9      0      0
  9       0      0      0      0      0      0      0      0      0      0
 10      10      0      0      0      0      0      0      0      0      0      0
 11       1      4      1     11      1     14      1     17      1     18      1     25
 12       1     26      1     28      1     32      1     34
 13       5   1000   1000    100     50      5      1     -1      0      0      0      1
 14    FLUID DYNAMICS PROBLEM CONTROL INPUT
 15   2.86000E-02             1
 16   1.46670E-02             5 1.46670E-02            11 1.46670E-02            12
 17   1.64000E-02            17 1.50000E-02            19 2.36700E-02            25
 18   1.20000E-02            26 2.73300E-02            29 3.18250E-02            33
 19   2.30800E-02            85
 20   0.5          0.0           -9.8          1.00000E-10
 21   1.00000E-04 1.00000E-06 1.00000E-04 1.00000E-04 1.00000E-08 5.00000E-02
 22   1.00000E-08 1.00000E-08 1.00000E-08 1.00000E-09 1.00000E-01 1.00000E-10
 23   0.0020       0.95          0.01          10.00         1.00000       0.00001
 24    FLUID DYNAMICS OUTPUT PARAMETERS
 25   0.0          0.0           0.0           0.0           0.0
 26   2.00000E-04 2.00000E-03 5.00000E-03 0.02          0.2           40.0
 27   0.0          1.00000E-03 0.010         0.60
 28   3.01000E-03 1.01000E-02 0.101         1.01          100.01        1000.0
 29   0.0          0.0           0.0           0.0
 30   2.00000E-04 5.00000E-04 1.00000E-03 0.50          10.0          100.0
 31   0.0          0.0           0.0           18.01
 32   1.01000E-03 1.01000E-02 0.101         5.01          100.01        1000.0
 33   0.0          0.0           0.0           0.0
 34   5.00000E-02 5.00000E-01 1.00000E 01 1.00000E 02 0.00000E 00 0.00000E 00
 35   0.00000E 00 0.00000E 00 0.00000E 00 0.00000E 00
 36   1.01000E-01 5.01000E 00 1.01000E 02 1.00000E 03 0.00000E 00 0.00000E 00
 37   0.00000E 00 0.00000E 00 0.00000E 00 0.00000E 00
 38   0.0          0.0           0.0           0.0           0.0           0.0
 39   0.0          0.0
 40   0.0          0.0           0.0           0.0           0.0           0.0
 41   0.0          0.0           0.0
 42   0.0          0.0           0.0           0.0           0.0           0.0
 43   0.0          0.0           0.0           0.0           0.0
 44   0.0          0.0
 45    VIEW FACTORS
 46
 47    TIME STEP CONTROL DATA
 48   0.0          1.00000E-05 1.00000E-12 3.00000E-01
 49   5.00000E-04 0.25          10.0          1.0           1.0           1.0
 50   0.0          0.0           0.0           0.0           0.0           0.0
 51    STRUCTURE AND SOLID FUEL PARAMETERS
 52   0.5          0.5           0.5           0.5           0.5           0.5
 53   0.5
 54   0.55         0.55          0.55          0.55
 55   100.0        100.0         100.0         100.0         100.0         10.0
 56   1.00000E 02 1.00000E 02 1.00000E 01
 57    STEEL INSTEAD OF FUEL DATA, M=1
 58   7.36500E 03 6.93000E 02 1.70000E 03 2.60000E 05 2.50000E 01
 59   6.10000E 03 7.50000E 02 1.60000E 00 2.00000E 01 5.36000E-03
 60   1.33800E 11 4.33700E 04 1.00000E 00 8.17000E 06 1.00000E 04 3.60000E-01
 61   4.92000E 02 1.26000E 00 1.64000E 00 0.00000E 00 5.60000E 01 7.70000E 03
 62   0.00000E 00 0.00000E 00
 63     ALUMINUM INSTEAD OF STEEL DATA, M=2
 64   2.70000E 03 8.50000E 02 1.10000E 03 4.00000E 05 2.50000E 02
```

```
 2.50000E 03 1.00000E 03 8.60000E-01 2.00000E 02 3.00000E-03
 4.75000E 10 3.04400E 04 1.00000E 00 9.38000E 06 1.00000E 04 3.60000E-01
 1.39000E 03 1.26000E 00 1.64000E 00 9.38000E 06 2.70000E 01 7.70000E 03
 0.00000E 00 0.00000E 00
   N-PROPANOL INSTEAD OF SODIUM DATA, M=3
 8.00000E 02 2.40000E 03 1.47000E 02 8.65000E 04 1.76000E-01
 8.00000E 02 5.12000E 03 1.42000E-02 1.38000E-01 2.50000E-04
 3.62412E 10 4.70270E 03 1.00000E 00 1.06020E 06 5.36800E 02 3.71300E-01
 1.80633E 03 1.04300E 00 4.54900E 00 0.00000E 00 6.00000E 01 5.77000E 02
 2.75000E 02 7.69200E 01
 1.06407E 03-8.86200E-01 0.00000E 00 2.59040E 00 3.75900E-01 0.00000E 00
   CONTROL DATA, SODIUM AT 6.1E4 SOUND SPEED, M=4
 1.54000E 03 1.30000E 03 2.38000E 02 2.70400E 04 1.34000E 02
 1.54000E 03 1.30000E 03 1.00000E 03 5.00000E 01 1.50000E-04
 3.22520E 09 1.21300E 04 1.00000E 00 4.81600E 06 2.50300E 03 3.41000E-01
 5.56300E 02 1.65000E 00 3.56700E 00 4.53500E 06 2.30000E 01 1.37500E 03
 2.14100E 02 4.67000E 01
    FISSION GAS DATA, M=5, USE AS COVER GAS, HELIUM PROPERTIES
 1.25000E 02 1.25000E 02 1.00000E 00 2.58000E 04 2.60000E-02
 1.25000E 02 1.25000E 02 7.77000E-02 2.60000E-02 1.80000E-05
 2.00000E 06 1.37500E 01 1.00000E 05 2.90000E 04 5.00000E 00 3.30500E-01
 3.19785E 03 1.65000E 00 2.56000E 00 0.00000E 00 4.00000E 00 1.00200E 01
 0.00000E 00 0.00000E 00
     COMPONENT PROPERTY DATA
 7.36500E 03 7.36500E 03 7.36500E 03 7.36500E 03 2.70000E 03 2.70000E 03
 1.54000E 03 1.25000E 02 1.25000E 02
 6.10000E 03 6.10000E 03 2.50000E 03 8.00000E 02 1.54000E 03 7.36500E 03
 7.36500E 03 2.70000E 03
 4.50000E 03 4.50000E 03 2.00000E 03 1.20000E 02 6.10000E 04 4.50000E 03
 4.50000E 03 2.00000E 03
  HEAT TRANSFER CORRELATION DATA
 1.00000E 00 1.00000E 00 1.00000E 00 1.00000E 00 1.00000E 00 1.00000E 00
 1.00000E 00 1.00000E 00 1.00000E 00 1.00000E 00 1.00000E 00 1.00000E 00
 1.00000E 00 1.00000E 00 1.00000E 00
 2.30000E-02 8.00000E-01 4.00000E-01 2.00000E 00
 2.50000E-02 8.00000E-01 8.00000E-01 5.00000E 00
 2.30000E-02 8.00000E-01 4.00000E-01 5.00000E 00
 2.30000E-02 8.00000E-01 4.00000E-01 2.00000E 00
 2.30000E-02 8.00000E-01 4.00000E-01 2.00000E 01
 3.70000E-01 6.00000E-01 3.30000E-01 2.00000E 00
     DRAG CORRELATION DATA
 1.00000E 00 1.50000E 01 5.00000E-07 5.00000E-07 1.00000E 00
 0.00000E 00 0.50000E 00 5.00000E-01 1.00000E 00 0.40000E 00 1.00000E 10
 8.30000E-02 -2.5000E-01 4.00000E-03 8.30000E-02 -2.5000E-01 4.00000E-03
 0.50000E 00
   PARAMETER REGION 1, CORE
 5.00000E 00 0.00000E 00 0.00000E 00 0.00000E 00 0.00000E 00 3.20000E-05
 0.00000E 00 0.00000E 00 8.32000E 01 0.00000E 00 0.00000E 00 1.93000E-01
 4.10000E-02 4.10000E-02 4.10000E-02 0.00000E 00 0.00000E 00 1.25000E 05
 1.95000E 03 6.40000E-01 0.00000E 00 2.30000E-05 1.00000E-17 3.00000E-03
 0.50000E-04 2.00000E 00 2.00000E 00
   PARAMETER REGION DATA FOR REGION 2, PISTON TRACK
 5.00000E 00 0.78796E 00 6.00000E 03 0.00000E 00 0.00000E 00 3.20000E-05
 0.00000E 00 0.00000E 00 6.20000E 01 0.00000E 00 0.00000E 00 0.78796E 00
 4.10000E-02 4.10000E-02 4.10000E-02 0.00000E 00 0.00000E 00 1.25000E 04
 1.95000E 03 6.40000E-01 6.00000E 03 2.30000E-05 1.00000E-17 5.00000E-04
 5.00000E-07 1.00000E 00 1.00000E 00
   PARAMETER REGION DATA FOR REGION 3, LOWER SPACER
 5.00000E 00 0.00000E 00 0.00000E 00 0.00000E 00 0.00000E 00 3.00000E-05
 0.00000E 00 0.00000E 00 6.02000E 01 0.00000E 00 0.00000E 00 1.17300E-01
 4.80000E-02 4.80000E-02 4.80000E-02 0.00000E 00 0.00000E 00 1.25000E 05
 1.95000E 03 6.40000E-01 0.00000E 00 2.30000E-05 1.00000E-17 1.00000E-05
 5.00000E-07 2.00000E 00 4.00000E 00
   PARAMETER REGION DATA FOR REGION 4, FUEL PIN ENTRANCE SECTION
```

```
 1.00000E 00 0.40000E 00 6.00000E 03 1.18999E-03 1.19000E-03 3.20000E-05
 4.96000E 02 4.96000E 02 0.56600E 02 2.20000E-01 1.00000E-04 1.20000E-01
 2.00000E-03 2.00000E-03 2.00000E-03 4.16000E 04 4.16000E 04 1.25000E 05
 1.95000E 03 6.40000E-01 6.00000E 03 2.30000E-05 1.00000E-17 5.00000E-04
 4.00000E-07 2.00000E 00 4.00000E 00
   PARAMETER REGION DATA FOR REGION 5, FUEL PIN BUNDLE
 1.00000E 00 0.46000E 00 6.00000E 03 1.18999E-03 1.19000E-03 3.20000E-05
 4.96000E 02 4.96000E 02 0.56600E 02 1.61000E-01 1.00000E-04 1.20000E-01
 2.00000E-03 2.00000E-03 2.00000E-03 4.16000E 04 4.16000E 04 1.25000E 05
 1.95000E 03 6.40000E-01 6.00000E 03 2.30000E-05 1.00000E-17 5.00000E-04
 5.00000E-07 1.60000E 00 3.20000E 00
   PARAMETER REGION DATA FOR REGION 6, SPACE BEFORE MIXING HEAD
 1.00000E 00 0.29000E 00 6.00000E 03 0.00000E 00 1.00000E-06 3.20000E-03
 0.00000E 00 1.00000E-03 5.60000E 01 0.00000E 00 1.00000E-04 1.20000E-01
 4.50000E-02 4.50000E-02 4.50000E-02 0.00000E 00 1.00000E 00 1.25000E 05
 1.95000E 03 6.40000E-01 6.00000E 03 2.30000E-05 1.00000E-17 5.00000E-04
 5.00000E-07 1.00000E 00 2.00000E 00
   PARAMETER REGION DATA FOR REGION 7, MIXING HEAD
 1.00000E 00 0.58000E 00 6.00000E 03 0.00000E 00 1.00000E-06 3.20000E-03
 0.00000E 00 1.00000E-03 0.93000E 02 0.00000E 00 1.00000E-04 1.00000E-01
 0.92000E-02 0.92000E-02 0.92000E-02 0.00000E 00 1.00000E 00 1.25000E 05
 1.95000E 03 6.40000E-01 6.00000E 03 2.30000E-05 1.00000E-17 5.00000E-04
 5.00000E-07 2.00000E 00 4.00000E 00
   PARAMETER REGION DATA FOR REGION 8, UPPER SPACE
 1.00000E 00 0.42000E 00 6.00000E 03 0.00000E 00 1.00000E-06 3.20000E-03
 0.00000E 00 1.00000E-03 5.01000E 01 0.00000E 00 1.00000E-04 0.60000E-01
 4.00000E-02 4.00000E-02 4.00000E-02 0.00000E 00 1.00000E 00 1.25000E 05
 1.95000E 03 6.40000E-01 6.00000E 03 2.30000E-05 1.00000E-17 5.00000E-04
 5.00000E-07 1.20000E 00 2.40000E 00
   PARAMETER REGION 9, LOWER CORE
 5.00000E 00 0.00000E 00 0.00000E 00 0.00000E 00 0.00000E 00 3.20000E-05
 0.00000E 00 0.00000E 00 8.32000E 01 0.00000E 00 0.00000E 00 1.93000E-01
 4.10000E-02 4.10000E-02 4.10000E-02 0.00000E 00 0.00000E 00 1.25000E 05
 1.95000E 04 6.40000E-01 0.00000E 00 2.30000E-05 1.00000E-17 3.00000E-03
 2.00000E-04 2.00000E 00 2.00000E 00
   MOVABLE PISTON
     1    34    85    30    34     1     1
     1     1     1     1     1     1
 0.36000E 00 1.50000E 02 2.58000E 03 1.20000E 00 2.04300E-03
   LOWER BOUNDARY INITIAL VELOCITIES
 0.00000E 00
 0.00000E 00
   MESH SET 1,  PROPANOL
     1     4     1     1     3     1     0     0     9
 0.00000E 00 0.00000E 00 0.00000E 00 0.00000E 00 0.00000E 00 5.21100E 02
 0.00000E 00 0.00000E 00 0.00000E 00
 0.00000E 00 0.00000E 00 0.00000E 00 4.52000E 02 0.00000E 00
 0.00000E 00 0.00000E 00 0.00000E 00 5.00000E 02 0.00000E-03 0.00000E 00
 0.00000E 00 0.00000E 00
 0.00000E 00 0.00000E 00 4.48000E 02 0.00000E 02 0.00000E 00 0.00000E 00
 0.00000E 00 0.00000E 00 0.00000E 00 3.16070E 01 0.00000E 00 3.66800E-03
 4.52000E 02
 0.00000E 00 0.00000E 00 0.00000E 00 0.00000E 00 5.00000E-08 5.00000E-08
   MESH SET 2,  PROPANOL
     5    11     1     1     3     1     0     0     1
 0.00000E 00 0.00000E 00 0.00000E 00 0.00000E 00 0.00000E 00 5.21100E 02
 0.00000E 00 0.00000E 00 0.00000E 00
 0.00000E 00 0.00000E 00 0.00000E 00 4.52000E 02 0.00000E 00
 0.00000E 00 0.00000E 00 0.00000E 00 5.00000E 02 0.00000E-03 0.00000E 00
 0.00000E 00 0.00000E 00
 0.00000E 00 0.00000E 00 4.48000E 02 0.00000E 02 0.00000E 00 0.00000E 00
 0.00000E 00 0.00000E 00 0.00000E 00 3.16070E 01 0.00000E 00 3.66800E-03
 4.52000E 02
 0.00000E 00 0.00000E 00 0.00000E 00 0.00000E 00 5.00000E-08 5.00000E-08
```

```
193     MESH SET 3,  PROPANOL VAPOR
194       12     12      1      1      3      1      0      0      1
195  0.00000E 00 0.00000E 00 0.00000E 00 0.00000E 00 0.00000E 00 5.21100E 02
196  0.00000E 00 0.00000E 00 0.00000E 00
197  0.00000E 00 0.00000E 00 0.00000E 00 4.52000E 02 0.00000E 00
198  0.00000E 00 0.00000E 00 0.00000E 00 1.00000E 00 0.00000E 00 0.00000E 00
199  0.00000E 00 0.00000E 00
200  0.00000E 00 0.00000E 00 4.48000E 02 0.00000E 02 0.00000E 00 0.00000E 00
201  0.00000E 00 0.00000E 00 0.00000E 00 3.16070E 01 0.00000E 00 3.66800E-03
202  4.52000E 02
203  0.00000E 00 0.00000E 00 0.00000E 00 0.00000E 00 0.00000E 00 5.00000E-08 5.00000E-08
204       MESH SET 4, AL, HE, LOWER SPACE
205       13     17      1      1      3      1      0      0      3
206  0.00000E 00 0.00000E 00 0.00000E 00 0.00000E 00 0.00000E 00 3.16700E 02
207  0.00000E 00 0.00000E 00 0.00000E 00
208  0.00000E 00 0.00000E 00 0.00000E 00 3.00000E 02 0.00000E 00
209  0.00000E 00 0.00000E 00 0.00000E 00 1.00000E-01 0.00000E-03 0.00000E 00
210  0.00000E 00 0.00000E 00
211  0.00000E 00 0.00000E 00 3.00000E 02 3.00000E 02 0.00000E 00 0.00000E 00
212  0.00000E 00 0.00000E 00 0.00000E 00 0.00000E 00 0.00000E 00 3.66800E-05
213  3.00000E 02
214  0.00000E 00 0.00000E 00 0.00000E 00 0.00000E 00 5.00000E-08 5.00000E-08
215       MESH SET 5, AL, STEEL, HE, 1.UCS
216       18     19      1      1      3      1      0      0      4
217  1.62000E 03 0.00000E 00 0.00000E 00 0.00000E 00 1.00000E-03 3.24000E 02
218  0.00000E 00 0.00000E 00 0.00000E 00
219  2.60000E 02 0.00000E 00 2.60000E 02 2.60000E 02 0.00000E 00
220  0.00000E 00 0.00000E 00 0.00000E 00 1.00000E-01 0.00000E-03 0.00000E 00
221  0.00000E 00 0.00000E 00
222  0.00000E 00 0.00000E 00 2.60000E 02 2.60000E 02 0.00000E 00 0.00000E 00
223  0.00000E 00 0.00000E 00 0.00000E 00 0.00000E 00 0.00000E 00 3.66800E-05
224  2.60000E 02
225  0.00000E 00 0.00000E 00 0.00000E 00 0.00000E 00 5.00000E-08 5.00000E-08
226       MESH SET 6, AL, HE, 2.UCS
227       20     25      1      1      3      1      0      0      5
228  1.18600E 03 0.00000E 00 0.00000E 00 0.00000E 00 1.00000E-03 3.24000E 02
229  0.00000E 00 0.00000E 00 0.00000E 00
230  2.57000E 02 0.00000E 00 2.57000E 02 2.57000E 02 0.00000E 00
231  0.00000E 00 0.00000E 00 0.00000E 00 1.00000E-01 0.00000E-03 0.00000E 00
232  0.00000E 00 0.00000E 00
233  0.00000E 00 0.00000E 00 2.57000E 02 2.57000E 02 0.00000E 00 0.00000E 00
234  0.00000E 00 0.00000E 00 0.00000E 00 0.00000E 00 0.00000E 00 3.66800E-05
235  2.57000E 02
236  0.00000E 00 0.00000E 00 0.00000E 00 0.00000E 00 5.00000E-08 5.00000E-08
237       MESH SET 7, AL, HE, SPACE BEFORE MIXING HEAD
238       26     26      1      1      3      1      0      0      6
239  0.00000E 00 0.00000E 00 0.00000E 00 0.00000E 00 1.00000E-03 3.24000E 02
240  0.00000E 00 0.00000E 00 0.00000E 00
241  0.00000E 00 0.00000E 00 2.54000E 02 2.54000E 02 0.00000E 00
242  0.00000E 00 0.00000E 00 0.00000E 00 1.00000E-01 0.00000E-03 0.00000E 00
243  0.00000E 00 0.00000E 00
244  0.00000E 00 0.00000E 00 2.54000E 02 2.54000E 02 0.00000E 00 0.00000E 00
245  0.00000E 00 0.00000E 00 0.00000E 00 0.00000E 00 0.00000E 00 3.66800E-05
246  2.54000E 02
247  0.00000E 00 0.00000E 00 0.00000E 00 0.00000E 00 5.00000E-08 5.00000E-08
248       MESH SET 8, AL, HE, MIXING HEAD
249       27     29      1      1      3      1      0      0      7
250  0.00000E 00 0.00000E 00 0.00000E 00 0.00000E 00 1.00000E-03 2.70000E 02
251  0.00000E 00 0.00000E 00 0.00000E 00
252  0.00000E 00 0.00000E 00 2.53000E 02 2.53000E 02 0.00000E 00
253  0.00000E 00 0.00000E 00 0.00000E 00 1.00000E-01 0.00000E-03 0.00000E 00
254  0.00000E 00 0.00000E 00
255  0.00000E 00 0.00000E 00 2.53000E 02 2.53000E 02 0.00000E 00 0.00000E 00
256  0.00000E 00 0.00000E 00 0.00000E 00 0.00000E 00 0.00000E 00 3.66800E-05
```

```
257  2.53000E 02
258  0.00000E 00 0.00000E 00 0.00000E 00 0.00000E 00 5.00000E-08 5.00000E-08
259       MESH SET 9, AL, HE, UPPER SPACE
260      30     33      1      1      3      1      0      0      8
261  0.00000E 00 0.00000E 00 0.00000E 00 0.00000E 00 1.00000E-03 1.62000E 02
262  0.00000E 00 0.00000E 00 0.00000E 00
263  0.00000E 00 0.00000E 00 2.52000E 02 2.52000E 02 0.00000E 00
264  0.00000E 00 0.00000E 00 0.00000E 00 1.00000E-01 0.00000E-03 0.00000E 00
265  0.00000E 00 0.00000E 00
266  0.00000E 00 0.00000E 00 2.52000E 02 2.52000E 02 0.00000E 00 0.00000E 00
267  0.00000E 00 0.00000E 00 0.00000E 00 0.00000E 00 0.00000E 00 3.66800E-05
268  2.52000E 02
269  0.00000E 00 0.00000E 00 0.00000E 00 0.00000E 00 5.00000E-08 5.00000E-08
270       MESH SET 10, PISTON TRACK, SAT. PROPANOL AT 293K
271      34     85      1      1      3      1      0      0      2
272  0.00000E 00 0.00000E 00 0.00000E 00 0.00000E 00 1.00000E-03 5.67000E 02
273  0.00000E 00 0.00000E 00 0.00000E 00
274  0.00000E 00 0.00000E 00 2.93000E 02 2.93000E 02 0.00000E 00
275  0.00000E 00 0.00000E 00 0.00000E 00 1.00000E-01 0.00000E 00 0.00000E 00
276  0.00000E 00 0.00000E 00
277  0.00000E 00 0.00000E 00 2.93000E 02 0.00000E 02 0.00000E 00 0.00000E 00
278  0.00000E 00 0.00000E 00 0.00000E 00 1.20000E 00 0.00000E 00 4.24133E-04
279  2.93000E 02
280  0.00000E 00 0.00000E 00 0.00000E 00 0.00000E 00 5.00000E-08 5.00000E-08
```

APPENDIX C

UPDATE FILE FOR HELIUM TEST CALCULATIONS

```
*ID LM01
*D FAM.98
      FHIG2=AMIN1(EPS,(ONE+XSGRD**(ONE/TFFN))**TFFN)
*D FAM.121,185
      HFIGJ=FIJG(IJ)*VELG(1)*VELG(1)*DTD(10)
      DG(IJ)=DG(IJ)+HFIGJ
*D XCHA.613,614
      CALL FHASE
*D FHAS.36,46
*D FHAS.158,1641
      IF(NCSC.EQ.ZERO) GO TO 8200
      IF(NCHT.EQ.ZERO) GO TO 8100
      HVS(1,5)=HGS*AFIN*FRACHT*SCRC
      HS(1,5)=HTCON(NCHT)*AFIN*FRACHT*SCRC
      HVSE(1,5)=HVS(1,5)*HS(1,5)/(HVS(1,5)+HS(1,5))
      STRGHT=RDGF(5)*CVG(5)*HVSE(1,5)*(TN(NCHT)-TGC)/(RDGF(5)*CVG(5)+
     *  DTT*HVSE(1,5))
      DG(IJ)=DG(IJ)+STRGHT
      DS(IJ+NCHT-1)=DS(IJ+NCHT-1)-STRGHT
 8100 CONTINUE
      IF(NCAT.EQ.ZERO) GO TO 8200
      HVS(2,5)=HGS*ACANW*FRACHT*SCRC
      HS(2,5)=HTCON(NCAT)*ACANW*FRACHT*SCRC
      HVSE(2,5)=HVS(2,5)*HS(2,5)/(HVS(2,5)+HS(2,5))
      STRGHT=RDGF(5)*CVG(5)*HVSE(2,5)*(TN(NCAT)-TGC)/(RDGF(5)*CVG(5)+
     *  DTT*HVSE(2,5))
      DG(IJ)=DG(IJ)+STRGHT
      DS(IJ+NCAT-1)=DS(IJ+NCAT-1)-STRGHT
 8200 CONTINUE
*I FAM.222
      RGGAM=RDGF(5)*RMAT(5)
*D N989.54,62
*D FAM.135
      KIJ(IJ)=ZERO
*I IMFL.938
      UL(IJ)=UG(IJ)
*I IMFL.961
      VL(IJ)=VG(IJ)
*I IMFL.985
      UL(IFJ)=UG(IFJ)
*I IMFL.989
      VL(IJF)=VG(IJF)
```